Geochronology of Permo-Mesozoic Sediments and Structures in the Eastern Greywacke Zone

Master Thesis

of

Isabella Haas

Technical University of Graz

Geocenter Graz

Institute of Earth Science

Ao.Univ.-Prof. Dr.phil. Harald Fritz

Graz, January 2017

EIDESSTATTLICHE ERKLÄRUNG

Ich erkläre an Eides statt, dass ich die vorliegende Arbeit selbstständig verfasst, andere als die angegebenen Quellen/Hilfsmittel nicht benutzt und die den benutzten Quellen wörtlich und inhaltlich entnommene Stellen als solche kenntlich gemacht habe.

Graz, am …… ……..

(Unterschrift)

STATUTORY DECLARATION

I declare that I have authored this thesis independently, that I have not used other than the declared sources / resources, and that I have explicitly marked all material which has been quoted either literally or by content from the used sources.

…… ……..

date (signature)

Für meine Eltern

1 Danksagung

An dieser Stelle möchte ich mich bei all jenen bedanken, die mich während der Anfertigung dieser Masterarbeit unterstützt haben.

Allen voran möchte ich hierbei Prof. Fritz danken, welcher meine Masterarbeit betreut hat. Ohne sein stets offenes Ohr für alle Fragen und Anliegen und die aufheiternden und motivierenden „Gschichtln“ wäre diese Arbeit nie zustande gekommen.

Großer Dank gebührt auch Magdalena Mandl, die mir alles nötige zur Zirkondatierung erklärte. Von der Aufbereitung bis hin zur Datenanalyse am Massenspektrometer war sie die größte Stütze, selbst wenn Messungen bis zwei Uhr morgens dauerten.

Ein weiterer Dank gebührt meiner Kollegin, Stefanie Eichinger, welche sozusagen mein „Partner in Crime“ bei der Zirkonanalyse war und mich stets motivierte.

Auch meinen Studienkollegen, Doria Haller, Anna Walch, Marlene Löberbauer, Philip Schantl und Silvia Weigand, sowie allen aus dem „Kellerloch“ möchte ich hiermit für ihre Freundschaft und Ermutigung danken, welche selbst die mühsamsten Tage und Arbeiten amüsant machten.

Abschließend möchte ich auch noch meiner Familie und meinen Freunden außerhalb des Studiums danken. Vor allem meine Eltern waren immer für mich da und ich wusste stets dass ich ihre volle Unterstützung hatte. Sie waren es auch, die mir mein Studium überhaupt erst ermöglicht haben.

Ich danke auch noch all jenen die namentlich hier nicht erwähnt wurden, aber dennoch zur Erstellung meiner Masterarbeit beitrugen.

Danke,

Isabella Haas

Graz, Jänner 2017

2 Kurzzusammenfassung

Die Post–Variszischen Deckgebirgseinheiten der einzelnen Decken der Grauwackenzone wurden bisher als etwa gleichaltrige, benachbarte Becken angesehen. Um dies zu überprüfen, wurden die selten beachteten Metasandsteine der Silbersberg Decke, der Veitscher Decke und der Präbichl Fm., sowie der Semmeringquarzit beprobt, um das Spektrum ihre detritären Zirkone mittels LA–MC–ICP–MS zu analysieren (U/Pb).

Es zeigte sich, dass die Liefergebiete der untersuchten Proben sehr unterschiedlich sind und die einzelnen Becken während ihrer Sedimentation vermutlich nicht benachbart waren. Der unmittelbare Untergrund der einzelnen Becken lag nach der Variszischen Gebirgsbildung frei und war der Erosion ausgesetzt. Trotzdem stammt der Detritus in den Sedimentbecken nur zum Teil aus diesem. Ein Vergleich der ermittelten Altersspektren mit publizierten Altern aus Grundgebirgsarealen der Ostalpen und Karpaten lässt folgende Liefergebiete vermuten:

- Die Altersverteilung der Zirkone im Silbersberg Metasandstein mit dem auffälligen Fehlen Ordovizischer Zirkone und einer Mitteldevonischen Population ist am ehesten mit Altern aus dem Kaintaleck Kristallin vergleichbar.
- Das wahrscheinlichste Liefergebiet des Semmeringquarzits mit der deutlichen Häufung Ordovizischer und Permischer Zirkone sind die Einheiten, die heute südlich des Tauernfensters liegen.
- Der Veitscher Metasandstein mit seinen dominanten Oberkambrischen bis Ordovizischen Altern aber auch Unterkarbonen detritären Zirkonen lässt sich mit den Tatrischen und Verporischen Einheiten der Karpaten vergleichen.
- Die Präbichl Fm. zeigt eine markante Unterkarbonische Altersgruppe und untergeordnet Ordovizische Zirkonpopulationen. Das Liefergebiet beinhaltet wahrscheinlich resedimentierte Paläozoische Anteile und Unterkarbone Magmatite.

Die Zirkonpopulationen aller Sedimente reflektieren die Stadien des Zerfalls von Gondwana bis zur Bildung Pangäas.

3 Abstract

The post-Variscan cover units of the different Greywackezone nappes were so far interpreted as juxtaposed sediment sources with similar ages. In order to examine this assumption, samples of the Silbersberg, the Veitscher and the Präbichl metasandstones as well as of the Semmering quartzite were taken and used for detrital U/Pb zircon analysis. The detrital zircon analysis was done with a LA-MC-ICP-MS.

The analysis demonstrated that the sediment sources were quite different, and therefore did not originate of the same sediment basins. The direct basement of the individual basins was exposed to erosion after the Variscan orogeny. Still, the detritus of the sediment basins originates only partly of the associated basement. If the age spectra of the detrital zircons are compared with the published ages of the basement terrains of the Alpine and Carpathian Realm, the following sources can be suggested:

- The age distribution of the Silbersberg metasandstone zircons lacks of Ordovician aged zircons and depicts middle Devonian population, which is most likely comparable to ages from the Kaintaleck Complex.
- The likeliest delivery area of the Semmering quartzite, which possesses an obvious accumulation of Ordovician und Permian zircons, are the units south of the current Tauern Window.
- The Veitscher metasandstone and the connected dominant Upper Cambrian to Ordovician ages, but also the Lower Carboniferous aged zircons, are quite similar to the age spectra of the Tatric and Veporic units of the Carpathian.
- A dominant Lower Carboniferous age group can be seen in the age spectra of the Präbichl Fm, as well as an Ordovician aged zircon population. The source area consists therefore probably of resedimented Paleozoic layers and Lower Carboniferous magmatites.

The zircon populations of all the samples reflect the break-up stages of Gondwana until the formation of Pangea.

4 Table of content

1 Danksagung V

2 Kurzzusammenfassung VII

3 Abstract VIII

4 Table of content IX

5 List of figures XIII

6 List of tables XVII

7 Introduction 1

8 Methods 2

8.1 Field work 2

8.2 Jawcrusher and roll crusher 2

8.3 Sieving 2

8.4 Gold panning 3

8.5 Magnetic Separation 3

8.6 Gravity separation 3

8.7 REM 4

8.8 LA –MC – ICP – MS 4

9 Geographical Overview 5

10 Geological Overview 7

10.1 Eastern Alps 7

10.1.1 The Helvetic nappes 7

10.1.2 Penninic nappes 7

10.1.3 Austroalpine 8

10.1.4 Southalpine 10

10.2 Variscian Orogeny 12

10.2.1 Model after Kroner & Romer, 2013: 12

10.2.2 Model after von Raumer et al., 2002: 14

10.3 Alpine Orogeny 15

10.4 Eastern Greywacke Zone 18

10.4.1 Veitsch Nappe 18

10.4.2 Silbersberg Nappe 19

10.4.3 Kaintaleck Nappe 19

10.4.4 Noric Nappe 20
11 Geological map 23
12 Thin section description 27
12.1 The Silbersberg Nappe 27
12.1.1 Metaconlgomerates 27
12.1.2 Greenschists 31
12.1.3 Phyllites 33
12.1.4 Riebeckite gneiss 35
12.1.5 Veins 37
12.1.6 Porphyritic Metatuff 38
12.2 The Veitsch Nappe 39
12.2.1 Metaconglomerates 39
12.2.2 Phyllite 40
12.3 Tattermann and Troiseck-Floning Complex 42
13 Deformation events 46
14 Quartz textures of the mapping area samples 48
15 Zircon data 52
15.1 Description of the analytical procedure of zircon dating with LA – MC – ICP - MS 53
15.1.1 Further data processing 54
15.2 Petrographic description of the geochronological samples 55
15.2.1 Sample G21: Silbersberg metasandstone 55
15.2.2 Sample G2: Semmering quartzite 56
15.2.3 Sample G1: Veitsch Nappe 56
15.2.4 Sample L1: Metasandstone of the Präbichl Formation 57
15.3 Description of the zircon samples through CL/BSE mixed images 58
15.3.1 Silbersberg metasandstone (G21) 59
15.3.2 Semmering Quartzite (G2) 60
15.3.3 Veitscher metasandstone (G1) 61
15.3.4 Metasandstein der Präbichl Formation (L1) 62
15.4 Concordia Plots of the measured samples 63
15.4.1 Silbersberg Metasandstein (G21) 64

15.4.2 Semmering quartzite (G2) 65
15.4.3 Veitscher Metasandstein (G1) 66
15.4.4 Metasandstein der Präbichl Formation (L1) 67
15.5 Age distribution of the samples displayed through Density Plots 69
15.5.1 Silbersberg metasandstone (G21) 69
15.5.2 Semmering quartzite (G2) 70
15.5.3 Veitscher metasandstone (G1) 71
15.5.4 Präbichl metasandstone (L1) 72
15.5.5 Comparison of the measured samples 73
15.5.6 Other possibilities to represent the measured age distributions 77
15.6 Differentiation of zircon development and the frequency of occurence in the different tectonic settings 82
15.6.1 Zircon formation and U/Th ratios 82
15.6.2 Preservation potential of zircons by means of their tectonic setting 84
15.6.3 Magmatic zircons and their tectonic settings 85
15.7 Plate tectonic developments during Earth's history 88
15.7.1 Pre-Cambrian 88
15.7.2 Cambrian 89
15.7.3 Ordovician 91
15.7.4 Silurian 94
15.7.5 Devonian und Carboniferous 95
15.7.6 Permian 99
15.7.7 The development of the Alps during the Pre – Variscian and Variscian events . 99
15.8 Interpretation of zircon ages and connected plate tectonic positions on the basis of cross sections 101
15.8.1 Pre- Cambrian 102
15.8.2 Cambrian (541 Ma - 485 Ma) 103
15.8.3 Ordovician (485 Ma - 443 Ma) 104
15.8.4 Silurian (443 Ma - 419 Ma) 105
15.8.5 Devonian (419 Ma - 358 Ma) 106

15.8.6 Carboniferous (358 Ma - 298 Ma) 107

15.8.7 Permian (298 Ma - 252 Ma) 110

15.9 Comments on the presumed origins of the different source areas, in relation to the pre-Alpine rock formation of the Alpine-Carpathian realm 117

15.9.1 Silbersberg metasandstone 117

15.9.2 Semmering quartzite 118

15.9.3 Veitscher metasandstone 119

15.9.4 Metasandstone of the Präbichl Formation 120

16 Conclusion 123

17 Reference list XIX

18 Appendix XXIX

18.1 Appendix A. sample register XXIX

18.2 Appendix B XXX

18.2.1 Silbersberg metasandstone (G21) XXX

18.2.2 Semmering quartzite (G2) XXXIV

18.2.3 Veitscher metasandstone (G1) XL

18.2.4 Metasandstone of the Präbichl Formation (L1) XLVII

18.3 Appendix C LII

18.3.1 Silbersberg metasandstone LII

18.3.2 Semmering quartzite LIII

18.3.3 Veitscher metasandstone LIV

18.3.4 Präbichl metasandstone LV

18.4 Appendix D LVI

18.5 Appendix E LXIX

5 List of figures

Fig. 1: Location of the mapping area (Digitaler Atlas Steiermark) 5
Fig. 2: Geological overview map of the Eastern Alps (after Schuster et al., 2013) 11
Fig. 3: Variscan orogeny after model of Kroner & Romer, 2013. It shows the opening of the Rheic ocean, the accretion of the detachment of the Amorican spur and the final collision of Gondwana and Laurussia. 13
Fig. 4: Paleogeographic overview of the eo-Alpine orogeny, with the opening of the oceanic arms and the closure of Meliata-Hallstatt (after Schmid et al., 2004). 17
Fig. 5: Tectonostratigraphic succession with lithologies of the Greywacke Zone, in two versions. Left Neubauer et al. (1994), right Schuster (2015) 22
Fig. 6: Mapping area close to Preiner Gscheid. It depicts the different lithologies as well as the dips and samples. 24
Fig. 7: Picture of the mapping area near to Preiner Gscheid. It shows the different lithologies, the dips as well as the sample numbers. The background of the map is given for orientation (Digitaler Atlas Steiermark). 25
Fig. 8: Thin sections of various samples of the metaconglomerate lithology. Picture A (with crossed polarizer) and B (without crossed polarizer) depict the typical augen-like texture of this lithology with components of mostly quartz grains. C is a close up of those component grains within the matrix. Picture D shows the fine sericitic felt and the finer grained quartz grains of the matrix. Photos E and F exhibit the matrix as well as components, but also show the retrograde chlorites of this lithology as components as well as in the matrix. The strain shadows of chlorite and quartz can also be seen in the pictures E and F. The occurring ores of metaconglomerates are shown throughout the pictures of this figure. 28
Fig. 9: This figure shows the composition and structure of the Greenschist lithology of the Silbersberg Nappe. Picture A to F all exhibit the main mineral compositions (see text). Picture B notable shows the remnants of epidote surrounded by chlorite in the epidote and chlorite abundant layer of sample P16. C and D, depict the small structural elements like normal faults and shear bands throughout the thin sections, while A shows a slight crenulation foliation too. 31
Fig. 10: This figure depicts the mineral composition and textures of the phyllites of the Silbersberg Nappe. All the pictures exhibit the typical mineralogical main composition of sericite, quartz and chlorite. Further, B also shows the shear bands and the “wavy” appearance of this rock type. Picture C depicts the few bigger mica grains, which can be interpreted as detritic mica parts, which are uncommon in the Silbersberg Nappe. A, D as well as E represent the typical veins of carbonate which penetrate the phyllites and are deformed in a later state. F shows a kink band which is part of coaxial shear bands. 34
Fig. 11: Parts A to D of this figure represent the Riebeckite gneiss of the Silbersberg Nappe. A (with crossed polarizer) and B (without crossed polarizer) show the smaller Riebeckites in the finer grained matrix, which are parts of the more foliated Riebeckite gneiss type. C depicts the big, already degrading Riebeckite of the less foliated rock type. Picture D exhibits the ore-filled cracks, which are to be found throughout the Riebeckite gneisses. 35
Fig. 12: Picture A (crossed polarizers) and B (without crossed polarizers) show the typical carbonate veins within this bigger vein complex, which possess a clearly visible displacement. Parts C (crossed polarizers) and D (without crossed polarizers) depict the notable chaotic strips of plagioclase. 37
Fig. 13: The composition of the porphyritic metatuff contains feldspar components, which are clearly visible in picture A (with crossed polarizers) and B (without crossed polarizers) and the matrix of sericitic white mica and fine grained quartz. 38
Fig. 14: This picture depicts the compostion of the metaconglomerates of the Veitsch Nappe, with the man components of detritic mica, quartz and feldspar. 39
Fig. 15: Picture A to D show the presence of the minerals quartz, feldspar, chlorite and mica, which is detritic white mica. C and D further exhibit a finer grained example of the Veitscher phyllites, while A and B show the shear band cleavage and the resulting wavy fabric of these rocks. 40
Fig. 16: The images A (with crossed polarizers) and B (without crossed polarizers) depict the typical structures of sample P 11. Notable are the visible K-feldspar recrystallization and the relatively high amount of carbonate. 42
Fig. 17: A (with crossed polarizers) and B exhibit the fabric of sample P 12 with the main components of white mica, chlorite, quartz and an high amount of feldspars. 43
Fig. 18: Along the main components, like quartz, white mica and chlorite, this pictures also show the crenulation foliation of sample P 13 which cannot be found in other lithologies of the mapping area. C (with crossed polarizers) and D (without crossed polarizers) also exhibit a quartz clast which is surrounded on both sides by highly folded white mica. 44

Fig. 19: These thin section pictures (with and without crossed polarizers) of sample P14 demonstrate the similarity to the metaconglomerates of the Silbersberg Nappe. The main components also are quartz and feldspar, next to sericitic white mica and chlorites, as well as similar structures. 45
Fig. 20. The structures of some of the thin sections of the mapping area allow the reconstruction of some deformation events. a) shows SC pattern throughout the thin section with a NW direction, b) depicts kink folding and crenulation foliation, c) carbonate vein which is folded and sheared to top SE, d) another carbonate vein which is folded and sheared to a N direction, e) shear bands, f) conjugated shear bands 47
Fig. 21: This figure shows the two types of cross girdles. Picture a) is cross girdle type I and picture b) type II after Passchier and Trouw, 2005. 49
Fig. 22: a) The different slip systems of quartz, depicted on a stereogram after Schmid and Casey, 1986. b) The other diagram shows Quartz c – axes opening angle plotted against the temperature in °C. The boxes are data after Kruhl, 1998 and the dashed line is the empirically determined connection between the opening angle and the temperature. The stereogram shows a cross girdle as well as the opening angle after Law (2014). 49
Fig. 23: Four different samples were analysed with a photometer and plotted in stereogram. Nr 1 and 2 are greenschists, while Nr. 3 and 4 depict Riebeckite gneiss. The black lines indicate their area of origin. 50
Fig. 24: a) This diagram dispalys the correlation between c-axes opening angle and temperature. b) The diagram after Grasemann et al., 1999, shows the curves for specific vorticity values, in comparison with the samples. 50
Fig. 25: The left picture depicts the sample G21 without crossed polarisation filter, while the sample G21 with crossed polarizing filter is shown on the right picture. The main minerals are Qu: quartz, Ch: chlorite, Cc: Calcite. 55
Fig. 26 The left picture indicates the sample G2 without crossed polarisation filter, while the sample G2 with crossed polarizing filter is shown on the right picture. 56
Fig. 27: The left picture represents the sample G1 without crossed polarisation filter, while the right picture depicts the sample G1 with crossed polarizing filter. The main minerals are Qu: quartz and Mu: muscovite. 57
Fig. 28: The left picture shows the sample L1 without crossed polarisation filter, while the right picture represents the sample L1 with crossed polarizing filter. The main minerals are Qu: quartz, Fsp: feldspar, Mu: serizitic gleams. 57
Fig. 29: Examples of representative zircon of the Silbersberg metasandstone. a) No. 20 round and not zoned; b) No. 28 round and zoned; c) No. 52 elongated and zoned; d) No. 73 elongated and not zoned; e) No. 91 round and sector zoned; f) No. 106 elongated and sector zoned. The red arrow shows the direction and form of the laser measurement. 59
Fig. 30: Examples of representative zircon of the Semmering quartzite. a) No. 152 elongated and zoned; b) No. 74 elongated and not zoned; c) No. 15 elongated and zoned; d) No. 32 round and not zoned; e) No. 64 round and zoned; f) No. 87 half pyramidal and zoned. The red arrow indicates the direction and form of the laser measurement.. 60
Fig. 31: This figure shows typical zircons of the Veitscher Metasandstone. a) No. 2 round and zoned b) No. 22 half pyramidal and zoned c) No. 74 half-pyramidal and zoned; d) No. 88 elongated and zoned; e) No. 51 elongated and zoned; f) No. 172 round and sector zoned. The red arrow displays the direction and form of the laser measurement. 61
Fig. 32: Some representative zircons of the Präbichl formation are shown here. a) No. 9 round and sector zoned; b) No. 16 elongated and zoned; c) No. 26 elongated and zoned; d) No. 28 round and zoned; e) No. 39 half-pyramidal and zoned; f) No. 56 round and zoned. The red arrow depicts the direction and form of the laser measurement. 62
Fig. 33: Four Concordia plots of the metasandstone of the Silbersberg are displayed. The two uppermost plots show the two main clusters, and every circle consists of a zircon measurement with a two Sigma error. Furthermore the concordance of all measurements can be seen. 64
Fig. 34: Four Concordia plots of the Semmering quartzite with the uppermost plots showing the two main ages. Similar to the earlier depiction every circle consists of a zircon measurement with two Sigma errors and a distinct concordance throughout the sample.. 65
Fig. 35: The Concordia diagrams of the metasandstone of the Veitsch Nappe exhibit clear concordance of all important age clusters. The upper plot on the left side and the right plot below represent the two main ages. Again, every circle consists of a zircon measurement with two Sigma errors. 66
Fig. 36: This representation of four Concordia diagrams of the metasandstone of the Präbichl formation displays a concordance of all important age groups. The left upper plot is the depiction of the main age. Every circle contains a zircon age with two Sigma error. 67

Fig. 37: Depiction of the Concordia plots of all samples with upper age limits between 800 and 1300 Ma. It exhibits, that nearly all zircon plots are concordant. 68
Fig. 38: Density plot of the Silbersberg metasandstone. On the x-axis the age in Ma is applied, while the y-axis shows the likelihood of appearance. The main age lies around 511 ± 3. 6 Ma and 390.3 ± 6.2 Ma. 69
Fig. 39: Density plot of the sample G2. On the x-axis the age in Ma is applied, while the y-axis exhibits the likelihood of appearance. The main ages are around 459.8 ± 2.5 Ma and 297.8 ± 2.5 Ma. 70
Fig. 40: Density plot of the G1 sample. The x-axis demonstrates the age in Ma, while the y-axis displays the likelihood of appearance. The main age lies around 465.4 ± 3.4 Ma, 498 Ma and 356.1 ± 2.6 Ma. 71
Fig. 41: Density plot of the sample L1. The x-axis represents the ages in Ma, while the y-axis is again the likelihood of appearance. The main age can be seen at 356.3 ± 3.9 Ma. 72
Fig. 42: Comparative representation of the similarities of the different analysed samples. Similarities and differences in the statistical frequencies of the zircon populations are highlighted (see text of chapter 15.5.5)..... 75
Fig. 43: Representation of the KDE plots of all measured samples with all age clusters. 76
Fig. 44: KDE und PDP plots in a directly compared way. The yellow age spectra represent the KDE diagrams, while red ones are the PDP plots. 78
Fig. 45: Depiction of the cumulative age distribution. The x-axis represents the million years, the y-axis shows the cumulative probability of appearance. 79
Fig. 46: The age distribution of the measured zircons is represented through the Normalized Age Probability plot (Gehrels, in 2007). The x-axis displays the age in Ma, while the y-axis contains relative values (no units). 81
Fig. 47: A chart representation of the differentiation through percentages of magmatic and metamorphic zircons. 83
Fig. 48: The number of the originating zircons in comparison to the magma volume is depicted. It is evident that the subduction area, in comparison to other tectonic environments, clearly generates most zircon (by Cawood et al., in 2013). 84
Fig. 49: This picture exhibits the amount in magma volume in comparison to the preservation potential. The marked area represents the balance between the magma formation and preservation in three possible tectonic settings (by Cawood et al., 2013). 85
Fig. 50: This graph representation depicts the percentages of long prismatic forms (volcanic zircons), short-prismatic forms (plutonic zirkons) and round forms (sedimentary zircons). 87
Fig. 51: Representation of the paleogeographical situation of the Late Cambrian till Early Devonian (after Stampfli & Borel, 2002). This depiction of the Tremadoc represents the detachment of Avlonia and the associated origin of the Rheic ocean. The Llandovery is characterised through the Ordovician orogeny in the eastern part due to the reunion of East-Avalonia with Gondwana. Ludlow displays the final detachment the now merged Hun terrain (opening Paleotethys) and the following Emsian exhibits the convergence of the Rheic ocean, as well as the opening of the Rheno-Hercynic ocean and the conditioned splitting off of the Hanseatic-terrain. 92
Fig. 52: Depiction of the paleogeographical situation during Middle Devonian till the Late Carboniferous (by Stampfli & Borel, 2002). During the Early Givetian the collision of the Hun terrain with the Hanseatic-terrain already had taken place. Many strike slip movements as well as the linked NW directed movement induced the Early Visean closure of the Rheno-Herzynic ocean and the collision of the Hanseatic Hunic terrain with Laurussia. The Bashkirian is characterised through the closure of the Paleotethys in the west and the correlated collision of Gondwana with Laurussia and therefore the formation of Pangea. 96
Fig. 53: Representation of the paleogeographical situation of the Late Carboniferous to Early Permian (by Stampfli & Borel, 2002). During the Kasimovian the formation of Pangea was finished and the rifting phases started in the Sakmarian, which are typical for the Permian. 98
Fig. 54: Depiction of a possible zircon population mixture. 102
Fig. 55: A plate tectonic profile depiction of the development Gondwanas at the end of the Precambrian with the differentiation of the future West-and East-Avalonia. The coloured circles represent the examined samples (violet s = Silbersberg metasandstone; green P = Präbichl metasandstone; black V = Veitscher metasandstone; orange Q = Semmering quartzite). The Proto-Tethys corresponds to the definition of Stampfli & Borel, 2002..... 103
Fig. 56: Plate tectonic development of the northern Gondwana margin during the Cambrian times. The samples are once more represented through coloured circles (legend like Fig. 55). 104

Fig. 57: A plate tectonic cross section through the different terrains of Gondwana in the Ordovician and a depiction of the orogeny in the eastern area (coloured circles are once more the sample positions with the same legend as in Fig. 55). 105
Fig. 58: Silurian development of Gondwana and its terrains, exhibited as cross sections (samples are again represented as in Fig. 55). 106
Fig. 59: Cross section representation of the plate tectonic developments during Devonian (with the same sample representation as in Fig. 55). 107
Fig. 60: This figure displays the collisions within the Hun terrain during the Carboniferous and Devonian (after von Raumer et al., in 2013). 109
Fig. 61: Plate tectonic development in represented through cross sections before and after the Variscian orogeny (once more the samples are shown as in Fig. 55). 109
Fig. 62: The blue circle exhibits the location of the analysed samples in the Permian. Permian extensional movements are also depicted (changed after Stampfli & Borel, 2002). 110
Fig. 63: Overall view of the plate tectonic development during the Paleozoic differentiated into West- and East-Avalonia (the legends and samples representation is similar to Fig. 55).). The Hun-terrain is depicted as coherent (in this and the earlier figures) although it presumably consisted of several continental blocks or ribbons. 111
Fig. 64: Paleogeographical representation of the earth from the Late Pre-Cambrian on up to Early Devonian (changed after Stampfli & Borel, 2002). The position of the analysed samples is exhibited in different colours (violet S = Silbersberg metasandstone, black V = Veitscher metasandstone, green P = metasandstone of the Präbichl Fm, orange Q = Semmering quartzite). 112
Fig. 65: Paleogeographical representation of the earth during Middle Devonian up to the Late Carboniferous (changed after Stampfli & Borel, 2002). The position of the single samples is again displayed in different colours (violet S = Silbersberg metasandstone, black V = Veitscher metasandstone, green P = metasandstone of the Präbichl Fm, orange Q = Semmering quartzite). 113
Fig. 66: Paleogeographical representation of the earth since Late Carboniferous up to Early Permian (changed after Stampfli & Borel, 2002). The position of the individual samples is again represented through different colours (violet S = Silbersberg metasandstone, black V = Veitscher metasandstone, green P = metasandstone of the Präbichl Fm, orange Q = Semmering quartzite). 114
Fig. 67: Classifications of the Precambrian age within the Silbersberg Metasandstone into typical zircon populations after Linnemann (2007). The picture depicts a Cambrian Rifting of this sample during the Pre-Cambrian. 115
Fig. 68: The classification of Precambrian aged zircons of the Semmering quartzite after Linnemann (2007). The picture exhibits a Cadomian back-arc during the Pre-Cambrian. 115
Fig. 69: The differentiation of the Precambrian aged zircons of the Veitscher metasandstone after the classification of Linnemann (2007). The depiction exhibits a Cadomian back-arc during the Pre-Cambrian. 116
Fig. 70: Classification of the Pre-Cambrian aged zircons of Präbichl metasandstone compared to the data of Linnemann (2007). The picture indicates a Cadomian back-arc during Pre-Cambrian. 116
Fig. 71: Supposed situation of the different source areas during the Permian (changed after von Raumer & Neubauer, 1993) 121
Fig. 72: The position oft he Präbichl sample can be located near the Tethys margin as the Tirolic-Juvavic nappes overlay those and there hast o be a crystalline hinterland. 122

6 List of tables

Table 1: Differentiation of zircon formation through the U/Th ratio 82
Table 2: This table lists all the samples taken during the mapping process XXIX
Table 3: Those tables depict the measured values of the zircons of the Silbersberg metasandstone, corrected through the EXCEL sheet LamTool U – Th – Pb VI of Košler und Klötzli (unpubl.). M257 (Nasdala et al., 2008), 91500 (Wiedenbeck et al., 1995) and Plešovice (Sláma et al., 2008) are the used standard samples. The crossed out measurements are discordant and were excluded of further steps. XXX
Table 4: Those tables depict the measured values of the zircons of the Semmering quartzite, corrected with the EXCEL sheet LamTool U – Th – Pb VI of Košler und Klötzli (unpubl.). M257 (Nasdala et al., 2008), 91500 (Wiedenbeck et al., 1995) and Plešovice (Sláma et al., 2008) are the used standard samples. The crossed out measurements are discordant and were excluded of further steps. XXXIV
Table 5: Those tables depict the measured values of the zircons of the Veitscher metasandstone, corrected with the EXCEL sheet LamTool U – Th – Pb VI of Košler und Klötzli (unpubl.). M257 (Nasdala et al., 2008), 91500 (Wiedenbeck et al., 1995) and Plešovice (Sláma et al., 2008) are the used standard samples. The crossed out measurements are discordant and were excluded of further steps. XL
Table 6: Those tables depict the measured values of the zircons of the Präbichl metasandstone, corrected with the EXCEL sheet LamTool U – Th – Pb VI of Košler und Klötzli (unpubl.). M257 (Nasdala et al., 2008), 91500 (Wiedenbeck et al., 1995) and Plešovice (Sláma et al., 2008) are the used standard samples. The crossed out measurements are discordant and were excluded of further steps. XLVII
Table 7: Register of the measured zircons of the Silbersberg metasandstone and the associated ages, two sigma errors and concordance. R: border of the zircon was measured, K: core of zircon was analysed, Diskor.: the analysed zircon is discordant..... LII
Table 8: Register of the measured zircons of the Semmering quartzite and the associated ages, two sigma errors and concordance. R: border of the zircon was measured, K: core of zircon was analysed, Diskor.: the analysed zircon is discordant. LIII
Table 9: Register of the measured zircons of the Veitscher metasandstone and the associated ages, two sigma errors and concordance. R: border of the zircon was measured, K: core of zircon was analysed, Diskor.: the analysed zircon is discordant.... LIV
Table 10: Register of the measured zircons of the Präbichl metasandstone and the associated ages, two sigma errors and concordance. R: border of the zircon was measured, K: core of zircon was analysed, Diskor.: the analysed zircon is discordant..... LV
Table 11: This table depicts the selected ages of the literature of the Alpine-Carpathian realm. LVI
Table 12: Occurence of ages in several areas oft he Eastern Alps in comparison to the measured sample ages. X: main ages of the samples. LXIX

7 Introduction

The geological units of the Greywackezone are composed of a repetitive succession of basement and cover sequences. Its cover units mostly consist of Permomesozoic sediments which so far were described in the literature as sediments of juxtaposed basins because of their similar appearance. Until now just $^{40}Ar/^{39}Ar$ data of detrital white mica, which exhibit the cooling history of the area around but not other techniques that record the early phases of intense magmatism and metamorphism, were made. In the course of this master thesis, U/Pb data of detrital zircons was produced, in order to prove or disprove the former assumptions.

Samples were taken from the Permian sediments of the Präbichl Formation (Noric Nappe), Silbersberg Formation (Silbersberg Nappe) and Carboniferous sediments of the Steilbachgraben Fm. (Veitsch Nappe), as well as from the Semmering quartzite as the cover of the Troiseck-Floning Complex. Zircons were separated out of these rocks samples and analysed by LA – MC – ICP – MS. The results were displayed through the evalution program of Isoplot diagrams. Theses Concordia diagrams, as well as probability plots, were used to interpret and locate the possible sedimentary sources.

It was further reviewed wether the detritus from these measured cover units could originate from the underlying basement, or if other basement units of the Alpine-Carpathian realm fed the sedimentary basins. Through the newly achieved information a paleogeographical development history of the sediment sources was tried to reconstruct, with the influence of the most important events throughout Earth's history. In order to be able to do these interpretations, the age distributions of the samples as well as the magmatic and metamorphic signature of the single zircons were used to reproduce the development of the sediments in a simplified way. The age cluster of the analysed samples were compared with tectonic events as shown on published paleogeographic maps, which was later on used to interpret the paleogeographical position of the sediment sources.

This thesis was intended to depict the development of the cover sequences of the Greywackezone in a comprehensible way.

It is necessary to mention that the zircon measurements and all the connected chapters were made in cooperation with the Master Thesis of Stefanie Eichinger, 2016.

8 Methods

8.1 Field work

In order to analyse the lithostratigraphic units of the Eastern Greywackezone a mapping of a particular area was done. Additional samples were taken to document the different lithologies.

Furthermore samples of an amount of 15 kg were taken to use them for the geochronological measurements. In all 35 samples for characterizing lithology and structures and 18 samples for the geochronology were taken. Table 2 of the Appendix lists all the samples, their coordinates and their orientation.

8.2 Jawcrusher and roll crusher

The Jawcrusher and the roll crusher from the company Siebtechnik were used to shred handpieces of rocks to fragments of about 125µm.
To achieve the coarser fracturing the Jawcrusher uses a wedge-shaped crushing chamber, where the moveable crusher jaw crumbles the probes. This crusher jaw can chop up rocks up until a Mohs' hardness of 8,5.
The final product of the Jawcrusher is later induced into the roll crusher, which is used to shred the probe into even smaller portions of rocks. Therefore the machine possesses two counter running rollers which allow a grinding of the samples up until the requested 125µm size.

8.3 Sieving

The final product of the roller crusher (see Retsch solutions in Milling & Sieving) contained grain size ranges from 2mm to smaller than 125µm. In order to separate the most important grain size for this work, which is the grain size range from smaller than 250µn to bigger than 125µm, Retsch "Analysesiebe" were used. For the differentiation of these grain size ranges, sieves were used in the following order and steps:

- 2mm
- 1mm
- 500µm
- 250µm
- 125µm

8.4 Gold panning

The gold panning-like procedure of the samples, after the sieving, was necessary to separate the heavier particles like zircons from the lighter grains. For that a gold pan from “Estwing” was used (see Geoscience News and Information; Estwing).

It is necessary to shake the particle-water mixture until all the material is floating in the pan. Afterwards, the lighter grains were gently washed out by slowly changing the angle of the pan and dipping it slightly into water. After some rounds of excluding the lighter material a small part of the sample, mostly dark materials like ores but also zircons, can be found on the bottom of the pan and be used for further methods.

8.5 Magnetic Separation

A magnetic separator from the S. G. Frantz Company Inc. was used to exclude magnetite or other magnetic minerals and grains out of the probes (S.G. Frantz Co).

The samples are slowly fed into the machine at one end and travel through a magnetic field, which is induced by an electromagnet. This leads to the separation of the stronger magnetic grains to the narrow side of the separator.

The separation can be influenced by manually changing the current, voltage and the vibration as well as the inclination. The used settings were the following:

- Inclination: 15°
- Vibration: 5
- Current: 0,4 to 2,5 Ampere

8.6 Gravity separation

For the gravity separation of the geochronological samples, sodium polytungstate was used as a heavy liquid (see TC-Tungsten Compounds). The sample is placed the specific heavy liquid, which is filled into glass cones. After few minutes, and repeated stirring of the liquid, the heavy particles of densities exceedingr 3,3g/cm^3 sunk deep into the cone, while the lighter grains are still floating on the surface.

After draining and drying the heavier particles, they can be used to finally handpick the zircons.

8.7 REM

A scanning electron microscope of type Joel JSM- 6310 at the Geocenter, Domain of Petrology and Geochemistry, was used to produce BSE and CL mixing pictures.

The grains were induced into high vacuum, where a bundled electron ray scans the surface of the sample. The interaction between the sample surface and the electrons produces emission, which is measured through detectors. The primary electrons (PE) are shot at the sample, where the energy of those PE and push processes knock out other electrons, the secondary electrons (SE; Holm, 1971).

The resulting BSE pictures can be used to identify the minerals, e.g. to differentiate between zircons and apatite. The combination of BSE and CL pictures allows the insight into zonation of the further used zircons and gives a better overview of cores and rims and the usability of the samples.

8.8 LA –MC – ICP – MS

The LA – MC – ICP – MS method is used for the Ionisation, the separation and detection of ions in the gas phase. The mass spectrometer itself consists of an ion source, a mass analyser and a detector, which are used in a high vacuum arrangement. It is a destructive method, meaning that small parts of the sample will be dissolved and cannot be used again. However, it uses only a few µg of probes (Gross, 2012).

The procedure of the measurement is used to separate ions according to their mass to charge ratio and determine the specific ratios in a qualitative and quantitative way.

For a further description see chapter 15.1.

9 Geographical Overview

The Eastern Greywacke Zone is to be found in the middle of Austria, which spreads from the east near Ternitz, Lower Austria, to the West near Liezen, Styria. Its extent is approximately a length of 200 km and a width of 20 km.

While the area of interest for the geochronological study extends through the entire Eastern Greywacke Zone, the particular area of interest for the mapping is located near Mürzzuschlag, between the Brandlberg to the west along the so called Preiner Gscheid Straße, until the Preiner Gscheid itself to the east. Fig. 1 indicates the exact position of the mapped area.

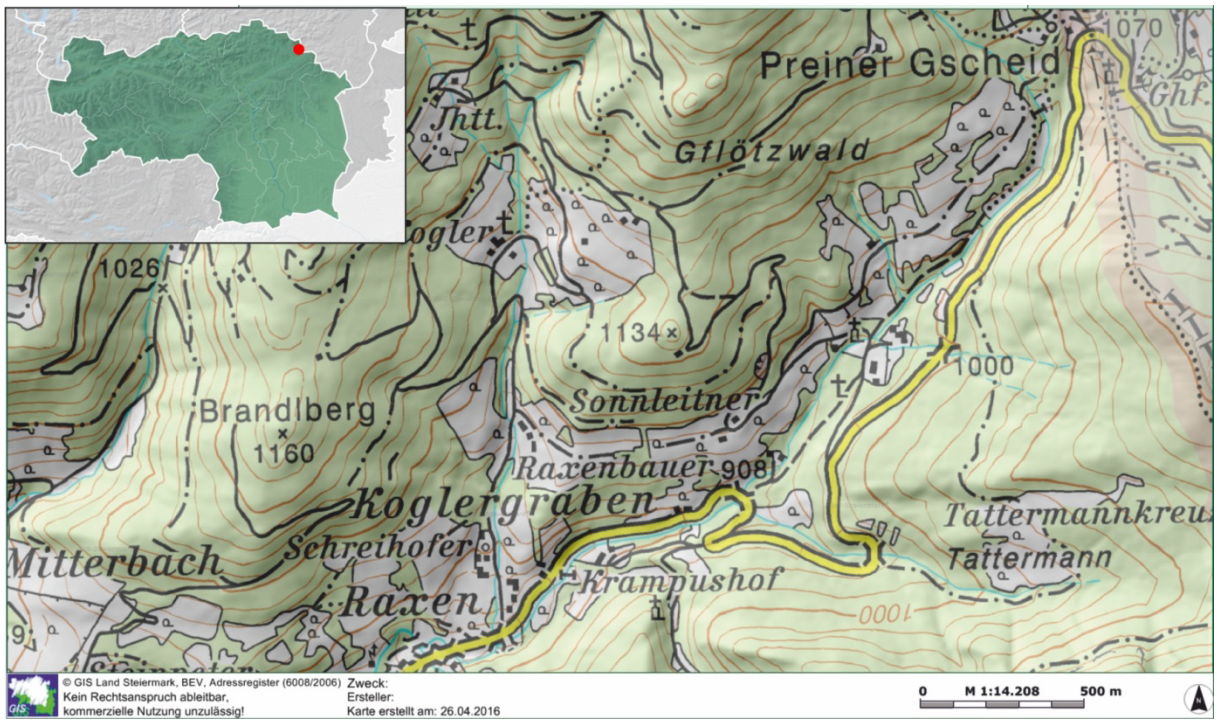

Fig. 1: Location of the mapping area (Digitaler Atlas Steiermark)

10 Geological Overview

10.1 Eastern Alps

The Alps extend over ca. 1200 km of length and are the most significant mountain chain in Central Europe. They are geographically divided into the Western, Eastern, Central and Southern Alps and continue to the East into the Carpathian arc.

The Eastern Alps are further differentiated into four tectonic super units (Schmid et al., 2004), namely:

- Helvetic nappe-complex
- Penninic nappes-complex
- Austroalpine nappe-complex
- Southalpine nappe-complex

10.1.1 *The Helvetic nappes*

The Helvetic nappe-complex is further divided into the Helvetic and the Ultrahelvetic nappes. They represent the European continental part during Mesozoic and Paleogene (Schuster et al., 2013).

The Helvetic nappes consist of heavily eroded metamorphic continental crust with a Variscan origin, and a cover of Carboniferous to Eocene sediment sequences. The Helvetic and Ultrahelvetic cover sequences in Austria were detached from their basement, the European lithosphere, and are interpreted as an thin-skinned fold and thrust belt by Neubauer et al., 2000. The Eastern Alps exhibit only small slices of those nappes, unlike the Western and Central Alps (Schmid et al., 2004; Schuster et al., 2013).

10.1.2 *Penninic nappes*

Above the Helvetic nappe-complex lie the Penninic nappes. These are the remnants of the Alpine Tethys Ocean, also known as Penninic Ocean, which opened during Jurassic and Early Cretaceous and was closed because of the Alpine Orogeny during Late Cretaceous and Paleogene (Froitzheim & Manatschal, 1996; Schuster et al. 2013). These Penninic Ocean derived complexes are subdivided into Valais, Brianconnais and Piemontais paleogeographical units in the Western Alps (Neubauer et al., 2000).

In Austria, the Penninic nappes are separated into the Lower, Middle and Upper Penninic nappes, with the Upper Penninic nappes being mostly derived from the Piedmont-Liguria Ocean as part of the Alpine Tethys (Schmid et al., 2004). In their model, the Middle Penninic nappes are correlated with the Brianconnais microcontinent and the Lower Penninic nappes with the Valais ocean. In the Eastern Alps, the Upper Penninic nappes can be seen as a part of nappe stacking process or as an accretionary wedge during Cretaceous times (Schmid et al., 2004; Froitzheim et al., 1994, Frisch et al., 1989) and forms the uppermost tectonic parts in the Tauern Window (Schuster et al., 2013). These Upper Penninic nappes are characterised by an Alpine overprint (Frey et al., 1999; Schmid et al., 2004). Remnants of the Lower Penninic nappes, mostly connected to the Valais ocean, are the Rhenodanubian Flysch present in the Alps and the Penninic nappes of the Tauern Window (Schuster et al. 2013).

Parts of the Middle Penninic nappes are rather found in the Central Alps than in the Eastern Alps, and represent parts of the Iberian-Brianconnais microcontinent (Schmid et al., 2004). This microcontinent, which rifted off stable Europe, separated the western part of the Penninic Ocean into the already former mentioned Piedmont-Ligurian and Valais Ocean (Schuster et al., 2013; Neubauer et al., 2000, Stampfli, 1993). The Upper Penninic nappe and the Lower Penninic nappe exhibit ophiolithes and metasediments, the upper nappe with an age of Jurassic to Cretaceous and the Lower with Cretaceous to Paleogene. The Middle Penninic nappes are rather characterised through basement rocks and Permo-Mesozoic metasediments as a cover (Schuster et al., 2013).

The Subpenninic nappes are lithologies from the former distal European margin, which unlike the other subsections, do not have contact with their lithospheric mantle (Schmid et al., 2004; Schuster et al., 2013). They were ductile deformed and are now the cover and basement nappes of the whole nappe complex basement (Schuster et al., 2013). Some of the basement units of the Subpenninic nappes exhibit Eclogites and can be interpreted as subducted and accreted material from the margin of the Penninic Ocean (Kurz & Froitzheim, 2002).

10.1.3 ***Austroalpine***

The Austroalpine lies above the Penninic nappes and is separated through the Periadriatic Lineament (further PAL) from the Southalpine (Schuster et al., 2013; Fig. 2). The Austroalpine is a residue of the Adriatic plate's continental crust with a Triassic passive continental margin sequence (Neubauer et al., 2000).

It contains parts of Cadomian continental crust (Neubauer et al., 2002) and metasediments of Paleozoic age as cover (Schuster et al., 2013). Within these Metasediments, magmatic rocks

can be found which are related to rifting and subduction processes up until Carboniferous times, and were later influenced by metamorphism and synorogenic magmatism (Schuster et al., 2013). This was followed by the deposition of post-orogenic sediments from the Carboniferous to Perm (Schuster et al., 2013). In Permian times a lithospheric extension and the connected high-temperature and low-pressure metamorphism followed (Schuster et al., 2013). It was subsequently succeeded by the deposition of the Permo-Mesozoic sediments which lead to a carbonate shelf and a Triassic passive continental margin next to Meliata Ocean, and a Jurassic passive margin towards the Penninic Ocean (Froitzheim & Manatschal, 1996; Neubauer et al., 2000; Schuster et al., 2013). The nappe stacking, and therefore the essential inner nappe structure occured during the Cretaceous orogenic event (Neubauer et al., 2000; Ratschbacher, 1986; Dallmeyer et al., 1998)

The nappe stack of the Austroalpine is further divided into two subunits: the Upper and the Lower Austroalpine unit (further UA and LA; Schmid et al., 2004). While the LA exhibits the former continental margin of the Piedmont-Ligurian part of the the Penninic Ocean, which was modified by extension and nappe stacking during the ocean evolution, the UA is an eo-Alpine nappe complex (Schuster et al., 2013). The Austroalpine was fromerly intersected in a different way by Tollmann (1977, 1985) into the Upper Austroalpine, the Middle Austroalpine and the Lower Austroalpine, whereas the Middle Austroalpine is nowadays seen as a part of the UA.

The UA is further subdivided into (Schuster et al., 2013):

- the Silvretta-Seckau nappe system, which is the lowermost part of the eo-Alpine nappe stack with a Variscan metamorphic basement and Permo-Triassic cover
- The Koralpe-Wölz nappe system tectonically overlies the Silvretta complex and is considered a high grade metamorphic extrusion wedge of the eo-Alpine. This nappe complex only contains pre-Alpine (poly)metamorphic basement nappes, as the cover was stripped off in the Lower Cretaceous in the course of the eo-Alpine orogeny.
- The Ötztal-Bundschuh nappe system is, from its composition similar to the Silvretta-Seckau system, but overlies the Koralpe-Wölz system tectonically
- the Greywacke Zone, which exhibits Palaeozoic nappes with an greenschist facies metamorphic print is, according to Schmid et al. (2004) tectonically emplaced over the Koralpe-Wölz system and is sedimentary contact with the
- Tirolic and Juvavic nappe systems of the Northern Calcareous Alps. These are the Permo-Mesozoic sediments of the Neotethyian shelf area, with the Juvavic being the most distal one, and are mostly un- or metamorphosed in greenschist facies.

- The Drauzug-Gurktal nappe systems holds, according to Schmid et al. (2004) the uppermost position in the eo-Alpine nappe stack of the Eastern Alps. It lies above the upper mentioned systems and exhibits a Variscan metamorphic basement, Palaeozoic metasedimentary sequences and Permotriassic cover sediments. The eo-Alpine metamorphism overprinted with very low grade up to amphibolite facies.
- The Gosau group represents the syn – to post - orogenic sediments of the Upper Cretaceous to Paleogene and terminated the eo – alpine orogeny.

The Meliata-Hallstatt unit, which has to be excluded from the other Austroalpine nappes, contains the remnants of the Meliata-Hallstatt Ocean, also called Neotethys, as a sedimentary infilling and can be found in the easternmost part of the Eastern Alps (Neubauer et al., 2000, Schuster et al., 2013). It contains sub-greenschist facies imprinted lithologies like serpentinites and deep water sediments of the Triassic, which are to be found in the Jurassic metasediments as redeposited material (Schuster et al., 2013).

10.1.4 ***Southalpine***

The Southalpine holds a southern, external retro orogenic wedge position of the Alps in the Miocene and continues into the External Dinarides (Neubauer et al., 2000; Schmid et al., 1996; Schmid et al., 2004; Schuster et al. 2013). It is further a continental unit, similar to the Austroalpine and is considered as the northern extension of the Adriatic microplate (Neubauer et al., 2000). The Southalpine shows just a slight deformation along the margins and seems to be in contact with the subcontinental lithosphere, which is visible in the Western Alps (Schuster et al. 2013). Furthermore, the Southalpine is interpreted as a S vergent fold-and-thrust-belt (Schmid et al., 2004).

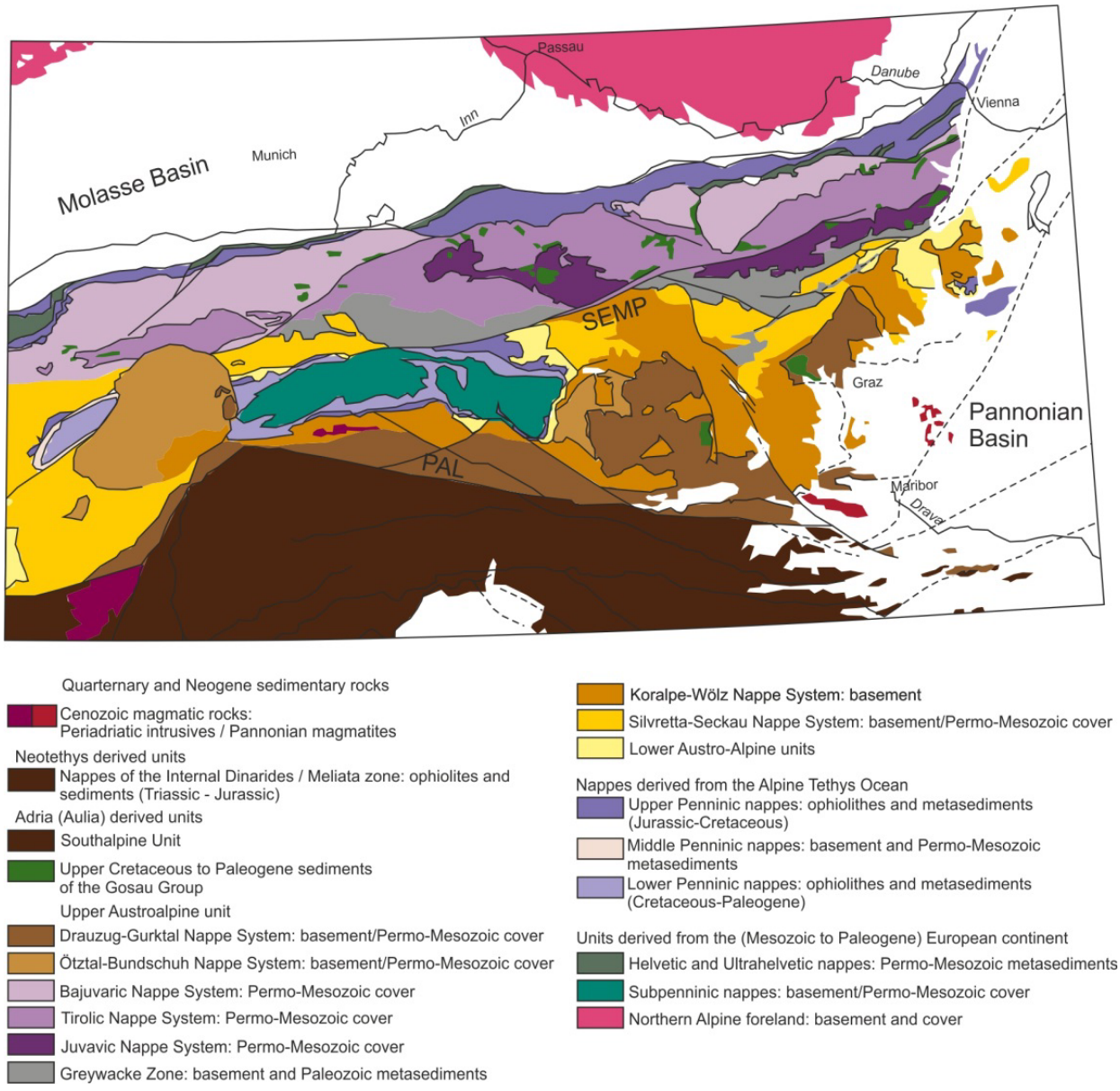

Fig. 2: Geological overview map of the Eastern Alps (after Schuster et al., 2013)

10.2 Variscian Orogeny

The Variscan Orogeny is mainly the outcome of the collision between the continents Gondwana and Laurussia and probably intermitted continental slivers (microcontinents), from the Upper Devonian to the Carboniferous (380-300 Ma), which created the supercontinent Pangea (Schuster et al., 2013; Kroner & Romer, 2013; von Raumer et al., 2002, 2003, von Raumer & Stampfli, 2008).

There are different theories about the involved continental pieces, timing and paleogeography of the Variscian Orogeny, and therefore two different possibilities will be discussed here.

10.2.1 ***Model after Kroner & Romer, 2013:***

One model is from Kroner & Romer (2013) who propose the theory that exclusively two major plates collided. These are the Gondwana plate, which contained oceanic crust of the Rheic Ocean as well as the Armorican Spur, and the Laurussia plate, which consists of the formerly accreted Avalonia Terrane, the East European Craton and the North American Craton.

The first step of the collision, during the subduction of the eastern Rheic Ocean, is believed to have occured in the Early Devonian where it lead to a deformation, which can be seen simultaneously to the initiation of continental subduction along the Armorican part of Gondwana and a back arc basin formation on both Amorican sides (e.g. the Rheno-Hercynian), and therefore also on Laurussia (Kroner & Romer, 2013). After the entering of the Armorican Spur (some kind of peninsula of northern Gondwana) into the subduction, the oceanic subduction of the Rheic Ocean stopped, because of the existence of thick and old Cadomian massifs which were unsubductable (Kroner & Romer, 2013). As further subduction stopped, a flip of subduction polarity was induced between the reorganised plate boundary zone of Gondwanan and North American Craton (Kroner & Romer, 2013). This first event and the evolving high pressure suites can be seen e.g. in the Bohemian massif. The subduction polarity flip lead to the subduction of Laurussia beneath Gondwana and additionally to the exhumation of e.g. the Mid-German Crystalline Zone (Kroner & Romer, 2013). Von Raumer et al. 2013 also mentions high-pressure eclogites in the Austroalpine basement with an age of about 360 to 300 Ma linked to the first parts of the Variscan Orogeny.

The collision was also the reason for a shift in the spreading axis of the Paleotethys, whose opening began in the Devonian on the Gondwana margin and was simultaneous to the subduction of the Rheic Ocean (Kroner & Romer, 2013; von Raumer et al. 2013).

The Devonian and Carboniferous were defined through the up-building on an orogenic wedge, which lead to a second suite of high-pressure rocks (Kroner & Romer, 2013). Around 340 Ma the peak of the high-pressure metamorphism was reached along intracontinental subduction zones, which were not associated with deformation/subduction along the Rheic suture zone (Kroner & Romer, 2013). The plate-driving forces and therefore the reason for the continent-continent-collision are considered by Kroner& Romer (2013) to be the ridge push of the Paleotethys ridge (Stampfli & Borel, 2002) and the slab pull of the Rheic Ocean (Nance et al., 2010) which subducted.

The transpressional stage, the final state of the Variscan Orogeny, started in the Carboniferous and was due to large scale escape tectonics (dextral and sinistral shear zones), which were induced through the ongoing collision and the thereby connected N-S compression (Kroner & Romer, 2013). Related to the transpression, isothermal exhumation processes occurred which lead to the Late Variscan high-temperature metamorphism (Kroner & Romer, 2013). This metamorphism was accompanied by large synkinematic intrusions of granites (Kroner & Romer, 2013; Cooke & O'Brien, 2001; Žák et al., 2011). Due to the compressional tectonics, the syn-orogenic basins were affected which lead to the Late Variscan fold and thrust belt until the compressional tectonic ceased around 300 Ma (Kroner & Romer, 2013).

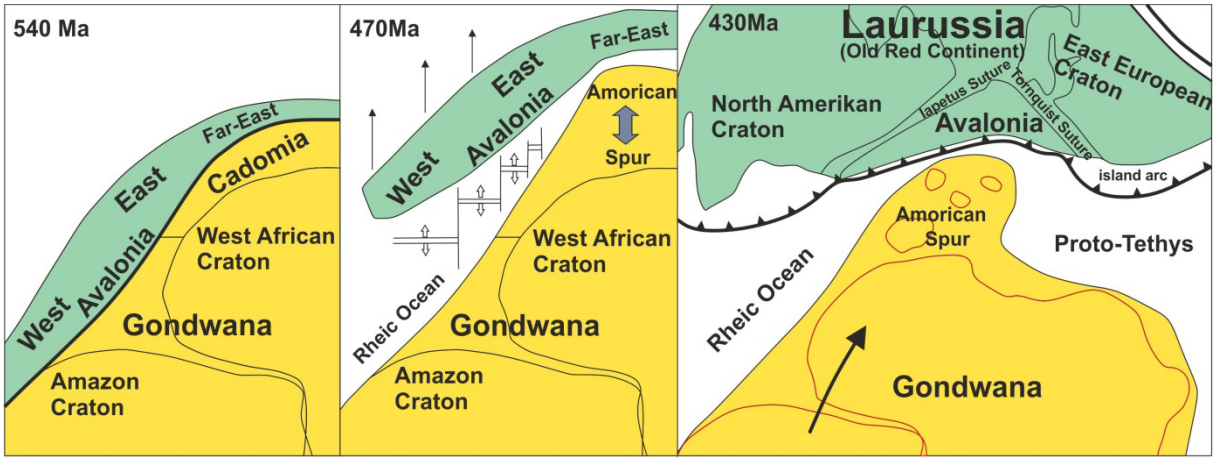

Fig. 3: Variscan orogeny after model of Kroner & Romer, 2013. It shows the opening of the Rheic ocean, the accretion of the detachment of the Amorican spur and the final collision of Gondwana and Laurussia.

10.2.2 ***Model after von Raumer et al., 2002:***

By contrast to the model of Kroner & Romer (2013), von Raumer et al. (2002) argues for the existence of microplates located between Gondwana and Laurussia. The formerly consolidated Gondwana broke up due to Cambrian back-arc rifting in combination with mantleplumes, which lead to the opening of the Rheic Ocean and the associated detachment of the Avalonia terrane (von Raumer & Stampfli, 2008; von Raumer et al., 2002, 2003; Domeier & Torsvik, 2014).

Ordovician times were characterised through ongoing opening of the Rheic ocean and the migration of the western Avalonia terrane to Laurussia (with a final collision during Silurian) and the connected subduction of the middle oceanic ridge of the Prototethys (von Raumer et al., 2002). The migration of the eastern part of Avalonia was prevented due to a still existing middle oceanic ridge of the Prototethys, which lead to destruction of the eastern Rheic arm and a collision between eastern part of Avalonia and Gondwana (Ordovician Orogeny; von Raumer, 1998, von Raumer et al., 2003; von Raumer & Stampfli, 2008). The collision and subsequent break-off of continental fragments along the Gondwana margin produced a complex terrane assemblage, which is further called the Hun super terrane (von Raumer et al., 2002; Frisch & Neubauer, 1989; Stampfli, 1996).

During Silurian times the opening of the Paleotethys occurred, combined with the subduction of the Rheic Ocean as well as the detachment of the Hun terrane from Gondwana (von Raumer et al., 2002). Simultaneously, terranes on the southern part of Laurussia rifted off (Hanseatic Terrane, von Raumer et al., 2013) in response to the Gondwana directed subduction of the Rheic Ocean and the connected opening of the Rheno-Hercynian Ocean during the Early Carboniferous (von Raumer et al., 2002; Stampfli et al., 2002). These Avalonia derived terranes collided with the Hun terrane during Late Carboniferous and lead therefore to the final closure of the Rheic Ocean (Stampfli et al., 2002). This collision is known as the eo-Variscian high pressure event (Stampfli et al., 2002).

Strike slip movements within the connected Hanseatic-Hun terrane occurred and are associated with the collision of the Hun terrane assemblage with Laurussia (Stampfli et al., 2002; von Raumer et al., 2013).

The last stage of the Variscian orogeny after this model is the final collision of Gondwana with Laurussia and the combined subduction of the Paleotethys and therefore the upbuilding of the Variscian mountain chain (Stampfli et al., 2002).

The piled up Variscan Orogen, visible eg. Bohemian Massif, started to break down again due to the thinning and magmatic activity between 340 and 310 Ma and the ongoing erosion lead to a planation of the orogen (Schuster & Stüwe, 2010). The oldest remnants of this event within the Eastern Alps are about 380 Ma old (Handler et al., 1997). The temperature peak of the metamorphism was around 340 Ma with medium pressure conditions, which was preceded by a low temperature, high pressure imprint of 350 Ma (Miller & Thöni, 1997; Schuster et al., 2013). In the Alps, the Greywackezone as well as the Carnic Alps and the Gurktaler Alps still show the sedimentary structures of the Palaeozoic deposits because they were located in a passive margin position from Silurian to Early Carboniferous times and show only minor overprint throughout the Alpine Orogeny (Schuster & Stüwe, 2010).

The Variscan orogeny was followed by deposition of Molassesediments in the Carboniferous), as well as by the Permian rifting, which is seen as the start of the Alpine tectonic evolution (Neubauer et al., 2000). The extensional event was caused through the dextral shear between the former continents Gondwana and Laurussia, which lead to E-W oriented rupture zones and a thinning of the lithosphere (Nebauer et al., 2000; Schuster & Stüwe, 2010).

10.3 Alpine Orogeny

The Alpine Realm experienced convergence and shortening between the Jurassic and the Lower Cretaceous through a convergence between the African, the Adriatic and the Eurasian Plate (Schuster et al., 2013). This lead to a first step of intra-oceanic subduction and accretion (Gawlick et al., 1999; Dallmeyer et al., 2008) followed by intracontinental subduction within the Austroalpine nappe system (Kurz & Fritz, 2003; Schuster, 2003). Subsequently, the Penninic Ocean was finally closed in the Eocene and the consequential continental collision lasts until recent (Schuster et al., 2013).

Thus, the Alpine Orogeny is grouped into two different stages: the eo-Alpine Event in the Jurassic/Early Cretaceous and the neo-Alpine Event in the Eocene (Schmid et al, 2004; Schuster et al, 2013). The eo-Alpine convergent event started in the Jurassic to Early Cretaceous, around 150-135 Ma, and is related to the final closure of the Meliata Ocean bay, with a formation of a deep sea trench and can only be recognised in lithologies of the Eastern Alps (Roßfeld basin; Neubauer et al., 2000; Schmid et al., 2004). This subduction led to emplacement of the Upper Juvavic nappes onto the later Apulian units at general nappe transport to NW and N (Neubauer et al., 2000; Handler et al, 1997; Ratschbacher, 1986; Ratschbacher & Neubauer, 1989; Handler, 1994). The subduction zone was filled with orogenic wedge sediments and trench-fill sediments (Schrambach & Roßfeld Fms.) now exposed in the UA nappes (Schuster et al., 2013).

Most of the Austroalpine nappes, the NW part of the Apulian plate, were set on the tectonical lower plate during this event, while the main part of the Adriatic plate, which represents now the Southalpine, was the upper plate (Handler et al., 1997; Schuster et al., 2013). Through the subduction and the consequent nappe stacking, the main part of the sedimentary cover was shaved off the basement (Schuster et al., 2013). During the Cretaceous, basement units were buried and faced up to eclogite facies conditions with the peak metamorphism around 92 Ma (Thöni, 2006; Schuster et al., 2013; Handler et al., 1997).

The following exhumation around 90 to 70 Ma lead to a medium pressure overprint and the eastern part exhumation was accompanied by NW thrusting and S to SE extensional tectonics (Hoinkes et al., 1999; Thöni, 1999; Schuster et al., 2013). Through the exhumation formed a metamorphic extrusion wedge with a lower inverted metamorphic field gradient part and an upper upright metamorphic field gradient (Schuster et al., 2013). Shortly after, from ca. 80 Ma onwards, the post-collisional Gosau Group sediments were deposited indicating cessation of the eo-Alpine collision in the Eastern Alps.

Due to a Rift stage from the Jurassic onwards the Penninic Ocean (Piemontais-Ligurian Ocean) opened (Fig. 4), while the southern part, the Valais basin, started opening in the Early Cretaceous (Neubauer et al., 2000). The Penninic Ocean was finally closed in the Eocene through subduction, which lead to the collision between the European continent and the Apulian plate from the Paleogene onwards. The Austroalpine units occupied an upper plate position while the European continental lithosphere and the Penninic domains experienced an high-pressure metamorphism (45 Ma; Schmid et al., 2013; Schuster et al., 2013; Neubauer et al., 2000). The final collision was driven mainly by the indentation of the Adriatic microplate into the alpine nappes (Neubauer et al., 2000).

This neo-Alpine Event formed the Penninic, the Subpenninic and the Helvetic nappes in the West and a high-pressure and low-temperature metamorphism in the Penninic and Subpenninic nappes of the Eastern Alps around 40 Ma (Schuster et al., 2013). This was followed by a Miocene E-W extension with accompanying exhumation and the formation of the Tauern Window, where the Penninic and Subpenninic nappes can be found in tectonic windows (Schuster et al., 2013). This exhumation and lateral extrusion to the E due to the WNW directed indentation of the Adriatic intender, lead to normal and dextral strike slip faults, which formed the morphology of the recent Alps, e.g. the exhumation of Saualpe-Koralpe complex or development of the Styrian basin (Neubauer et al., 2000; Schmid et al., 2004; Schuster et al., 2013). The major strike slip faults are known as the PAL or the SEMP (Salzach – Ennstal – Mariazell – Puchberg; Schuster et al., 2013).

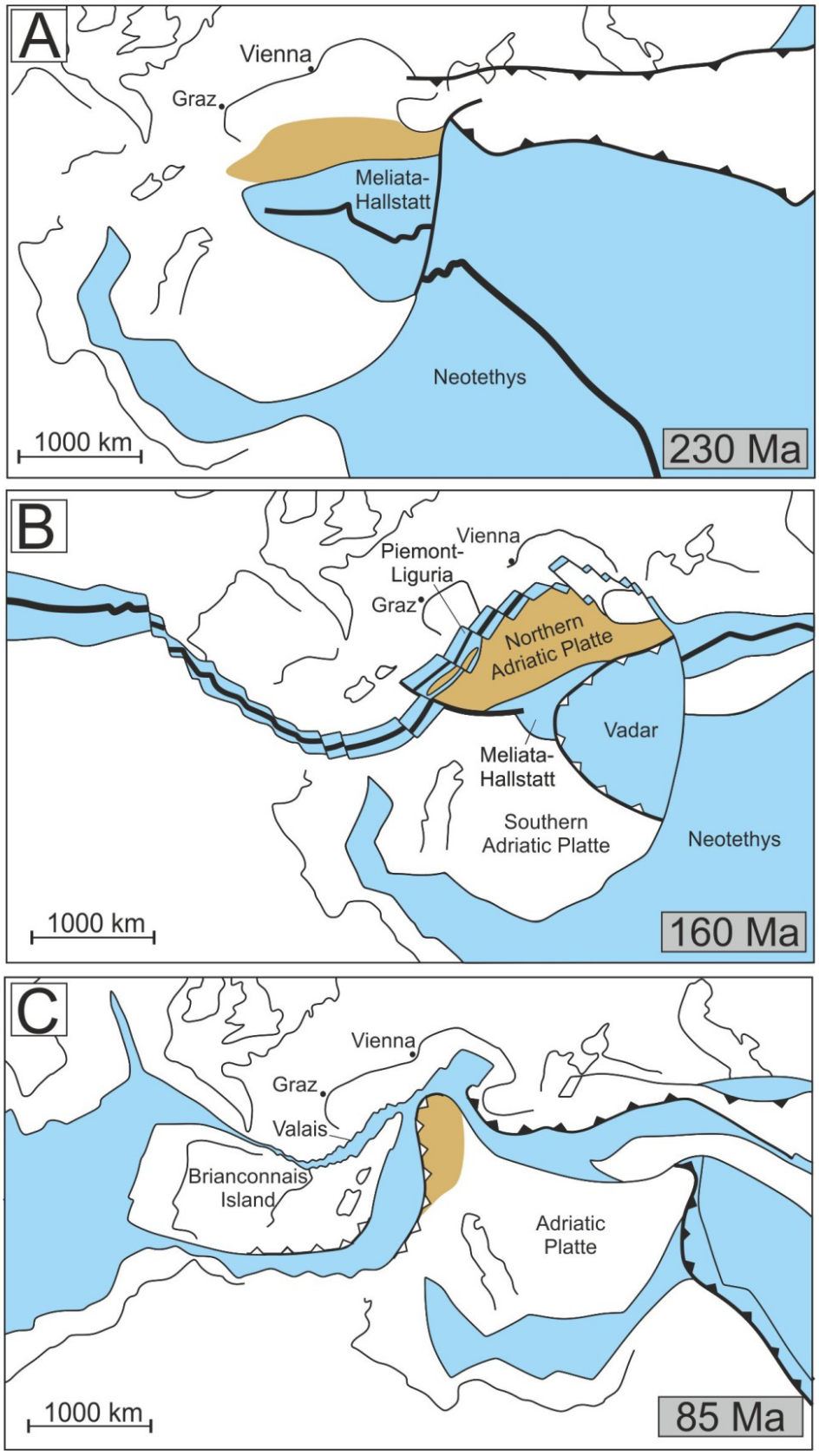

Fig. 4: Paleogeographic overview of the eo-Alpine orogeny, with the opening of the oceanic arms and the closure of Meliata-Hallstatt (after Schmid et al., 2004).

10.4 Eastern Greywacke Zone

The Eastern Greywacke Zone is known to be a unit containing a Palaeozoic basement with Permomesozoic cover elements as parts of the Northern Calcareous Alps (further referred to as NCA) and is supposed to be a complex of individual thrust sheets (Neubauer et al., 1994).

Neubauer et al., 1994 divided the Greywacke Zone into four distinct nappes (Fig. 5):

- The Veitsch Nappe
- The Silbersberg Nappe
- The Kaintaleck Nappe
- The Noric Nappe

The units of the Greywacke zone underwent a lower Greenschist facies metamorphism in the Cretaceous, which was preceded by Paleozoic sedimentary, magmatic and metamorphic events (Neubauer et al., 2002). The Palaeozoic sedimentary sequences of the Greywacke are overlien by Permian to Mesozoic strata of the Tirolic nappes of the NCA (Neubauer et al., 1994).

Schuster 2015 divides the Eastern Greywacke Zone just in three nappes, the Veitsch, the Silbersberg and the Noric-Tirolic nappe and introduces the nape “Greywacke Zone Nappe System”. In this interpretation the Silbersberg Nappe is interpreted as sedimentary cover of the Kaintaleck Complex composed of high-grade metamorphosed rocks (Schuster, 2015).
Individual nappes are separated by shear zones which are interpreted to possess a polyphase development, beginning in the Cretaceous until the Neogene (Schuster, 2015). The Tirolic-Noric Nappe system on top contains Paleozoic rocks, Ordovician to Carboniferous metasediments and metavolcanics. Above those metasediments follows the Präbichl Fm and the Werfener schist, which grades into the Triassic layers of the Tirolic nappes in the NCA.

10.4.1 *Veitsch Nappe*

The lowest nappe of the Greywacke Zone exposed along the southern part of the Greywacke Zone, is the Veitsch Nappe, which was divided by Ratschbacher (1987) into three formations. These are the Steilbachgraben Formation, the Triebenstein Formation and the Sunk Formation, while Neubauer & Vozarová (1990) added another formation, the Graschnitz Formation. Whereas the Steilbachgraben Fm consists of clastics and in fewer portions carbonate, the Triebenstein Fm contains carbonates and some greenschists. The composition of the Sunk Fm is to be described as quartz conglomerates, although there are also graphite deposits present (Neubauer et al., 1994). The Sunk Fm further seems to grade into the Graschnitz Fm, which can

only be found near Frauenberg east of Bruck/Mur. The Graschnitz Fm is characterised by phyllites but also brownish to reddish sandstones and quartz breccias which are mostly intercalated within phyllites (Neubauer & Vozarová, 1990).

Overall, the formations can be seen as post eo-Variscan shelf to molasse-type sequence with an Early Carboniferous to Permian age (Neubauer et al. 2002; Handler et al. 1997). These molasse type sediments are interpreted by Handler et al. 1997 to be deposited in a transtensional basin setting which was elongated. On the southern border of the Veitsch Nappe Miocene faults can be frequently found, which seem to have a steep inclination and are the contact to the Silvretta Seckau Nappe System. In this study are this nappe system is represented by the Troiseck-Floning Complex, which contains Paragneiss and Amphibolites (Schuster, 2015; Nievoll, 2015). Additionally magnesites can be found in lenses throughout the Veitsch Nappe (Nievoll, 1984).

Detrital white mica of the Carboniferous molasses-type rocks of the Veitsch Nappe were dated as 310.5 +- 1.2 Ma with the 40Ar/39 Ar – method (Handler et al., 1997).

10.4.2 ***Silbersberg Nappe***

The Silbersberg Nappe, which is lying on top of the Veitsch Nappe, is made up of quartzphyllites, carbonate-chlorite schists, the Riebeckite gneiss and Silbersberg conglomerate. The carbonate–chlorite schists, as well as the quartzphyllites, are mainly found in the base of the nappe (Neubauer et al., 1994). The Riebeckite gneiss of this nappe has a mylonitic fabric and suggests through its geochemical signature to have an protolith of highly fractionated volcanic origin (Paulus, 1991). This gneiss is not well dated, scattered ages point to a Jurassic age(Schuster, 2015).

The main rock type of the Silbersberg Nappe, the quartzphyllite, often possesses intercalated layers of acidic tuff and quartz breccias, and is considered of Early Palaeozoic age (Neubauer et al., 1994; Neubauer et al., 2002). Nowadays, most of the sedimentary sequences of this nappe, namely the Silbersberg conglomerate is considered a Permian sediment. Detrital white mica of these conglomerates showed ages of 359.6 ± 1.1 Ma (Neubauer et al., 2002; Handler et al., 1997).

10.4.3 ***Kaintaleck Nappe***

The Kaintaleck Nappe is often called “Kaintaleck slices” or “Kaintaleck Complex” and is to be found along a thrust within the Greywacke Zone and cannot be found as a continuous nappe (Neubauer et al., 1994). The sequence itself is subdivided into three complexes, which was

mainly conducted through Neubauer und Frisch (1993): the Ritting complex, the Frauenberg complex and the Prieselbauer complex.

The Ritting complex, whose protolith age is arguable, contains amphibolites (with garnet and zoisite), serpentinites, micaschists and marble, which is mostly thin-layered (Neubauer et al., 1994).

The Frauenberg complex is composed of amphibolite (with plagioclase), marble lenses and a great amount of paragneiss (Neubauer et al., 1994). Due to an U-Pb analysis of zircons, there are data for a upper intercept age of 2,53 Ga as the protolith age, and a lower intercept age of 516 Ma which is interpreted as a Late Cadomian metamorphism (Neubauer et al., 1989)

The Prieselbauer complex consists of migmatic augen paragneiss and micaschist, but also amphibolites as well as aplites occur (Neubauer et al., 1994).

Two of the complexes, namely the Frauenberg and the Ritting, are further covered in a transgressive way by gneiss conglomerates, which seem to be equivalent to the Kalwang Conglomerate. The orthogneiss fragments, which can be found in the conglomerate, are from their geochemical signature acidic plutonic rocks that were formed in a supra-subduction zone environment (Neubauer et al., 1994).

Ductile shear zones split the Kaintaleck slices from other nearby units and are also found within the nappe itself which forms “pseudoconglomerates”, which contain boudins of lithologies of a higher competence in a mica-rich matrix (Neubauer et al., 1994). Ar ages of white mica gave an age of 360 to 380 Ma (Devonian)is interpreted as cooling below 400°C (Handler et al. 1999; Schmidt 1999; Schuster et al. 2001).

10.4.4 ***Noric Nappe***

The sedimentary and magmatic rocks of the Noric Nappe can be divided into three groups. The Ordovician to Early Silurian succession includes acidic volcanoclastic rocks and shists, from the Silurian to Devonian shelf sediments of a passive continental margin developed, that are overlain by Permian conglomerate and siltstones (Neubauer et al. 2002, Neubauer et al. 1994).

More specifically, the Gerichtsgraben Fm. builts the base of the Paleozoic sedimentary sequnece and is composed of sericitic phyllites, with an arkosic part, containing greenstone layers as well as metasandstones, quartzites and acidic tuffs (Schönlaub 1982; Nievoll und Suttner 2015).

The Ordovician Blasseneck Porphyroid on top of the Gerichtsgraben Fm., which originated from ignimbrite is widespread in the Eastern Greywacke Zone (Nievoll und Suttner 2015). It is followed by the Upper Ordovician Polsterquartzite and "Cystoideen-Limestone". The Polster quartzite is characterised through "Metaquartzwacken" with large monocrystalline quartz grains (Nievoll und Suttner 2015).

The Silurian succession starts with the Rad Phyllites or Rad Fm., which consists of slates and phyllites containing acidic tuff layers, greywackes and lydites (Nievoll 1987; Nievoll und Suttner 2015). These phyllites are followed by Devonian limestones and shaly limestones (Nievoll, 1987). The Stocker Fm, that occurs in the eastern part of the Eastern Greywackezone is seen as probably time equivalent of the Rad Fm. and consists of Metavolcanites and quartzites (Nievoll und Suttner 2015).

Above the Rad Phyllites and the Stocker Fm lie variable carbonate rocks that have been given different names in different areas (eg. the Fe-ore bearing Sauberg limestone). The Permian Präbichl Fm and the Triassic Werfener Fm are partly in transgressive contact to the limestones (e.g. at location Leobner Hütte – Polster), in other places they are in tectonic contact above different Paleozoic formation (e.g. in the study area). The succession is characterised through their metasandstones (Schuster, 2015). The Präbichl Fm contains quartz conglomerate and coarse sandstones, which represent former distal alluvial fan deposits (Nievoll, 2015; Handler et al., 1997).

The Noric Nappe and its sedimentary record leads to an interpretation of an extensional geodynamic environment where the continental crust was continuously subsided from the Ordovician until the Early Carboniferous (Neubauer et al., 2002).

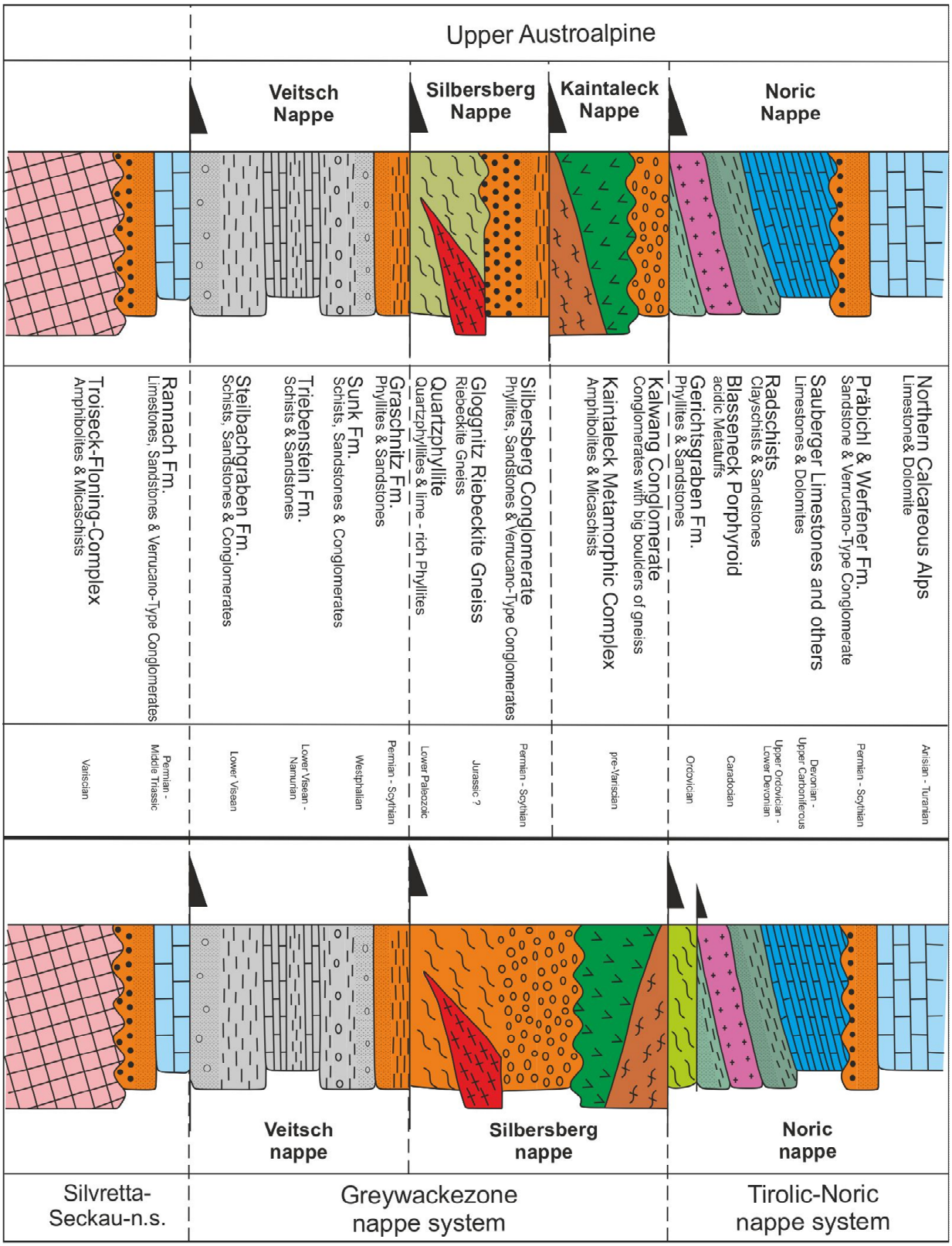

Fig. 5: Tectonostratigraphic succession with lithologies of the Greywacke Zone, in two versions. Left Neubauer et al. (1994), right Schuster (2015)

11 Geological map

A geological map of the area around Preiner Gscheid was produced, which includes most of the nappes of the Greywackezone.

From the bottom to the top in this map those are (Fig. 6, Fig. 7):

- Veitsch Nappe
- Silbersberg Nappe
- Noric-Tirolic Nappe

The Kaintaleck Nappe or any high-grade metamorphosed rocks that may be part of this nappe were not found in the study area.

To the south of the tectonic footwall boundary of the Veitsch Nappe, two units occur that were not included into the mapping project. These are the “Tattermann Schuppe” and the Troiseck-Floning Complex. The “Tattermann Schuppe” is of historical importance as, according to Tollmann (1977), these sericite schists were considered part of a small sliver of “Mittelostalpin” which lies tectonically above the “Unterostalpin” of the Semmering System (Tollmann, 1964). Recently the Troiseck-Floning Complex is considered part of the Upper Austroalpine Silvretta-Seckau System (Schuster, 2015), and was formerly the Middle Austroalpine (Tollmann, 1977). The Troiseck-Floning Complex consists mainly of gneisses. The Permian Semmering quartzite, the sedimentary cover of the Troiseck-Floning Complex, will be later discussed as one of the geochronological samples of this thesis (see chapter 15).

In the study area the Veitsch Nappe consists of graphitic schists, sandstones and, in basal parts, metaconglomerates. Variable lithologies occur throughout the Silbersberg Nappe, including phyllites, metaconglomerates, greenschists and Riebeckite gneisses. It appears that the lithological succession is duplicated, possible due to duplex structures within the Silbersberg Nappe. The base of the Noric Nappe is represented by the Blasseneck Porphyroid. The thrust disconformly cuts through individual lithologies of the Silbersberg Nappe.

The foliation of the lithologies as well as thrust surfaces dip overall to NW or N, with an average angle of about 40°.

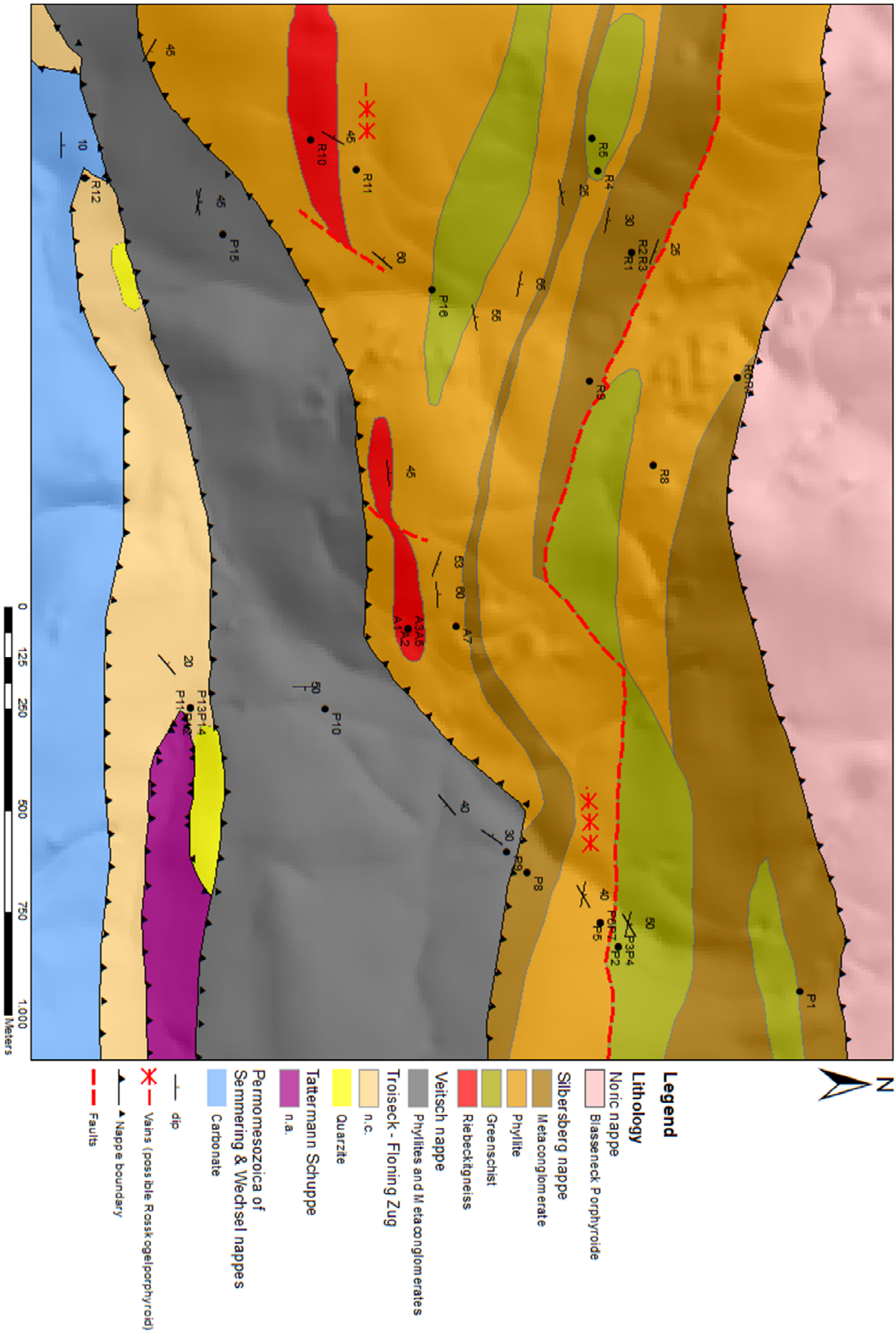

Fig. 6: Mapping area close to Preiner Gscheid. It depicts the different lithologies as well as the dips and samples.

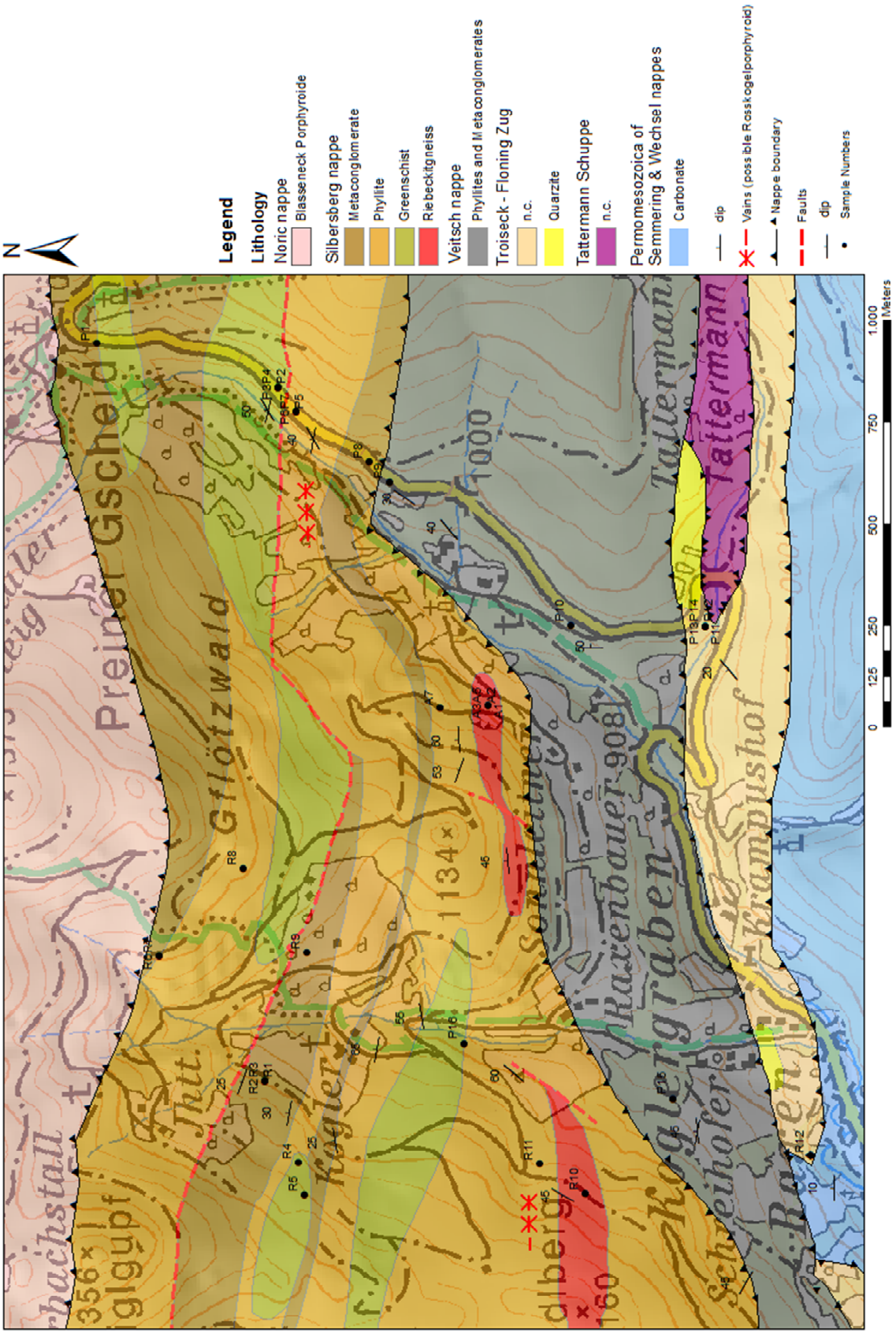

Fig. 7: Picture of the mapping area near to Preiner Gscheid. It shows the different lithologies, the dips as well as the sample numbers. The background of the map is given for orientation (Digitaler Atlas Steiermark).

12 Thin section description

This first part of the thin section description is dedicated to the rocks and lithologies of the mapping area between “Brandlberg” and “Preiner Gscheid” in Styria. The following lithologies can be categorised into the nappes of Silbersberg and Veitsch of the Greywackezone, the “Troiseck-Floning-Zug” and the “Tattermann Schuppe”.

The description of these thin sections follows the systematics given in the book “Microtectonics”(Passchier und Trouw 2005).

12.1 The Silbersberg Nappe

Within the Silbersberg Nappe different lithologies, such as metaconglomerates, phyllites and Greenschists occur. These rocks are characterised mostly by sericitic mica and numerous quartz components. An unusual feature in these siliciclastic dominated rocks is the Riebeckite gneiss.

12.1.1 ***Metaconlgomerates***

The metaconglomerates of the Silbersberg Nappe have a distinct mineral association. The most common components are quartz grains or lesser common plagioclase grains. Those grains are found in an augen texture, with components and a matrix which seems to flow around those grains. The foliation of this lithology is well developed which assists the wavy and augen texture like appearance (Fig. 8*, A & B*).

The matrix of these metaconglomerates can be described as a fine grained mixture of sericitic white mica, chlorite and another, smaller, quartz generation.

Additional components of the rocks are Fe-oxides which form brown streaks throughout the thin sections and are often accompanied by opaque ore kernels (Fig. 8*, E & F*). As accessories, zircons, rutile, titanite as well as tourmaline can be found. Some of the metaconglomerate probes also show lithic components which are composed of mainly quartzite. Further feldspar and chlorite can be seen.

The component feldspar of the metaconglomerates possesses growth twinning and seems to be mostly undeformed and monocrystalline, similar to the component quartz of this lithology. Although the main parts of the components show this undeformed behaviour, it is to be said, that some components are broken and even exhibit some stretching marks.

Sericite not only occurs as part of the matrix but also as the product of sericitisation of plagioclase in most of the thin sections.

The very common chlorite of the metaconglomerates could be originated from former biotite or even hornblendes.

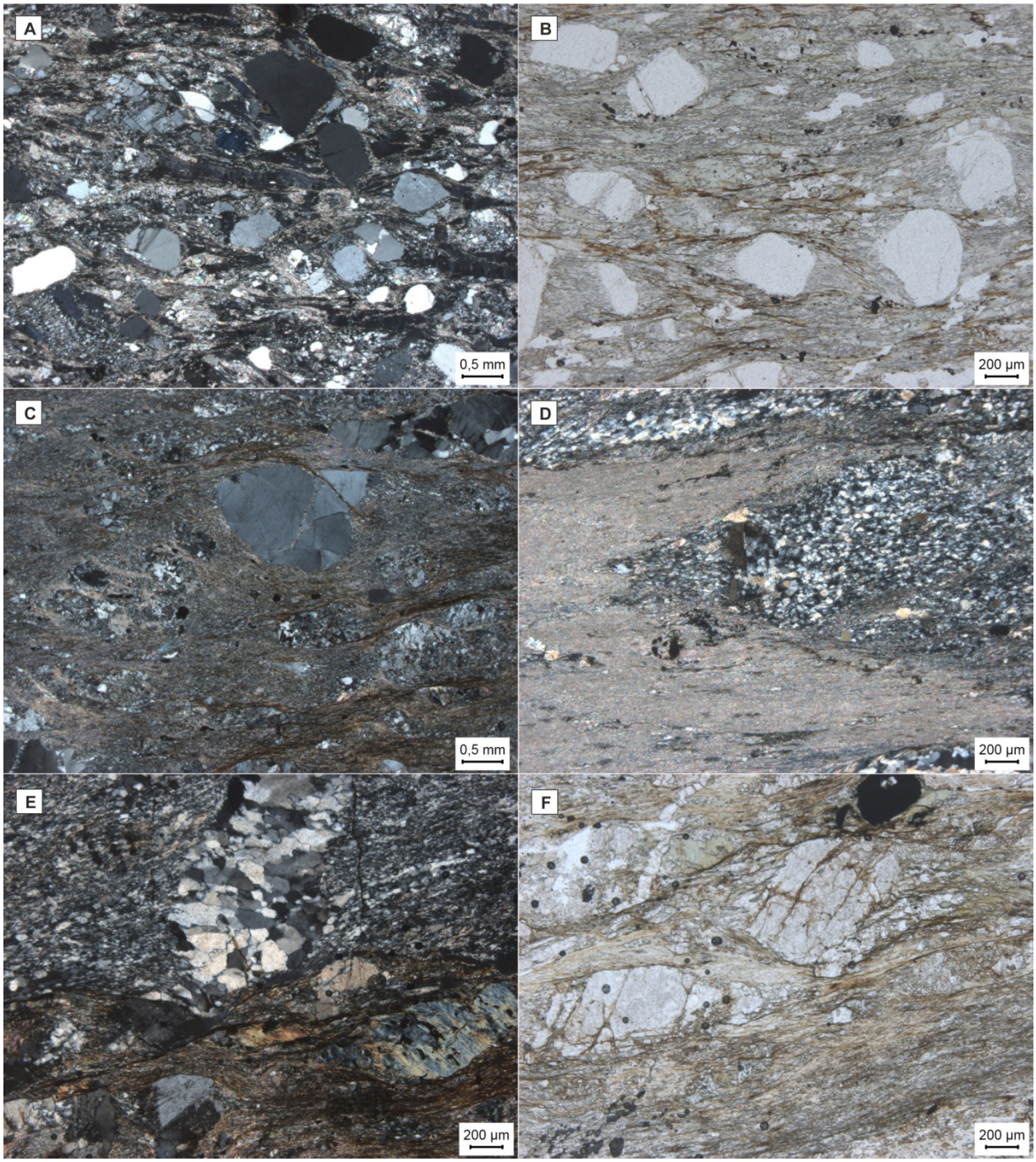

Fig. 8: Thin sections of various samples of the metaconglomerate lithology. Picture A (with crossed polarizer) and B (without crossed polarizer) depict the typical augen-like texture of this lithology with components of mostly quartz grains. C is a close up of those component grains within the matrix. Picture D shows the fine sericitic felt and the finer grained quartz grains of the matrix. Photos E and F exhibit the matrix as well as components, but also show the retrograde chlorites of this lithology as components as well as in the matrix. The strain shadows of chlorite and quartz can also be seen in the pictures E and F. The occurring ores of metaconglomerates are shown throughout the pictures of this figure.

Textures & Structures

Quartzes of the metaconglomerates from the Silbersberg Nappe are characterised by subgrain rotation (SGR; Passchier und Trouw 2005) up to grain boundary migration (GBM, Passchier und Trouw 2005). Also, some larger grains that escaped from intense deformation still show undulose extinction (Fig. 8*, D*).

SGR is characterised through dislocations that concentrate along grain boundaries. New grain boundaries are formed that typically have small angles between crystal crystallographic axes. At increasing temperatures free climbing dislocations develop, which climb up the lattice planes. Therefore, the angle between the lattices of the subgrains increases with temperature and creates as such a new, smaller grain. The initial grain shows some ductile and elongating deformation, while new round subgrains are resulting (Passchier und Trouw 2005). This often leads to core-and-mantle structures, where an old grain stays intact in the core, while the subgrains are developing all around the older grain, which is called the mantle (Passchier und Trouw 2005). This process is a hint for beginning grain boundary migration.

GBM is attributed to higher temperatures as SGR and is known to be an increase in the grain boundary mobility of the former generated subgrains. As soon as subgrain boundaries are formed there is an increase in the mobility of them. With a variable grain size, but mostly larger than the former subgrains and a lobate shape, they can be differentiated from SGR (Passchier und Trouw 2005).

The quartz rich layers of the metaconglomerates show both SGR and GMB but also, in finer grained rocks, pressure solution occurs. The wide range of deformation mechanisms points to a larger temperature interval between 300°C and 500°C. Deformation increments developed at decreasing temperatures, most probably during exhumation. Greenschist facies deformation is also evident from appearance of chlorite and solution-precipitation processes are dominant in fine grained layers producing sericite strain caps.

Typical microstructures that can be found in the metaconglomerate are small normal faults and shear bands. These shear bands can be partly identified as C’ type shear bands. C’ type shear bands are known to be inclined to the shear zone boundary as well as to the former foliation of the deformed rocks (Passchier und Trouw 2005). Quartzes as well as chlorites are found in strain shadows and, additionally, whole strain caps of chlorite are present (Fig. 8*, F*).

The main deformation, however, seems to be characterised by pressure solution. Pressure solution originates due to a high stress on particular grains which do have, along their contact, a high angle to the direction of instantaneous shortening (Passchier und Trouw 2005). This results into dissolution of grain parts on these high stress points and the repeated deposition of those parts. Further all the structures do have a highly asymmetric appearance. Sense of shear derived from microstructures is dominantly top N to top W.

12.1.2 ***Greenschists***

The greenschists of the Silbersberg Nappe are dominated by fine grained chlorite and quartz, and frequently very large epidote minerals. White mica and plagioclase can rarely be found (Fig. 9). Further carbonate occurs often in veins and is interpreted as a late phase.

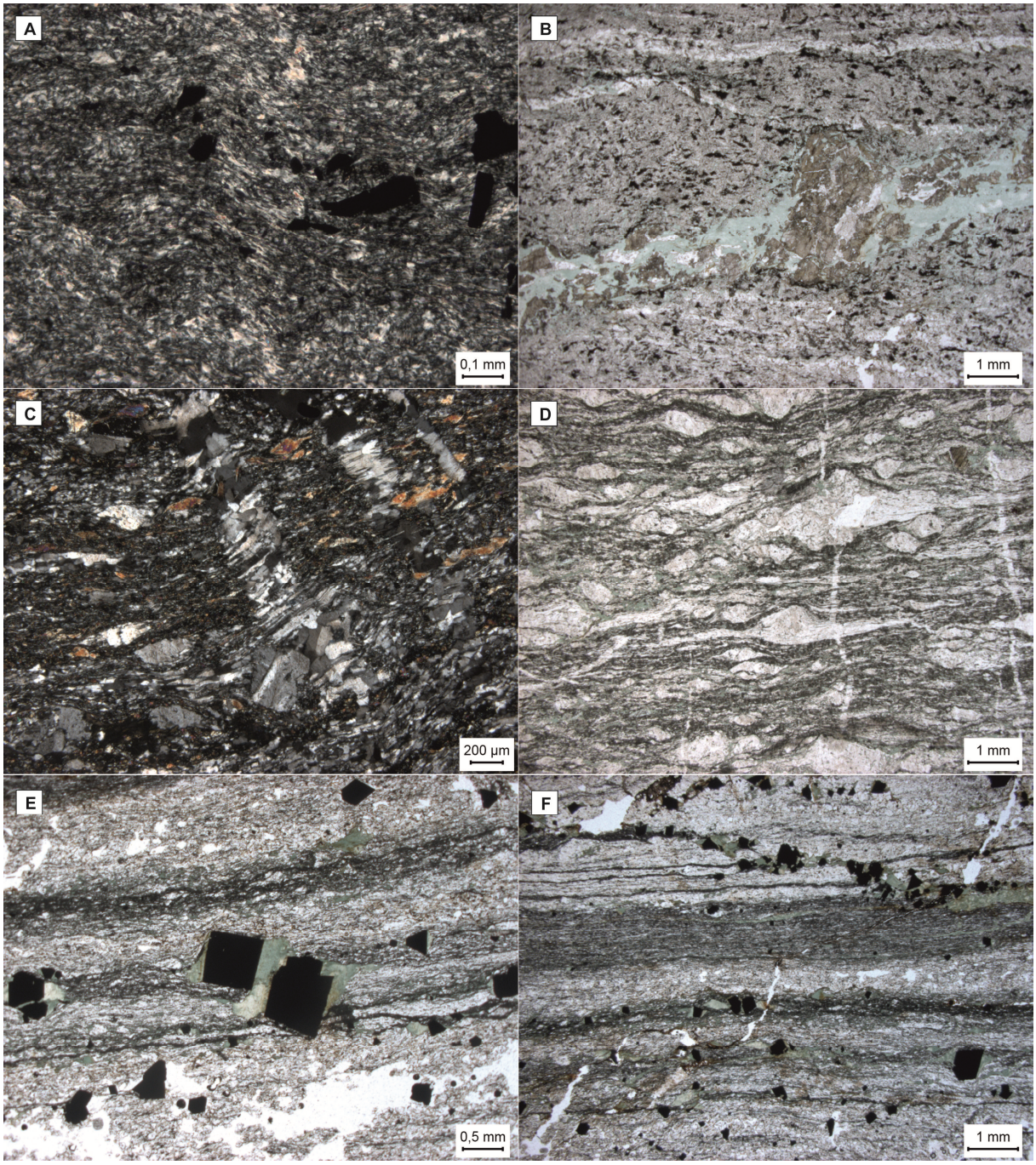

Fig. 9: This figure shows the composition and structure of the Greenschist lithology of the Silbersberg Nappe. Picture A to F all exhibit the main mineral compositions (see text). Picture B notable shows the remnants of epidote surrounded by chlorite in the epidote and chlorite abundant layer of sample P16. C and D, depict the small structural elements like normal faults and shear bands throughout the thin sections, while A shows a slight crenulation foliation too.

Similar to most lithologies of the Greywackezone Fe-minerals can also be found in the thin sections, like euhedral pyrites with chlorite as strain shadows (Fig. 9*, E & F*). The chlorite of the greenschist can also be seen as a secondary, retrograde, formation.

A special feature of the greenschist thin sections are the numerous epidotes, which sometimes seem to be stretched. Those epidotes can be seen as a metamorphic growth or remnants of crystal tuff. As an example for these epidotes, sample P16 shows two distinct layers in the thin section. There is a brighter, feldspar and quartz rich layer and a darker, chlorite and epidote abundant one (Fig. 9*, B*). The sample R3 does have another special feature, as hornblendes can still be found as relicts.

The possible protolith of some of these greenschists may be metatuff, as there are specific fuzzy textures and a fine grained fabric.

Overall, there is a clear foliation, frequently mylonitic, in these rocks and an inequigranular grain distribution. The fine grained matrix mostly contains quartz and chlorite, which seems to flow around bigger feldspars and quartz components as well as epidotes.
Fractures filled with quartz and feldspar can also be found.

Textures & Structures

The quartz rich layers of this lithology seems to be deformed by SGR and GBM, while the bigger quartz layers mostly show SGR and the smaller matrix grains GBM. This leads to the assumption that the last deformation of this rocks was in greenschist facies with a temperature area of 350°C till 500°C.
Furthermore, typical core-and-mantle structures are also to be found.

Notable structures of the greenschist are mostly shear bands, which leads to a wavy appearance. Further, stretched crystals in veins occur which do have an oblique orientation to the foliation, and small normal faults, can be found (Fig. 9*, A, C &D*). One of the greenschist samples, namely P2, shows a crenulation foliation.

12.1.3 ***Phyllites***

The fine grained phyllites of the Silbersberg Nappe are typically abundant in sericitic white mica, which builds up the flowing texture around more competent grains like quartz and the rare feldspar (Fig. 10). Accordingly, some of the phyllites possess a distinct foliation which is pierced in different positions by veins filled with carbonate (Fig. 10*, A & D*). Others do not have an obvious penetrative structure, because of the finely granulated fabric.
Further minerals are chlorite, which is located next to the white mica in the flow textures, tourmaline and titanite. Ores and Fe-oxides, shown as brown streaks, are also common in the phyllites, as well as the accessory mineral zircon.

Some samples, for example P3, do have alternating layers of mica-rich, mica-scare and carbonate-rich parts, although the carbonates are found as bigger vein minerals too. It is noteworthy that the sample P3 shows some detritic white mica, which is scarce in the Silbersberg Nappe (Fig. 10*, C*).
The feldspars of this nappe often exhibit sericitisation and growth twinning.

Textures & Structures

The phyllitic quartzes of the Silbersberg Nappe are mainly characterised by SGR. This leads to possible temperatures of around 400°C.

Strain caps, as well as shear band cleavage (c-type) and isolated low angle shear bands are noteworthy structures of the phyllites (Fig. 10*, B & F*). The carbonate veins can be seen as the latest deformation in the brittle field (Fig. 10*, A & E*). Further structures are kink bands, which were induced through coaxial shear bands.
Again the main deformation process can be identified as pressure solution.

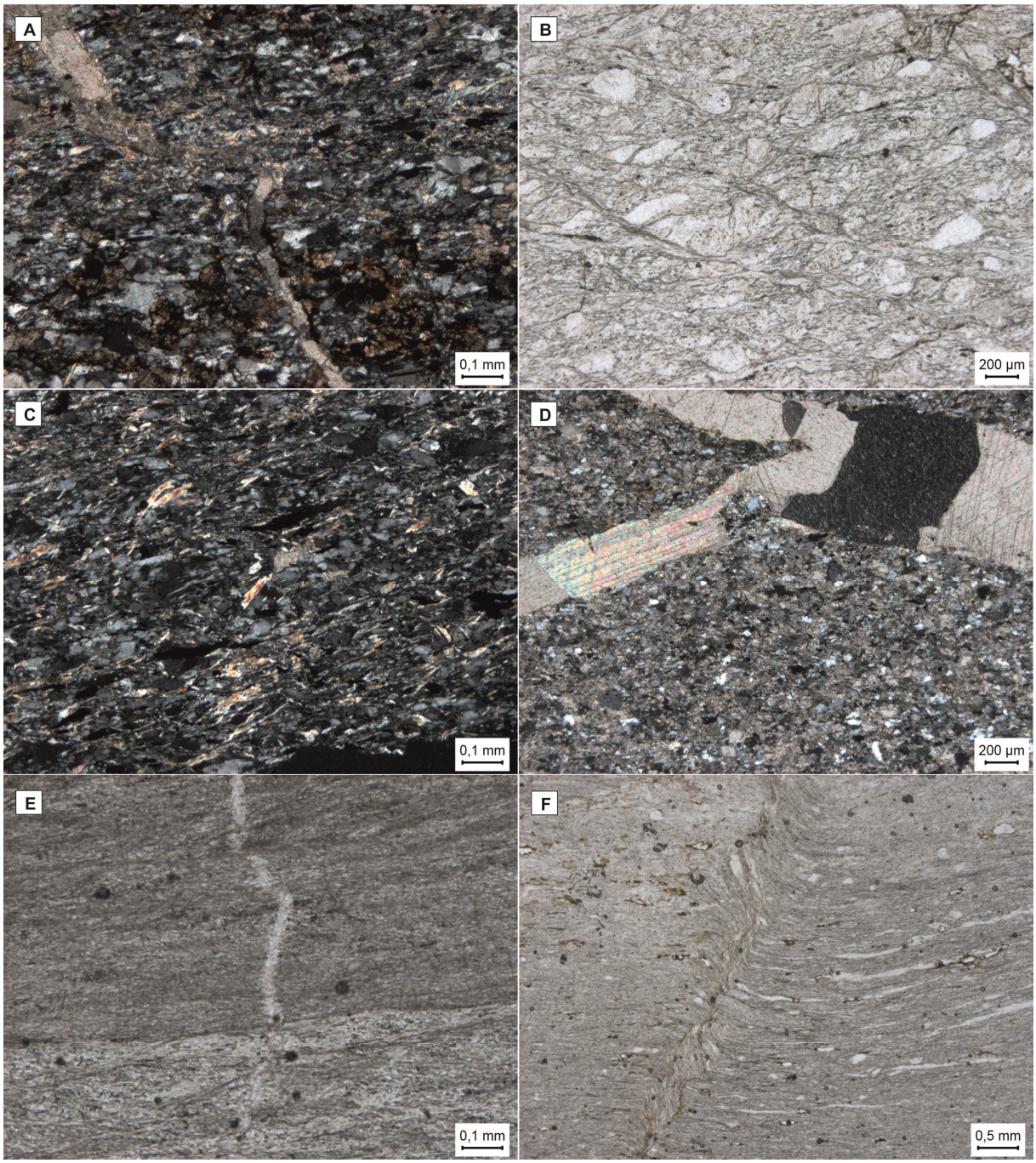

Fig. 10: This figure depicts the mineral composition and textures of the phyllites of the Silbersberg Nappe. All the pictures exhibit the typical mineralogical main composition of sericite, quartz and chlorite. Further, B also shows the shear bands and the "wavy" appearance of this rock type. Picture C depicts the few bigger mica grains, which can be interpreted as detritic mica parts, which are uncommon in the Silbersberg Nappe. A, D as well as E represent the typical veins of carbonate which penetrate the phyllites and are deformed in a later state. F shows a kink band which is part of coaxial shear bands.

12.1.4 ***Riebeckite gneiss***

The Riebeckite gneiss of the Silbersberg Nappe is a speciality in itself. The Riebeckite gneiss can be interpreted as a magmatic effusive rock, although it has a metamorphic overprint (Fig. 11*;* Paulus, 1991).

Due to grain size, degree of deformation and metamorphic overprint it is possible to distinguish different types within the Riebeckite gneiss. On the one hand, there are the finer grained samples which mostly exhibit the original magmatic textures. The bigger Riebeckite-porphyroclasts of these samples show the minerals characteristic of deep blue to light greenish colour, although they have already started to degrade (Fig. 11*, C*). Smaller streaks of these Riebeckites, with a lighter blue appearance can also be found and are an indication that even those more magmatic Riebeckite gneisses did see a metamorphic overprint of some degree.

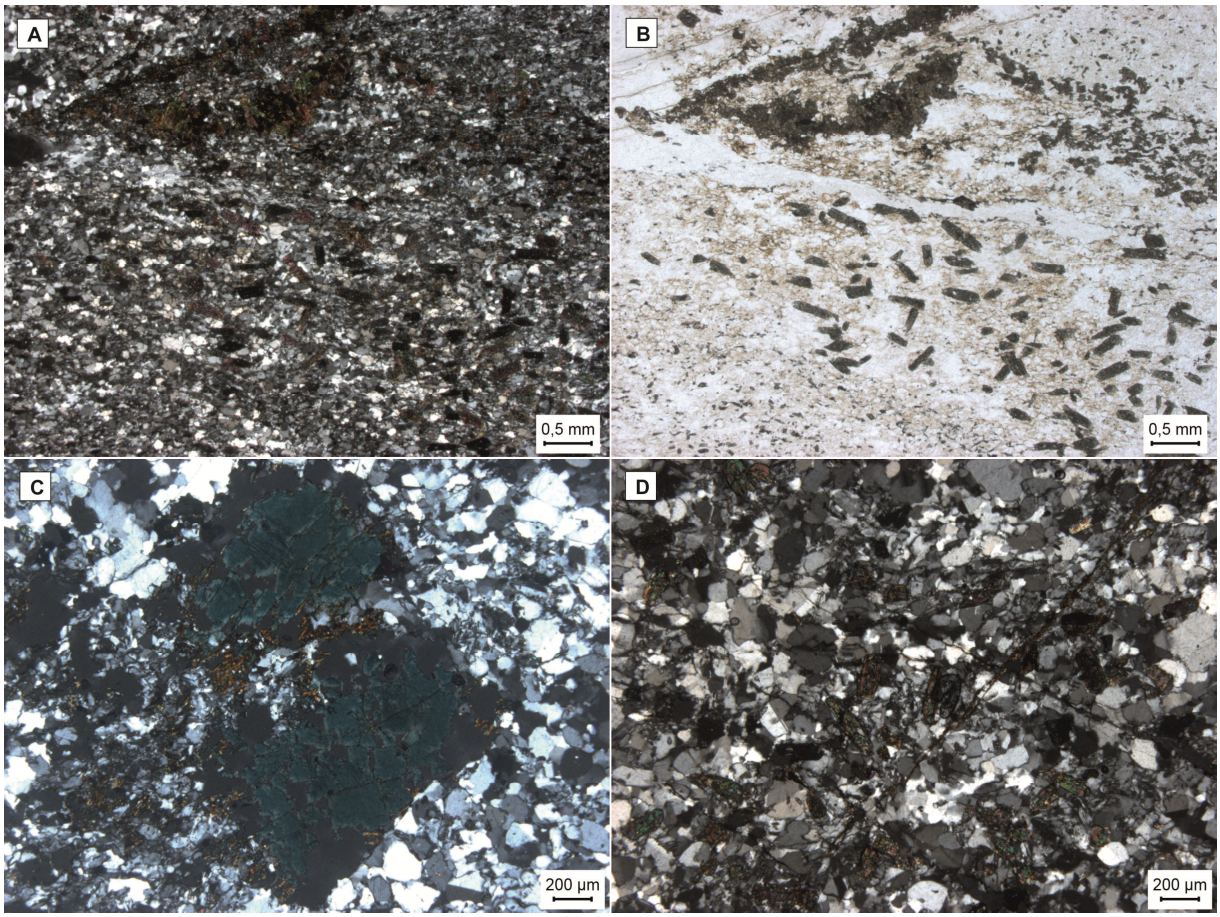

Fig. 11: Parts A to D of this figure represent the Riebeckite gneiss of the Silbersberg Nappe. A (with crossed polarizer) and B (without crossed polarizer) show the smaller Riebeckites in the finer grained matrix, which are parts of the more foliated Riebeckite gneiss type. C depicts the big, already degrading Riebeckite of the less foliated rock type. Picture D exhibits the ore-filled cracks, which are to be found throughout the Riebeckite gneisses.

On the other hand, there are samples with distinct foliation, where the smaller, secondary Riebeckites are adjusted along the cleavage (Fig. 11*, A & B*). These more foliated samples are from a distinct area, which could hint at a localised shear zone, as some even appear to have mylonitic foliation. The existence of localised shear zone is also confirmed through an outcrop, which presents mylonitic and cataclastic rocks and more sheared Riebeckite gneisses. Another mineral that can be found in those more deformed samples are retrograde epidotes.

Riebeckites are alkali-amphiboles and occur preferential in quartz-containing rocks (Paulus 1991). Further are the Fe-richer, Al-scarce end members of the alkali-amphiboles like Riebeckite known to form in magmatic rocks (Paulus 1991).

Abundant minerals in the Riebeckite gneisses are also quartz and feldspar, often as plagioclase strips. Further components of the samples are the accessories Apatite and Fe-oxides.
Throughout the thin sections cracks can be found, which are mainly filled with quartz.

Textures & Structures

Again it is necessary to differentiate between the more sheared and the original, magmatic fabric Riebeckite gneisses. The un-sheared samples show mainly none to low-grade dynamic recrystallization like bulging (BLG, Passchier und Trouw 2005). BLG is interpreted as a mobility of the grain boundaries at rather low temperatures, where the boundary of one grain bulges into the neighbouring crystal, which possesses a higher dislocation density (Passchier und Trouw 2005).
The samples which underwent some kind of metamorphic overprint exhibit mostly SGR to beginning GBM.
This leads to a temperature range of 300°C to 450°C for the deformed samples and about 300°C for those nearly without metamorphic influence.

Furthermore, some brittle faults, which seem to be the last part of any deformation, can be found and were filled with Fe-oxides (Fig. 11*, D*).

12.1.5 ***Veins***

Within the Silbersberg Nappe of the Greywackezone occur veins with apparent magmatic rocks, mainly next to the Riebeckitgneiss. These vein rocks have similar appearance to fault breccia and are characterised through a high amount of plagioclase. This plagioclase is mostly aggregated as chaotic strips (Fig. 12*, C & D*).

Besides the plagioclase, there are also minerals like quartz, chlorite, carbonate and sericite, which are present in nearly all of the other lithologies in the Silbersberg Nappe too. The common cracks in these veins are also filled with carbonate. These veins were deformed afterwards and now show variable amount of displacement (Fig. 12*, A & B*).

Although the whole fabric of the rocks does not hint at mylonitic texture, there are some components like the carbonates which seem to possess a wavy appearance.

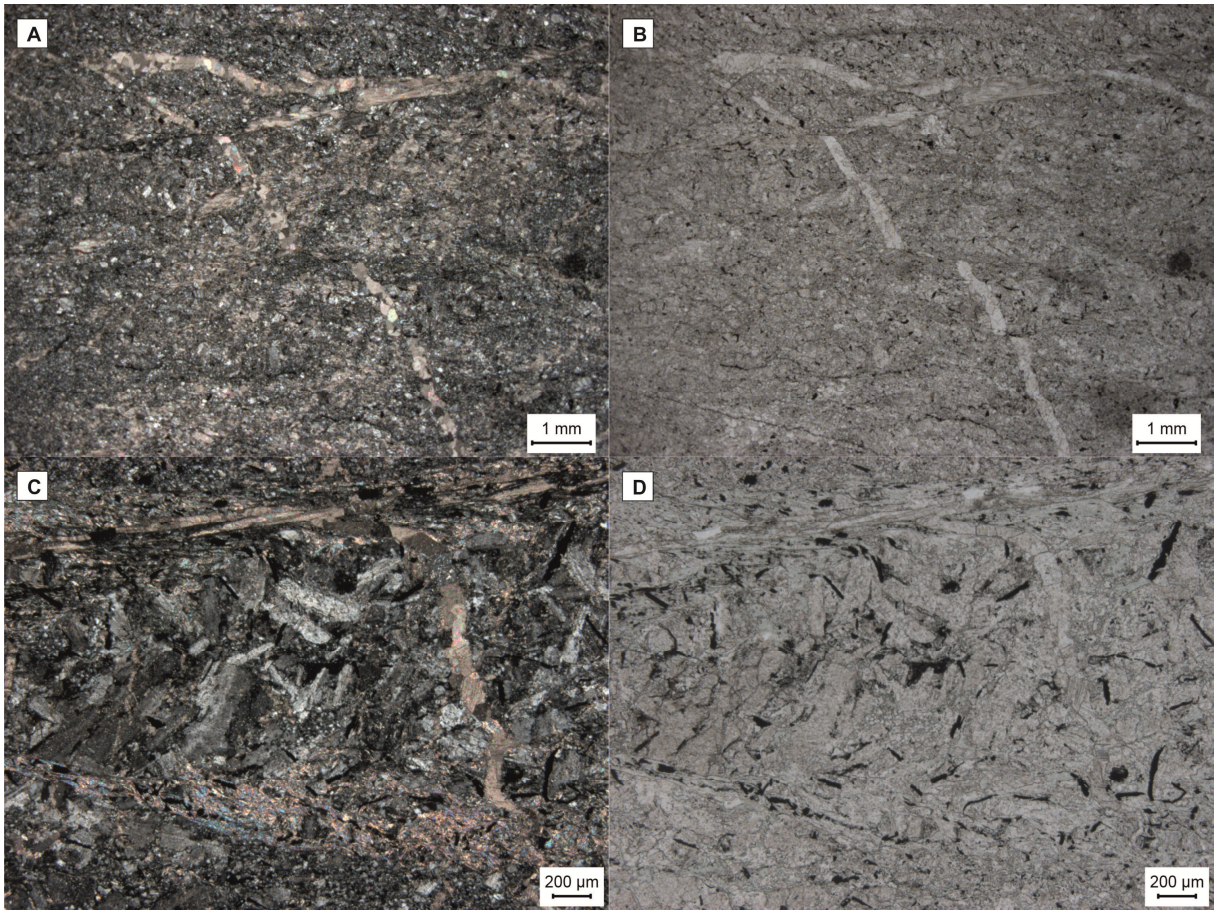

Fig. 12: Picture A (crossed polarizers) and B (without crossed polarizers) show the typical carbonate veins within this bigger vein complex, which possess a clearly visible displacement. Parts C (crossed polarizers) and D (without crossed polarizers) depict the notable chaotic strips of plagioclase.

12.1.6 *Porphyritic Metatuff*

Another peculiarity of the Silbersberg Nappe is the porphyritic tuff which was found on the location Brandlberg (see chapter 11).

This metatuff contains lots of feldspar components which are located in a fine grained quartz and sericitc white mica matrix (Fig. 13). Further, there are Fe-oxides amongst the accessories zircon and titanite. The whole sample possesses a clearly visible foliation.

Unlike other samples of the Silbersberg Nappe the bigger components of this rock are not quartz but rather plagioclase and additionally K – feldspar. Noteworthy are the glass-remnants, which also differentiate this rocks from the typical Silbersberg lithologies.

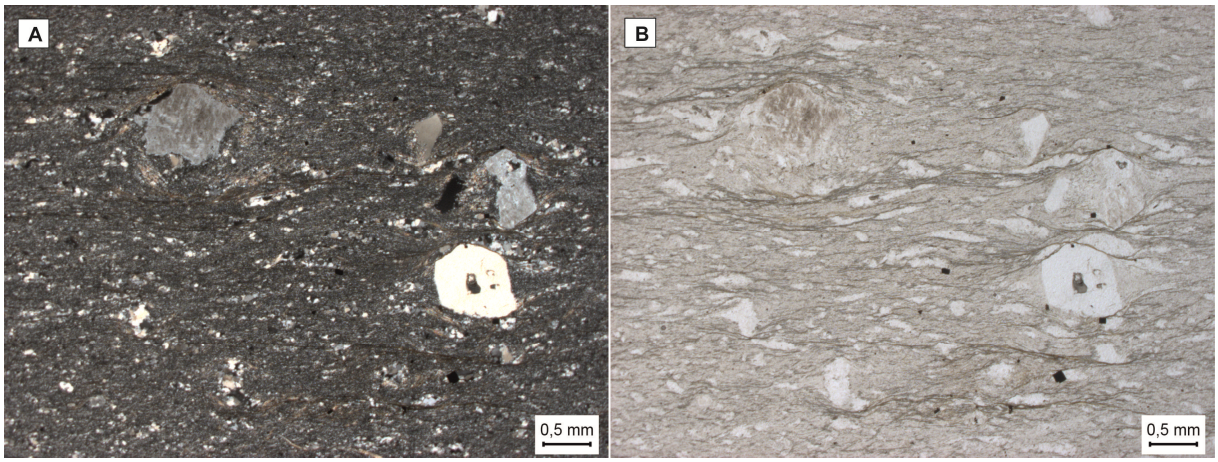

Fig. 13: The composition of the porphyritic metatuff contains feldspar components, which are clearly visible in picture A (with crossed polarizers) and B (without crossed polarizers) and the matrix of sericitic white mica and fine grained quartz.

Textures & Structures

The quartz grains of the matrix mostly hint at SGR and therefore represent a temperature range of 300°C to 400°C.

The metatuff of the Silbersberg Nappe features various strain shadows as well as strain caps. These strain shadows are symmetric and point to coaxial deformation. The whole appearance of these rocks seems to be mylonitic.

12.2 The Veitsch Nappe

Similar to the Silbersberg Nappe, the Veitsch Nappe of the Greywackezone contains also metaconglomerates and phyllites. Distinctive features are abundant graphite and detrital white mica.

12.2.1 ***Metaconglomerates***

The main components of the metaconglomerate of the Veitsch Nappe are quartz, feldspar and white mica. These white mica grains have two different habits, as there is the fine grained sericitic white mica and the larger detritic one. The detritic mica is not always adjusted to the foliation within the thin sections (Fig. 14).

Among these main components, there are also tourmaline, zircons, titanite, Fe-oxides and ores to be found.

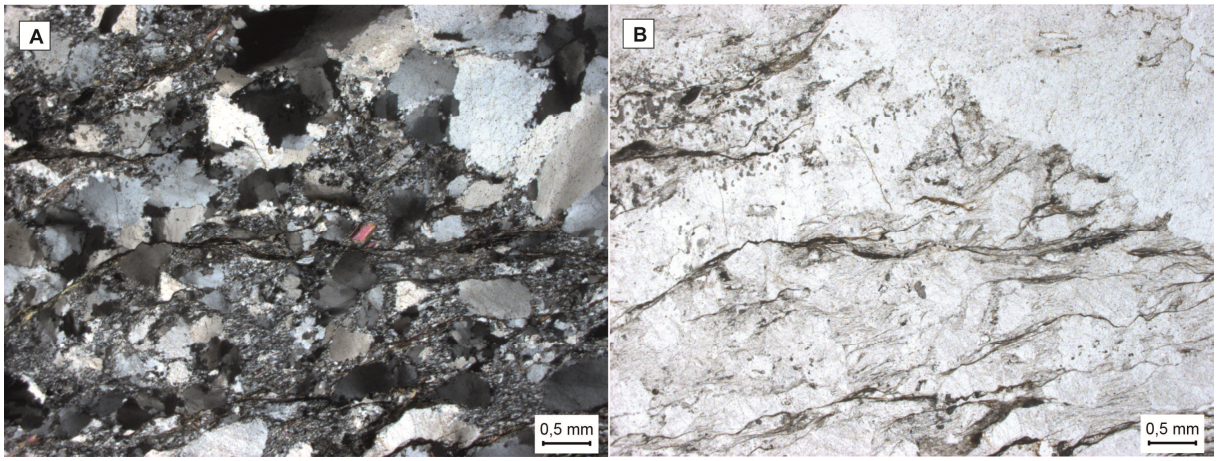

Fig. 14: This picture depicts the compostion of the metaconglomerates of the Veitsch Nappe, with the man components of detritic mica, quartz and feldspar.

Textures & Structures

Throughout the thin sections, there are thick quartz veins which are undeformed or to the upmost deformed by bulging.

Matrix quartz is characterised through BLG to beginning SGR, which leads to mantle-and-core textures within the thin section. Therefore, the temperature range is around 300°C to at maximum 400°C.

12.2.2 ***Phyllite***

The fine grained phyllite of the Veitsch Nappe is mainly characterised through its mineral content quartz, feldspar, chlorite and white mica (Fig. 15). Like the metaconglomerate of this nappe, the white mica occurs either as sericitic pelt or as larger detrital grains. Other special features are graphite layers, which can also be found in many phyllite samples.
Noteworthy accessories are tourmaline, zircons, titanite and rutile.
The chlorite of the phyllites not only occurs as fine grains in the fabric, but also as chlorite fish, and do have about the same size as the detritic white mica.

Similar to many of the already described lithologies, Fe-oxid streaks could be found. Additionally some lithic components are contained in the pyhllitic fabric.

The cleavage is clearly developed and tends to possess a wavy texture of fine white mica and chlorite around the more competent grains, although there is no “augen” texture per se.

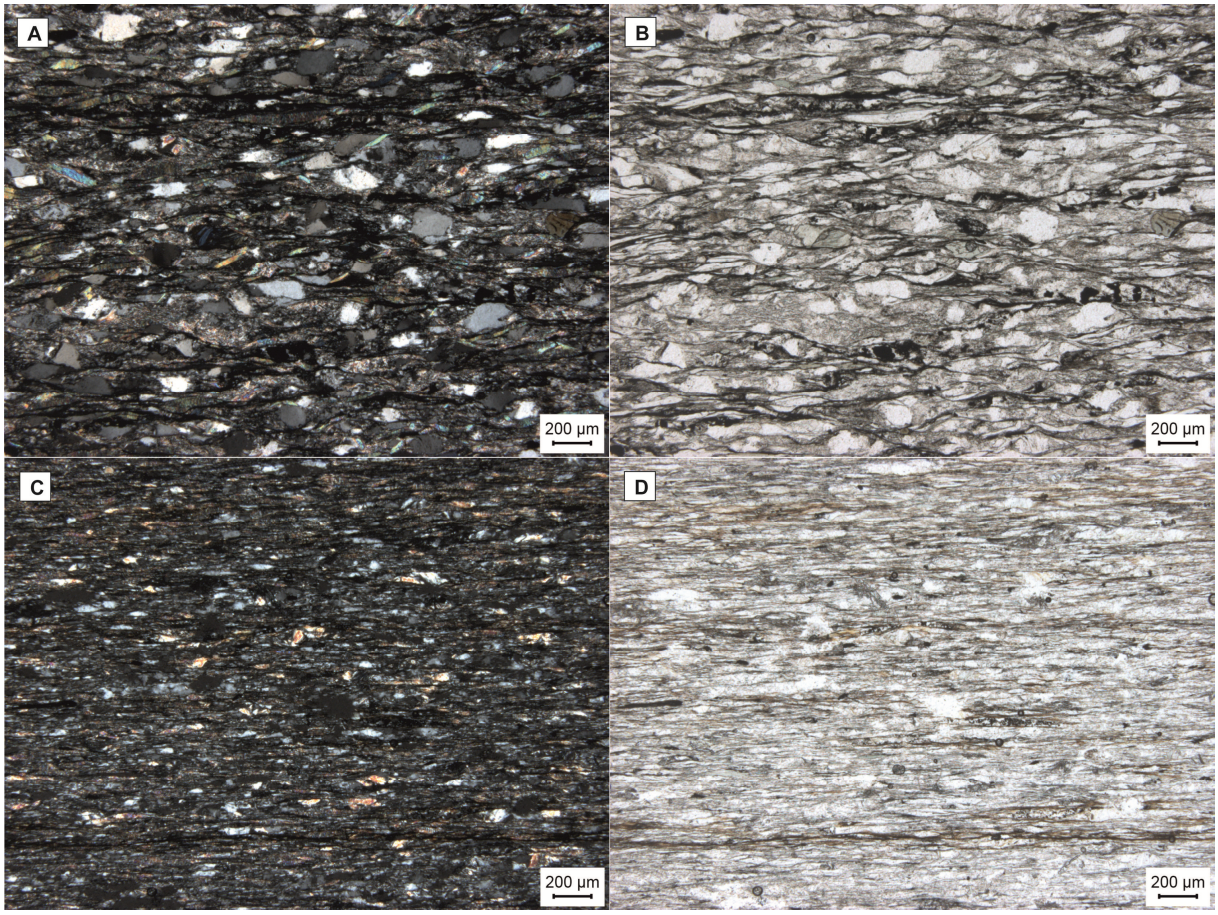

Fig. 15: Picture A to D show the presence of the minerals quartz, feldspar, chlorite and mica, which is detritic white mica. C and D further exhibit a finer grained example of the Veitscher phyllites, while A and B show the shear band cleavage and the resulting wavy fabric of these rocks.

Textures & Structures

The dominant deformation mechanism in phyllites is pressure solution. Bulging is recognised in quartz rich layer. Both point to temperatures of around 300°C to 400°C. This connotes the greenschist facies, which matches the low grade facies conditions a phyllite requires.

Although the small grain sizes of the phyllites blur the structures, it is possible to recognise shear band cleavage (c-type) in some samples (Fig. 15*, A & B*), which leads to an overall wavy fabric in them. Others possess a mainly planar fabric with few small shear bands.

12.3 Tattermann and Troiseck-Floning Complex

Rocks from the Tattermann and the Troiseck-Floning Complexes are hard to differentiate (if it is possible at all) in the small parts mapped. In the study area the narrow stripe to the south of the Veitsch Nappe is characterised by metaclastic rocks of variable grain size.

Sample P11

Sample P11 which can be classified as metasandstone, mainly consists of quartz, plagioclase and some K-feldspar. This feldspar-dominated rock does also contain sericitic white mica and a high amount of carbonates, although those carbonates are possibly brought into the system as a last phase through fluids. Further minerals are chlorite and zircons, but also Fe-oxides and ores can be found within the thin section. The feldspars are considerably bigger than those of the Greywackezone nappes and more frequent (Fig. 16*)*.

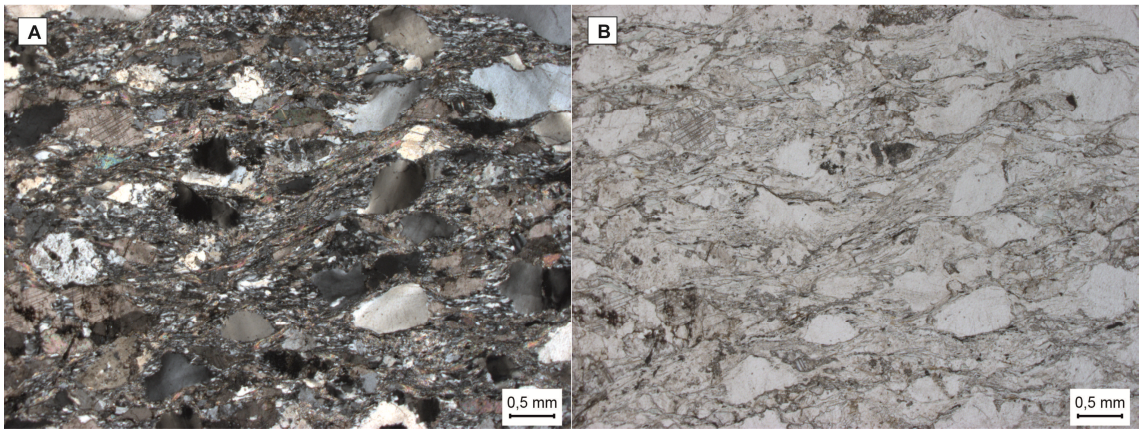

Fig. 16: The images A (with crossed polarizers) and B (without crossed polarizers) depict the typical structures of sample P 11. Notable are the visible K-feldspar recrystallization and the relatively high amount of carbonate.

Textures & Structures

The K-feldspars of this sample show some features of beginning dynamic recrystallisation like BLG and points to a temperature of around 500°C (Passchier und Trouw 2005).

The main deformation process in this sample, however, is a rather low temperature, with pressure solution and fracturing.

Sample P12

This other sample contains quartz, plagioclase and K-feldspar. The plagioclase exhibits growth twinning and a high amount of sericitisation. Further fabric components are white mica, which mostly occur as bands within the thin section, and chlorite that has a blotched appearance (Fig. 17). Ores can be found too, but unlike in the nappes of the Greywackezone, they are not as abundant in these units.

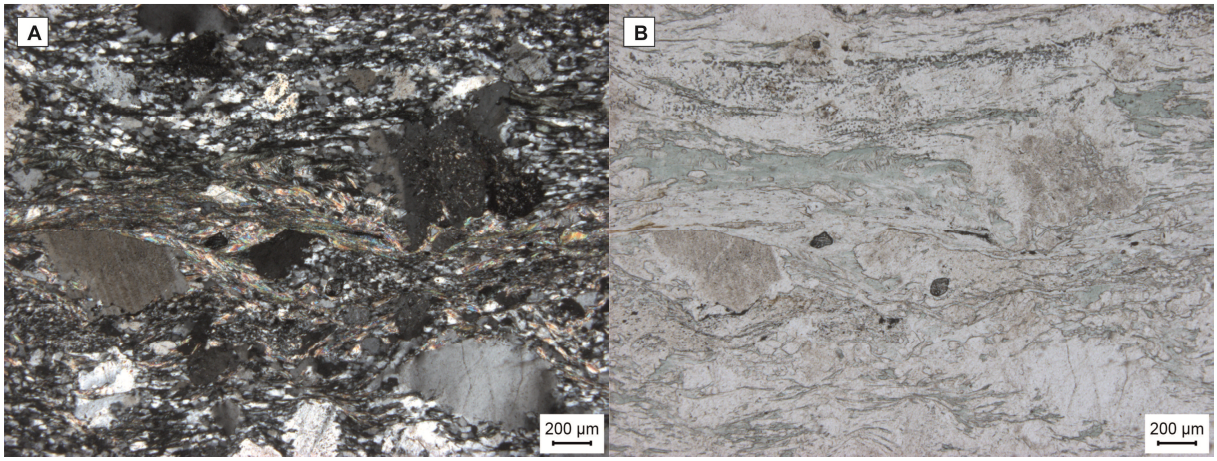

Fig. 17: A (with crossed polarizers) and B exhibit the fabric of sample P 12 with the main components of white mica, chlorite, quartz and an high amount of feldspars.

The metasediments have an immature look on it and can be interpreted as a rock with a magmatic source.

Textures & Structures

The quartzes of sample P12 exhibit core-and-mantle textures as well as SGR and can be counted as two different quartz generations. This leads to temperature assumptions of about 300°C to 500°C. Although there are some small normal faults to be found, as well as sigma clasts, it is not possible to detect a significant shear direction, as the sample was taken unoriented.

Sample P13

The finer grained metasandstone of sample P13 contains mostly quartz, white mica and chlorite. There are some bigger quartz components too (Fig. 18, C & D) as well as Fe-oxide streaks.

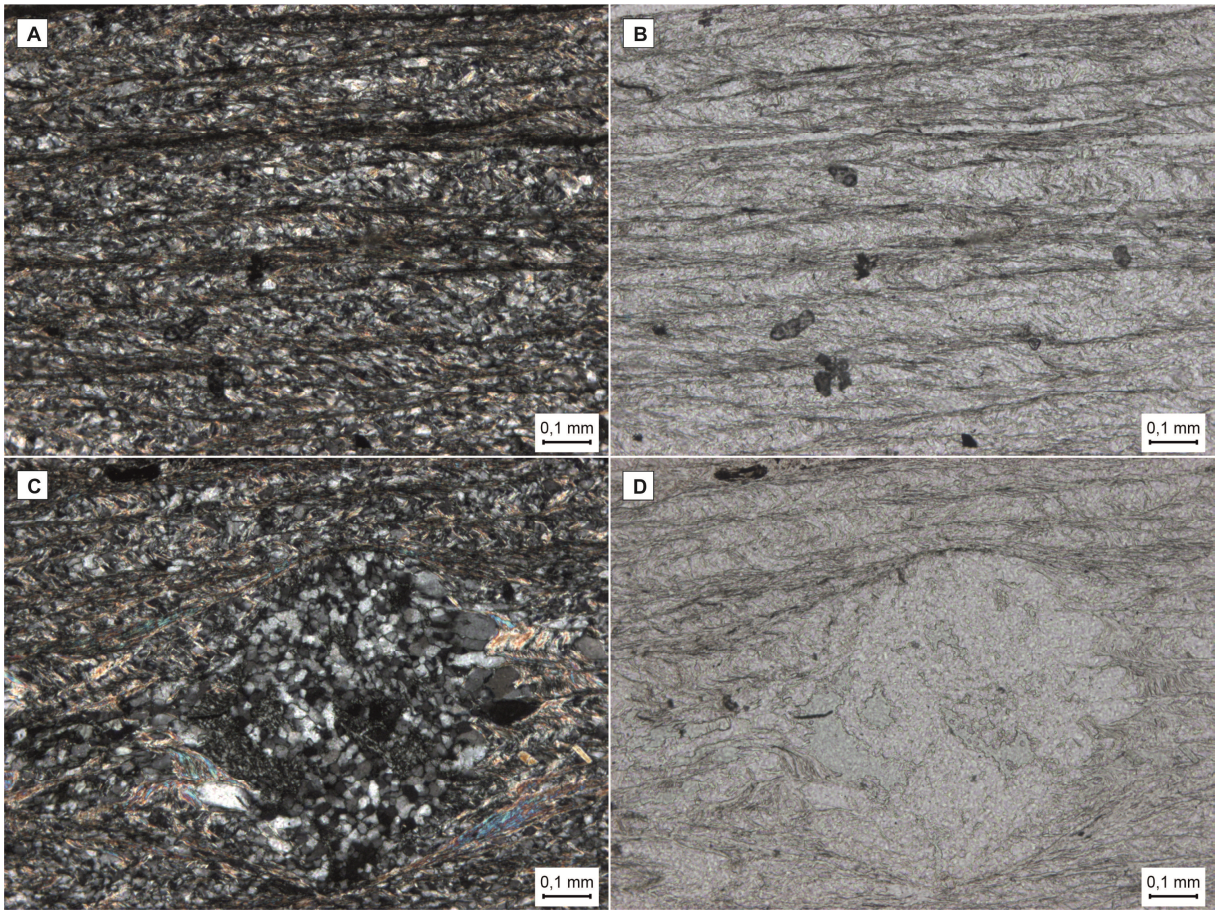

Fig. 18: Along the main components, like quartz, white mica and chlorite, this pictures also show the crenulation foliation of sample P 13 which cannot be found in other lithologies of the mapping area. C (with crossed polarizers) and D (without crossed polarizers) also exhibit a quartz clast which is surrounded on both sides by highly folded white mica.

Textures & Structures

The quartz components indicate the dynamic recrystallisation type SGR, which marks a temperature range of 300°C to 400°C.

Chlorite can be found in strain shadows and the sample is overall good texturized. The mineralogical composition and the strain shadows indicate greenschist-facies as the last deformation facies. A notable structure through this sample is the crenulation foliation, which was not found in the other lithologies of the mapping area (Fig. 18).

Sample P14:

Sample P14 has similarity to the metaconglomerate of the Silbersberg Nappe. Alike these metaconglomerates, there are quartz and plagioclase grains as components which are found in a matrix of sericitic white mica, but also smaller quartz grains. Chlorite is also very common, as well as Fe-oxide streaks and ores (Fig. 19).

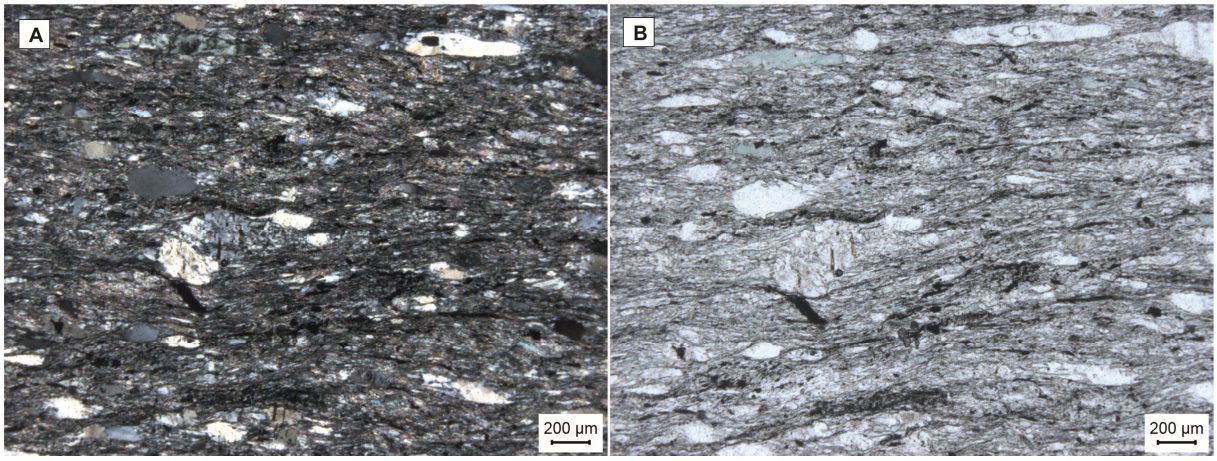

Fig. 19: These thin section pictures (with and without crossed polarizers) of sample P14 demonstrate the similarity to the metaconglomerates of the Silbersberg Nappe. The main components also are quartz and feldspar, next to sericitic white mica and chlorites, as well as similar structures.

Textures & Structures

The quartz textures of this sample are containing core-and-mantle structures as well as GBM which indicates temperatures of about 450°C-500°C.

The most common structures in this sample are shear bands, which even seem to form c-type shear band cleavage in some parts. Further shear sense indicators are quartz sigmoids, which seem to hint at a deformation in a NW direction.

13 Deformation events

Although few oriented samples were taken, it was possible to establish deformation events throughout observation from thin sections and variation of microstructures.

The first deformation event (D1) is a penetrative deformation, which can be seen in most of the samples throughout the mapping area. This deformation shows a shear direction to NW as can be exemplarily seen in Fig. 20a. Associated structures to this event are mostly defined through SC patterns.

This first deformation was followed by a second event (D2), which is characterised through W-E compression. This compression can mainly be seen in kink folding, which lead to an overall crenulation foliation (Fig. 20b). Localised shear zones are associated with this deformation.

A third event (D3) is best shown in carbonate veins. These veins where brought into the system through cracks and later shortened and folded in top SE direction (Fig. 20c & d).

In the Troiseck-Floning and Tattermann complex can also other crenulation deformation be seen, which overprints an older deformation event.

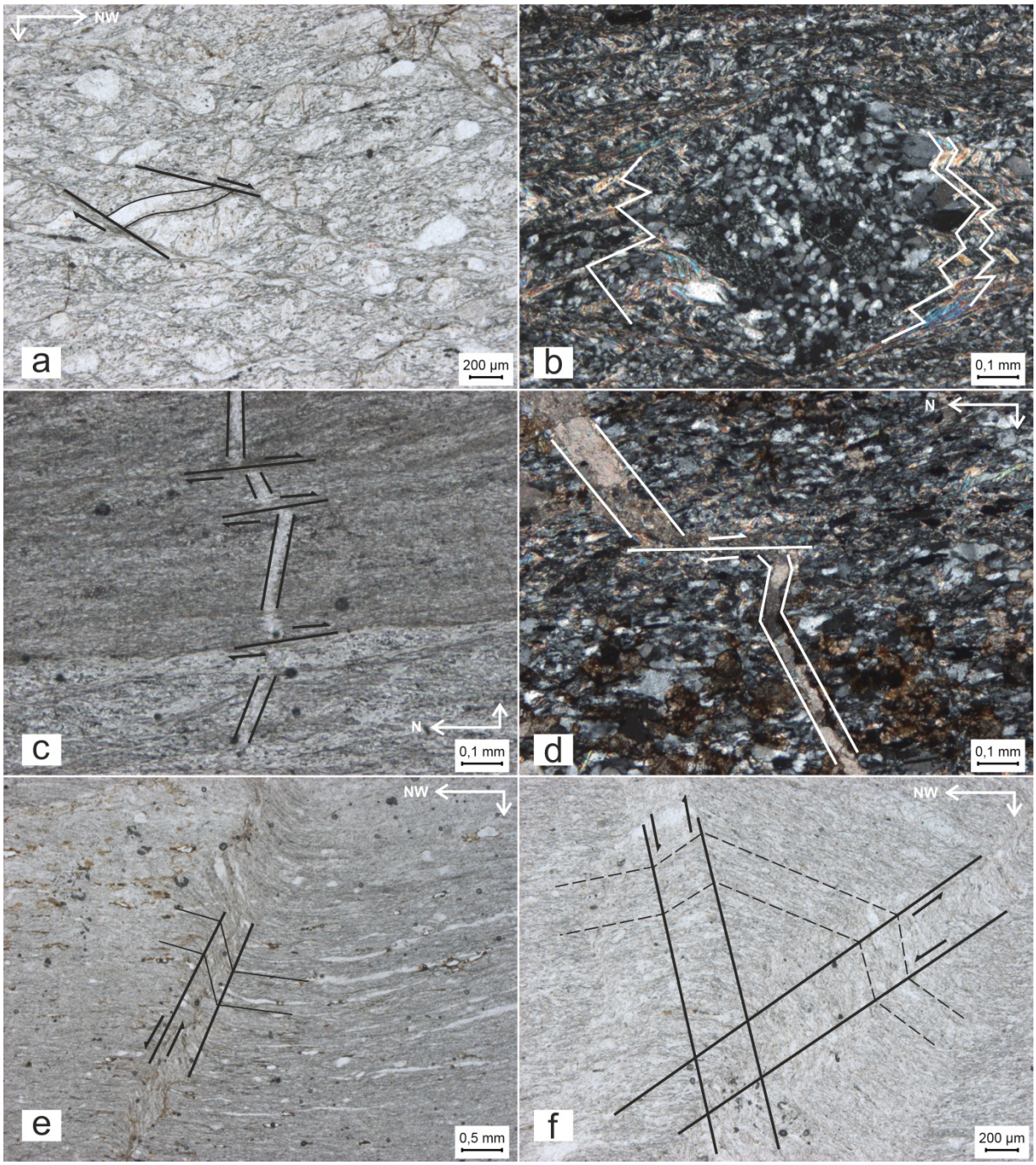

Fig. 20. The structures of some of the thin sections of the mapping area allow the reconstruction of some deformation events. a) shows SC pattern throughout the thin section with a NW direction, b) depicts kink folding and crenulation foliation, c) carbonate vein which is folded and sheared to top SE, d) another carbonate vein which is folded and sheared to a N direction, e) shear bands, f) conjugated shear bands

14 Quartz textures of the mapping area samples

The thin sections of the mapping are mainly described petrographical, but they were also examined through their lattice preferred orientation pattern (LPO). Glide systems in quartz together with the fabric opening angle method after Kruhl (1996) were used to estimate syn-tectonic temperatures and direction of shear. For this method Kruhl (1996) analysed a relation between temperatures and quartz c-axis opening angle (Passchier & Trouw, 2005). In addition, the activation of different glide systems in quartz is dependend on the temperature and the strain rate.

The orientation of the different quartz grains can be determined through a photometer und are later plotted into a stereogram. The resulting c-axes patterns are characteristic for different slip systems. To maintain strain compatibility, more than one slip system is active possibly resulting in cross girdles from which information upon temperatures during the deformation can be derived (Law, 2014; Fig. 22).

Quartz possesses five different slip systems, which are differentiated after Schmid and Casey (1986, Figure Fig. 22):

- Basal <a> slip, which is connected with a low temperature
- Rhomb <a> slip, due to a middle temperated system
- Prism <a> slip, a high temperature slip system
- Prism <c> slip, a slip system connected with high temperature and additional shear strain

Cross girdles can have two different appearances. Type I mainly results because of flattening strain, while type II is governed by constrictional strain (Passchier & Trouw, 2005; Fig. 21). As pure shear and simple shear can both be present, most of the cross girdles are not vertically to the lineation but rather inclined to the shear direction, which is then called an asymmetric cross girdle.

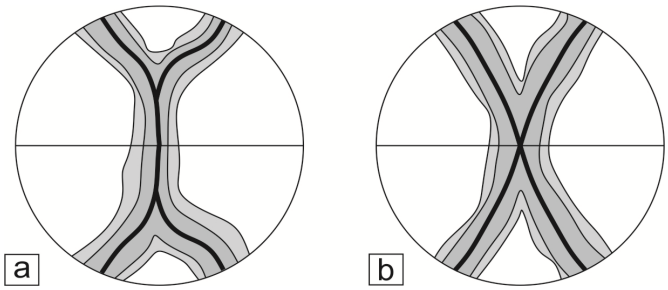

Fig. 21: This figure shows the two types of cross girdles. Picture a) is cross girdle type I and picture b) type II after Passchier and Trouw, 2005.

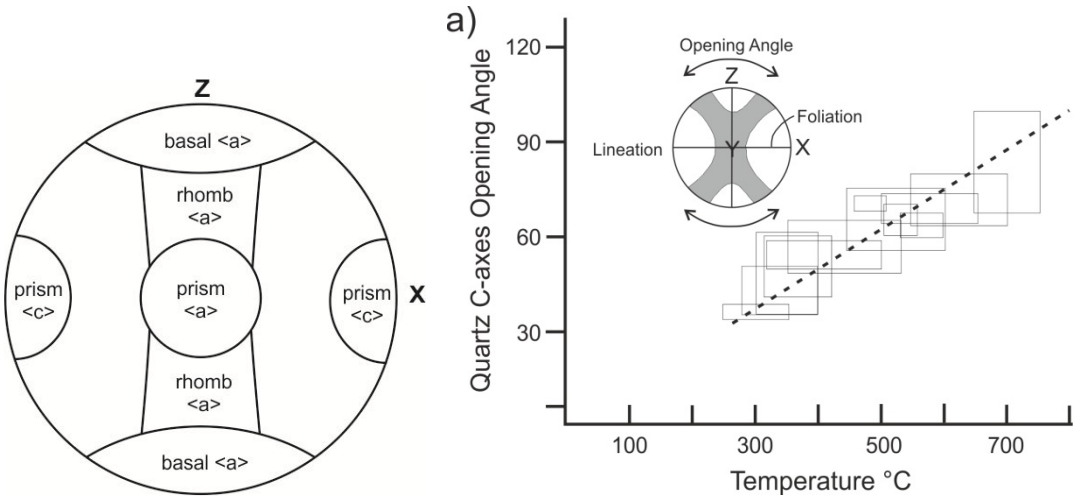

Fig. 22: a) The different slip systems of quartz, depicted on a stereogram after Schmid and Casey, 1986. b) The other diagram shows Quartz c – axes opening angle plotted against the temperature in °C. The boxes are data after Kruhl, 1998 and the dashed line is the empirically determined connection between the opening angle and the temperature. The stereogram shows a cross girdle as well as the opening angle after Law (2014).

In order to estimate the vorticity of the sample rocks, the ellipticity of the strain ellipsoid (Rf) as well as the angle between flattening and shear plane (β) are set in correlation. The angle β is therefore a function between vorticity and finite strain, which results in curves for specific vorticity-values in a diagram after Grasemann et al. (1999; Fig. 24). After this principle it is possible to use the measured values of the samples, plot them in the diagram and obtain the vorticity.

The LPO method was applied on two greenschists of mapping area (Nr. 1 and 2 of Fig. 23), as well as on two Riebeckite gneisses of the area around Brandlberg (one of them not oriented, Nr. 3 and 4 of Fig. 23).

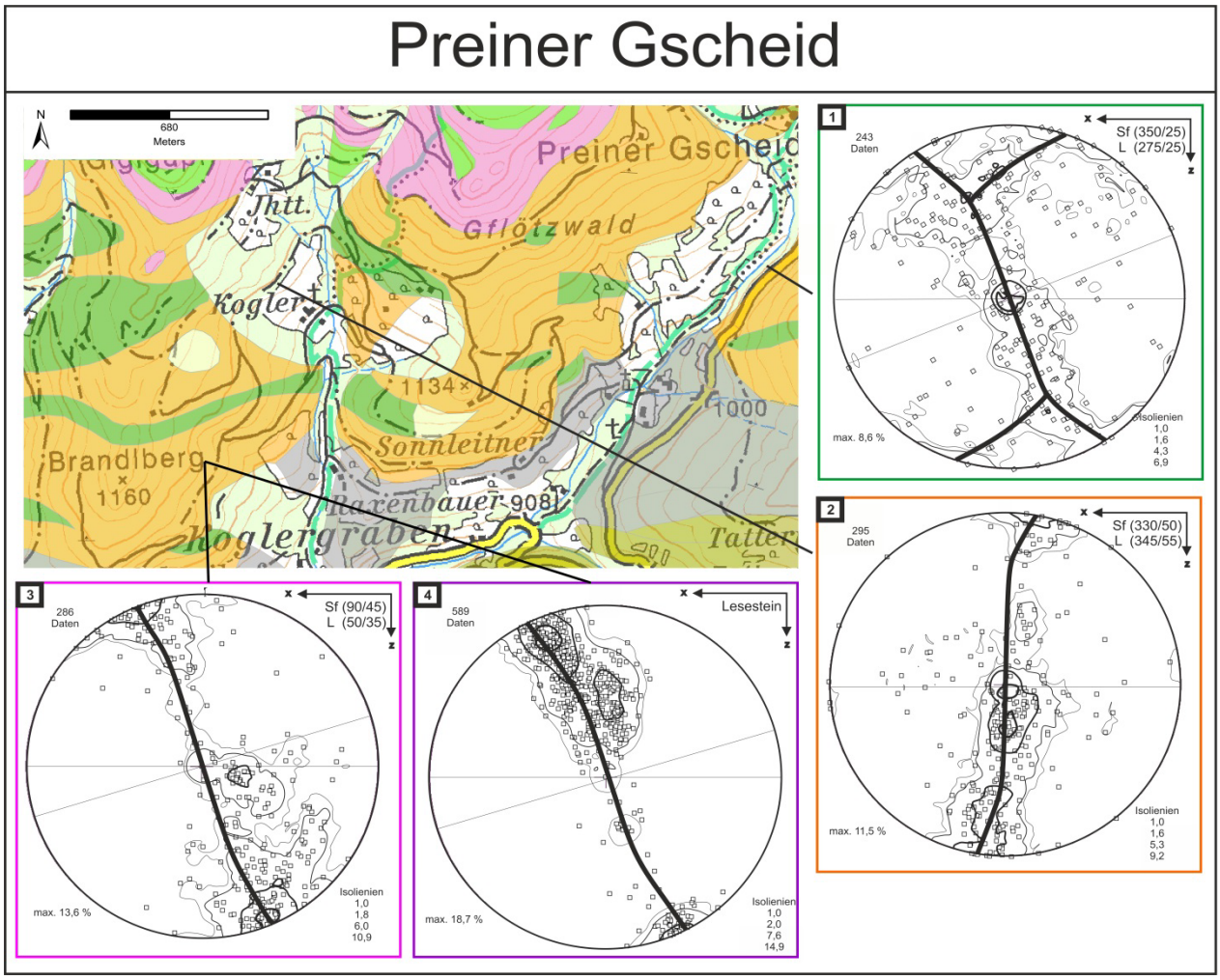

Fig. 23: Four different samples were analysed with a photometer and plotted in stereogram. Nr 1 and 2 are greenschists, while Nr. 3 and 4 depict Riebeckite gneiss. The black lines indicate their area of origin.

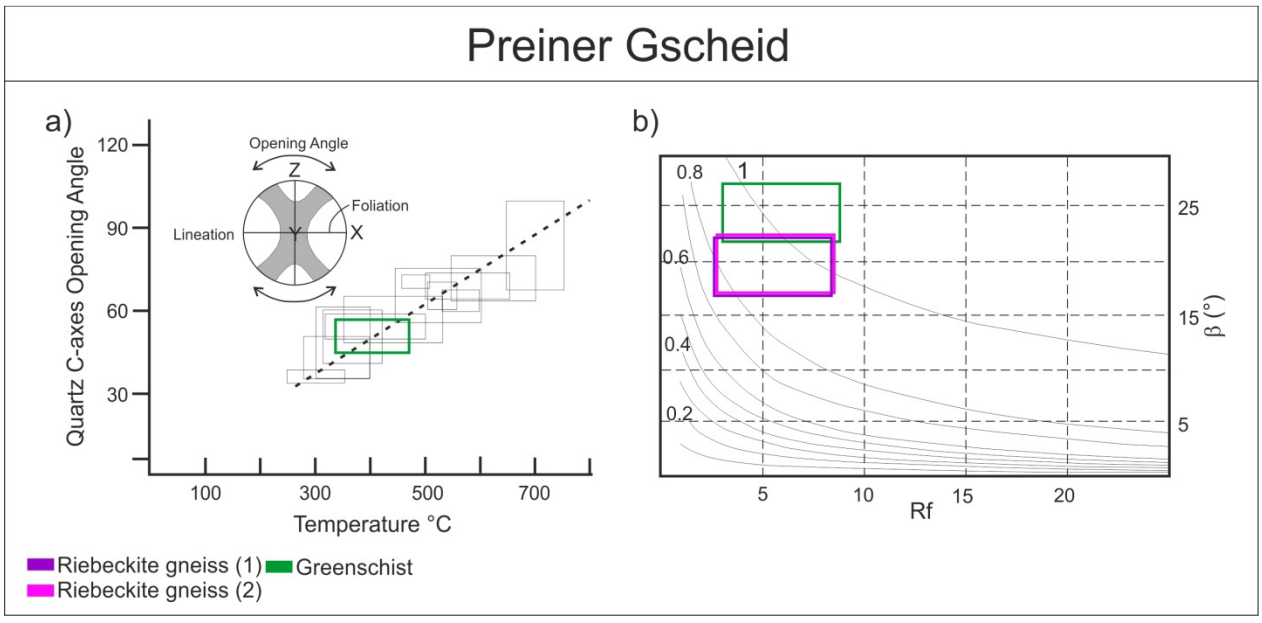

Fig. 24: a) This diagram dispalys the correlation between c-axes opening angle and temperature. b) The diagram after Grasemann et al., 1999, shows the curves for specific vorticity values, in comparison with the samples.

The greenschist of Nr. 1 exhibits an asymmetric cross girdle with a shear direction to W. Further it is noticeable that there were different slip systems active, like basal <a>, rhomb <a> and prism <a> gliding. Dominance of basal <a> glide suggests a temperature of around 350 °C, which correlates with resulting temperature out of the opening angle versus temperature diagram (Fig. 24).

As the greenschist (Nr. 1) exhibits a combination of simple and pure shear, it was further analysed through the vorticity values diagram (Fig. 24). Hence it is evident that the greenschist possesses a Wm (mean vorticity number) between 0.6 and 1. Overall the greenschist is characterised through mostly general shear to simple shear and temperatures around 350°C.

The second greenschist of the mapping area is a single girdle which makes it impossible to use diagram b of Fig. 24. It displays, however, a combination of basal <a>, rhomb <a> and prism <a> glide, dominance of basal <a> glide system suggests temperature of around 300°C to 400°C.

Both Riebeckite gneisses (Nr 3 and 4 in Fig. 23) with dominant basal <a> glide suggest again temperatures around 300°C to 350°C. LPO pattern are highly asymmetric suggesting deformation close to simple shear (top N to NE).

15 Zircon data

The following chapters describe the procedure of dating detrital zircons and provide an interpretion of the plate tectonic position of the source areas throughout the Paleozoic aerathem.

Descriptions to the analytical part, the petrographical investigations of the zircons samples, the depiction through CL/BSE mixed images, Concordia plots, Density Plots, differentiation through zircon formation, plate tectonic development through Earth's history, interpretation of zircon ages as well as comments to the possible origin of the source areas. The order of descriptions follows hereby the order of the processing.

Here I comment that this part of the thesis was made in collaboration with the master thesis of Stefanie Eichinger, 2016. This includes the sampling, the separation of the zircons as well as the dating procedure. Therefore the following chapters are largely identical to those of the Master Thesis of Stefanie Eichinger.

15.1 Description of the analytical procedure of zircon dating with LA – MC – ICP - MS

The measurement of the zircons was performed with a LA-MC-ICP-MS, where a New Wave 193 nm ArF Excimer-Laser as well as a Nu Plasma II Mass Spectrometer was used. The samples were measured at the Geocenter Graz, in the NAWI Graz Central Lab for Water, Minerals and Rocks.

A laser frequency of 8 Hz and a scan velocity of 10µm s^{-1}, as well as laser energy of 5.5 Jcm^{-2} were used for the measurement. The laser beam was focused on the sample surface and the approximate scan line length was about 120 µm at a zircon intersection of 10µm.

The used carrier gas was helium (0.7 l min^{-1}), to which argon gas of 0.75 l min^{-1} was added, before the gas mixture reached the torch of the mass spectrometer. Additionally 0.8 l min^{-1} Ar gas was brought into the system as a help, as well as 15 l min^{-1} Ar-gas for cooling purposes.

The Nu Plasma II Mass spectrometer consists of 16 Faraday Cups with 5 ion counter, which measure the following signals:

- Faraday Cups:
  - H9 – ^{238}U
  - H7 – ^{232}Th
- Ion Counter:
  - IC0 – ^{208}Pb
  - IC1 – ^{207}Pb
  - IC2 – ^{206}Pb
  - IC3 – $^{20}4Pb$
  - IC4 – ^{202}Hg

The ratio of $^{238}U/^{235}U$ was taken as 137.88, after the work of Steiger & Jäger, 1977.

Measurement time was around 280 seconds, with a warm up time of 30 seconds and a measured length between 50µm and 200µm. As an internal standard the Plešovice zircon (Sláma et al., 2008) was used, as well as the zircons M257 (Nasdala et al., 2008) and 91500 (Wiedenbeck et al., 1995) as external standard.

15.1.1 *Further data processing*

Through the EXCEL sheet LamTool U-Th-Pb VI, which was created by Košler und Klötzli (unpublished), the former measured ratios of $^{206}Pb/^{238}U$, $^{207}Pb/^{235}U$ and $^{207}Pb/^{206}Pb$ were corrected. In order to reduce the influence of Pb containing inclusions, incorrect ratios were removed.

The EXCEL plug-in Isoplot (Version 3.75, Ludwig, 2012) of the Berkley Geochronology Center was used to calculate Concordia Plots, which were depicted as diagrams with an error of 2 σ. Zircons with a concordance of less than 0.1 were seen as discordant and therefore not considered for further assessments.

Subsequently, the data was brought into the Density Plotter 7.1 of Vermeesch, 2012, and plotted with KDE (Kernel Density Estimation) and PDP (Probability Density Plot) to generate age distributions. For further classification and verification, the data was also brought into the EXCEL Macros Normalized age probability plots (2003) and Cumulative age probability plots (2003) of Gehrels, 2007.

15.2 Petrographic description of the geochronological samples

Four different samples from Carboniferous to Permian sediments were taken. Three to five kilograms of sample material were taken at the different localities throughout the eastern Greywackezone.

15.2.1 *Sample G21: Silbersberg metasandstone*

The metasandstone of the Silbersberg Nappe was taken at the type locality of Silbersberg in the area of Gloggnitz in Lower Austria. This sample is out of the upper sequence north of the Gloggnitz railway station, immediately below the northern border to the Kaintaleck crystalline complex. The sample location has the coordinates

N	E
47°40,883'	15°56,056'

Detrital white mica components can already be seen in the field. The sample is foliated and slightly weathering. The colour can be described as greyish green and further bigger clasts of lithic components and quartz are possible to be found.

The thin sections reveal quartz, feldspar, chlorite, carbonate, sericite, muscovite, epidote, titanite and common opaque phases as well as zircons (Fig. 25). Small extension gashes occur and detrital white mica is found in the thin section. The sample can be described as fine grained metasandstone, with well-rounded components, and can therefore be classified as rather mature sediment.

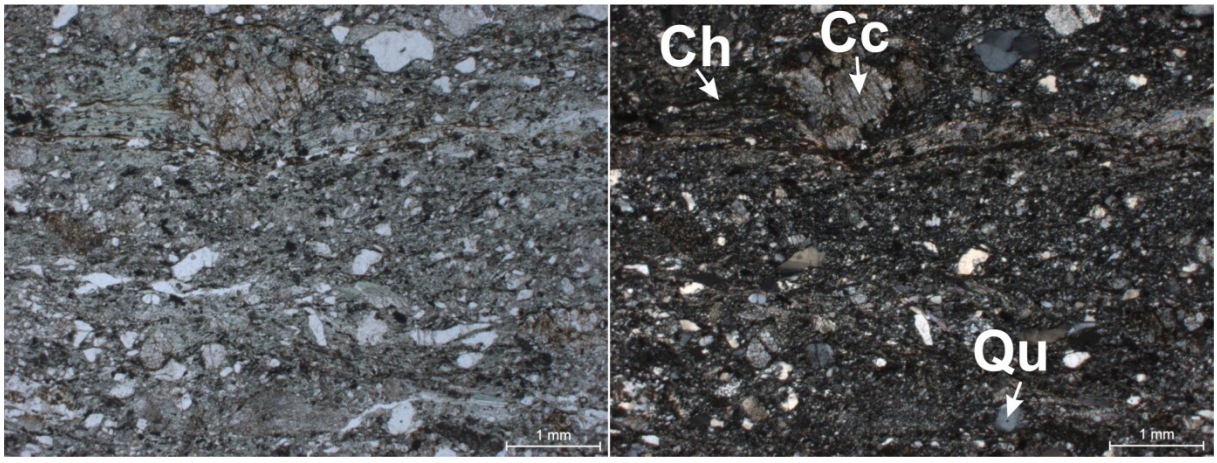

Fig. 25: The left picture depicts the sample G21 without crossed polarisation filter, while the sample G21 with crossed polarizing filter is shown on the right picture. The main minerals are Qu: quartz, Ch: chlorite, Cc: Calcite.

15.2.2 *Sample G2: Semmering quartzite*

This sample was taken at a stone pit near Waldbach bei Raxen, around 5 km east of Kapellen at the coordinates of

N	E
47°39,14'	15°41,34'

The field samples exhibits the typical conchoidal fracture of quartzite and is bulky with a greyish colour.

Sericitic mica, quartz with SGR and sericitic mica are dominant minerals in the thin sections (Fig. 26); zircons appear frequently. The components of the sample are well-rounded, which is an indication of a far source transport.

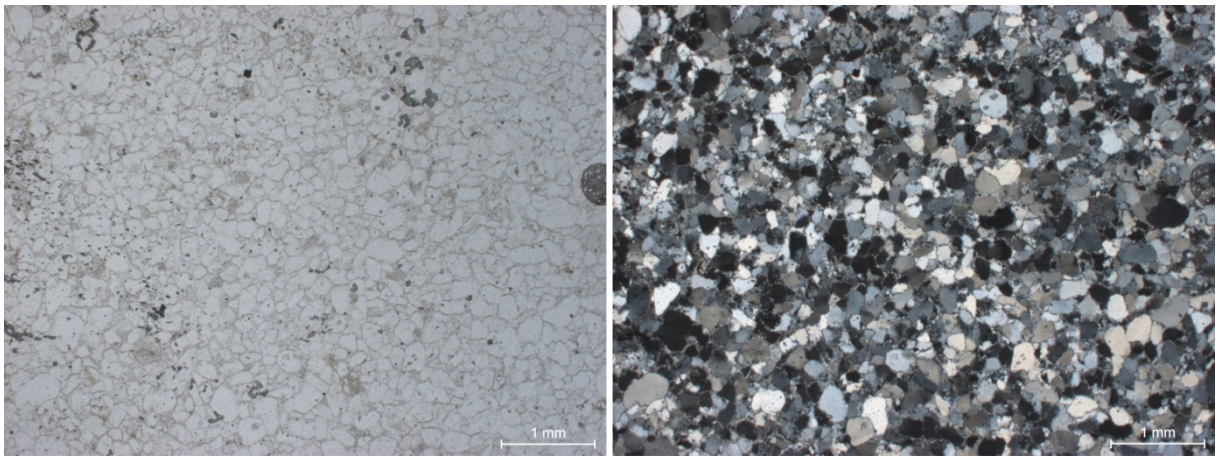

Fig. 26 The left picture indicates the sample G2 without crossed polarisation filter, while the sample G2 with crossed polarizing filter is shown on the right picture.

15.2.3 *Sample G1: Veitsch Nappe*

At the Preiner Gscheidstraße, about 1.5 km south of the Preiner Gscheid, the sample of the Veitscher metasandstone was taken. The coordinates are:

N	E
47°40,14'	15°43,08'

The sample can be characterised as dark grey, fine to middle-grained with lamellar fractions. Detrital white mica can also be identified.

The thin section depicts graphite, quartz, sericite, detrital white mica, feldspar, tourmaline, chlorite, titanite and zircon as can be seen in Fig. 27, with an overall fine-grained feature. The quartz components are often not that well-rounded as the former sample G2. Sigmoidal forms of quartz are common as well as white mica fish.

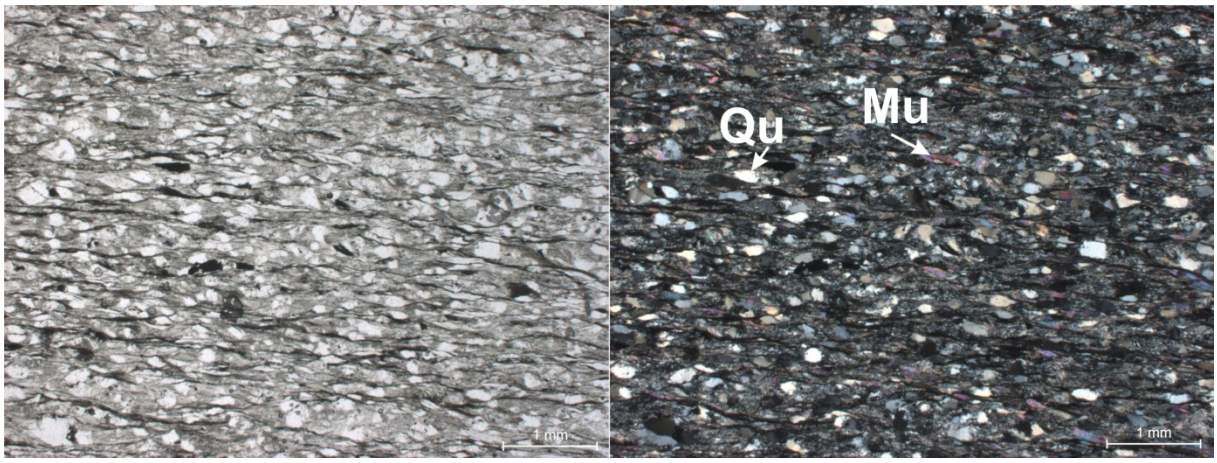

Fig. 27: The left picture represents the sample G1 without crossed polarisation filter, while the right picture depicts the sample G1 with crossed polarizing filter. The main minerals are Qu: quartz and Mu: muscovite.

15.2.4 *Sample L1: Metasandstone of the Präbichl Formation*

L1 was taken at the type locality of the Präbichl Formation at the Leobner Hütte on the Präbichl itself. The coordinates are:

N	E
47°32,03'	15°58,28'

Violet colours dominate this sample which is massive and not foliated. Quartz and feldspar grains can already be recognised at the field, which leads to a porous appearance.

The thin section depicts a granular matrix with quartz, partial sericitic white mica, titanite, plagioclase, rutile, zircon and a few opaque phases (Fig. 28). Overall, this sample can be described as coarser grained than the other samples and not that well-rounded.

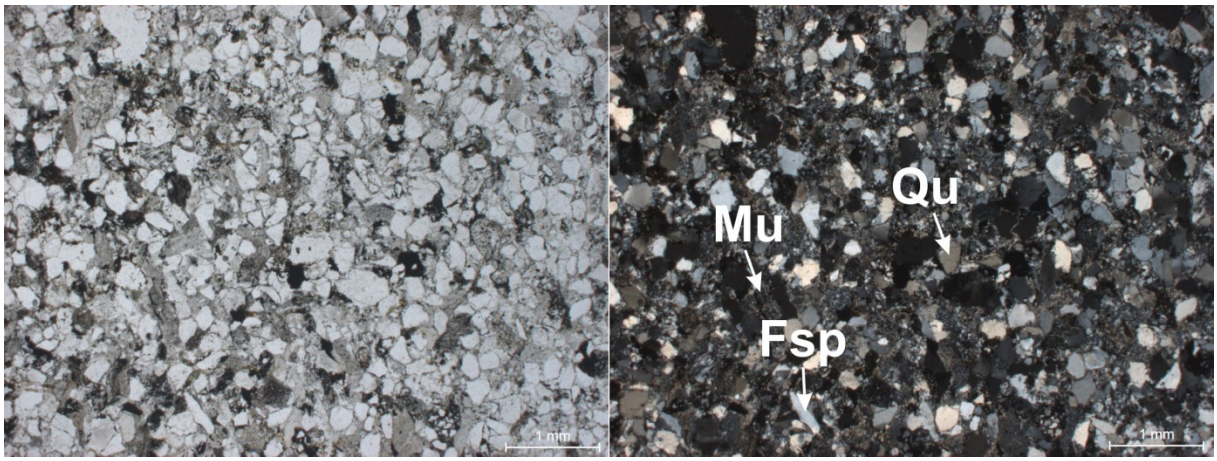

Fig. 28: The left picture shows the sample L1 without crossed polarisation filter, while the right picture represents the sample L1 with crossed polarizing filter. The main minerals are Qu: quartz, Fsp: feldspar, Mu: serizitic gleams.

15.3 Description of the zircon samples through CL/BSE mixed images

In order to identify growth patter, to choose homogneous areas for dating and to identify possible inclusions in zircon CL/BSE images at the REM were produced. The zircons were further differentiated on grounds of their form (e.g. round, short – or long – prismatic), as well as on their zonation (e.g. zoned, not zoned, sector zoned; Fig. 29, Fig. 30, Fig. 31, Fig. 32).

15.3.1 ***Silbersberg metasandstone (G21)***

The zircons of the Silbersberg metasandstone are dominated by magmatic zonic zonation and sector zonation. Metamorphically grown margins are rather rare and were excluded from the measurement because of their small size. Fig. 29 depicts representative examples with grains sizes between 50µm and 100µm.

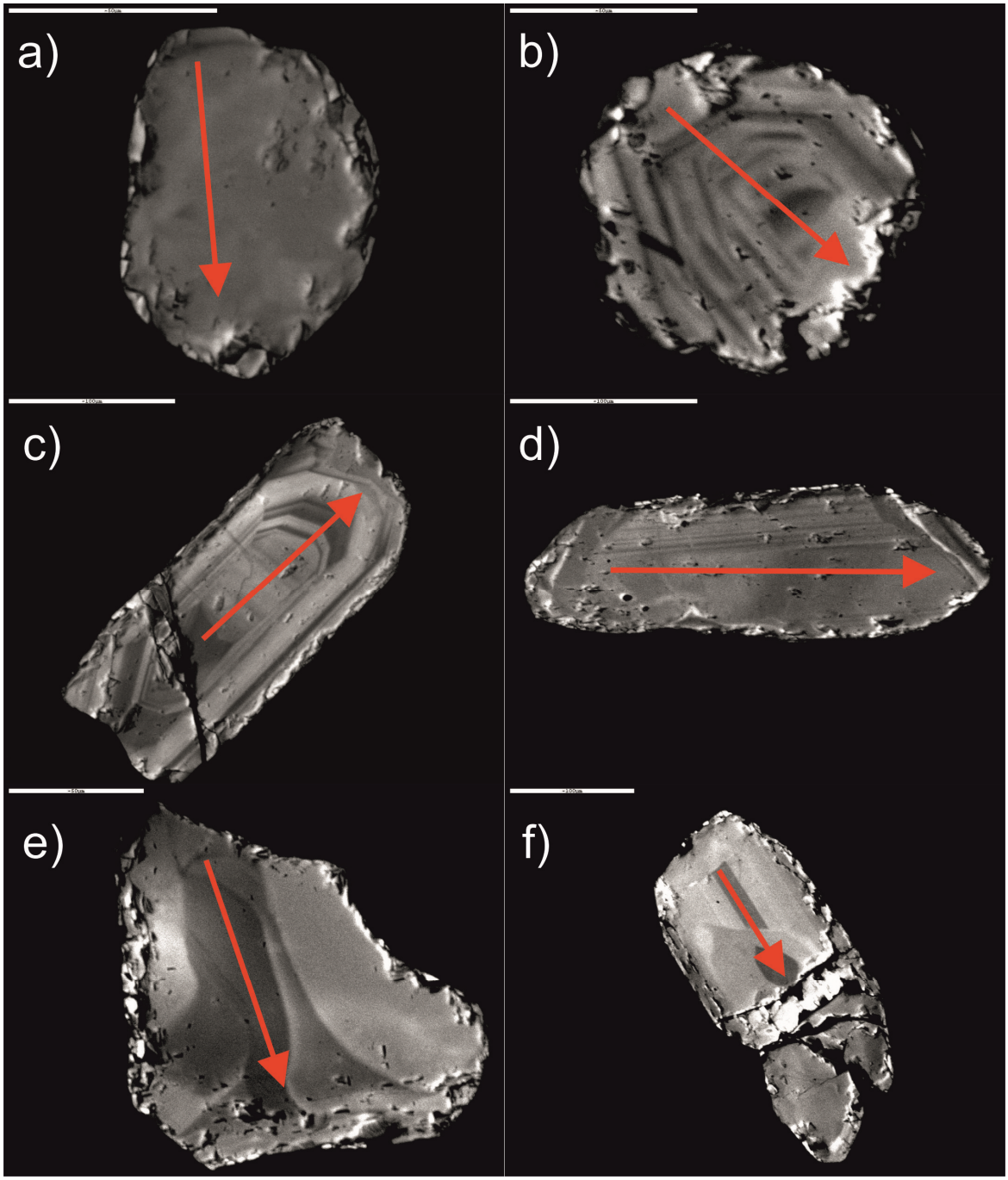

Fig. 29: Examples of representative zircon of the Silbersberg metasandstone. a) No. 20 round and not zoned; b) No. 28 round and zoned; c) No. 52 elongated and zoned; d) No. 73 elongated and not zoned; e) No. 91 round and sector zoned; f) No. 106 elongated and sector zoned. The red arrow shows the direction and form of the laser measurement.

15.3.2 *Semmering Quartzite (G2)*

This sample is characterised through magmatic concentric zonations, and also, but seldom by sector zonation. The rare metamorphically grown margins were not dated. Fig. 30 depicts a representative excerpt of these samples zircons, with an average grain size of 70µm.

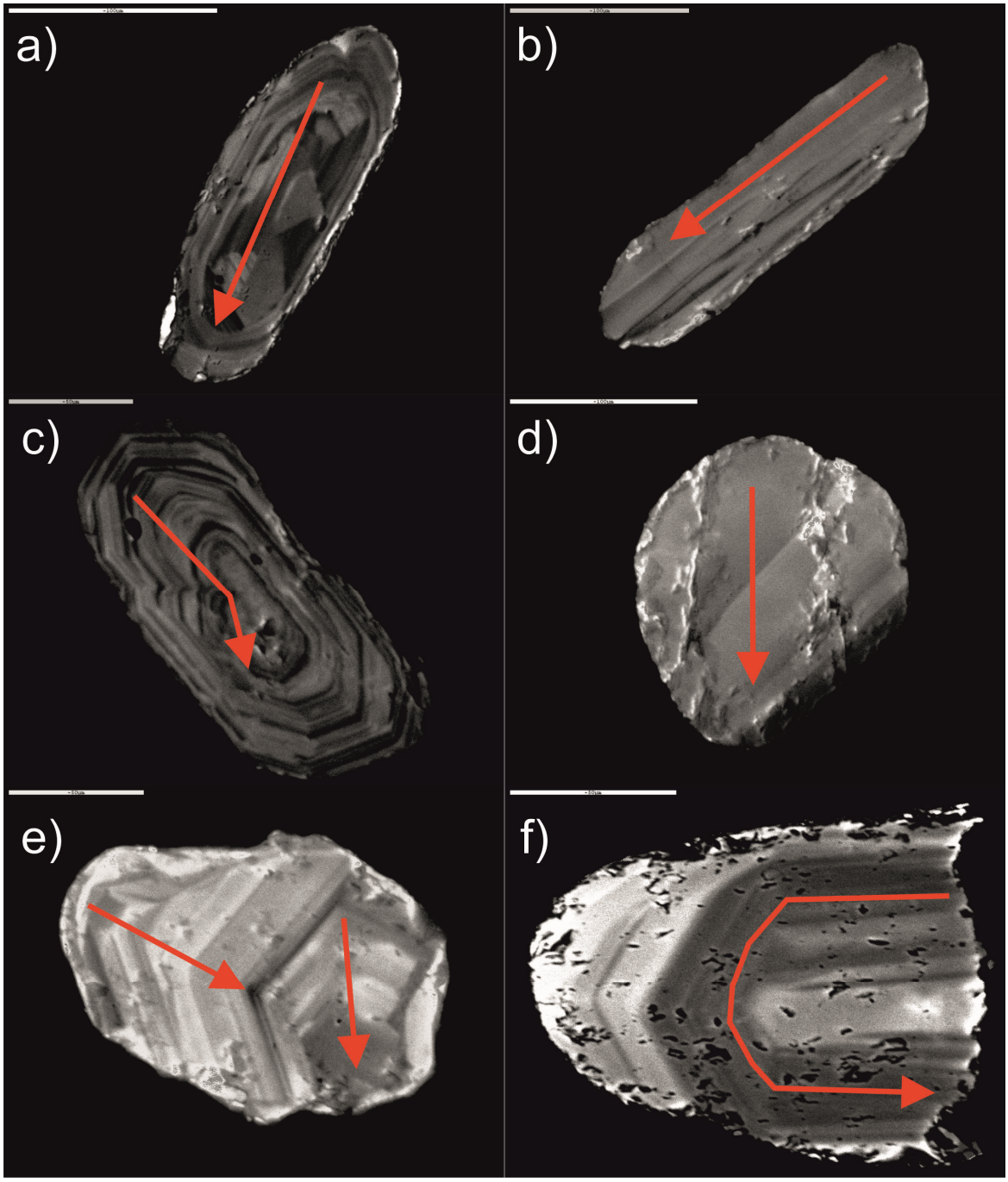

Fig. 30: Examples of representative zircon of the Semmering quartzite. a) No. 152 elongated and zoned; b) No. 74 elongated and not zoned; c) No. 15 elongated and zoned; d) No. 32 round and not zoned; e) No. 64 round and zoned; f) No. 87 half pyramidal and zoned. The red arrow indicates the direction and form of the laser measurement..

15.3.3 ***Veitscher metasandstone (G1)***

Zircons from this sample have grain sizes between 100µm and 50µm and exhibit, similar to the other samples, mainly magmatic concentric zoning as well as sector zoning. Metamorphic grown margins are again dismissed and Fig. 31 depicts a variation of representative zircons of the Veitscher metasandstone.

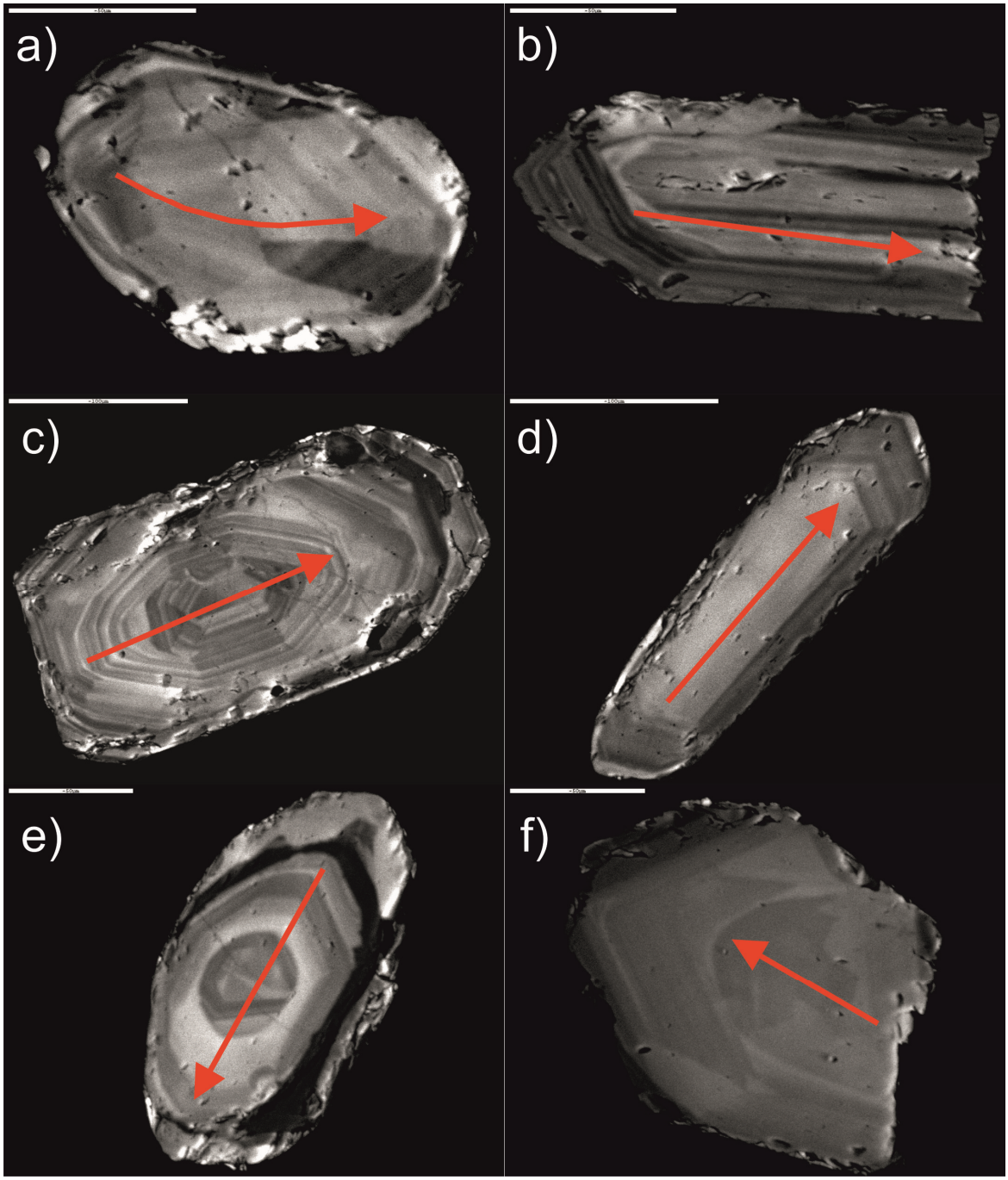

Fig. 31: This figure shows typical zircons of the Veitscher Metasandstone. a) No. 2 round and zoned b) No. 22 half pyramidal and zoned c) No. 74 half-pyramidal and zoned; d) No. 88 elongated and zoned; e) No. 51 elongated and zoned; f) No. 172 round and sector zoned. The red arrow displays the direction and form of the laser measurement.

15.3.4 ***Metasandstein der Präbichl Formation (L1)***

The metasandstone of the Präbichl Formation exhibits mostly zircons with concentric magmatic growth zonation, and some few ones with sector zonation. Fig. 32 depicts a variation of these zircons, which mostly are smaller than the zircons of the other samples, with a mean length of about 50µm.

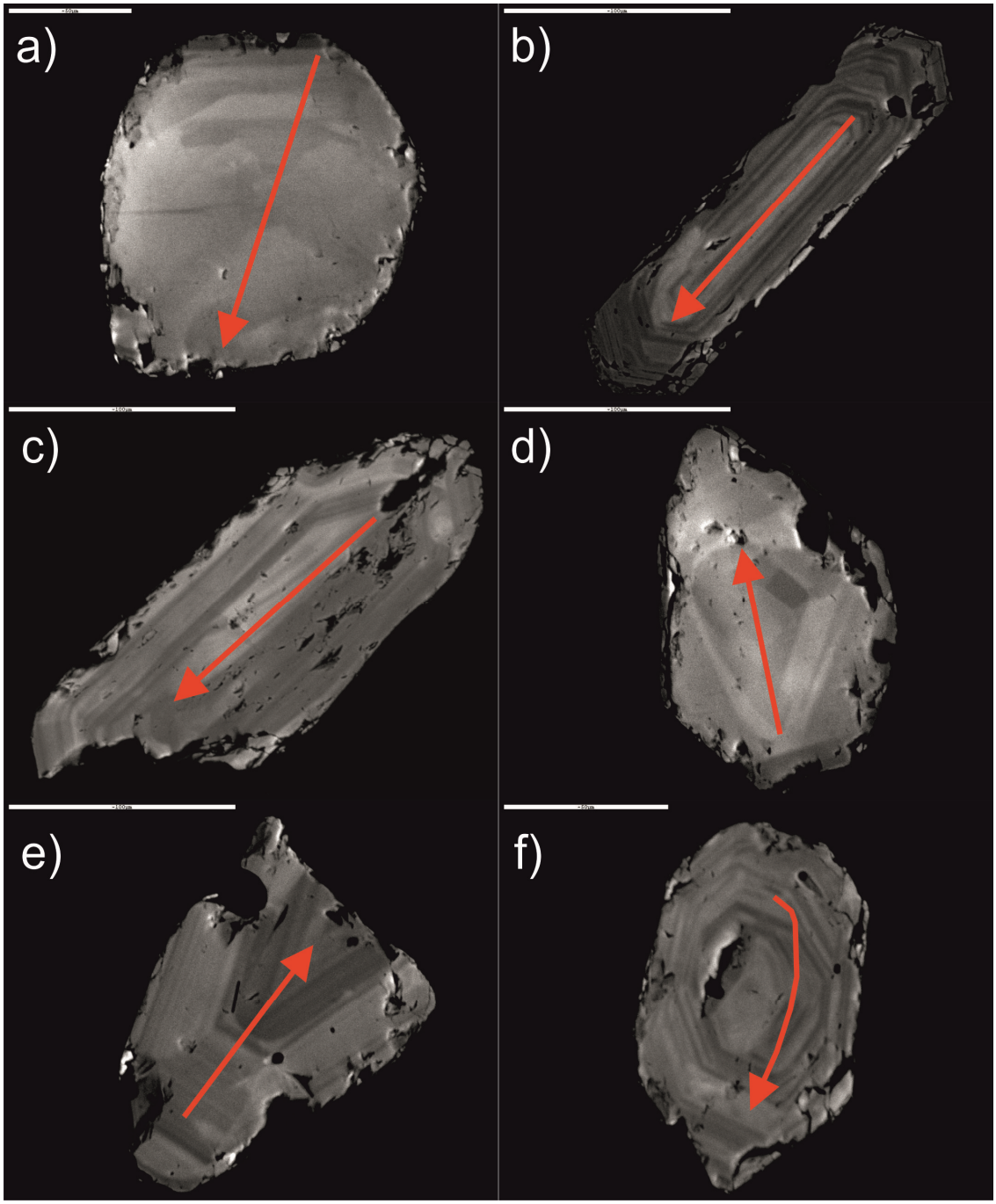

Fig. 32: Some representative zircons of the Präbichl formation are shown here. a) No. 9 round and sector zoned; b) No. 16 elongated and zoned; c) No. 26 elongated and zoned; d) No. 28 round and zoned; e) No. 39 half-pyramidal and zoned; f) No. 56 round and zoned. The red arrow depicts the direction and form of the laser measurement.

15.4 Concordia Plots of the measured samples

The EXCEL plug-in Isoplot (Version 3.75, Ludwig, 2012) was used to produce age clusters of measured zircons. The data sets, which were used in the EXCEL plug-in to produce the Concordia Plots, are to be found in the appendix.

Zircon cluster plotted on Concordia diagrams show overwhelming concordant data. While Fig. 33, Fig. 34, Fig. 35 andFig. 36 depict the four most important age cluster of each sample in order to give an overview, Fig. 37 shows all the age data of the different samples until an age border of 1100 Ma.

The most important age groups of the sample G21 (Silbersberg metasandstone) are around 571 ± 9 Ma, 546 ± 6 Ma, 511 ± 4 Ma and 390 ± 6 Ma (Fig. 33), with overall 47 zircons measured. The concordant ages of individual age groups overlap within their errors.

The Semmering quartzite is dominated by age clusters around 662 ± 8 Ma, 618 ± 8 Ma, 460 ± 2 Ma and 298 ± 3 Ma, which can be seen in Fig. 34. The single measured ages are again mostly concordant and have overlapping errors. 111 zircons of the Semmering quartzite were measured.

G1, the sample of the Veitscher metasandstone, where 105 zircons were measured, shows age clusters at 601 ± 6 Ma, 555 ± 6 Ma, 498 ± 3 Ma and 465 ± 3 Ma (Fig. 35). Again the sample depicts continuous concordant age measurements with overlapping errors.

The age clusters of the highest importance of the Präbichl metasandstone are to be found around 578 ± 8 Ma, 519 ± 8 Ma, 466 ± 6 Ma und 356 ± 4 Ma (Fig. 36). Similar to the other measured sample, the metasandstone of the Präbichl Formation also displays concordant ages with overlapping errors and overall 53 zircons were measured.

Fig. 37 exhibits the Phanerozoic and Neoproterozoic ages in one Concordia diagram. Most of the data are concordant and the rare discordant ages and measurements with large errors were not considered to generate a statistical data distribution (Probability Plots).

15.4.1 *Silbersberg Metasandstein (G21)*

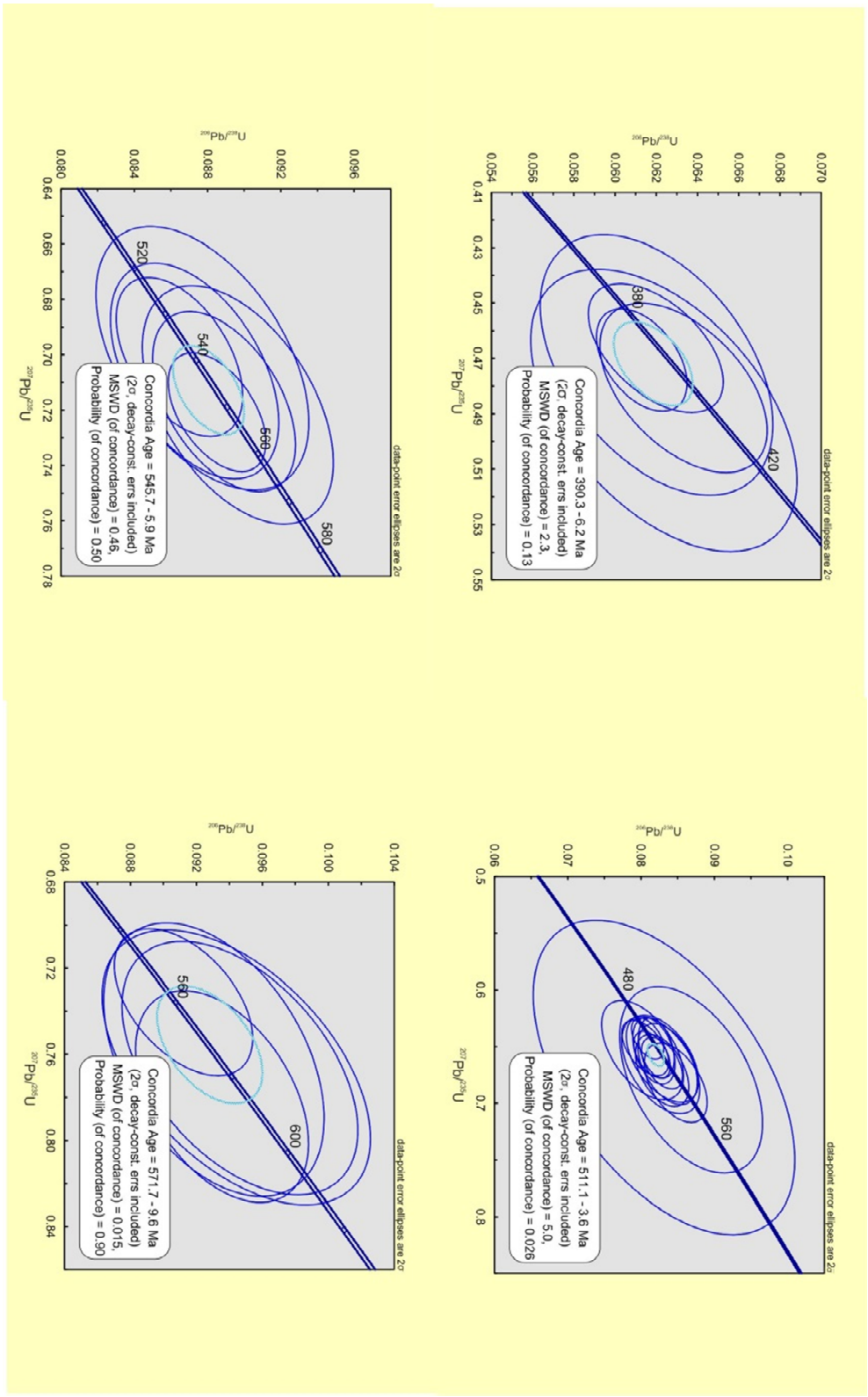

Fig. 33: Four Concordia plots of the metasandstone of the Silbersberg are displayed. The two uppermost plots show the two main clusters, and every circle consists of a zircon measurement with a two Sigma error. Furthermore the concordance of all measurements can be seen.

15.4.2 ***Semmering quartzite (G2)***

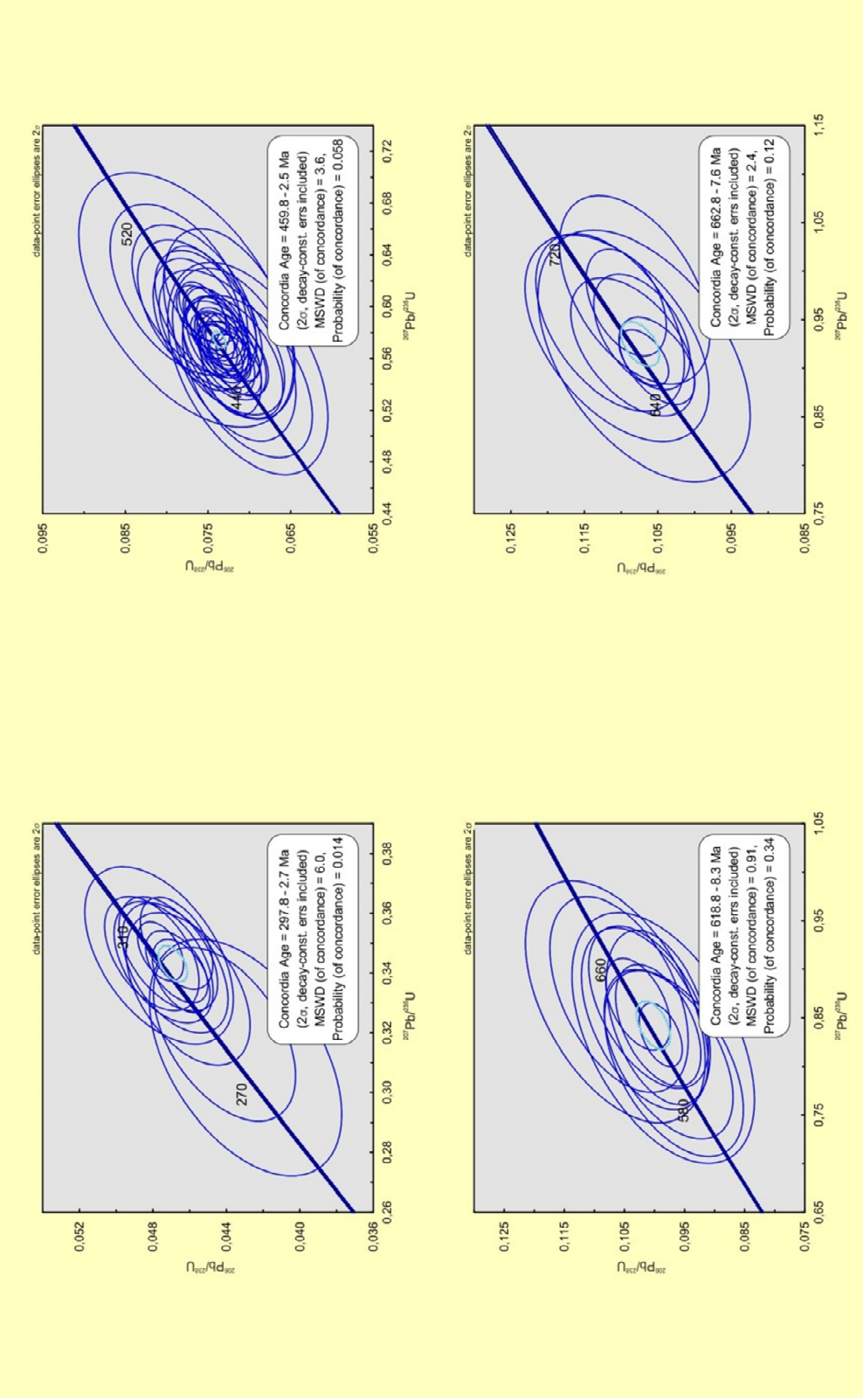

Fig. 34: Four Concordia plots of the Semmering quartzite with the uppermost plots showing the two main ages. Similar to the earlier depiction every circle consists of a zircon measurement with two Sigma errors and a distinct concordance throughout the sample..

15.4.3 *Veitscher Metasandstein (G1)*

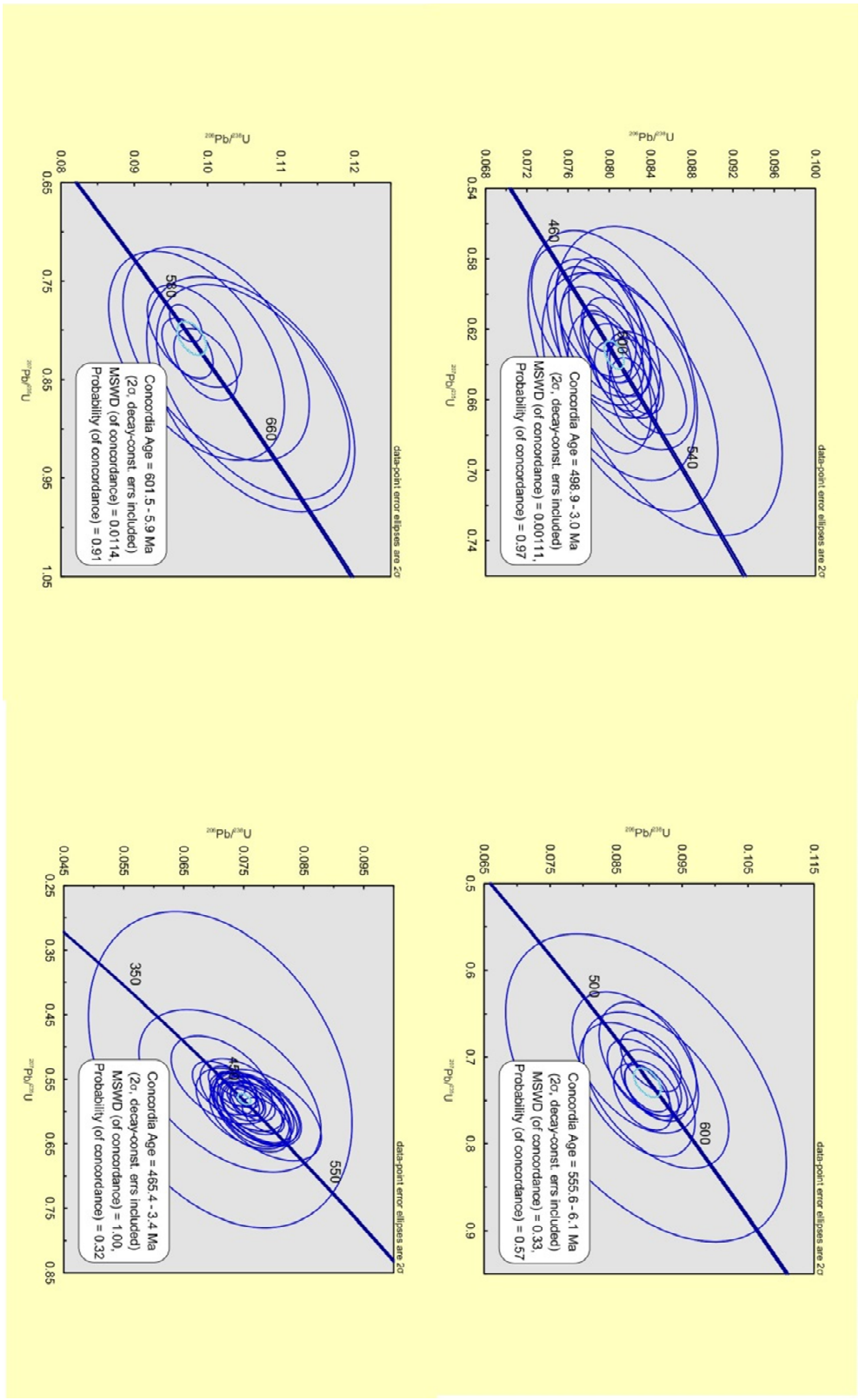

Fig. 35: The Concordia diagrams of the metasandstone of the Veitsch Nappe exhibit clear concordance of all important age clusters. The upper plot on the left side and the right plot below represent the two main ages. Again, every circle consists of a zircon measurement with two Sigma errors.

15.4.4 ***Metasandstein der Präbichl Formation (L1)***

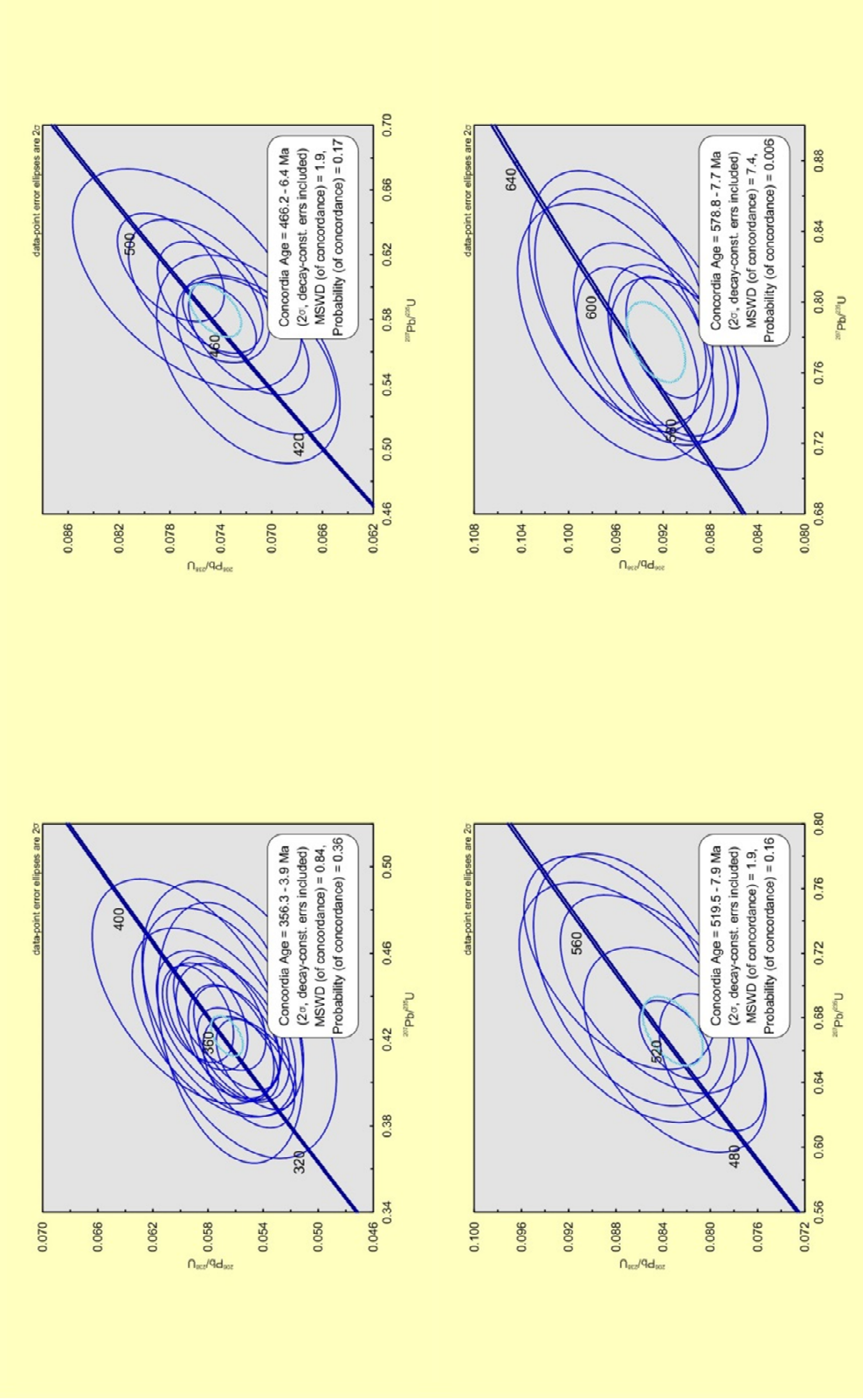

Fig. 36: This representation of four Concordia diagrams of the metasandstone of the Präbichl formation displays a concordance of all important age groups. The left upper plot is the depiction of the main age. Every circle contains a zircon age with two Sigma error.

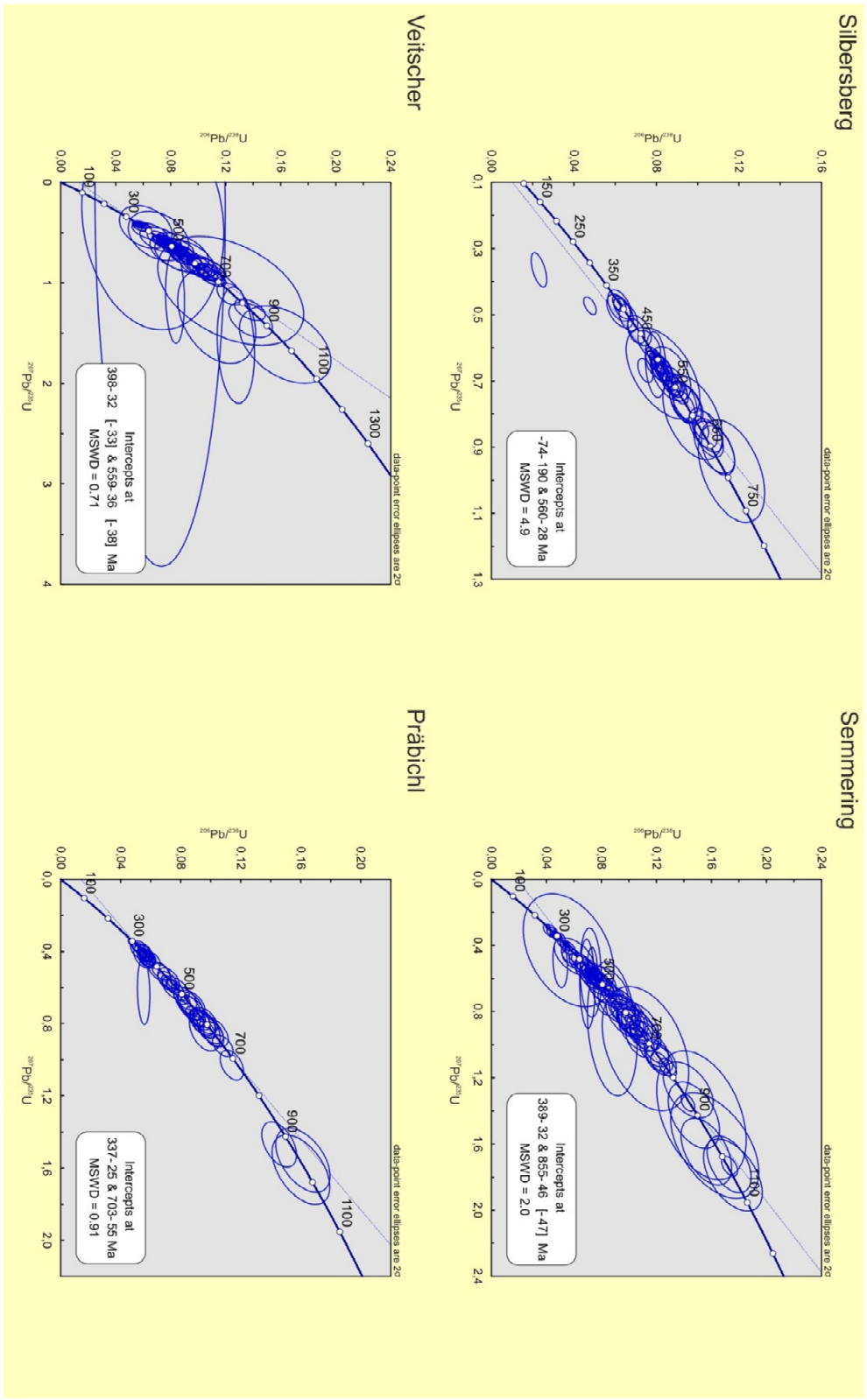

Fig. 37: Depiction of the Concordia plots of all samples with upper age limits between 800 and 1300 Ma. It exhibits, that nearly all zircon plots are concordant.

15.5 Age distribution of the samples displayed through Density Plots

In order to display the statistical age distribution of the single, measured samples, the Density Plotter of Vermeesch, 2012, was used to produce KDE diagrams (Kernel Density Estimation).

15.5.1 ***Silbersberg metasandstone (G21)***

52 concordant zircons were used to determine the statistical age distribution of the Silbersberg metasandstone (Density Plot), where 47 of those display ages between 350 Ma and 980 Ma. Around 511 ± 3.6 Ma is the highest relative probability, others occur around 545 Ma and 571 Ma. The oldest zircon ages are around 2 Ga, 2.4 Ga, 2.7 Ga and 2.8 Ga, which can be seen only in a low percentage of measured zircons, and there is also a Mesoproterozoic age gap.
The youngest age group to be found in this sample is around 390.3 ± 6.2 Ma, with a youngest single measured zircon age of 387.9 ± 9.1 Ma (Fig. 38).

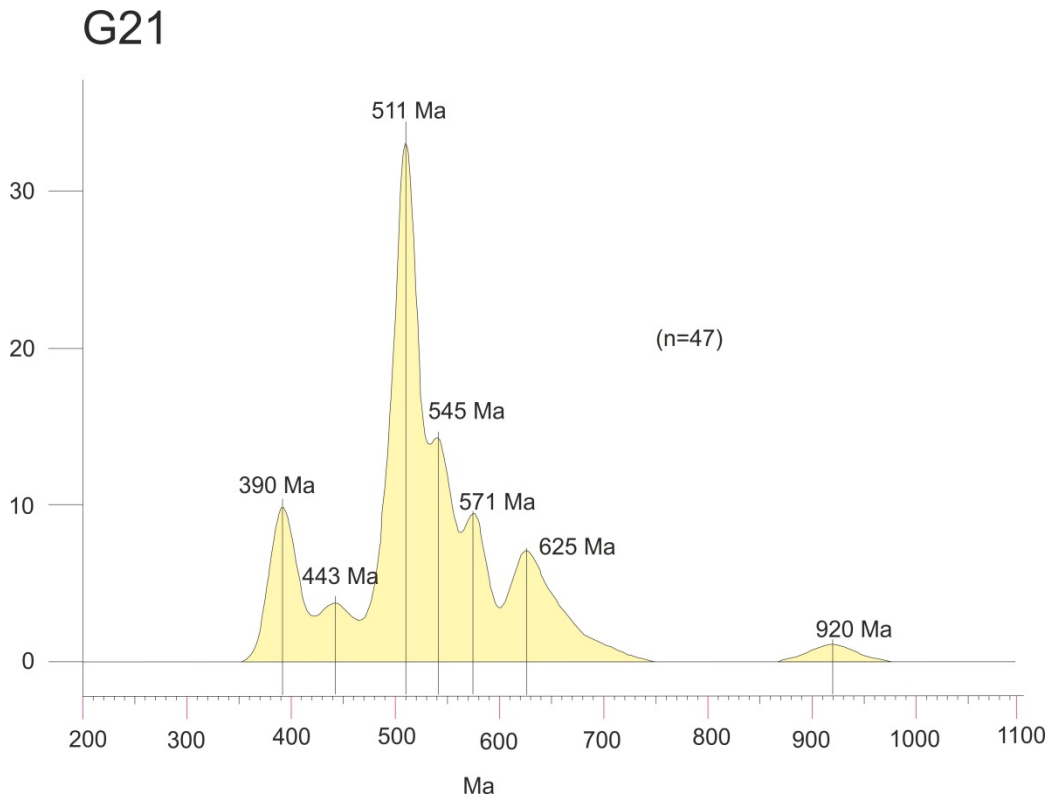

Fig. 38: Density plot of the Silbersberg metasandstone. On the x-axis the age in Ma is applied, while the y-axis shows the likelihood of appearance. The main age lies around 511 ± 3. 6 Ma and 390.3 ± 6.2 Ma.

15.5.2 *Semmering quartzite (G2)*

From the Semmering quartzite 114 zircons were measured, where 111 pieces produced ages between 200 Ma and 1100 Ma. The most important age group, with numerous zircons, is around 459.8± 2.5 Ma, while the youngest plotted age can be found at 297.8 ± 2.5 Ma (Fig. 39).

Age groups older than 1100 Ma could be disregarded, as there are just three single zircons showing those ages which lie at 1.6 Ga and 2 Ga. Overall the youngest zircon of the quartzite is at 260.2 ± 7.8 Ma.

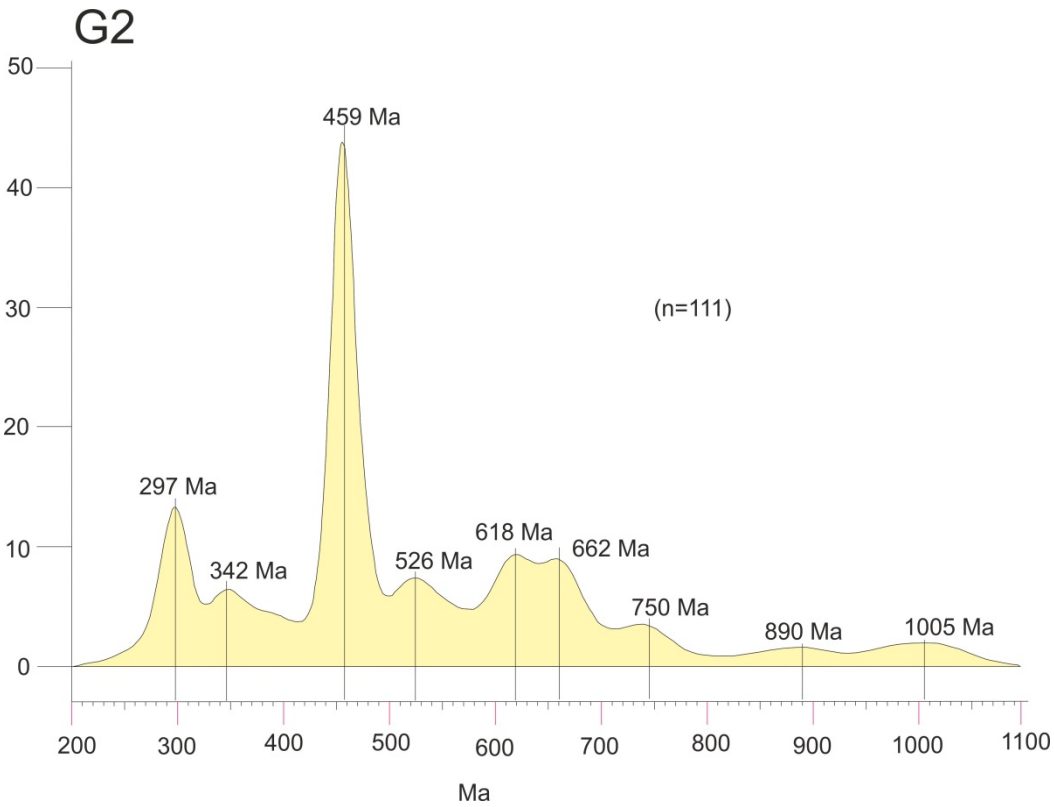

Fig. 39: Density plot of the sample G2. On the x-axis the age in Ma is applied, while the y-axis exhibits the likelihood of appearance. The main ages are around 459.8 ± 2.5 Ma and 297.8 ± 2.5 Ma.

15.5.3 ***Veitscher metasandstone (G1)***

For the measurement of the Veitscher metasandstone, 113 zircons have been separated, where 105 of those depict ages between 300 Ma and 1050 Ma. The main age groups are at 465.4 ± 3.4 Ma, 498 Ma and 356 Ma (Fig. 40). Ages around 351 ± 7.6 Ma are the youngest cluster.

Similar to the other samples, the few old aged zircons of the Veitscher metasandstone also exhibits a Mesoproterozoic age gap, with groups at 2 Ga, 2.5 Ga, 2.7 Ga and 2.85 Ga.

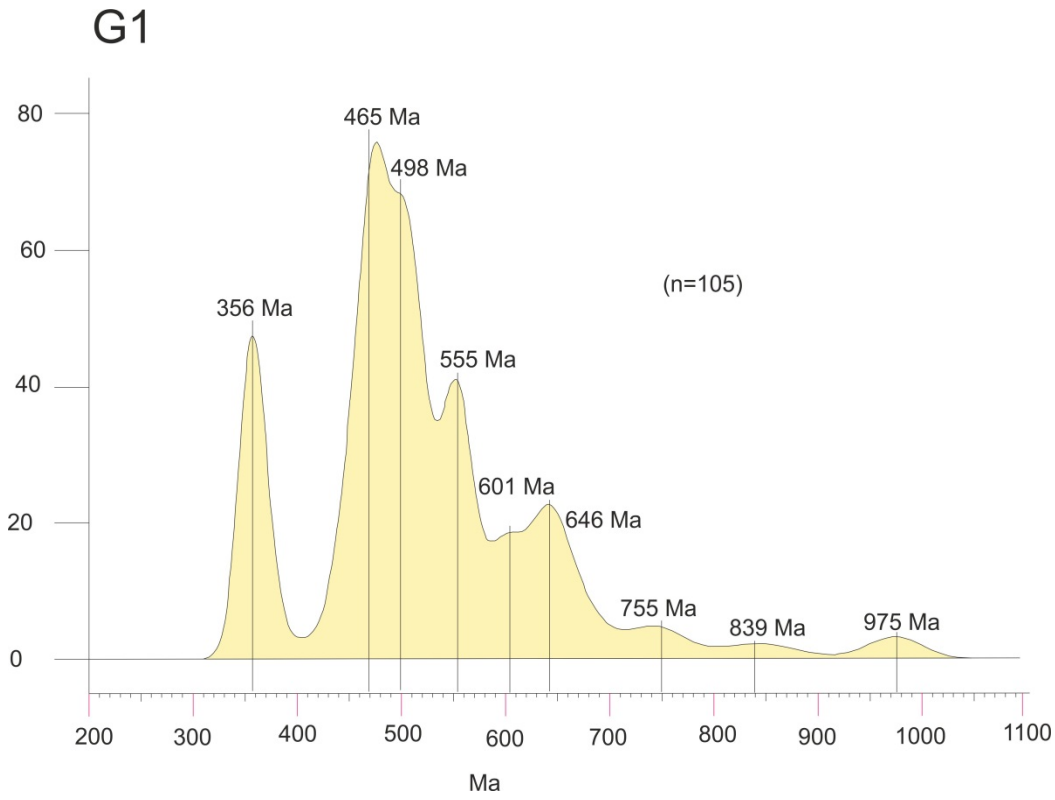

Fig. 40: Density plot of the G1 sample. The x-axis demonstrates the age in Ma, while the y-axis displays the likelihood of appearance. The main age lies around 465.4 ± 3.4 Ma, 498 Ma and 356.1 ± 2.6 Ma.

15.5.4 *Präbichl metasandstone (L1)*

The Präbichl metasandstone was dated through 61 detrital zircons, where 53 of them display ages between 250 Ma and 1000 Ma. The age cluster around 356.3 ± 3.9 Ma can be recognized as the most important, while the youngest one is around 317 Ma. Other age clusters can be found between 466 Ma and 617 Ma (Fig. 41).

A zircon with the age of 304 ± 12 Ma could be identified as the youngest measured zircon, while there are again a few old ones at ages around 2 Ga, 2.3 Ga, 2.6 Ga and 2.75 Ga, which also depict a Mesoproterozoic age gap.

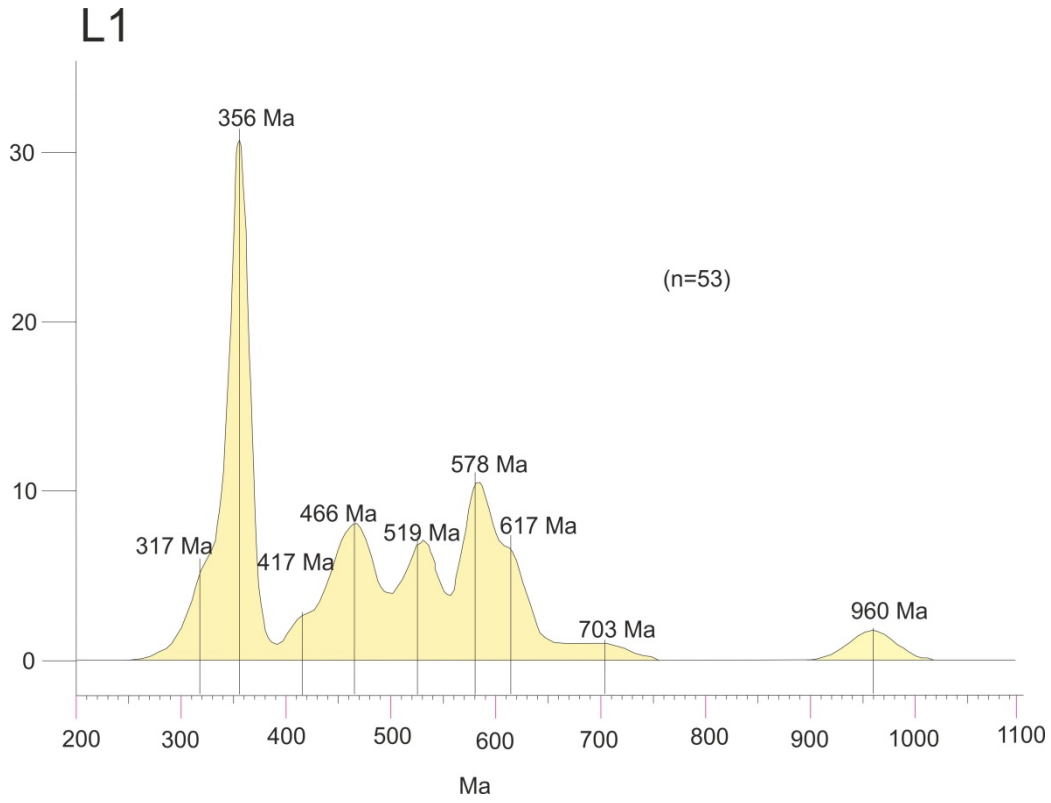

Fig. 41: Density plot of the sample L1. The x-axis represents the ages in Ma, while the y-axis is again the likelihood of appearance. The main age can be seen at 356.3 ± 3.9 Ma.

15.5.5 ***Comparison of the measured samples***

A comparison of the different age groups in the probability plots (Fig. 42) display similarities as well as peculiarities. None of the analysed sample zircon spectra can be compared fully to each other and therefore the source areas are different for the samples.

The Semmering quartzite is the only sample, with an Early Permian age cluster and possesses therefore the youngest zircon age of all (297 Ma). A source area for the detrital zircons with similar ages cannot be excluded for the Veitsch Nappe, as the sedimentation age of this sample is interpreted as Carboniferous (Steilbachgraben Fm., Neubauer et al., 1994).

Young Variscian ages are solely seen as a shoulder cluster (317 Ma) around the main age of the Präbichl Fm. The other samples rather depict older Variscian Events between 340 Ma and 390 Ma, although again they differ somehow from sample to sample.
There are some matches between the Veitsch Nappe and the Noric Nappe (Präbichl Fm.), as both have main age cluster around 356 Ma (Lower Carboniferous). Differing of those two samples, the Silbersberg metasandstone depicts a distinct age group around 390 Ma (Middle Devonian). The source area of the Semmering quartzite does not have a distinct age at these times, but rather a few magmatic/metamorphic singular zircons exhibiting an age around 342 Ma.
A magmatic/metamorphic event around the border of Middle to Upper Ordovician is best seen in the Semmering quartzite (main age group at 459 Ma) and in the Veitsch Nappe (main age group at 465 Ma). The Präbichl Fm. does display a small age group around 466 Ma, while the Silbersberg metasandstone differs here completely and does not have an Ordovician age at all.
Cambrian ages on the other side are to be found in all the nappes, with different frequency. The main Cambrian age can be noticed in the Veitsch Nappe, which exhibits a distinct age group around 498 Ma.
Late Neoproterozoic ages are also represented in all the samples, with ages between 570 Ma and 545 Ma being the most abundant ones (Silbersberg Nappe, Veitsch Nappe, Präbichl Fm and fewer in the Semmering quartzites). Similar to these ages, there are also Neoproterozoic cluster between 600 Ma and 1000 Ma to be found in all the samples, even if those are not very common and just represented by a few singular zircons.
An important peculiarity is the lack of Ordovician aged zircons in the age spectra of the Silbersberg metasandstone, as the Ordovician ages are pretty common around the basement areas of the Eastern Alps.

Another important feature are the mainly eo-Variscian zircons in the data base (e.g. 365 Ma), as well as the source material of the Silbersberg Nappe, which had experienced a Middle Devonian metamorphic, magmatic event. These features differentiate the Silbersberg Nappe clearly from the other samples.

Further a depiction of the whole age spectra of all samples is given in Fig. 43. This documents the existence of different aged Archean zircons as well as the lack of Mesoproterozoic ages in the samples, except the Semmering quartzite.

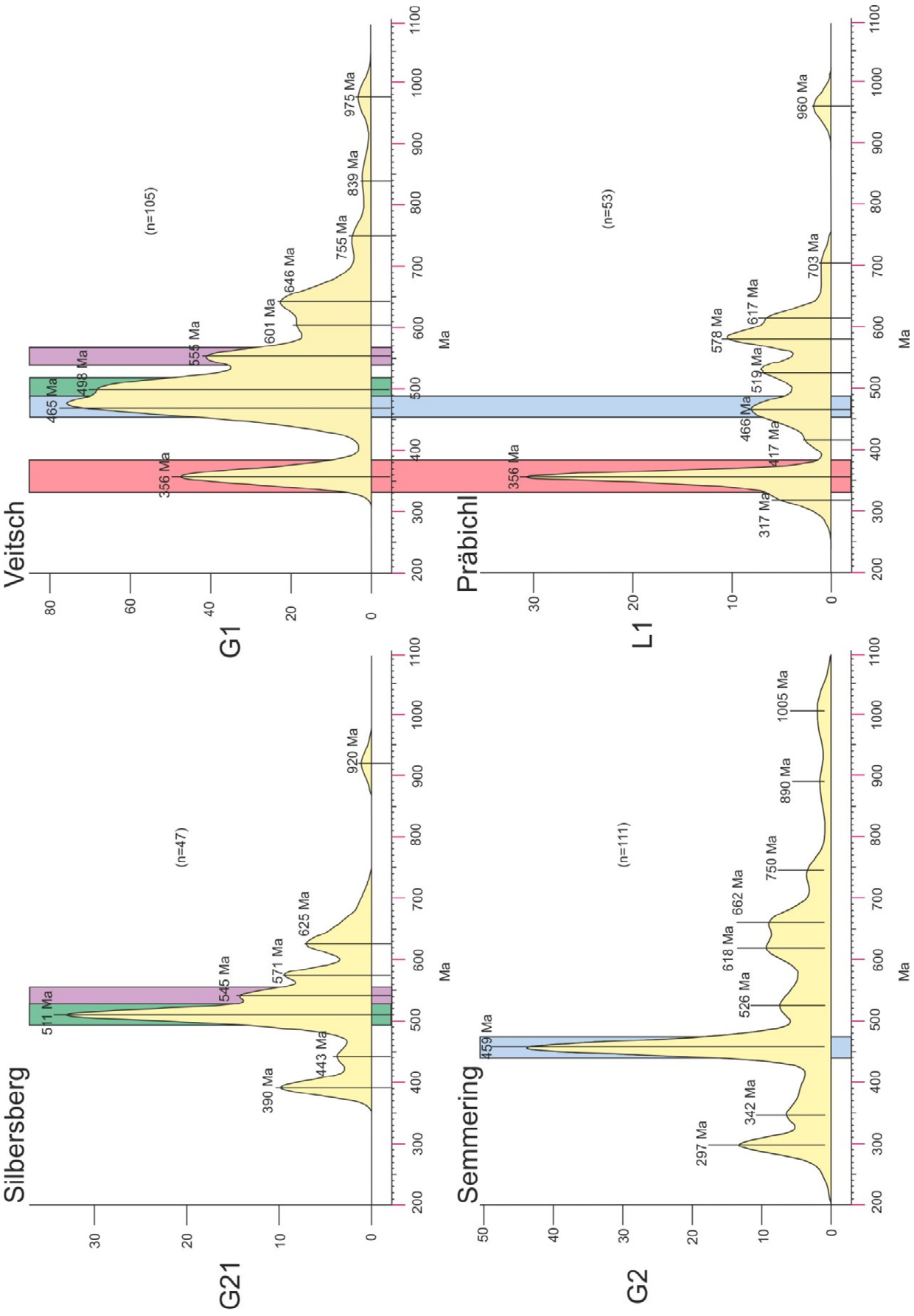

Fig. 42: Comparative representation of the similarities of the different analysed samples. Similarities and differences in the statistical frequencies of the zircon populations are highlighted (see text of chapter 15.5.5)

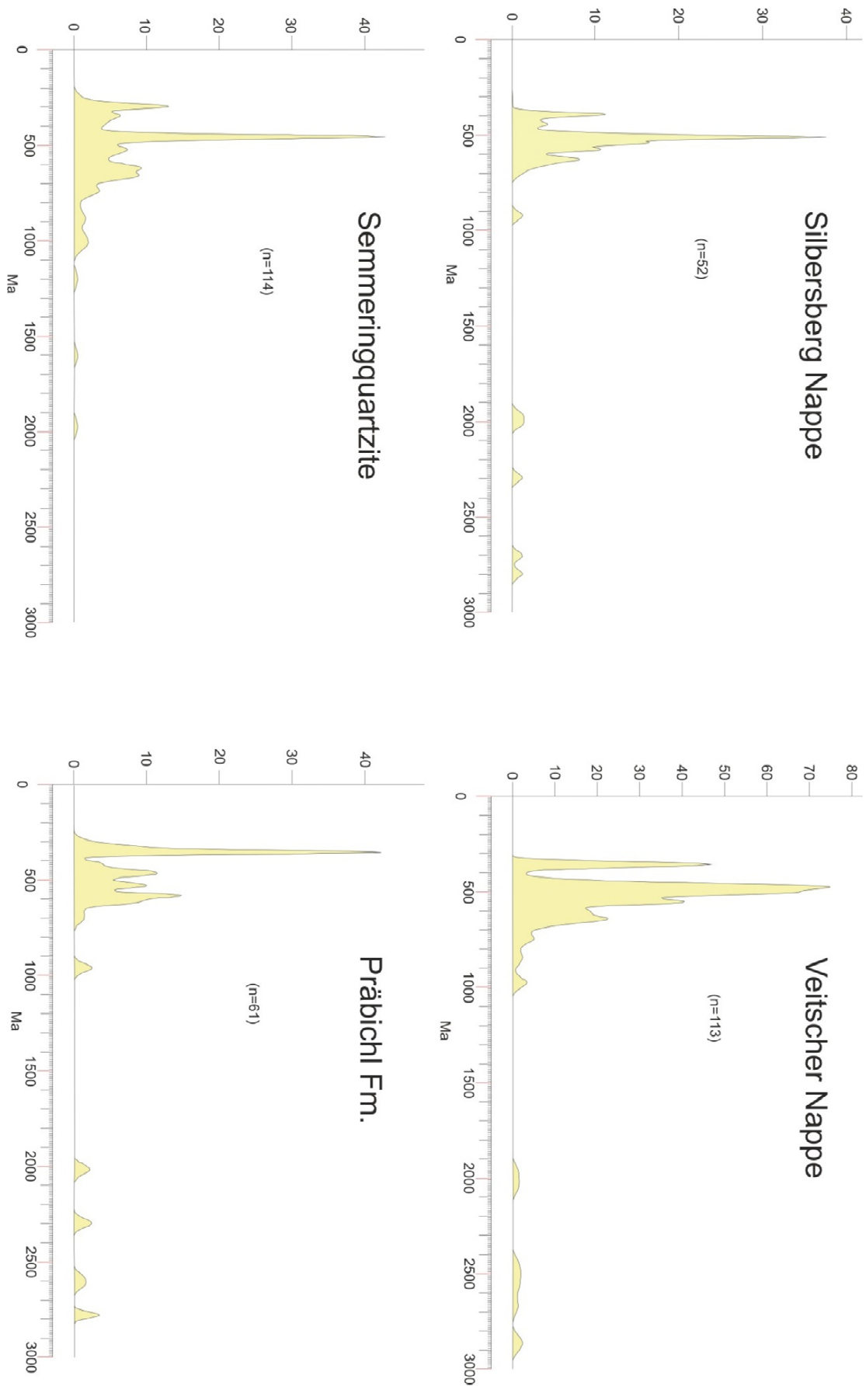

Fig. 43: Representation of the KDE plots of all measured samples with all age clusters.

15.5.6 ***Other possibilities to represent the measured age distributions***

Although the KDE display after Vermeesch, 2012, was used mainly to interpret the age distributions, there are also other calculation and depiction possibilities.

To verify the data, the PDP and the KDE Plot after Vermeesch, 2012, were compared, as well as the Normalized age probability plots and the Cumulative age probability plot after Gehrels, 2007, were produced. Now it was possible to analyse significant deviations of the age group probabilities based on the different methods.

15.5.6.1 PDP – KDE comparison

Both options of depiction are characterised through normal distribution and exhibit age distributions. Vermeesch, 2012, mentions that the PDP Plot is rather problematic to display the age distributions, as the ages are over smoothed and therefore do not show the real probabilities.

The PDP as well as the KDE Plots were produced with the same band width of 8 in order to be up for comparison. In Fig. 44 can now be seen, that all the measured samples depict the same ages with both methods and a small possible difference of 1 Ma or 2 Ma, although the PDP Plot always indicates higher probabilities. The varying statistical computation therefore does not have a significant influence on the age spectra distribution.

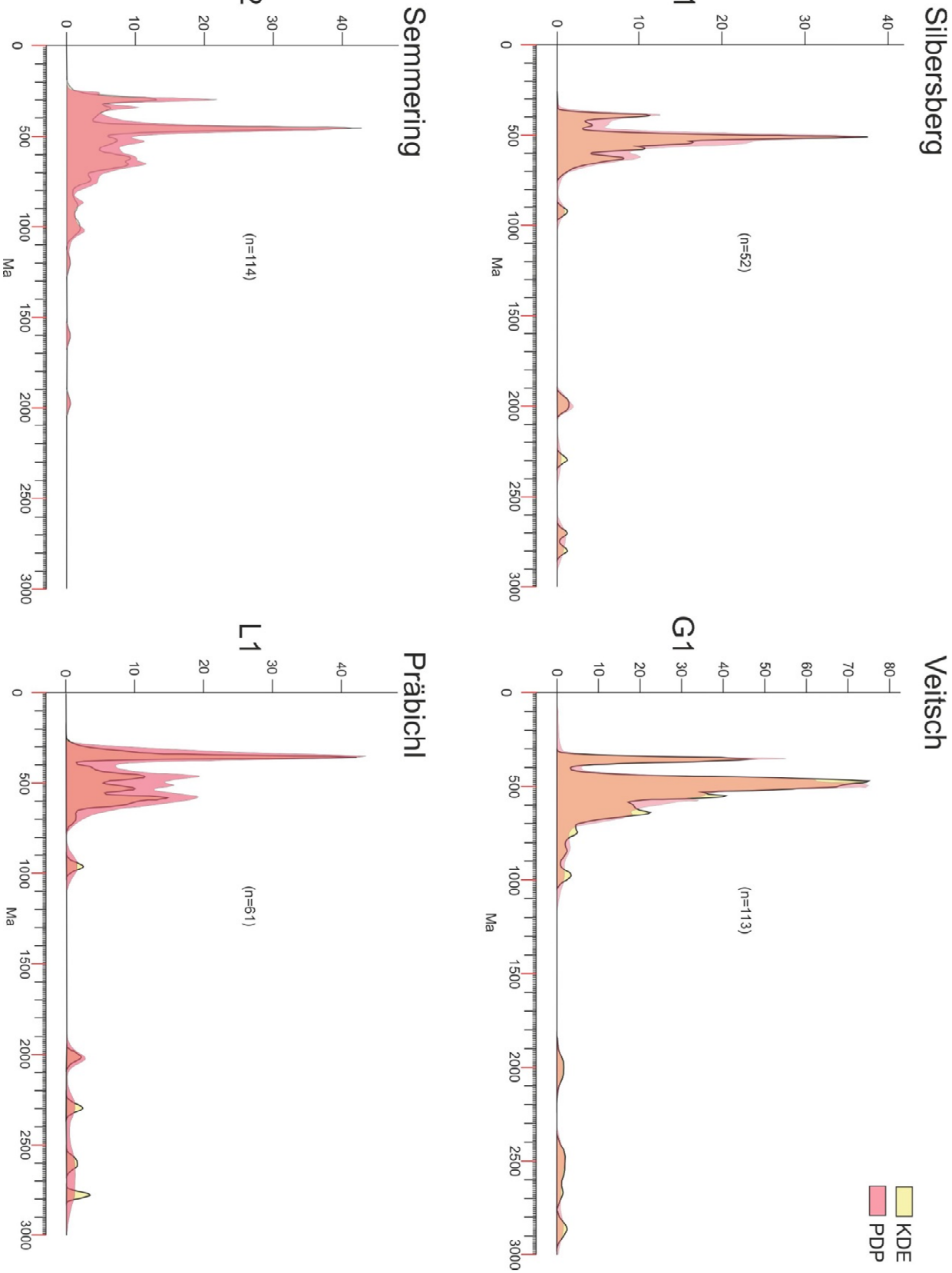

Fig. 44: KDE und PDP plots in a directly compared way. The yellow age spectra represent the KDE diagrams, while red ones are the PDP plots.

15.5.6.2 Cumulative age probability plot

The EXCEL plug-in by Gehrels, 2007, was used to produce a "cumulative age probability" plot and therefore to depict the likelihood of occurrence.

Age gaps are displayed as horizontal parts of curves, as for example in Fig. 45 around 700 Ma. Steep sections of the curve show frequent occurring ages of the different zircon populations.

Ma are seen on the x-axis of Fig. 45 and therefore it is possible to recognise that most of the measured ages are to be found between 250 Ma and 700 Ma. Crossing curve areas depict different zircon populations with e.g. the metasandstone of the Präbichl Fm. having a similar age of 356 Ma which is missing in the Semmering quartzite.

If this plot is applied on the Silbersberg metasandstone, it depicts its strongest steepening between 500 Ma and 550 Ma, which correlates with a Concordia age cluster around 511 Ma (Fig. 38). The equivalent steepening of the Semmering quartzite can be seen between 420 Ma and 480 Ma and therefore confirms the main age group of 459 Ma (Fig. 39).

The main age of the Präbichl metasandstone around 356 Ma (Fig. 41) can also be recognised in the cumulative age probability plot, which displays the main steepening between 340 Ma and 380 Ma.

The curve progression of the Veitscher metasandstone is more complex and therefore it is not possible to reduce the age range further than between 450 Ma and 530 Ma. This age range is still comparable to the two main age groups of this sample at 465 Ma and 498 Ma (Fig. 40).

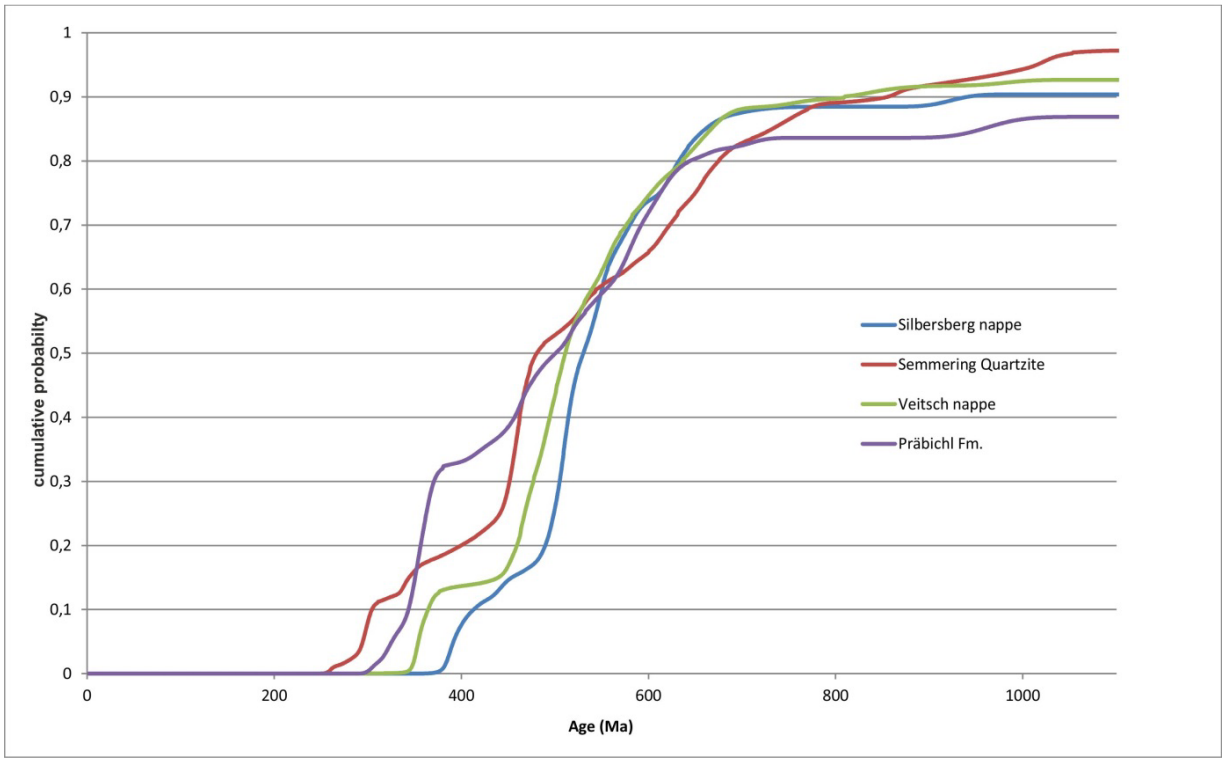

Fig. 45: Depiction of the cumulative age distribution. The x-axis represents the million years, the y-axis shows the cumulative probability of appearance.

15.5.6.3 Normalized age probability plots

The Normalized age probability plot EXCEL plug-in by Gehrels, 2007, was used to compare the data with the Density Plots, plotted through the programme by Vermeesch, 2012.

The comparison of those two methods brought up several significant differentiations to the Density Plots:

The differences of Density Plots and Normalized age probability plots are severe in the Silbersberg metasandstone (Fig. 38, Fig. 46). This sample depicts its main age around 511 Ma and another significant age around 390 Ma in the Density Plots (which correlates with the Concordia Plots), while the plug-in by Gehrels, 2007 solely shows a main age group at 350 Ma.

Similar to the Silbersberg sample, the Semmering quartzite also displays different age distributions in both depiction possibilities. The Density Plot shows a common age group around 459 Ma, while the Probability Plot rather exhibits several age clusters between 380 Ma and 520 Ma (Fig. 39, Fig. 46).

Both plot possibilities are the most alike in the Veitscher metasandstone, where the main age of 465 Ma is shown. Although both display the same main age, another age group of 356 Ma is exclusively shown in the Density Plots, while this age group seems to be shifted to 290 Ma in the Probability Plot (Fig. 40, Fig. 46). Another age cluster of about 498 Ma does not even appear at the Probability Plot.

The main differentiation point of both methods in the Präbichl metasandstone is the most common age group. While the Density Plot exhibits this age around 356 Ma, the Probability Plot possibly combines a few different age groups between 460 Ma and 600 Ma to a bigger one (Fig. 41, Fig. 46).

Because of this obvious mismatching of both Plot methods and the non-conformity of the Probability Plot with the Concordia diagrams at chapter 15.4 (e.g. main age of Silbersberg metasandstone at 511 Ma), the additional plot method of Probability Plot can be rejected.

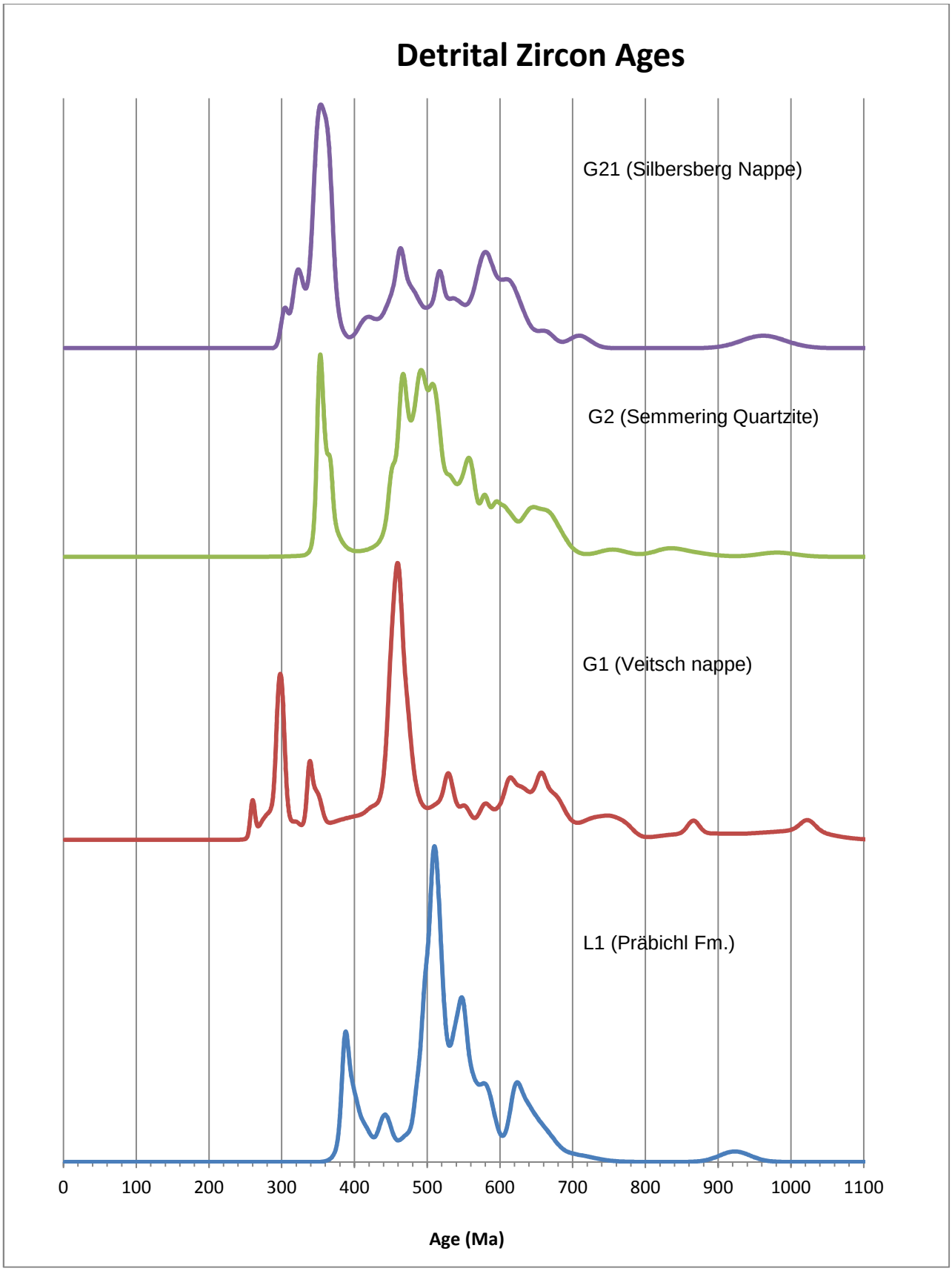

Fig. 46: The age distribution of the measured zircons is represented through the Normalized Age Probability plot (Gehrels, in 2007). The x-axis displays the age in Ma, while the y-axis contains relative values (no units).

15.6 Differentiation of zircon development and the frequency of occurence in the different tectonic settings

In order to be able to interpret the measured samples of the sediments in a proper way, it is necessary to follow the development of their sources during earth's history and identify their origin and the accompanying tectonic setting, as well as their preservation potential.

15.6.1 *Zircon formation and U/Th ratios*

Zircons can grow during a magmatic event or a high grade metamorphic event. Uranium – Lead ratios can be used to differentiate zircons by means of their formation (Rubatto, 2002). This ratio can be classified as following (Rubatto, 2002):

Table 1: Differentiation of zircon formation through the U/Th ratio

U/Th ratio	Origin
<0,1	Metamorphic Origin
>0,1	Magmatic Origin

Although the ppm – contents of Uranium and Lead were not measured it is still possible to use this differentiation, as 99% of the natural occuring Uranium consists of ^{238}U and 100% of the Thorium is ^{232}Th. Due to the relatively high U/Th ratio, it was possible to identify the origin of the zircons as mostly magmatic events, even if the ratios vary strongly from sample to sample (Fig. 47).

The most metamorphic zircons of all the analysed samples can be found in the Silbersberg metasandstone, where the amount of metamorphic zircons decreases with the age. The most characteristic age clusters of this sample are around 511 Ma and 390 Ma, the latter with a percentage of 60% metamorphic zircons. Ages around 511 Ma possesses a lower amount of metamorphic zircon about 15%. Differently as the Silbersberg sample, the Semmering quartzite exhibits just a small percentage of metamorphic zircons, with 30% being the highest amount in the age cluster of 459 Ma and the youngest Concordia age of 297 Ma consisting solely of magmatic zircons. Zircons of the Veitsch Nappe (age groups of 498 Ma, 465 Ma and 356 Ma) are mostly of magmatic origin, with the youngest age being 100% magmatic. Although the magmatic originated zircons are overall dominating, the sample of the Präbichl Fomration is, through the U/Th ratio, the only one solely consisting of them.

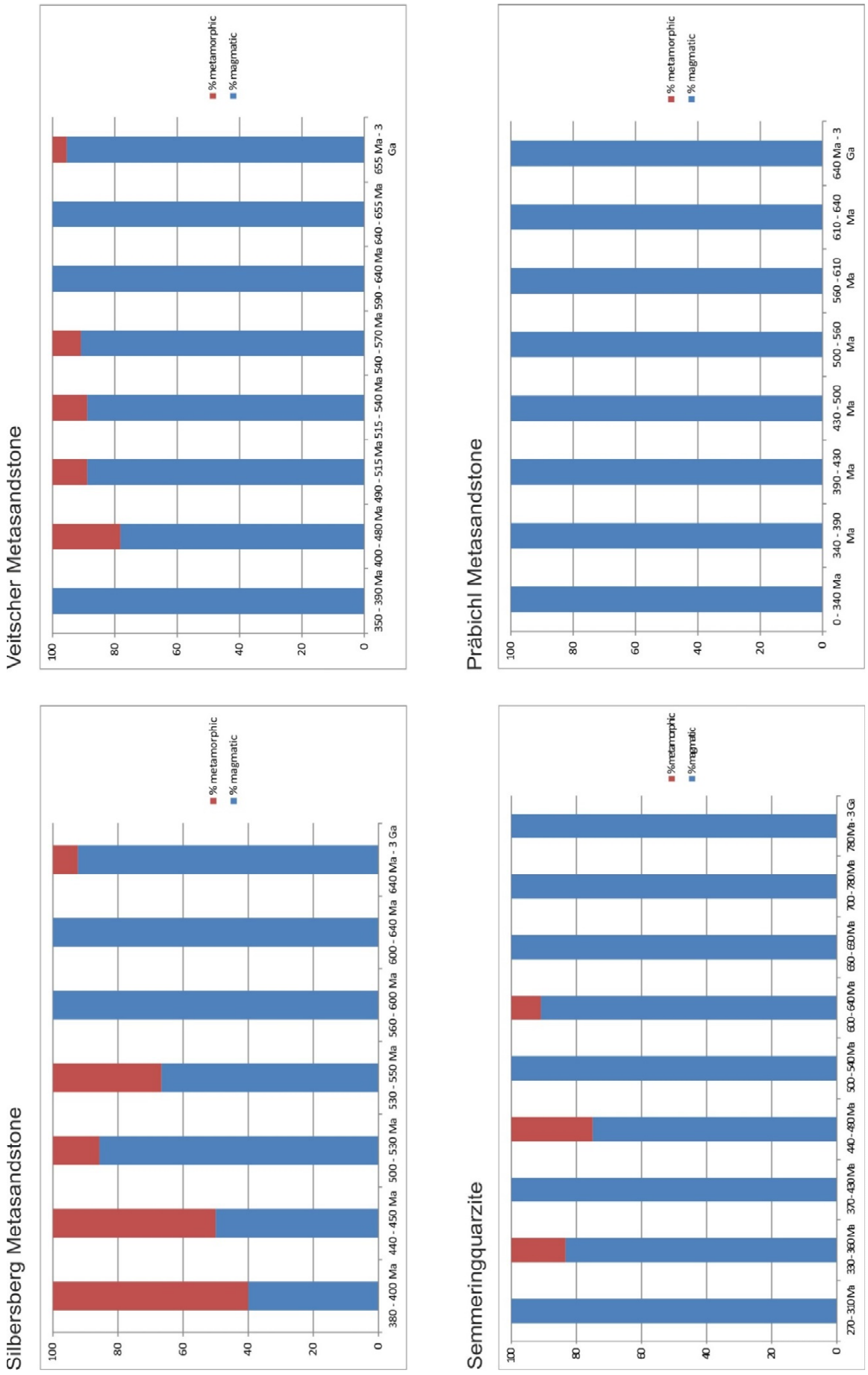

Fig. 47: A chart representation of the differentiation through percentages of magmatic and metamorphic zircons.

15.6.2 *Preservation potential of zircons by means of their tectonic setting*

The potential of preservation of zircon minerals is defined as a function of probability of formation in proportion to the probability of preservation. Most intermediate magma is produced around subduction zones and therefore the formation of zircons is high too. The amount of produced magma volume, as well as the frequency of zircon occurrence, is lower in collisional Orogens and lowest during rifting events which form mainly alkaline magmatites (Cawood et al., 2013; Fig. 48).

Although the magma production is highest around subduction zones, the percentage of produced zircons per magma volume is lower than in collisional areas (Cawood et al., 2013; Moecher & Samson, 2006; Dickinson, 2008). Overall the number of crystallised zircons formed in subduction zones is still higher than in collision phases, as there is also more magma produced (Cawood et al., 2013).

Generally the potential of preservation in a convergent environment and during continental break up is low. During collisional events as well as in the last phase of subduction on the other hand, zircons are distinctly better preserved (Cawood et al., 2013; Fig. 49). Therefore, it is unlikely that zircons formed in a rifting event will be preserved.

The analysed zircons can be mostly identified as magmatic derived and can hence be associated with magmatism at an active continental margin or formation during syn-collisional magmatism.

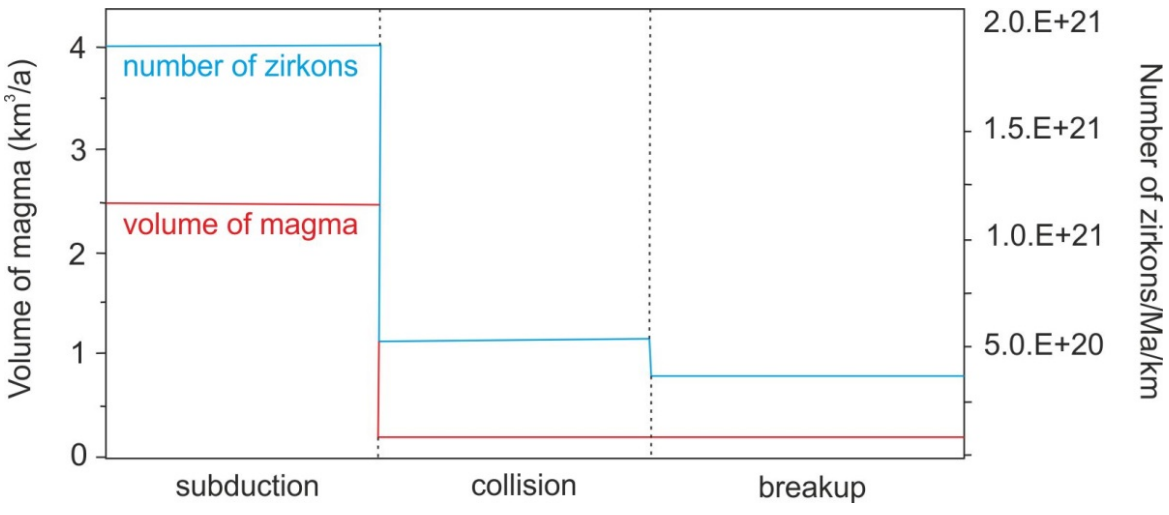

Fig. 48: The number of the originating zircons in comparison to the magma volume is depicted. It is evident that the subduction area, in comparison to other tectonic environments, clearly generates most zircon (by Cawood et al., in 2013).

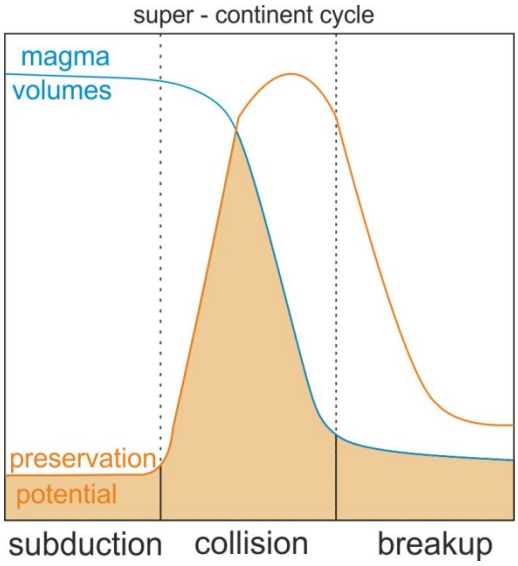

Fig. 49: This picture exhibits the amount in magma volume in comparison to the preservation potential. The marked area represents the balance between the magma formation and preservation in three possible tectonic settings (by Cawood et al., 2013).

15.6.3 *Magmatic zircons and their tectonic settings*

To find out which tectonic setting lead to the formation of the analysed magmatic zircons, diagrams like Fig. 50 were produced. These diagrams base on Fig. 47, where the distinction between magmatic and metamorphic zircons was made.

Zircons formed during magmatic events can be mostly differentiated as volcanic or plutonic derived. While volcanic exemplars (e.g. vulcanite above subduction zones) are known for their long prismatic habit, the plutonic ones (collisional event or root of magmatic arc) develop a short prismatic shape. A third form could be identified, round zircons, which can be explained by prior transportation and cannot be assigned to either magmatic form.

Due to this classification it was possible to relate the analysed zircon samples to different possible tectonic settings.

The magmatic zircons of the Silbersberg Nappe show mainly a volcanic origin, with the youngest cluster at 380 Ma to 400 Ma and another one between 440 Ma and 450 Ma, which lead to long prismatic zircon habitus. Even though the magmatic forms indicate volcanic formation, the source area still suffered a collisional event, as the main percentages of similar aged zircons are metamorphic ones (Fig. 47). Older zircons around 500 Ma to 530 Ma exhibit all three zircon shapes. This could be connected to a denudation during a rifting, as volcanism, plutonism and sedimentation occur.

Two age groups are dominant in the Semmering quartzite, 297 Ma and 459 Ma (Fig. 39). The younger zircons are mainly volcanic with only about 20% of plutonic origin, while the older ones about 459 possess all zircon forms, although the volcanic ones prevail. Because of the relatively high amount of metamorphic zircons in the older age group of the quartzite, this age could be correlated to an orogeny. The youngest age possesses a volcanic percentage of 80%, with 20% plutonic ones, and can therefore be associated with a volcanic event.

The ratio of metamorphic to magmatic zircons and the high magmatic zircon occurrence in the Veitsch Nappe sample is similar to the one in the Semmering quartzite. Ages around 498 Ma, 465 Ma and 356 Ma (Fig. 40) are interpreted as the most important ones, with the youngest and the oldest one being connected with an active continental margin. They differ with their amount of metamorphic and magmatic zircons, which leads to the assumption that they have been at different positions on the active margin at different times. Most metamorphic zircons of this sample can be found at the age cluster around 465 Ma, which exhibit as many volcanic as plutonic specimen and are therefore assigned to an orogeny.

Just magmatic zircons can be found in the metasandstone of the Präbichl Formation, which display their main ages around 578 Ma, 466 Ma and 356 Ma (Fig. 41). The first age cluster is dominated by plutonic forms and is interpreted as derived from a plutonic, granitic magmatism. As the distribution of plutonic and round zircons at the age group of 466 Ma is 50:50, with a small amount of plutonic ones, an active continental margin can be assumed as the setting of origin. The main age group of 356 Ma is dominated by volcanic zircons, with a lower percentage of plutonic and round forms, and is also associated with an active continental margin.

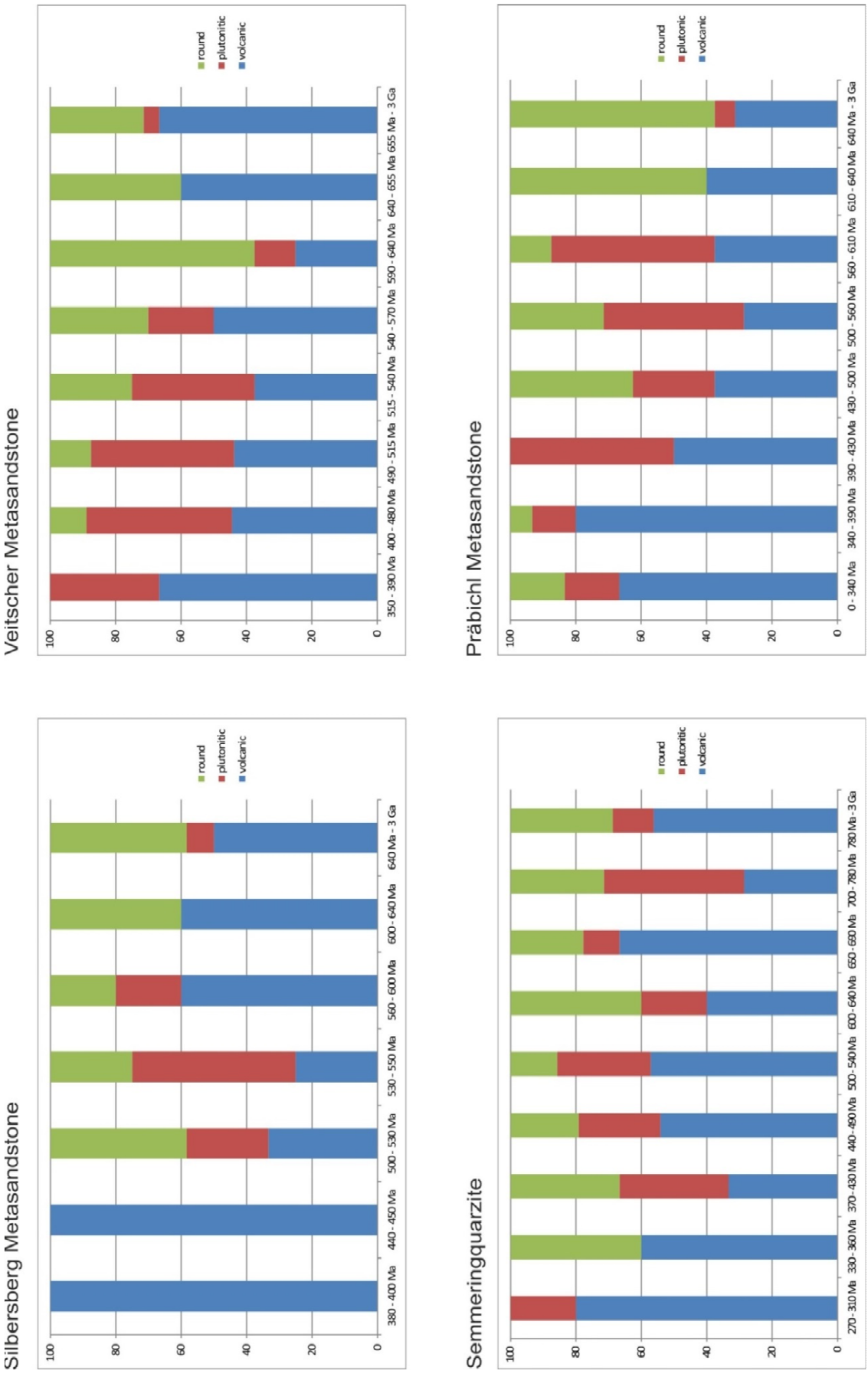

Fig. 50: This graph representation depicts the percentages of long prismatic forms (volcanic zircons), short-prismatic forms (plutonic zirkons) and round forms (sedimentary zircons).

15.7 Plate tectonic developments during Earth's history

The comprehension of the stage of devlopment of the plate tectonic situation during the Phanerozoic and Neo-Proterozoic is significant to be able to interpret the zircon data and therefore this overview was created. It should be mentioned that the plate tectonic model by von Raumer et al. (2002, 2003) and von Raumer & Stampfli (2008) was mainly considered, as it is a consistent paleogeographical depiction. This model additionally exhibits the most plausible arrangement of oceans and continents, which can be associated with the analysed zircon age patterns. The numeric ages (e.g. 390 Ma) and their connected eras and stages are after the stratigraphical chart of Cohen et al., 2013.

15.7.1 *Pre-Cambrian*

At the end of Pre-Cambrian times the African continent was the centre of the super continent Gondwana and consisted of various Archean cratons and Paleo- Meso- and Neoproterozoic girdles (Abdelsalam et al., 2002). Zircons which exhibit ages around 2.5 Ga can be correlated with the cratons of Africa, while the only Paleoproterozoic ages (2.5 Ga - 1.6 Ga) can be found in East Africa at Usagaran and Ubedian Belt, which are east and southwest to the Tanzania craton (Fritz et al., 2013). Most zircons of these belts possess ages around 1.8 Ga and can be identified due to their Mesoproterozoic age gap (e.g. Fritz et al., 2013). Solely the Irumide Belt of Mosambique exhibits Mesoproterozoic ages (1.6 Ga to 1 Ga; Fritz et al., 2013). Ages between 1.3 Ga and 0.9 Ga (Grenville ages) are typically found in Western Africa (Linnemann et al., 2007). These West African shields consist of Archean and Paleoproterozoic granites and gneiss, which are overlain by Late Proterozoic to Phanerozoic sediments. West Africa and Brasiliano (1.3 Ga - 1.1 Ga) are mainly characterised through the Grenville Orogeny (1.3 - 0.9) after Linnemann et al., 2007. Therefore, West Africa as well as South America could be excluded as origin for the analysed samples, as both are dominated by the Grenville Orogeny and the samples do not exhibit such age cluster (Linnemann et al., 2007; Fig. 44). Ages between 1.1 Ga and 0.9 Ga on the other side are considered to be originated of the Arabian Nubian Shield (ANS), as several magmatic arcs were formed there (Fritz et al., 2013).

This information leads to the assumption that East Africa and the bordering Sahara metacraton can be identified as the origin of the older analysed zircons.

The ages between 1000 Ma and 800 Ma are characterised through the break-down of Rodinia, which lead to a sea floor spreading and the formation of voluminous island and magmatic arcs and therefore to frequencies in the zircon data between 900 Ma and 1000 Ma (Johnson et al., 2011). This is connected to the "Proterozoic Mantle Mobilisation Event", which is also documented in some Austroalpine units and the Penninic rocks of the Alps (Johnson et al.,

2011; von Raumer et al., 2013). It also led to magmatic events during the ongoing consolidation of Gondwana because of the accretions in the Arabian Nubian shield between 900 Ma and 600 Ma (Johnson et al., 2011).

Between 890 Ma - 710 Ma and 640 Ma - 580 Ma closures of oceans and formation of island arcs and granitoids happened (Johnson et al., 2011). This is the reason for the numerous granitoids in the ANS, which are connected to development and the break-up of Gondwana. The ANS can hereby be seen as the suture between West and East Africa (Linnemann et al., 2007; Sirevaag et al., 2016). East Africa is generally characterised through granitoids of 650 Ma to 550 Ma ages.

After Johnson et al., 2011 there are different groups of Cryogenic-Ediacaric magmatism in the ANS:

- *Syn-collisional calc-alkaline accretion - granitoids: 650 Ma - 610 Ma.* These granitoids are typically connected to TTG suite and exhibit an island arc formation during the East-West Gondwana convergence
- *Post-collisional alkaline granitoids: 620 Ma - 550 Ma.* These granitoids are to be found in Northern Africa and are connected to the break-up of Africa. This break-up was induced due to a northward extrusion, which was assigned to mantle delamination around 570 Ma. Due to that delamination a subduction zone was formed which is declared as Avalonian-Cadomian-Active-Margin in the north of Gondwana (Linnemann et al., 2007).

The change of magmatism, in relation to the mantle delamination, lead to a northward detachment of some continental Gondwana derived blocks in the Late Pre-Cambrian (Candan et al., 2015).
This detachment can be arranged into three main steps (between Late Cambrian and Carboniferous):
Firstly, the Avalonian blocks drifted off in the Early Ordovician, which was later followed by the European Hun-Terrain in Late Silurian and concluded by the eastern Asiatic Hun-Terrain in the Early Devonian (von Raumer et al., 2002).

15.7.2 ***Cambrian***

The Cambrian is mainly characterised through extension phases (von Raumer & Stampfli, 2008). North of Gondwana existed a active margin, which is also called Avalonian-Cadomian-Active-Margin (Linnemann et al., 2007), and at the border back-arc movements formed during Early and Middle Cambrian, which are known as Cadomian back-arc (von Raumer & Stampfli,

2008; Linnemann et al., 2007). After the characterisation of Linnemann et al. (2007) the biggest amount of the analysed samples should have been somewhere near this back-arc during the Cambrian (Fig. 67, Fig. 68, Fig. 69).

Simultaneously intra-continental rift basins formed at other places, which were connected to a post-Pan-African extension phase, especially in Africa (von Raumer & Stampli, 2008). These Cadomian-Pan-African events are also documented in age data of detrital white mica in the Austroalpine (von Raumer et al., 2013; Neubauer et al., 2007). During the Upper Cambrian, Avalonia started to rift off of Gondwana and therefore opened the Rheic ocean and formed oceanic crust, which is seen as an oceanisation of margin correlated basins in relation to back-arc rifting (von Raumer & Stampfli, 2008; von Raumer et al., 2002; Domeier & Torsvik, 2014). The sample of the Silbersberg metasandstone is the only one containing this event (Fig. 66).

Chemical data of the Bohemian Massif by Floyd et al. (2000) was interpreted by Crowley et al. (2000) as Cambrian continental break off as a consequence of mantle plume formation during time. Mantle plumes played an important role as a preparation of the rifting of the Rheic ocean, but rifting as cause of tension on the plate margins during the ongoing back-arc opening is similar important for the positioning of the oceanic basins (von Raumer at al., 2003).

The Alps exhibit this tectonic evolution in the Speik complex of the Gleinalpe (Melcher & Meisel, 2004). This complex includes the Kraubath serpentinites, which possess an age of around 550 Ma, and show an oceanisation in the north of Gondwana as a result of the first off drifting of Peri-Gondwanan-terrains (Melcher & Meisel, 2004). Further clues for this oceanisation during Upper Cambrian to Early Ordovician times are the Chamrousse ophiolites in France, which display ages of 500 Ma and document the first rifting as relics within this ophiolites are similar to the Rheic ocean (von Raumer & Stampfli, 2008; Ménot et al., 1987, 1988). Garnet-hornblende-plagioclase gneiss of the Silvretta group also depict ages of 532 Ma and are interpreted as oceanic derived plagiogranites, which are seen as part of an ophiolite sequence which formed during the break-up of the Gondwana continental shelf during the Cambrian (Müller et al., 1996, Faryad et al., 2002). These can be correlated with the Ötztal-Stubai nappe eclogites (530 Ma - 521 Ma; Faryad et al., 2002).

15.7.3 ***Ordovician***

The Ordovician times continued with the rifting and seafloor spreading, which was combined with sedimentation gaps, thermic uplifts and ongoing volcanic evolutions (von Raumer & Stampfli, 2008; von Raumer et al., 2013). During Late Cambrian and Early Ordovician (500 - 480 Ma) the break off of Avalonia was finalised and followed by a northward drifting, which lead to the opening of the Rheic ocean (von Raumer et al., 2002; Domeier & Torsvik, 2014; see 490 Ma at Fig. 51). This event is mainly to be recognised in the sample of the Veitscher metasandstone (Fig. 40). The break off was induced by the subduction of the middle oceanic ridge of the Proto-Tethys (von Raumer et al., 2002). Within the eastern continental blocks the northward drifting of Avalonia and therefore the opening of the Rheic ocean was hindered by the still existing oceanic ridge of the Proto-Tethys (von Raumer et al., 2003). Therefore, the east was a witness to the Ordovician collison, which was the collison of the former detached terrains with Gondwana as those terrains drifted back and destroyed the eastern Rheic ocean (von Raumer et al., 2003; von Raumer, 1998; von Raumer & Stampfli, 2008, see 440 Ma at Fig. 51). This eastern arm of the Rheic ocean was thereby subducted beneath Gondwana (von Raumer et al., 2002).

Within the Avalonian terrains amalgamation of volcanic arcs and continental ribbons with Gondwana happened (von Raumer et al., 2003; von Raumer, 1998), which lead to the closure of the Cambrian back-arcs and to the stacking of the Cambrian Chamrousse ophiolites (von Raumer & Stampfli, 2008). This event, which is also known as Ordovician orogeny, was short lived (von Raumer et al., 2002; von Raumer et al., 2003), but exhibited in nearly all of our analysed samples, except the Silbersberg metasandstone (Fig. 42).

The Ordovician collision conducted a complex terrain assemblage on the northern margin of Gondwana, which is known as Noric composite terrains or Hun-Superterrain (von Raumer et al., 2002; Frisch & Neubauer 1989; Stampfli, 1996), and contains an accretion wedge, volcanic arcs and parts of the eastern Rheic ocean as well as the Middle Ordovician suture of the failed eastern arm of the Rheic ocean (von Raumer et al., 2002, 2003). Parts of this suture, which are also known in the Alpine area, were accreted and thrusted on the Gondwana margin (Stampfli et al., 2002). The Hun-Superterrains is further an accumulation of continental blocks, which include Armorica, the inner alpine Basement and microcontinents which were part of the eastern Avalonia (von Raumer et al., 2002; Stampfli, 1996).

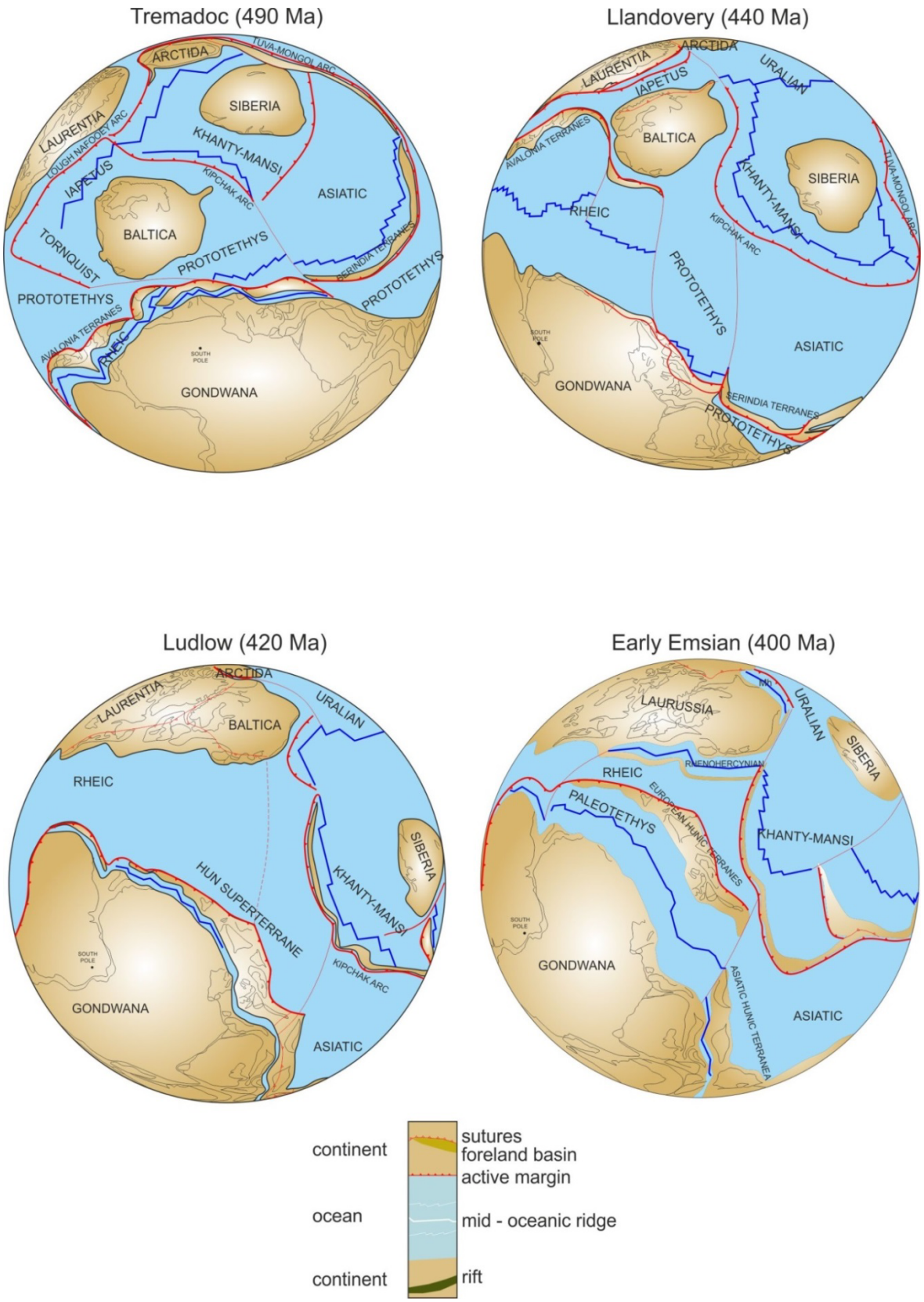

Fig. 51: Representation of the paleogeographical situation of the Late Cambrian till Early Devonian (after Stampfli & Borel, 2002). This depiction of the Tremadoc represents the detachment of Avlonia and the associated origin of the Rheic ocean. The Llandovery is characterised through the Ordovician orogeny in the eastern part due to the reunion of East-Avalonia with Gondwana. Ludlow displays the final detachment the now merged Hun terrain (opening Paleotethys) and the following Emsian exhibits the convergence of the Rheic ocean, as well as the opening of the Rheno-Hercynic ocean and the conditioned splitting off of the Hanseatic-terrain.

After Avalonia was separated from Gondwana, the plate tectonic evolution of the eastern microcontinent started to be different, and therefore Armorica and the inner alpine basement developed in another way from now on (von Raumer et al., 2002; von Raumer & Stampfli, 2008). At the same time porphyroids and granitoids were formed because of the subduction of the middle oceanic ridge and after von Raumer et al. (2013), magmatic pulses around 490 Ma, 480 - 470 Ma and 460 - 450 Ma can be identified (Stampfli et al., 2002). This subduction zone was the reason for a back-arc spreading during Middle Ordovician times, which ultimately induced the opening of the Paleotethys in Silurian (Stampfli et al., 2002). The opening of the Paleotethys can be connected with two rifting events, one of them happening in the Late Ordovician and the second one in the Silurian (von Raumer et al., 2013). The Silurian event was connected to flood basalts and lead to the main opening of the Paleotethys and went on until Devonian (von Raumer et al., 2013). The western part of Avalonia drifted from Early to Middle Ordovician northwards, towards Baltika and Laurentia (Golonka, 2000; 2002; 2009; 2012; Golonka & Gaweda, 2012).

Magmatic rocks played an important role during the plate tectonic development of the Gondwana derived microcontinents in Cambrian and Ordovician times (von Raumer et al., 2003). Maniar und Piccoli (1989) produced a diagram for plate tectonic differentiation, which exhibits the trend of a chemical development of magmatic rocks over time. The granitoids plot thereby in fields, which are attributed to a specific plate tectonic position (Maniar und Piccoli, 1989). Cambrian plagiogranites of different localities, e.g. Chamrousse or Silvretta plagiogranites, are connected to formation of oceanic crust during the opening of the Rheic ocean (von Raumer et al., 2003). Cambrian and Early Ordovician alkaline granitoids represent rifting phases of thicker crust, which were also in relation with the opening of the Rheic ocean (von Raumer et al., 2003). Early Ordovician calc-alkaline metaluminous granites are possibly connected to a Cambrian-Ordovician active margin, while younger 450 Ma calc-alkaline peraluminous granitoids rather bear characteristics of a post-orogenic development (von Raumer et al., 1999, 2002, 2003). The chemical development of those granitoids reflects the overall evolution of the Cambrian-Ordovician rifting, the Cambrian-Ordovician active margin and the Ordovician collision (Stampfli et al., 2002).

Around 480 Ma to 470 Ma, voluminous calc-alkaline volcanites were formed and their relicts can be identified in Spain, Massif Zentral and the Bohemian Massif, as well as in the Alps (von Raumer et al., 2002). Ordovician ages are overall common, as they appear in the Carpathians (e.g. 480 Ma - 470 Ma, Putis et al., 2008), in the Western Alps and in the Penninic units of the Tauern Window (488 Ma, Eklogit, von Quadt et al., 1997). Further occurences of these ages are

in the Austroalpine, west and south of the Tauern (470 Ma - 450 Ma, Schulz et al., 2008; Gabbros and Granitoids of about 510 Ma - 470 Ma, Schaltegger et al., 1997) as well as in the Gleinalmkristallin (480 Ma, Neubauer et al., 2003).

During Middle Ordovician times (460 Ma) felsic magma emplaced in the Greywackezone (Blasseneck Porphyroid, 468 Ma, Söllner et al., 1991, Loth et al., 2001), in the Carnic Alps (Comelico Porphyroid, Hubich und Löschke, 1993) and in the Gurktaler nappe (Golzeck Porphyroid, Neubauer & Pistotnik, 1984, Hubmann et al., 2013).

The mountain chain which developed during the Ordovician as result of the subduction of the middle oceanic ridge of the Proto-Tethys, was already decaying during Late Ordovician, which lead to a rift opening of the future Paleotethys in the following Silurian times (von Raumer et al., 2003; Stampfli, 2000).

15.7.4 *Silurian*

The time periods which followed after the Ordovician amalgamation, is characterised through successive subduction steps and up-building of an accretion wedge as well as arc volcanism on the active margin of Gondwana (von Raumer et al., 2002).

The formation of an active margin on the northern Hun-Superterrain margin during Early Silurian times supports the south directed subduction zone of the Rheic Ocean (von Raumer et al., 2002; Stampfli et al., 2002). Eclogites of the Tauern Window exhibit the Silurian events (von Raumer et al., 2002; von Quadt et al., 1997) and Late Ordovician to Silurian crustal extension periods and riftings lead finally to the opening of the Paleotethys (von Raumer et al., 2013).

During the Late Silurian the Hun-Superterrain detached of Gondwana and opened the Paleotethys (von Raumer at al., 2002; see 420 Ma in Fig. 51). This opening is represents a back arc opening along the Gondwana margin and is connected with the Gondwana directed subduction of the Rheic ocean (Stampfli et al., 1991, 2002; Stampfli, 2000; von Raumer at al., 2002). Paleomagnetic data indicate a northward, Laurussia directed, drifting of the Hun-Superterrain after the final detachment (von Raumer et al., 2002; Bachtadse et al .1995; Schätz et al .1997; Tait et al .1998; Torsvik et al .1994; Torsvik and Eide 1998). Silurian flood basalts occurred simultaneously with the beginning of the seafloor spreading (Stampfli et al., 2002). The Pre-Variscian blocks detached at different times from Gondwana and assembled again during the Variscian orogeny (von Raumer et al., 2003).

Data of the Alps of Schaltegger (1993), Thöni & Miller 2004(Ötztal) and Schulz et al. (2003, 2004) exhibit a Silurian rift event between 450 Ma and 430 Ma. The extension and subsidenz

at the passive margin is known from the Greywackezone, the Paleozoica of Graz, the Gurktaler nappe and the Carnic Alps (Hubmann et al., 2013).

Avalonia collided with Baltica during Late Ordovician-Early Silurian and eventually also with Laurentia in the Middle Silurian (Golonka & Gaweda, 2012). This collision is known as the Caledonian orogeny and from then on the continents Baltica, Avalonia and Laurentia were summed up as Laurussia (Golonka & Gaweda, 2012).

15.7.5 ***Devonian und Carboniferous***

In the following Early Devonian the eastern, Asiatic Hun-Terrain detached from Gondwana (Stampfli et al., 2002). Armorica and the other Hun-Terrains (Ligeria and Galatia), which formed a ribbon-like, not necessarily connected Superterrain, were not far from Gondwana in Early Devonian (Stampfli et al., 2002; von Raumer et al., 2013). The terrain consisted of an active margin with high pressure girdle to the north and a passive margin at the south (Stampfli et al., 2002, 2011, von Raumer et al., 2013). Its passive margin lead to a formation of platform carbonates at certain areas during the Upper Devonian/Lower Carboniferous. A roll-back of the Rheic plate against Laurussia after the Ordovician subduction of the middle oceanic ridge was the reason for the drifting off of the European Hun-Terrain of Gondwana during the Middle Devonian (Stampfli et al., 2002).

The strong forces of the subduction of the Rheic plate induced rift events within the southern passive margin of Laurussia during the Early Devonian and lead to the opening of the Rheno-Hercynian basin (Stampfli et al., 2002; see 400 Ma at Fig. 51). Its oceanic nature is verified through ophiolitic relicts and pelagic sediments, e.g. within the Harz nappes (Stampfli et al., 2002). During this rift event several blocks detached from Laurussia (Hanseatic terrain), which collided eventually with Armorica in the Middle Devonian (Stampfli et al., 2002, von Raumer et al., 2013; see 380 Ma at Fig. 52). The collision between the Gondwana derived European Hun-Terrains with those from Laurussia formed an accretion of a bigger terrain along the European part of the passive continental margin of Laurussia, which resulted in the final closure of the Rheic ocean (Stampfli et al., 2002). This Middle Devonian eo-Variscian high pressure event

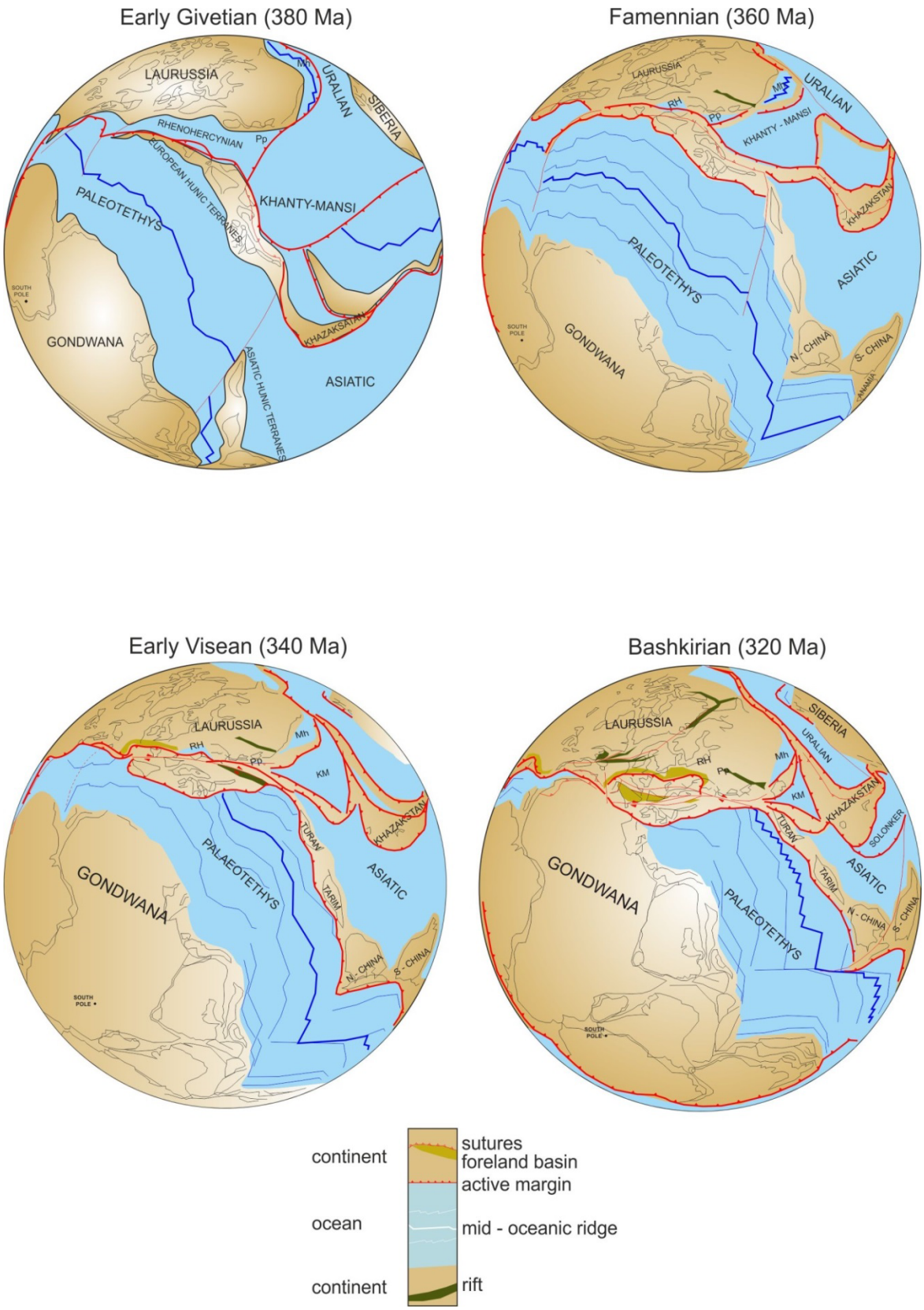

Fig. 52: Depiction of the paleogeographical situation during Middle Devonian till the Late Carboniferous (by Stampfli & Borel, 2002). During the Early Givetian the collision of the Hun terrain with the Hanseatic-terrain already had taken place. Many strike slip movements as well as the linked NW directed movement induced the Early Visean closure of the Rheno-Herzynic ocean and the collision of the Hanseatic Hunic terrain with Laurussia. The Bashkirian is characterised through the closure of the Paleotethys in the west and the correlated collision of Gondwana with Laurussia and therefore the formation of Pangea.

can be seen in mostly all metamorphich areas of the Variscian orogeny, as well as in the Silbersberg metasandstone sample (Stampfli et al., 2002; Fig. 38).

Some terrains suffered a strong metamorphism, while others were affected by it later in the Visean (Middle Carboniferous 340 Ma; Stampfli et al., 2002). The formation of Flysch started in some areas not before the Late Carboniferous (310 Ma), so some blocks were not involved in the first phase of metamorphism because of their position as just the front margin of the Superterrain was affected and in connection with the subduction and suture of the Rheic ocean (Stampfli et al., 2002). The northern part of the Superterrain is interpreted as active continental margin, while the other areas were excluded of those tectonic and thermic activities and formed a passive margin (Stampfli et al., 2002). Until the Late Devonian this situation was predominate, but in the Carboniferous strike slip events occurred in the eastern part of the Superterrain, which induced a west directed movement and collisions within the terrain and therefore consolidated the Hun-Terrain and the Hanseatic Terrain, which can be seen in the samples of the Veitsch Nappe and Präbichl Formation (Stampfli et al., 2002, von Raumer et al., 2013; see 360 Ma at Fig. 52; Fig. 40, Fig. 41).

Connected to those collisions were widely spread Flysch formations, e.g. Hochwipfelflysch, and lead to a first up-building of the Viseanic mountain belt and the closure of the Paleotethys (Stampfli et al., 2002; Diener et al., 2001). A confirmation of these events is to be found in petrographical and geochemical investigations of the Hochwipfelflysch, which exhibits Viseanic and Westfalic ages (Diener et al., 2001). Examinations showed that there was a pattern of strike-slip affected deposition areas for the Hochwipfel sedimentation, which lay along the northern active margin of the Paleotethys (Diener et al., 2001). REE-analysis further displayed an increase of volcanogenic input (Diener et al., 2001). The collisions also induced a stacking of basement nappes (von Raumer et al., 2013).

The suture of the Rheic ocean is indicated along the northern active margin of the Hun-Terrain (between Hanseatic and Hun-Terrain), while the Paleotethys suture was positioned at the southern border of the Superterrain (Stampfli et al., 2002, 2013). Because of the former subduction of the Rheic ocean on the northern margin, now high temperature deformations in the connected continental block of Armorica, Ligera and Galatia occurred, especially along the former through eclogites defined suture (around 350 Ma; von Raumer et al., 2013).

Gondwana eventually collided with Laurussia during Late Carboniferous. Laurussia now contained the former accreted terrains (Hanseatic-Hunnic-Terrain), because of the former closure of the Paleotethys in the West (Stampfli et al., 2002; see 320 Ma at Fig. 52). This

suggests an accretion of the European Hun-Terrains on Laurussia due to the northward subduction of the Paleotethys, which changed the passive margin of the Hun-Terrain to an active one, and a southward subduction of the Rheno-Hercynian ocean (Stampfli et al., 2002, 2013). This indicates that there has been an active margin at the northern and southern margin of the Hanseatic-Hun-Terrain. The subduction of the middle oceanic ridge of the Paleotethys triggered later the final Variscian orogeny, which was during the Carboniferous (Stampfli et al., 2002; see 300 Ma at Fig. 53).

The eo-Variscian event is represented in the Alps, e.g. in the Ötztal eclogites (380 Ma), which were later overprinted by a granulite formation (e.g. Hoinkes et al., 1997).

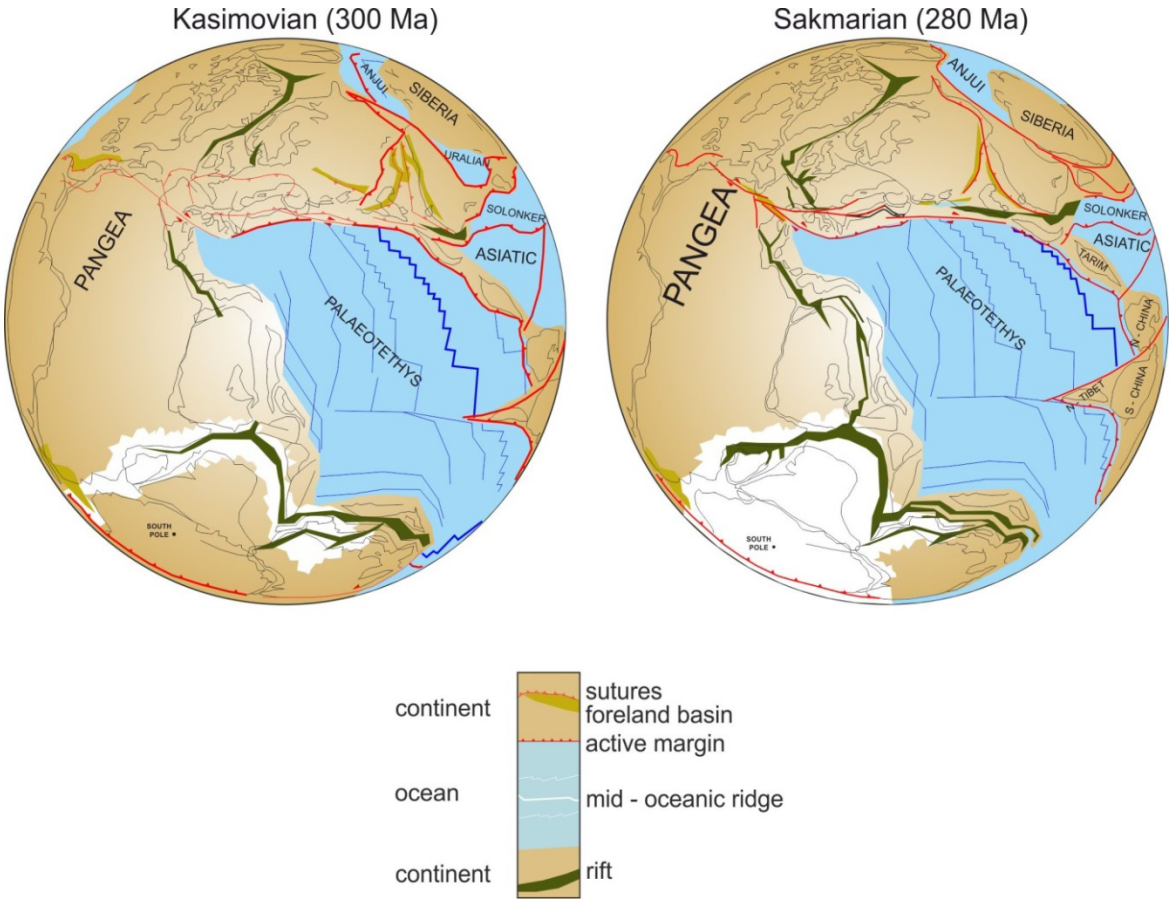

Fig. 53: Representation of the paleogeographical situation of the Late Carboniferous to Early Permian (by Stampfli & Borel, 2002). During the Kasimovian the formation of Pangea was finished and the rifting phases started in the Sakmarian, which are typical for the Permian.

15.7.6 ***Permian***

From the Late Carboniferous on, the subduction of the Paleotethys caused a slab roll-back which lead to extension events in the Variscian orogeny from the Early Permian on (Stampfli et al., 2002; see 280 Ma at Fig. 53). These north to south directed extensions triggered the opening of numerous back arc basins during Early Permian, which formed basaltic magma in earth's mantle and partly melted the lower crust because of the thinning of the lithosphere (Stampfli et al., 2002, Schuster & Stüwe, 2010, Schuster et al., 2013). Only the Semmering quartzite depicts the Permian event (Fig. 39).

During Permian times also wide spread quartz rich volcanism happened, as some of the magma reached earth's surface (Schuster & Stüwe, 2010, Schuster et al., 2013).

The Variscian evolution can be differentiated into three phases after von Raumer et al., (2013):

- Subduction of the oceanic crust beneath Gondwana, Laurussia as well as opening of Paleotethys
- Visean collision, between Laurussia and Peri-Gondwanan terrains
- Final collision of Gondwanan with Laurussia and the correlating subduction of the Paleotethys

Due to the Variscian orogeny, Carboniferous strike slip events occurred as well as rotation to suture duplication (von Raumer et al., 2002; Edel, 2000, 2001).

15.7.7 ***The development of the Alps during the Pre – Variscian and Variscian events***

The Alpine Realm is connected to the northern margin of Gondwana and was after von Raumer et al. (2013) affected by the following events:

- Active margin at northern part of Gondwana during Neoproterozoic and Early Cambrian times (e.g. Penninic & Austroalpine basement, Frisch & Neubauer, 1989)
- Complex Ordovician development at the northeastern margin of Gondwana with connected intra-arc magmatism and extension, as well as subduction, collision and the correlating opening of the eastern Rheic ocean
- Passive continental margin from the Late Ordovician on and following crustal extension, which continued until the Devonian opening of the Paleotethys
- Polyphase convergence and collision events during the Middle Devonian to Lower Carboniferous

Those events can be related to various rocks of the Alps:

Island arc metadiorites, which can be found in the Silvretta nappe, exhibit an age of 610 Ma and also show gabbroitic and tonalitic intrusion of an 520 Ma - 530 Ma age, which were eclogitised and are connected to an active margin (von Raumer et al., 2013).

The basement of the Austroalpine suffered a stepwise magmatic development which formed I- and S-type granitoids which display ages between 470 Ma and 450 Ma (von Raumer et al., 2013). Additionally a 450 Ma to 430 Ma old thermic events, which is associated with anatectic melt, can be identified within the Alpine Realm. This lead to an emplacement of 450 Ma old gabbros and to an extrusion of acidic volcanic rocks in the Noric terrain and are interpreted to be an indication for a diverging crust (von Raumer et al., 2013).

Further examples can be found in the Grazer Paleozoic with the alkali metabasits and Early Silurian middle oceanic ridge basalts and intra plate basalts, which formed because of the Late Ordovician to Silurian crustal extension phase (Fritz & Neubauer, 1988; von Raumer et al., 2013).

Within the alpine area also intrusions of granitic and meta-alkaline rocks developed during Silurian times, which can now be looked on at the Alpine tholeiitic and alkaline within plate basalts of 430 Ma age in the Ordovician units of the Austroalpine basement (von Raumer et al., 2013). Visean flysch initiated the Late Variscian events in the Austroalpine and can be traced in the pelagic depositions of red limestone and radiolarite (von Raumer et al., 2013). Some Variscian granites, resulting from the Viseanic collision, can be found within the Alps as I-type granites of a 330 Ma age and high K-Mg type of 330 Ma to 340 Ma age (von Raumer et al., 2013).

During the Late Carboniferous the Alpine basement was subjected to strong exhumation and erosion, which lead to a deposition of molasses-like detritic sediments throughout the Alps (von Raumer et al., 2013).

Around 300 Ma to 250 Ma there can be indications found which are connected to high temperature low pressure events in the Austroalpine, which are a result of crustal extension and correlate with pegmatites along the southern Ötztal basement, south of the Tauern window and along Kor- and Saualpe (von Raumer et al., 2013; Thöni, 1999).

15.8 Interpretation of zircon ages and connected plate tectonic positions on the basis of cross sections

Zircon populations of clastic sediments contain information about dynamic developments of the source area, which contains in this case, the time between Archean and Permian. This information helps to reconstruct the possible development, which can be depicted as a migration of crustal blocks over time in paleogeographical maps. If the source areas underwent separate evolutions, a reconstruction would be simple. As this is seldom the case it has to be expected that single crustal blocks amalgamated during the different orogenies between Pre-Cambrian and Permian and were connected no earlier than the last Pre-Permian orogeny. It is possible that e.g. two different crustal blocks were united during the Ordovician orogeny, which would have had a separate development before, but a similar one after that (Fig. 54).

As these scenarios are hard to reproduce, the following text tries to reconstruct a simple evolution history with the help of the measured main ages of the zircon spectra. A possible approach to decode a complex development history is a systematically examination of the zircon populations of different aged cover unit sediments. Further it has to be mentioned, that the zircon populations depict only magmatic and high temperature metamorphic events. Orogenic processes, which are connected to low grade metamorphic facies and where therefore not accompanied by magmatic processes, can not be identified through this technique.

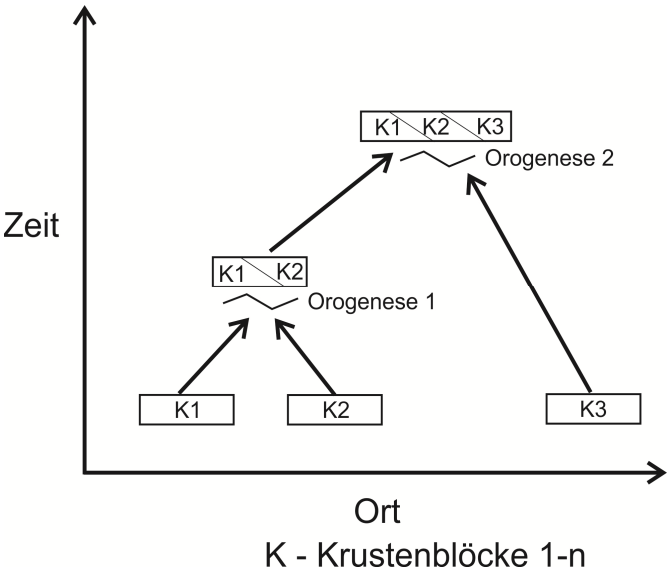

Fig. 54: Depiction of a possible zircon population mixture.

It was tried to reconstruct the time and space development of the source areas, which was the origin of the Late Paleozoic sediments of the Greywackezone. In order to be able to perform the reconstruction the age distribution and the morphological and chemical features as well as the phases of plate divergence, convergence or collision were considered. The paleogeographical positions were reproduced for every time step with the help of already published paleogeographical maps and published concepts of the formation of Europe through repeated docking of Gondwana fragments. The interpretation mainly follows the works of von Raumer et al., 2002, as these are coherent works, which are consistent in itself and follow the whole time range of Neoproterozoic to Permian. It was tried to identify the position of the sediment source throughout the different time steps and portrayed in idealized cross sections and paleogeographical maps.

15.8.1 ***Pre- Cambrian***

At the end of the Pre-Cambrian, especially during the Ediacarian (630 Ma – 540 Ma, Cohen et al., 2013), a change of calc-alkaline to alkaline magmatism occurred, which was correlated to the mantle delamination and the following drifting of continental part against the north (Candan et al., 2015). The crustal blocks which were later part of the source are of the analysed samples were possibly located along the northern part of the eastern Gondwana, around the modern ANS and the Sahara metacraton. Every sample and their zircon populations depict common ages around 1000 Ma - 900 Ma and 700 Ma - 550 Ma (Fig. 43). This ages can be interpreted as typical west-gondwanan ages (eastern part of modern Africa), but are not enough for a distinct association to the northwest or northeast of Africa, as just a small amount of Pre-Cambrian ages alone is an uncertain allocation.

Ages of around 1600 Ma and 1100 Ma are considered to be typically Laurentian or Baltican ages, but cannot be found in the analysed samples, which excludes those positions as a sediment source (Dörr et al., 2015).

The Silbersberg metasandstone sample depicts a different development compared to all other samples as it does not display the Ordovician event. This leads to the assumption that the source area was positioned on the north-western margin of Gondwana, which suffered extension directly after the Cadomian orogeny (Fig. 55). This assumption is also verified by the classification of Linnemann et al., 2007, which correlated the Silbersberg metasandstone with a Cambrian rifting during Pre-Cambrian times, while all the other samples are through a Cadomian back arc (Fig. 67 in comparison to Fig. 68, Fig. 69, Fig. 70).

Because of the division of magmatic zircons into volcanic and plutonic ones (Fig. 50), all the samples except the Semmering quartzite could be connected to a plutonic magmatism. After Crowley et al. (2002) a mantle plume formation due to delamination occurred and produced numerous granitoids, which confirms the assumed tectonic situation of the analysed samples.

The former development was preceded by the break off of the first Gondwana fragments (Avalonia, Cadomia) and therefore was the position of the Silbersberg source area in the earliest stages at the western Avalonian/Cadomian girdle, while the other samples position on the eastern part, which collided later on again with Gondwana.

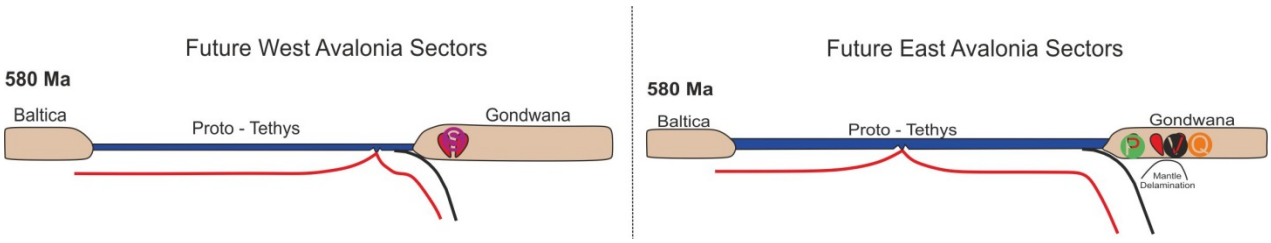

Fig. 55: A plate tectonic profile depiction of the development Gondwanas at the end of the Precambrian with the differentiation of the future West-and East-Avalonia. The coloured circles represent the examined samples (violet s = Silbersberg metasandstone; green P = Präbichl metasandstone; black V = Veitscher metasandstone; orange Q = Semmering quartzite). The Proto-Tethys corresponds to the definition of Stampfli & Borel, 2002.

15.8.2 *Cambrian (541 Ma - 485 Ma)*

The beginning of the Paleozoic is characterised through extension phases and the formed rift basins, which were facilitated through the Pre-Cambrian mantle delamination (von Raumer et al., 2003; von Raumer & Stampfli, 2008). This was followed in the Late Cambrian by a starting removal of Avalonia from Gondwana and the correlated opening of the Rheic ocean (von

Raumer & Stampfli, 2008; von Raumer et al., 2002). Stampfli et al. (2002) and von Raumer et al. (2002) interpret the Rheic ocean as subducted in a Gondwana directed way, which lead to an active margin on the northern part of Gondwana.

These developments can be retraced in the samples of the Silbersberg metasandstone (main age around 511 Ma) and in the Veitsch Nappe (main age around 498 Ma), but even to a smaller zircon age amount in the Präbichl Formation. Because of the magmatic differentiation of the zircons it is possible to identify a break off in the Early Cambrian times and an active margin in the Upper Cambrian (Fig. 50). This magmatic signature represents therefore a position at the northern margin of Gondwanan for most of the samples source areas (Fig. 56, Fig. 64). Divergent of this is only the Semmering quartzite which does not possess suitable ages, which leads to the assumption that its source was not positioned directly on the active margin or the extension area behind it (Fig. 56).

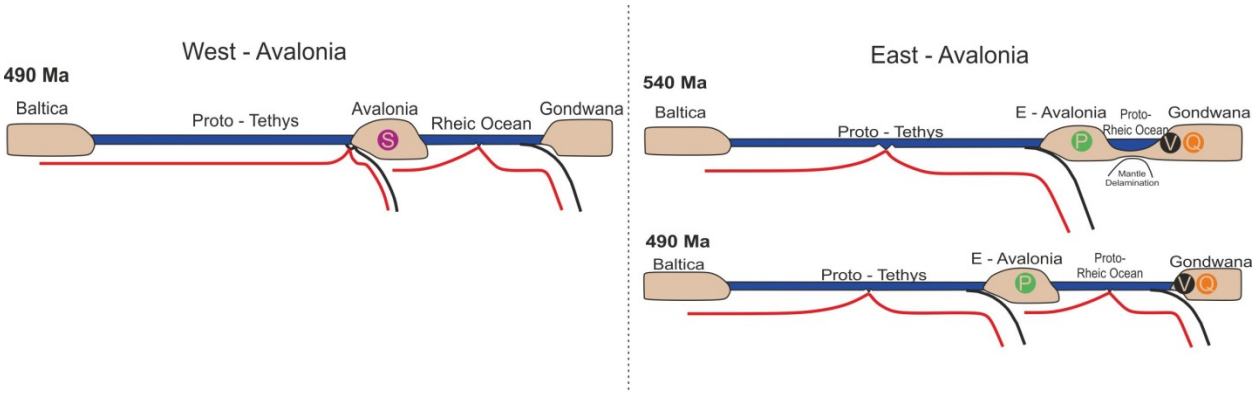

Fig. 56: Plate tectonic development of the northern Gondwana margin during the Cambrian times. The samples are once more represented through coloured circles (legend like Fig. 55).

15.8.3 *Ordovician (485 Ma - 443 Ma)*

During the Ordovician times Avalonia finally broke up from Gondwana due to the subduction of the middle oceanic ridge of the Proto-Tethys (von Raumer et al., 2002; Domeier & Torsvik, 2014). While the western part of Avalonia was able to drift uninterrupted northwards, the still remaining ridge of the Proto-Tethys in the east stopped the development and lead to a back-drifting of East-Avalonia to Gondwana (von Raumer et al., 2003; Golonka & Gaweda, 2012). This back-drifting induced a collision between Avalonia and Gondwana and the destruction of the eastern Rheic ocean. This collision is known as the Ordovician orogeny and triggered a complex terrain assemblage, which was later called Hun-Terrain (von Raumer et al., 2003, 2002).

The samples of the Veitscher metasandstone, as well as the sediments of the Präbichl Fm and the Semmering quartzite display ages between 450 Ma and 480 Ma. Those are even the main age groups of the Veitsch Nappe and the Semmering quartzite (465 Ma and 459 Ma), while the Silbersberg Nappe does not show this age at all. The source area of the Silbersberg metasandstone therefore must have been farther away of the influence area of the Ordovician magmatic arc, which again hints at a position at the western Avalonia terrain (Fig. 57). West-Avalonia did not experience the Ordovician orogeny and is therefore a suitable position for the Silbersberg source (Fig. 64).

The Präbichl metasandstone depicts just a small amount of Ordovician aged zircon, and can hence be interpreted as occupying a position on the western margin of East-Avalonia after the detachment from Gondwana (Fig. 42). By means of the magmatic zircon signature it was also possible to characterise the formation position as an active margin rather than an orogeny and hints again at an East-Avalonian location.

The Veitscher metasandstone as well as the Semmering quartzite exhibit distinct Ordovician ages, which can be connected to the orogeny. This leads to a sediment source position still at the northern margin of Gondwana, which was strongly affected by the orogenic event, and can be approved through the magmatic signature (Fig. 50, Fig. 57).

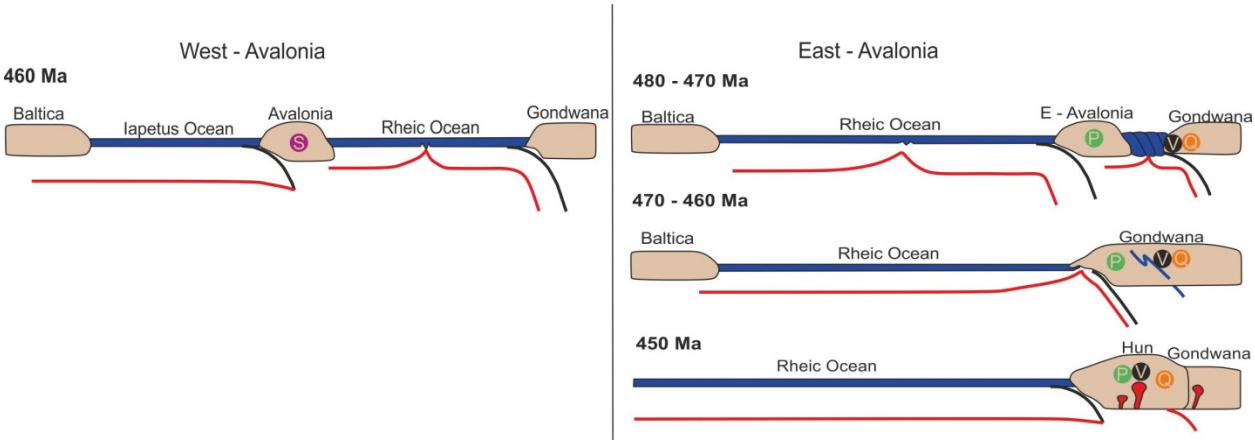

Fig. 57: A plate tectonic cross section through the different terrains of Gondwana in the Ordovician and a depiction of the orogeny in the eastern area (coloured circles are once more the sample positions with the same legend as in Fig. 55).

15.8.4 *Silurian (443 Ma - 419 Ma)*

Due to the Late Ordovician-Silurian crustal extensions and the closure of the Rheic ocean, the Silurian opening of the Paleotethys occurred and detached the Hun-Terrains in the north from Gondwana (Stampfli, 1996, von Raumer et al., 2002, 2013). At the same time period the

western part of Avalonia collided with Baltica, converged during Middle Silurian times with Laurentia and built up the north positioned continent Laurussia (Golonka & Gaweda, 2012).

The only sample displaying an age as well as a magmatic zircon signature for this event is the metasandstone of the Silbersberg Nappe (443 Ma). This confirms again the paleotectonic position of the sediments sources for the Silbersberg Nappe at the western terrain of Avalonia. Overall the Silbersberg metasandstone exhibits stronger diverging age distribution in comparison to the other samples sources, which mostly resided on the Hun-terrain (Fig. 58, Fig. 64 and Fig. 42).

All the other samples depict further steps of development and the sediment sources were hence located on the Hun-terrain. If they would have been positioned on Gondwana during Silurian, they would not indicate further events.

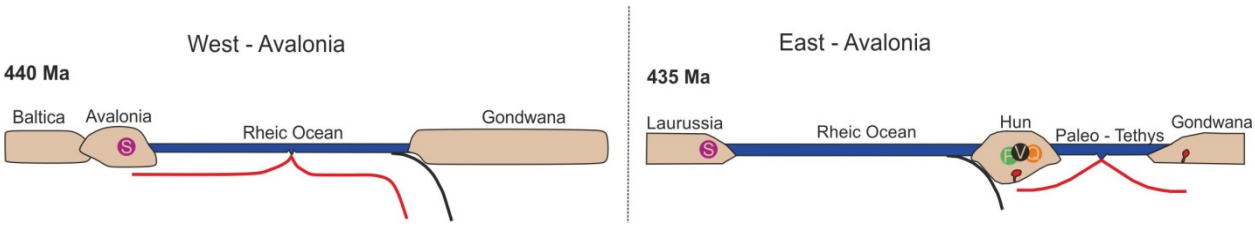

Fig. 58: Silurian development of Gondwana and its terrains, exhibited as cross sections (samples are again represented as in Fig. 55).

15.8.5 *Devonian (419 Ma - 358 Ma)*

Devonian times are connected to the off drifitng of the Hun-terrain and the continuing opening of the Paleotethys (Stampfli et al., 2002; von Raumer et al., 2002). The Hun-terrain is interpreted as continental slivers that were not necessarily connected, which consisted of Armorica to the west and Ligeria and Galatia to the east (von Raumer et al., 2013). The northern part of this terrain contains an active margin with high pressure girdles, while the southern part represents a passive continental margin (Stampfli et al., 2002, 2011, von Raumer et al., 2013).

During the Devonian the opening of the Rheno-Hercynian ocean occurred at the southern passive margin of Laurussia, which lead to the detachment of continental blocks (Stampfli et al., 2002). These blocks collided with the Hun-terrain in the Middle Devonian and closed thereby the Rheic ocean through subduction beneath the Hun-terrain (eo – Variscian event; Stampfli et al., 2002).

The sample of the Silbersberg metasandstone is the only one displaying a distinct Devonian age (390 Ma), which was interpreted with the help of magmatic zircon signatures as an orogenic formed age (Fig. 47). This leads to the assumption that this samples source was involved in the eo-Variscian metamorphism and rested on the southern margin of Laurussia detached continental block (Hanseatic block) in a upper plate position. Because of this position the sediments sources of the samples did not see any further events. As the other samples do not exhibit similar ages and a Hun-terrains position is assumed, the crustal blocks which served as source probably were located on the mainly protected middle part of the Hun microcontinent (Fig. 59, Fig. 65).

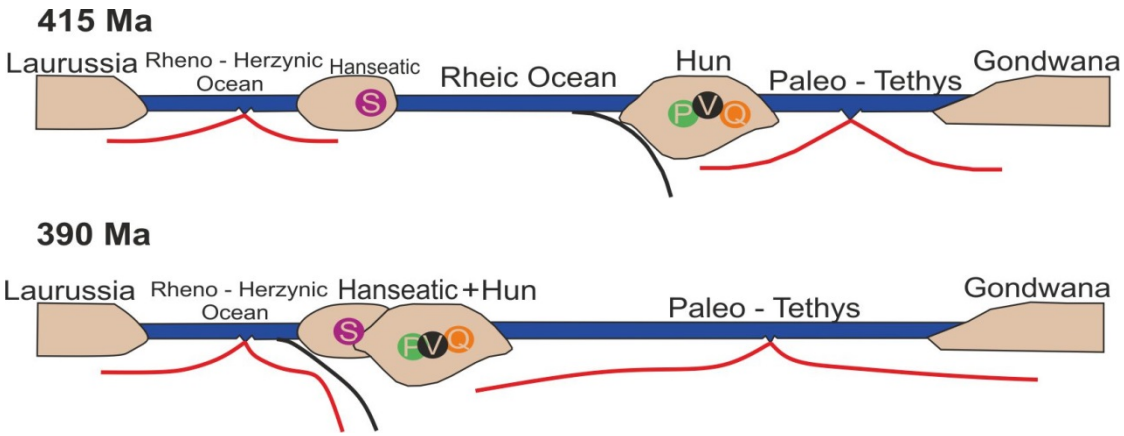

Fig. 59: Cross section representation of the plate tectonic developments during Devonian (with the same sample representation as in Fig. 55).

15.8.6 *Carboniferous (358 Ma - 298 Ma)*

The Carboniferous is characterised through various strike slip movement, which lead to collisions within the terrain, where e.g. Armorica collided with Ligeria/Galatia (von Raumer et al., 2013; Fig. 60). These collisions, which were triggered through a dextral convergence, occurred around 350 Ma along the former subduction zone of the Rheic ocean und induced a high temperature deformation in the now consolidated sliver of Armorica, Ligeria and Galatia (Hun-terrain, von Raumer et al., 2013). In the northern and southern part of this terrain a new subduction zone formed (von Raumer et al., 2013).

Within the Late Carboniferous a northwest migration of the Hanseatic-Hunic-terrain occurred and conducted into a collsion with Laurussia, which is now known as Viseanic event (Stampfli et al., 2002). A north-directed subduction of the Paleotethys followed because of the approach Gondwanas (Stampfli et al., 2002, 2013), which resulted into the collision with Laurussia and

the connected formation of the super-continent Pangea (Variscian orogeny, Stampfli et al., 2002, 2013).

Because of the former events all of the sediment sources for the samples were now united on the Hun-terrain (Fig. 65), although an accurate determination of the position is not possible due to the strike slip movement.

The source of the Silbersberg metasandstone is the only sample displaying an age cluster at 390 Ma and can therefore be located near the northern subduction zone of the Ligeria-Galatia-terrain (Fig. 60), whereas all the other samples sources can be settled on the southern passive margin. Main age cluster of the Präbichl and the Veitsch Nappe are around 356 Ma, while others, like the Semmering display smaller amount of similar aged zircons (342 Ma) or have an age gap in their zircon population (Silbersberg). This indicates a central lower plate position during the collision of Armorica with Galatia/Ligeria of the Präbichl Fm and the Veitsch Nappe around 350 Ma (Fig. 60). Located on the northern border of the aggregated, near to the continental margin of the Rheno-Hercynian ocean, the source of the Silbersberg metasandstone was not involved in the collision. The Semmering quartzite with its low amount of zircons around 342 Ma was still influenced by the orogeny and farther south than the Silbersberg but farther north than the Veitsch Nappe, as well as in a upper plate position (related to the intra-Hun-suture; see Fig. 61).

The Präbichl metasandstone sample is the only one hinting at a later Variscian event at 317 Ma, so the source area of it was either beneath the Late Variscian strike slip movements or near the south of the Hun-terrain placed subduction zone.

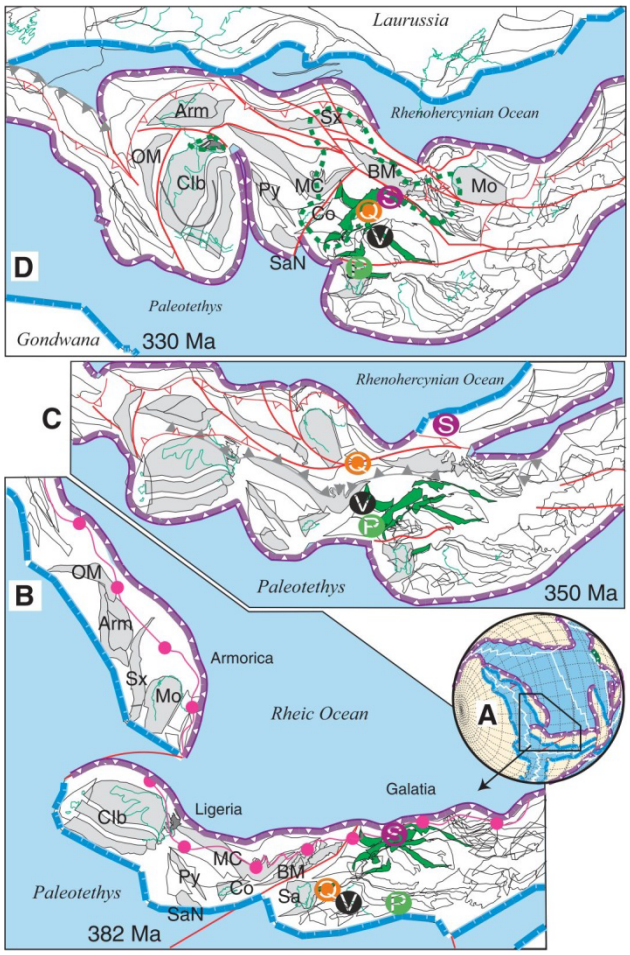

Fig. 60: This figure displays the collisions within the Hun terrain during the Carboniferous and Devonian (after von Raumer et al., in 2013).

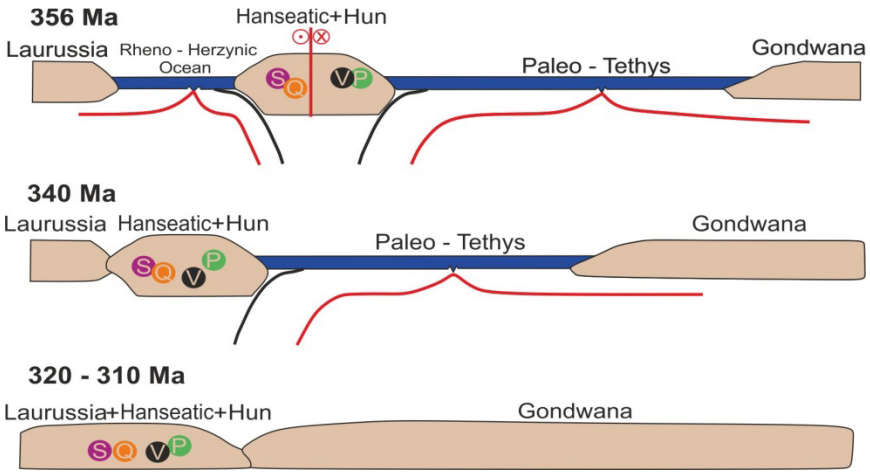

Fig. 61: Plate tectonic development in represented through cross sections before and after the Variscian orogeny (once more the samples are shown as in Fig. 55).

15.8.7 *Permian (298 Ma - 252 Ma)*

The only sample to display a distinct Permian age is the Semmering quartzite, although such ages cannot be totally excluded at source area of the Veitsch Nappe, as the sedimentation there (Steilbachgraben Fm.) stopped during the Carboniferous. The Semmering quartzites source was located near the Permian girdle in the Alps, which was influenced by intensive magmatism and high pressure metamorphism (Fig. 62).

The Permian paleogeography is not outlined in detail because all the areas of the analysed samples were now juxtaposed and all the original sources were near the continental margin of the Paleotethys. Further various Permian through existed within the continental areas, which were possibly bound to the strike slip events. Fig. 62 displays that the strike slip faults reached far into the continental areas. Such transform faults are known from the Permian as well as the Jurassic (Frank & Schlager, 2006; Schuster & Frank, 1999), where they might have dislocated crustal blocks of the future Alps to a bigger extent.

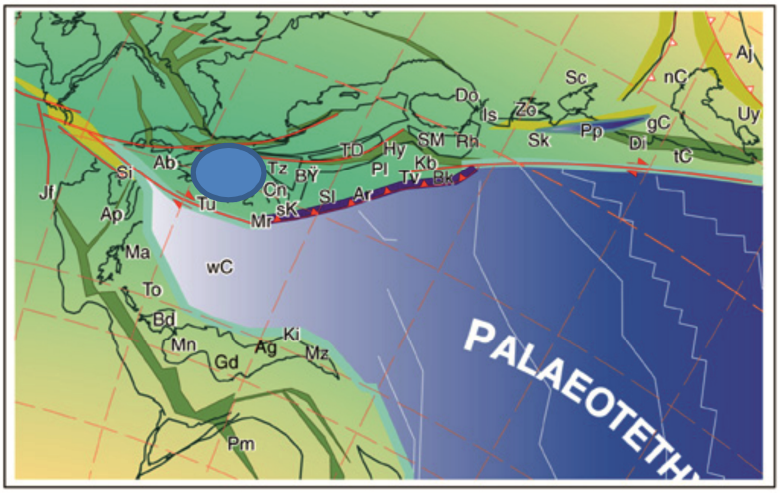

Fig. 62: The blue circle exhibits the location of the analysed samples in the Permian. Permian extensional movements are also depicted (changed after Stampfli & Borel, 2002).

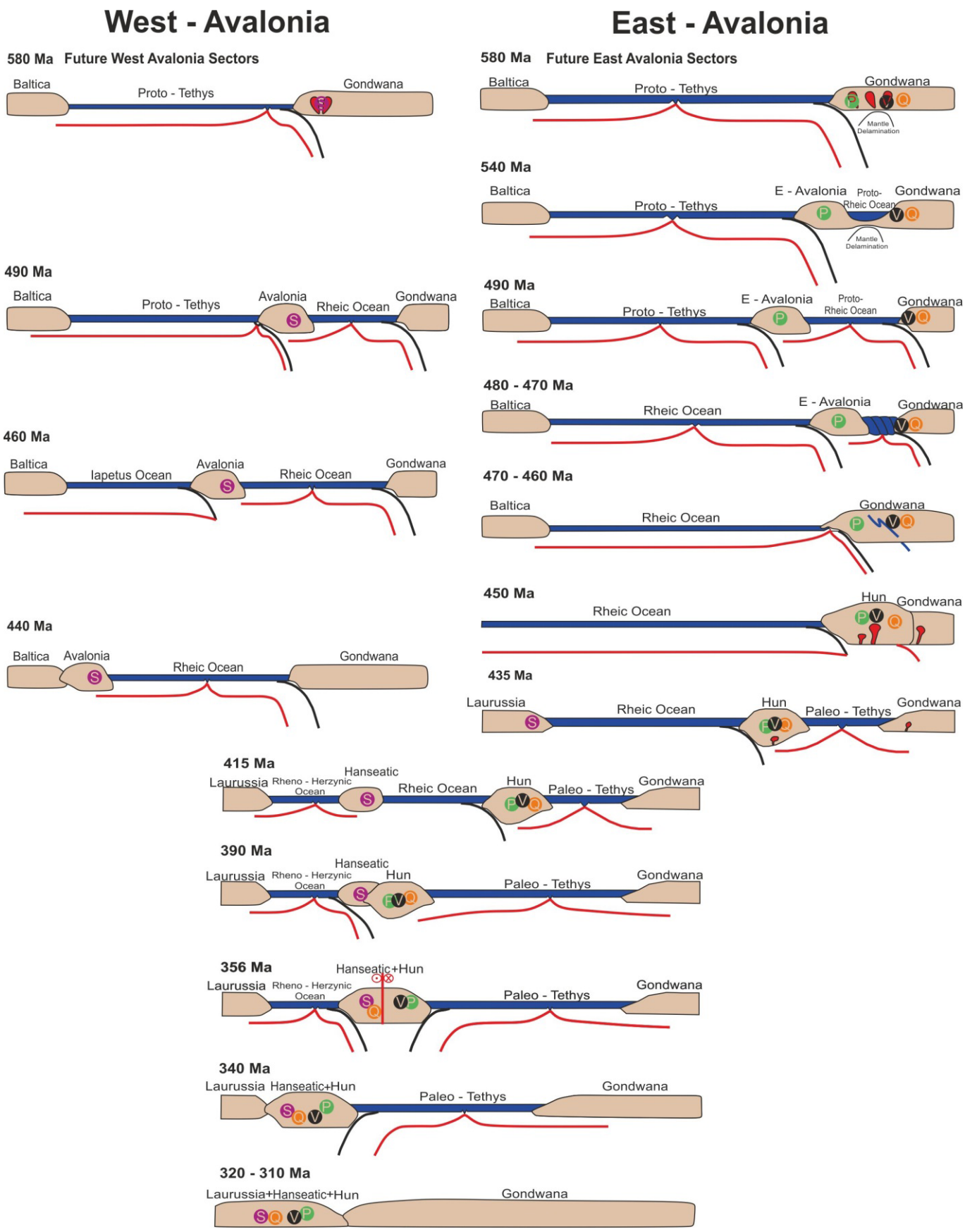

Fig. 63: Overall view of the plate tectonic development during the Paleozoic differentiated into West- and East-Avalonia (the legends and samples representation is similar to Fig. 55).). The Hun-terrain is depicted as coherent (in this and the earlier figures) although it presumably consisted of several continental blocks or ribbons.

The following figures were changed after Stampfli and Borel, 2002, with an addition of the paleogeographical position of the analysed samples throughout the different geological eras.

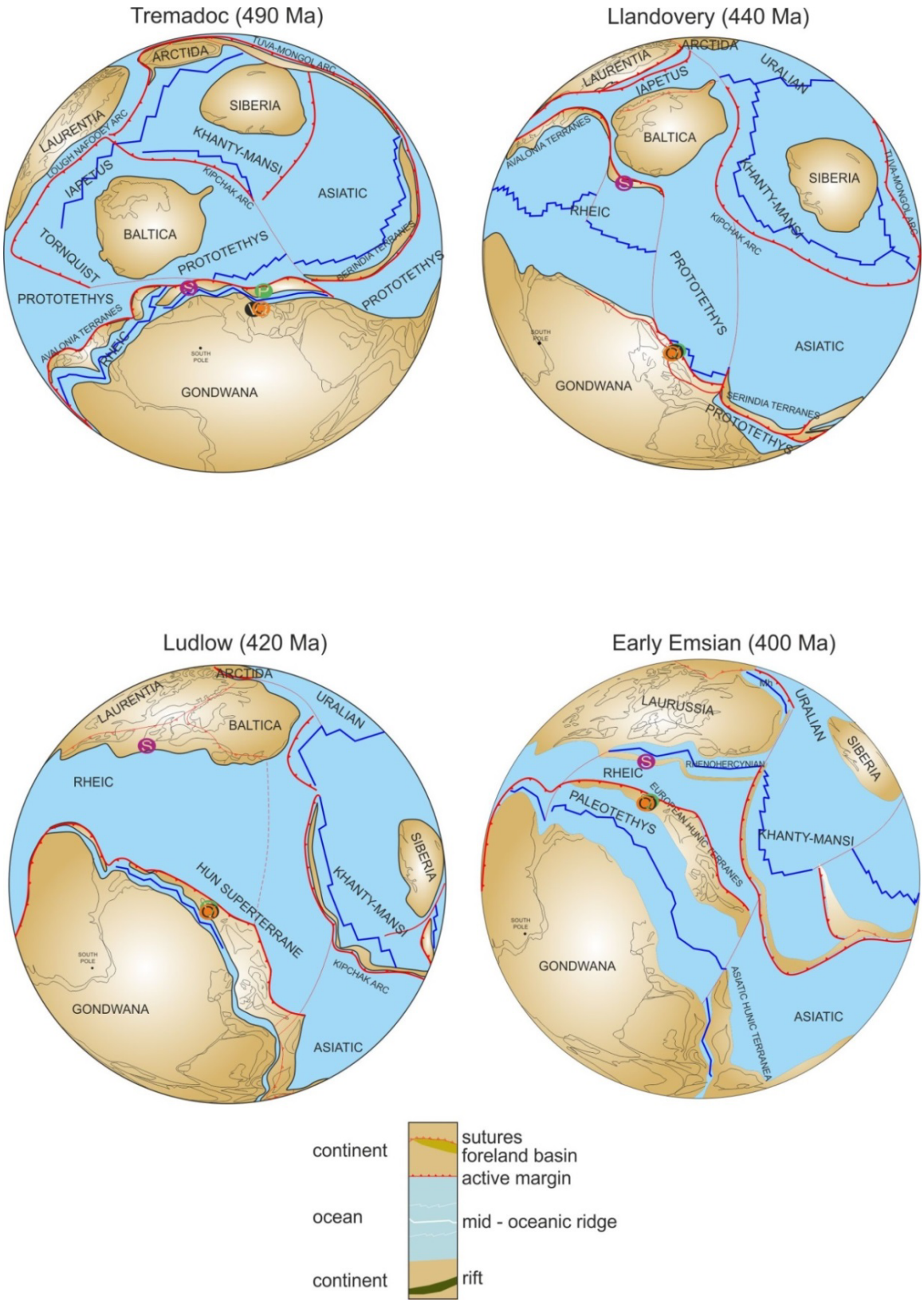

Fig. 64: Paleogeographical representation of the earth from the Late Pre-Cambrian on up to Early Devonian (changed after Stampfli & Borel, 2002). The position of the analysed samples is exhibited in different colours (violet S = Silbersberg metasandstone, black V = Veitscher metasandstone, green P = metasandstone of the Präbichl Fm, orange Q = Semmering quartzite).

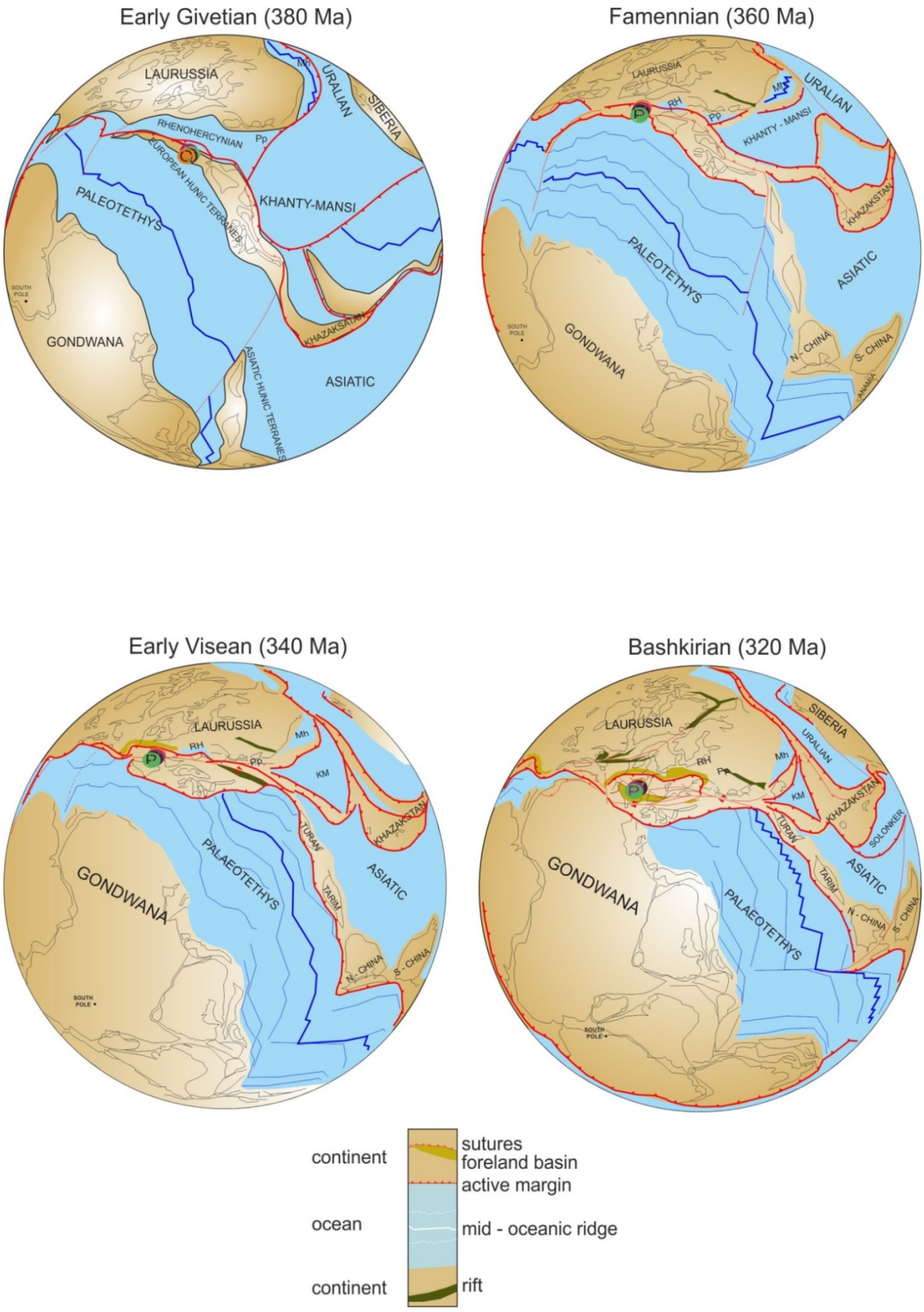

Fig. 65: Paleogeographical representation of the earth during Middle Devonian up to the Late Carboniferous (changed after Stampfli & Borel, 2002). The position of the single samples is again displayed in different colours (violet S = Silbersberg metasandstone, black V = Veitscher metasandstone, green P = metasandstone of the Präbichl Fm, orange Q = Semmering quartzite).

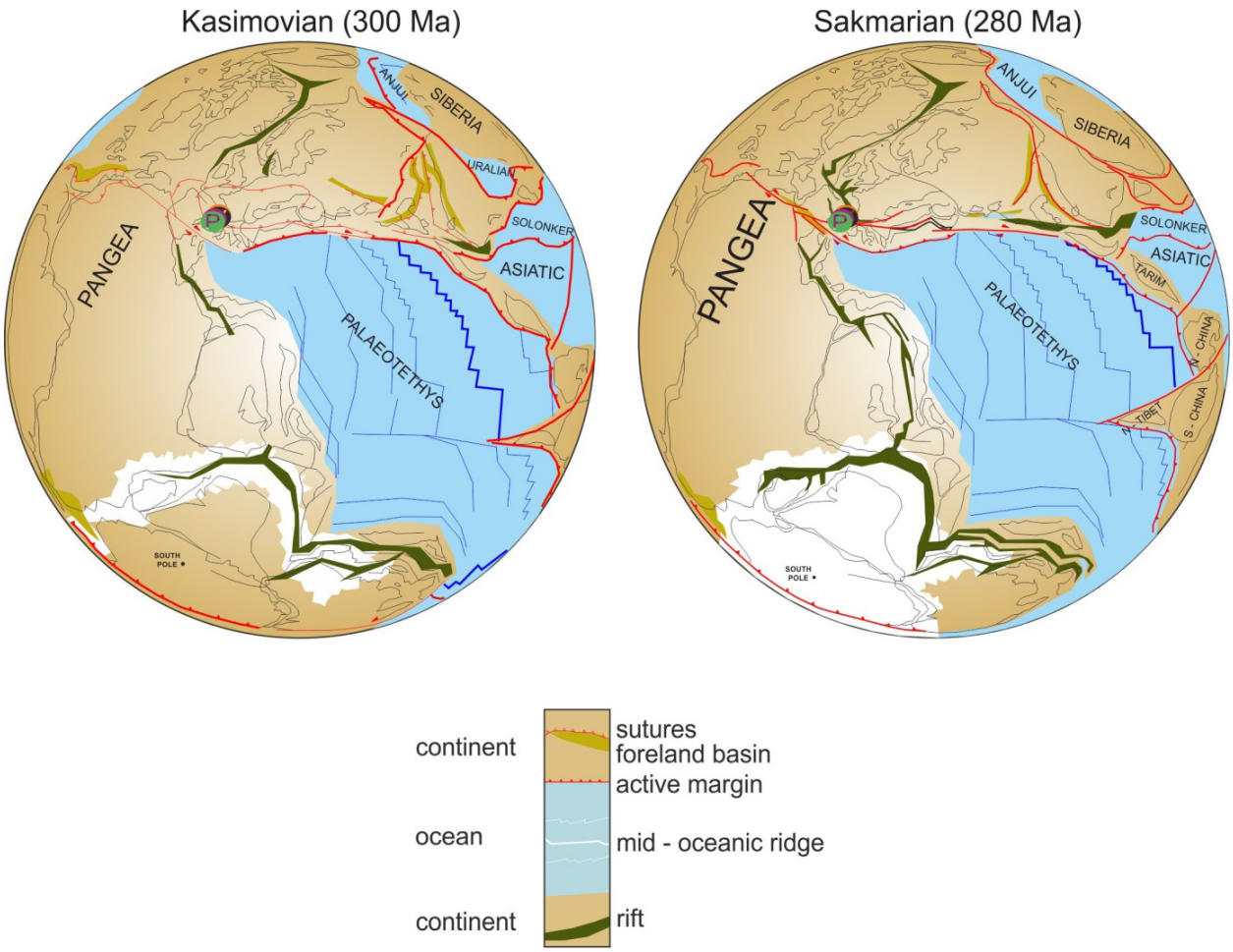

Fig. 66: Paleogeographical representation of the earth since Late Carboniferous up to Early Permian (changed after Stampfli & Borel, 2002). The position of the individual samples is again represented through different colours (violet S = Silbersberg metasandstone, black V = Veitscher metasandstone, green P = metasandstone of the Präbichl Fm, orange Q = Semmering quartzite).

Silbersberg Metasandstein (G21)

Nummer	Alter(Ma)	Fehler (2σ)
100	495	10
108	496	24
52	497	17
69	503.2	8.4
106	507	12
118	507	21
90	509	10
94	509	12
72	510.2	9.5
60R	515	18
103	516	11
91	516	20
59	518	16
107	518	14
122	522	66
104	527	16
38	530	37
105	540	22
78	541	17
37	551	19
56	561	15
112	575	26
21	578	29
47	579	26
58	582	20
3	601	54
40R	621	14
42R	624	25
1	630	26
30	639	24
19	654	33
28	662	30

Nummer	Alter(Ma)	Fehler (2σ)
17	923	43
84	1966	31
36	2014	24
55	2296	70
86	2704	42
111	2799	51

	Anzahl	Prozent
Kambrian Rifting	17	44.74
Cadomian retroarc	2	5.26
Cadomian back arc	13	34.21
Rodinia break - up	0	0.00
Grenvillian	1	2.63
Eburnean	3	7.89
Liberian	2	5.26
Leonian	0	0.00
Summe:	38	100.00

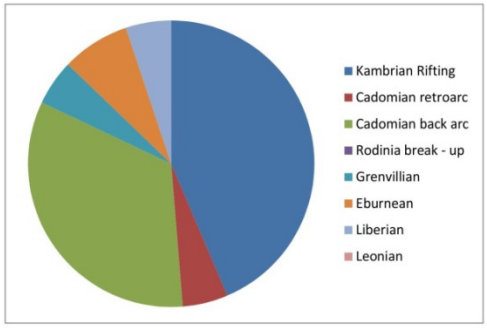

Fig. 67: Classifications of the Precambrian age within the Silbersberg Metasandstone into typical zircon populations after Linnemann (2007). The picture depicts a Cambrian Rifting of this sample during the Pre-Cambrian.

Semmeringquarzit (G2)

Nummer	Alter(Ma)	Fehler (2σ)
75	507	42
21	510	23
89	512	58
84	519	37
86	522	21
102	528.5	9.6
9	533	14
50	552	16
54	554	85
111	574	53
152	579	15
47	581	32
64K	598	42
64R	603	38
156	611	55
22	613	13
66	617	26
85	618	34
127	624	39
163	628	36
23	632	20
131	639	52
128	641	41
138	653	18
142	657	12
40	657	52
144	663	29
165	667	24
115	670	43
93	678	36
14	680	21
41	683	38

Nummer	Alter(Ma)	Fehler (2σ)
60	720	39
112	725	30
101	743	33
154	747	39
26	755	25
149	774	21
13	906	120
139	973	99
36	974	61
82	1019	50
62	1023	18
134	1041	63
61	1974	34

	Anzahl	Prozent
Kambrian Rifting	7	15.56
Cadomian retroarc	0	0.00
Cadomian back arc	25	55.56
Rodinia break - up	6	13.33
Grenvillian	6	13.33
Eburnean	1	2.22
Liberian	0	0.00
Leonian	0	0.00
Summe:	45	100.00

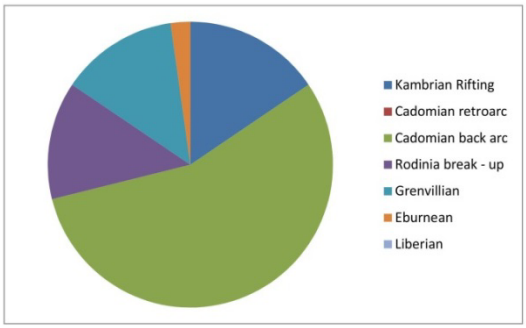

Fig. 68: The classification of Precambrian aged zircons of the Semmering quartzite after Linnemann (2007). The picture exhibits a Cadomian back-arc during the Pre-Cambrian.

Veitscher Metasandstein (G1)

Nummer	Alter(Ma)	Fehler (2σ)	Nummer	Alter(Ma)	Fehler (2σ)
182	493	21	105	578.9	5.2
2	494	15	102	584	27
136	498	13	209	594.2	8.1
88	495.8	9.3	13	601	23
35	499	32	178	604	13
21	503	24	111	614	46
10	505	13	192	609	45
19	508	10	104K	615	16
170	504.7	9	210	636	46
57	515	41	14	637	50
74	502	17	11	641	24
156	511	14	91	642	25
83	511	32	54	649	29
39	511.9	9.5	172	652	37
183	516	11	125	655	34
29	515	12	50R	666	19
1	518	27	20	668	35
116	523	19	174	679	21
187	522	34	24	685	29
109	530	26	42	746	190
118	531	12	100	755	37
147	534	84	173	736	120
194	545	16	151	975	110
62	543	36	7	981	49
34	552	20	137	1970	58
38	559	19	48	2044	61
144	558	79	31	2451	60
60	558	12	188	2510	57
117	555	34	205	2573	98
166	561	41	202	2671	83
154	561	15	146	2852	59
195	560	17	59	2880	74
149	582	14			

	Anzahl	Prozent
Kambrian Rifting	22	33.85
Cadomian retroarc	2	3.08
Cadomian back arc	28	43.08
Rodinia break - up	3	4.62
Grenvillian	2	3.08
Eburnean	3	4.62
Liberian	5	7.69
Leonian	0	0.00
Summe:	65	100.00

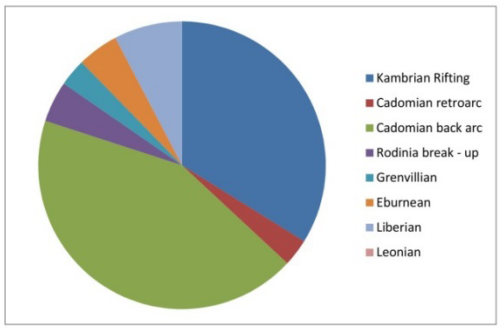

Fig. 69: The differentiation of the Precambrian aged zircons of the Veitscher metasandstone after the classification of Linnemann (2007). The depiction exhibits a Cadomian back-arc during the Pre-Cambrian.

Präbichl Metasandstein (L1)

Nummer	Alter(Ma)	Fehler (2σ)
36	503	18
61	515	29
71	517	11
21	533	29
38	534	34
1	568	24
39	574	20
59	581	20
35	581	25
85	589	31
44	589	32
97	594	30
45	604	42
82	612	20
73	616	31
87	624	34
105	628	26
96	663	25
56	709	30
66	955	56
48	971	60
86	2006	49
68	2030	27
54	2290	50
83	2308	130
62	2584	110
58	2625	77
69	2781	150
25	2782	73

	Anzahl	Prozent
Kambrian Rifting	5	17.24
Cadomian retroarc	0	0.00
Cadomian back arc	13	44.83
Rodinia break - up	1	3.45
Grenvillian	2	6.90
Eburnean	4	13.79
Liberian	4	13.79
Leonian	0	0.00
Summe:	29	100.00

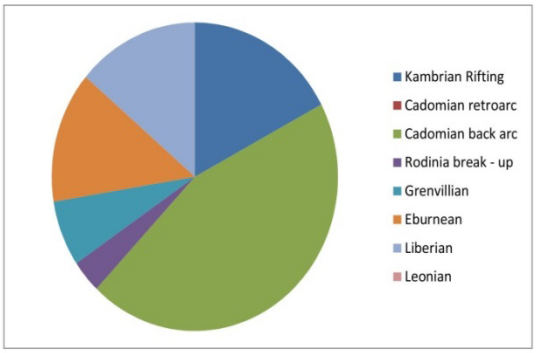

Fig. 70: Classification of the Pre-Cambrian aged zircons of Präbichl metasandstone compared to the data of Linnemann (2007). The picture indicates a Cadomian back-arc during Pre-Cambrian.

15.9 Comments on the presumed origins of the different source areas, in relation to the pre-Alpine rock formation of the Alpine-Carpathian realm

The analysed samples and their age distribution was compared to ages of basements in several areas of the Eastern Alps and the Western Carpathians, in order to find similarities and to define the source area for some of the sediments (see 18.5 Apendix E). By means of differentiation between plutonic, volcanic and metamorphic zircons, nature and timing of the orogenic phases and/or rifting phases could be defined. As zircons can just be formed at considerable magmatism and high grade metamorphism it must be stated that just the high graded events can be depicted. Because of that it was not possible to recognise low grade orogenic events and rocks which were not near the center of the orogen.

Additionally, the basement rocks beneath the particular analysed metasediments were examined to include or exclude them as source area. The names of the basements are their geographical ones, where e.g. Seckau Crystalline is not to be confused with the Silvretta/Seckau nappe system, which is connected to its tectonic position after the eo-Alpine orogeny and not to the position before the deposition of Paleozoic sediments.

15.9.1 *Silbersberg metasandstone*

The possible basement of the Silbersberg metasandstone is currently under discussion. Neubauer et al. (1994) interprets the Silbersberg Nappe as a tectonic unit with a Paleozoic phyllitic basement, the Gloggnitzer Riebeckite gneiss and a sedimentary cover consisting of the Silbersberg conglomerate. The low grade phyllitic basement as well as the poorly dated Riebeckite gneiss will not deliver Paleozoic zircons. After the hypothesis that the Paleozoic basement was the source area for the metasandstones, the former mentioned rocks should deliver Pre-Paleozoic zircons.

Schuster (2015) rather sees the Silbersberg Nappe connected to the Kaintaleck Complex, which can also be a potential supply area. The Kaintaleck Complex consist of Archean gneiss, garnet gneiss (514 Ma), the Kalwang conglomerate (498 - 502 Ma) and aplitic gneiss (365 Ma; Neubauer et al., 1994). Detritic white mica of the Silbersberg conglomerate, which hint at a cooling after an at least Greenschist facies event, displays an age of 359 Ma, while the Kalwang gneiss conglomerate shows ages of 386 Ma (Handler et al., 1997) and is part of the Silbersberg Nappe for Schuster (2015). If this basement is the source area, all of these ages, except the cooling ages, have to be found in the metasandstones.

The metasandstone of the Silbersberg Nappe exhibits two dominant age cluster, one around 511.1 ± 3.6 Ma and the other around 390.3 ± 6.2 Ma (G21, Fig. 42). This indicates a source area which suffered a Lower to Middle Cambrian orogeny, possibly at a magmatic arc, and a Middle Devonian event. Smaller amounts of zircons also depict ages of 443 Ma, 545 Ma, 571 Ma, 625 Ma, 920 Ma as well as older one from the Archean. Due to the main ages (511 Ma and 390 Ma) there is possible relation to the Kaintaleck Complex, although the metamorphic and magmatic ages around 360 Ma of this crystalline basement are not exhibited in the Silbersberg Nappe. The main age cluster of the metasandstone of 511 Ma and 390 Ma are distinctly magmatic and metamorphic and can therefore be related to an orogeny. Detritical white mica of 383 Ma and 359 Ma ages confirm through local cooling an orogenic phase.

Ordovician ages are common throughout the basements of the Alps, but have to be excluded as a source because of the lack of Ordovician ages in the metasandstone. This excludes the crystalline areas west and east of the Tauern as well as the Alpidic Koralpe-Wölz system, which do not depict Pre-Alpidic events. Further excluded were the basements which do not show an age cluster at 390 Ma, as well as around 511 Ma. Due to these limitations just the areas of the Kaintaleck Complex and possible the units of the Carpathians (especially Tatric and Gemeric) remain as delivery areas as those have a distinct 511 Ma age (see 18.5 appendix E). Also the Klátov unit of the northern margin of the Gemeric units (containing of amphibolites and paragneiss) are often compared to the Kaintaleck Complex (Schuster, 2015).

15.9.2 *Semmering quartzite*

The Semmering quartzite from the Mürztal (G2) superposes the Troiseck-Floning Complex as a part of the Silvretta/Seckau nappe system. Although there is no geochronological data of the Troiseck-Floning Complex available, there is some data from the correlating Rennfeld crystalline and the Seckauer Tauern as a basement of the Rannach Fm. (similar to the Semmering quartzite). The Rennfeld crystalline displays Proterozoic detrital zircons, which formed after an anatectic event between 470 Ma and 420 Ma and a second magmatic and metamorphic event between 367 Ma and 353 Ma (Neubauer et al., 2003).

The most important ages of 459.8 ± 2.5 Ma (Lower Upper Ordovician) and 297.8 ± 2.7 Ma (Lower Perm) as well as lower amounts of zircon populations at 340 Ma, 526 Ma and 618 Ma can be used to characterise the Semmering quartzite (G2, Fig. 42). Those ages do not correlate with the Troiseck-Floning equivalents and are therefore not the only source area. Only the Rosskogel porphyroid would be relatable because of the Permian ages.

As a focus of this sample is again on the Ordovician age cluster, once more all the basements without equivalent ages are excluded. This leads to the elimination of many East Alpine areas, e.g areas around the Tauern Window, the Koralpe-Wölz system and the Semmering-Wechsel system. The Permian ages are quite exceptional, which seems to guide to a source area beneath the Permian, metamorphic girdle (areas south of the Tauern Window). So the most logical area of delivery are the areas beneath the Texel crystalline, as well as crystalline areas south of the Tauern Window, the western Greywackezone and the Carpathians (Tatric, Veporic and Gemeric; see 18.5 Apendix E).

15.9.3 *Veitscher metasandstone*

The Veitsch Nappe does not possess a basement, which means there is no information about possible basement area erosion. A striking fact about the sedimentary development of the Veitsch Nappe is the shallow water evolution with molasses-like character (Steilbachgraben Fm., Neubauer et al., 1994) which started in the Early Visean (around 340 Ma). This formation of shallow water environment similar to the Veitsch Nappe is not common in the Alpine realm, but relates possibly to the Karbon von Nötsch and the Ochtiná unit in the Gemeric of the Carpathian. Because of this, those units are often combined as a Veitsch/Nötsch-Szabadbattyán-Ochtiná-zone (Ebner et al., 2008; Vozárová et al., 2009). The crystalline of Nötsch, which is tectonically beneath the Karbon von Nötsch, is an Ordovician aged metamorphic complex, which exhibits a Late Ordovician to Silurian cooling (earlier than 420 Ma) following an amphibolite facies metamorphism (Neubauer, Genser unpublished data). This crystalline was correlated with the Kaintaleck Complex because of the similar tectonic position and the relatable ages (Neubauer per. Comm).

Age groups of 498.9 ± 3 Ma, 465.4 ± 3.4 Ma and 356.1 ± 2.6 Ma dominate the metasandstone of the Veitsch Nappe (G1, Fig. 42) and point out events during Upper Cambrian, Middle Ordovician and Upper Devonian/Lower Carboniferous times. Detrital white mica of the Veitsch Nappe are dated 303 Ma and indicates therefore a similar source area as the Präbichl metasandstone of the Noric Nappe. The Ochtiná group was already analysed through detrital zircons of Lower Carboniferous deep water turbidites (Hradok Fm.; Vozarova et al., 2013) and exhibit dominant ages around 355 Ma as well as ages between 723 Ma and 554 Ma and 2,3 Ga – 2,6 Ga.

The Ordovician Smrencinka Fm. of the volcano sedimentary Rakovec group displays besides Proterozoic ages (dominating 577 Ma, 609 Ma and 644 Ma) also Upper Carboniferous and Permian samples with a most important age density around 360 Ma.

The Gemeric units of the Carpathians, especially the detrital zircons of the Ochtiná group are not comparable to the Veitsch Nappe. Particularly the dominant Ordovician ages of the Veitscher metasandstone are not available in the spectra of the Carboniferous Gemeric sediments. Additionally, the Permian sediments (Krompachy group) of the Gemeric unit depict distinct age maxima (477 Ma 352 Ma, 300 Ma and 281 Ma) which leads to the assumption that different crustal blocks amalgamated during the Variscian orogeny, while Ordovician metamorphosed rocks were brought into the system later on.

The remaining Carpathians (Tatric, Veporic) are the only possible units to show similar ages to all important age cluster of the metasandstones and are therefore most likely area of origin. Basements like Seckau and Ötztal can be excluded because of the lack of Ordovician ages (see 18.5 Apendix E).

15.9.4 *Metasandstone of the Präbichl Formation*

The Präbichl Formation is underlain by the massive Ordovician aged Blasseneck Porphyroid, and therefore it would be plausible to find zircons of this porphyroid in the sample. Additionally detrital zircons of the also occurring Ordovician to Devonian clastics of the Gerichtsgraben Fm., Rad Fm. and Polster Fm could have been redeposited. The Gerichtsgraben Fm as well as the Rad Fm further depict detrital white mica with an age of 562 Ma and 607 Ma and document an existence of a Late Neoproterozoic metamorphic event (Cadomian orogeny). Detrital white mica of the Permomesozoic Präbichl Fm itself, reveals ages of 303 Ma, but cannot be directly compared to the analysed zircon age spectra.

Detrital white mica of Silurian and Devonian sediments of the Western Greywacke Zone (Schattberg Fm., Löhnersbach Fm.) werde dated at 500 – 550 Ma, 600 – 700 Ma and 900 Ma (Panwitz, 2006). The Neo-Proterozoic ages of these mica correlate with the ages of the Präbichl Fm, although mica ages do have other implications than zircon ages, but the source area was possibly imprinted in a Pan –African way. Additionally there is a small variation of mica ages throughout the Ordovician to Lower Carboniferous and therefore hints at a homogenous, non-changing erosion area. Data of Permian cover sediments (Gröden Fm., Alpiner Bundsandstein) exhibited Variscan ages between 341 Ma and 308 Ma (Panwitz, 2006). The youngest dated mica is about 271 Ma old and therefore the maximum age of sedimentation (Panwitz, 2006). This again correlates with the zircon data of the Präbichl Fm. (age at 356 Ma and a youngest age at 304 Ma).

Because of the main age of 356 Ma (L1, Fig. 42) in the Präbichl sample it is possible to exclude the direct basement, which does not show any metamorphic event around 356 Ma. Ordovician

zircons, possible from the Blasseneck Porphyroid, additionally appear to just a small amount. Due to the main age of the sample, the source area must have suffered an Early Variscian metamorphism/magmatism. Young Variscian detrital white mica out of this sequence are also common (Handler et al., 1997). Further age cluster can be found around 466 Ma to 519 Ma and 578 Ma to 617 Ma, but also older ones with 703 Ma and 960 Ma appear. Overall the Präbichl metasandstone possesses highly heterogeneous zircon spectra, which points at a re-sedimentation of Paleozoic strata series.

The most important age of 356 Ma depicts an Early Variscian event, and match with the detrital white mica ages of 303, which could be interpreted as the cooling after another event which is displayed by the minor zircon age of 317 Ma. The age of 356 further indicates that a Early Variscian source area was eroded.

It is difficult to specifiy the crystalline source area, as the age group of 356 Ma can be found in various units. As the Präbichl Formation, which is overlain by Tirolic units of the Northern Calcareous Alps, can be located somewhere near the Tethys margin, it was tried to specify the position of the source area with these highly speculative figures (Fig. 71, Fig. 72). These figures try to locate the source areas in reference to the Permian, magmatic girdle and Pre-Alpidic arrangement.

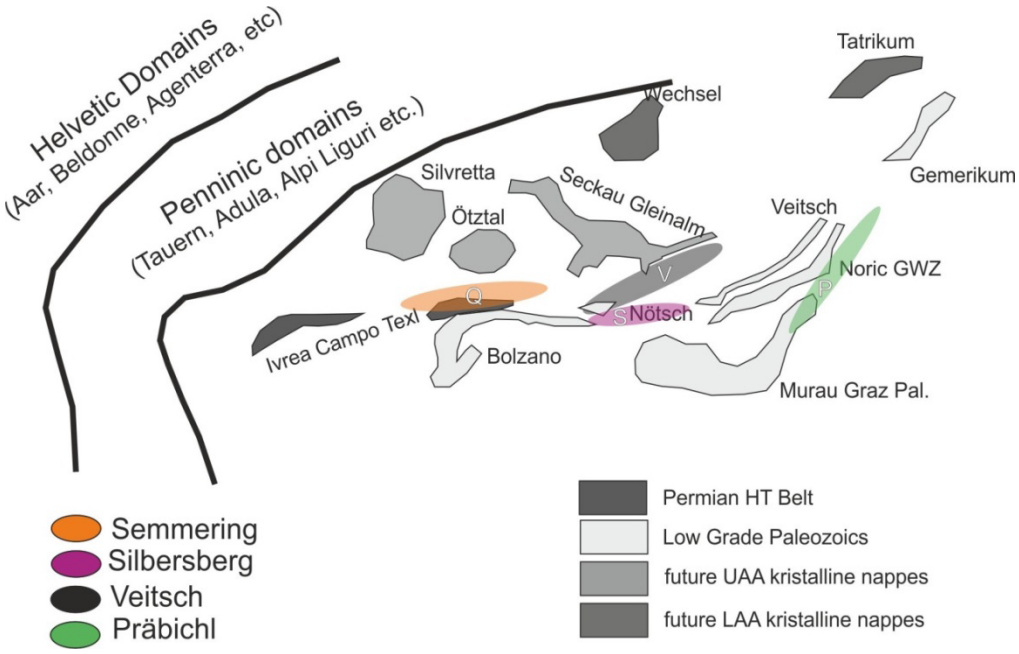

Fig. 71: Supposed situation of the different source areas during the Permian (changed after von Raumer & Neubauer, 1993)

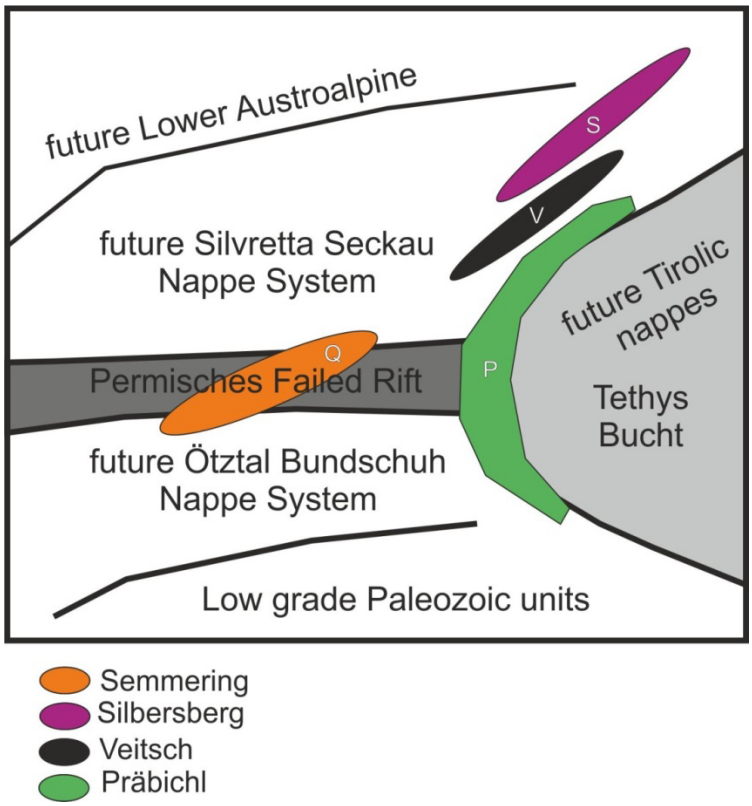

Fig. 72: The position oft he Präbichl sample can be located near the Tethys margin as the Tirolic-Juvavic nappes overlay those and there hast o be a crystalline hinterland.

16 Conclusion

Due to the preceding chapters it is now evident, that the measured zircons and hence the source area of the late Paleozoic cover metasediments do differ in their age spectra and therefore were located at different positions during Earth's history. The main propositions are:

1) The source areas of the sampled metasandstones and the quartzite differ distinctly. This implies elevated during the Carboniferous and Permian, which supplied different detrititus into not necessarily juxtaposed sedimentary basins. The erosional areas consisted of heterogenous rocks, which were merged during earlier orogenies.
2) The direct basement of the sedimentary cover is not the source area of the metasediments. The analysed age spectra were compared to ages of the Alpine-Carpathian realm in order to include or exclude delivery areas. Zircon ages of the Silbersberg metasandstone correlated best with the ages of the Kaintaleck Complex, which lacked of Ordovician ages too, and can therefore be assumed as the source area.

   A crystalline origin of the Semmering quartzite zircons could be found in the units south of the todays Tauern Window, which exhibits as the only crystalline basement, Ordovician and Permian overprints.

   Units of the Carpathians (especially Tatric and Gemeric units) resemble the age spectra of the Veitscher metasandstone, which is seen to be the most probable source area. The Veitsch Nappe cannot be compared to any crystalline area of the Alps and is rather similar to the Karbon von Nötsch and the Ochtiná unit of the Gemeric (Carpathians).

   The allocation of the Präbichl metasandstone was the most challenging one. It was not possible to connect the sample with an unique Alpine crystalline area, because of the divergent age distribution. Therefore it must be assumed that this metasandstone consists of several re-deposited Paleozoic strata. The main age of this sample (356 Ma) cannot be found in the direct basement of the Präbichl Fm and has to be excluded as an area of origin. Further to mention is, that a metamorphic/magmatic area delivered detritus into the deposition area of the Präbichl Fm, which was further north than the Permo-Mesozoic shelf.
3) Although the Greywackezone is just a small strip in the Eastern Alps, the measured age data still exhibits high variation and points at a complex development with different source areas. Due to the nappe arrangement within the Greywackezone it can be assumed that the different nappes came into contact through long-distance transport. This transport includes the the Alpine nappe stacking but the heterogeneity of the source areas still points at large-scale strike-slip movement as they are known of the Jurassic.

4) The Silbersberg metasandstone depicts through the plate tectonic position of the source area, a deviating development since the Pre- Cambrian, compared to the other samples. For this reason, the source area of the Silbersberg sample was likely located on a different position on West-Avalonia. Linnemann, 2007, confirms this, through the classification of the Silbersberg metasandstone to a Cambrian rifting (511 Ma), while the other entire samples exhibit a Cadomian back arc. Further, the Silbersberg Nappe does not display Ordovician ages in the zircon populations, which confirms the position at the western Avalonian terrain. The other sediment sources were rather located at East-Avalonia and suffered the Ordovician orogeny (Veitscher metasandstone and Semmering quartzite; about 460 Ma).

During the Ordovician orogeny, which influenced the Veitscher metasandstone, the Semmering quartzite and the Präbichl Fm., the Silbersberg metasandstone migrated with West-Avalonia to Baltica and finally collided in Silurian times (about 440 Ma), making West-Avalonia a part of southern Laurussia.

The Veitscher metasandstone, the Semmering quartzite and the Präbichl Fm. were now united on the Hun-Terrain after the Ordovician orogeny, which already disconnected from Gondwana during Silurian and migrated towards Laurussia. In the following Devonian, the samples were again united on the Hanseatic-Hun-terrain during the eo-Variscian event, because of the former detachment of the Hanseatic block from Laurussia. This Devonian collision is solely depicted in the Silbersberg sample at around 390 Ma and is the last event to be seen in the zircon data, possibly because of the protected position within the upper plate.

The other source areas were located aside and underwent a metamorphic overprint at 356 Ma, due to strike slip movement in the Early Carboniferous. These movements lead to intra-continental collsions and can be seen in the Veitscher metasandstone as well as in the Präbichl Formation. Triggered through the strike slip movements, the Hanseatic-Hun-terrain finally collided with Laurussia and built up the Viseanic mountain chain. This is possibly displayed in the Semmering quartzite through the age of 342 Ma.

The final subduction and the connected collision between Laurussia and Gondwana can be interpreted as 320 Ma, and is shown in similar aged zircons of the Präbichl Fm.

17 Reference list

Abdelsalam, M. G., Liégeois, J. P., & Stern, R. J. (2002). The saharan metacraton. *Journal of African Earth Sciences*, *34*(3), 119-136.

Adamija, S., Abesadze, M., Chkhouta, T., Kekelia, M., & Tsimakuridze, G. (1992). Tectonices in the Variscan crystalline assemblages of the Greater Caucasus and Ďumbier massif of the Western Carpathians. Spec. Vol. IGCP, 276, 7-19.

Bachtadse, V., Torsvik, T. H., Tait, J. A., & Soffel, H. C. (1995). Paleomagnetic constraints on the paleogeographic evolution of Europe during the Paleozoic. In Pre-Permian geology of central and eastern Europe (pp. 567-578). Springer Berlin Heidelberg.

Bertrand, J. M., & Leterrier, J. (1997). Granitoïdes d'âge Paléozoïque inférieur dans le socle de Vanoise méridionale: géochronologie U-Pb du métagranite de l'Arpont (Alpes de Savoie, France). Comptes Rendus de l'Académie des Sciences-Series IIA-Earth and Planetary Science, 325(11), 839-844.

Borsi, S., Del Moro, A., Sassi, F. P., & Zirpoli, G. (1973). Metamorphic evolution of the Austridic rocks to the south of the Tauern Window (Eastern Alps): radiometric and geopetrologic data. Mem. Soc. geol. ital, 12, 549-571.

Brack, W. (1977). Geochronologische Untersuchungen an Gesteinen des Altkristallins in der Schobergruppe, Österreich. na.

Burda, J., Gawęda, A., & Klötzli, U. (2013). U-Pb zircon age of the youngest magmatic activity in the High Tatra granites (Central Western Carpathians). Geochronometria, 40(2), 134-144.

Bussy, F., Derron, M. H., Jacquod, J., Sartori, M., & Thelin, P. (1996). The 500 Ma-old Thy on metagranite: a new A-type granite occurrence in the western Penninic Alps (Wallis, Switzerland). European Journal of Mineralogy, 565-576.

Bücksteeg, A. (1999). Zur Geologie des Kristallins der Schobergruppe (Osttirol/Österreich). Aachener Geowiss Beitr, 33, 1-206.

Cambel, B., & Kral, J. (1989). Isotopic geochronology of the Western Carpathian crystalline complex: the present state. Geologicky Zbornik Geologica Carpathica, 40(4), 387-410.

Candan, O., Koralay, O. E., Topuz, G., Oberhänsli, R., Fritz, H., Collins, A. S., & Chen, F. (2016). Late Neoproterozoic gabbro emplacement followed by early Cambrian eclogite-facies metamorphism in the Menderes Massif (W. Turkey): Implications on the final assembly of Gondwana. Gondwana Research, 34, 158-173.

Cawood, P. A., Hawkesworth, C. J., & Dhuime, B. (2013). The continental record and the generation of continental crust. Geological Society of America Bulletin, 125(1-2), 14-32.

Cliff, R. A. (1980). Uranium-lead isotopic evidence from zircons for lower Palaeozoic tectonic activity in the Austroalpine Nappe, the Eastern Alps. Contributions to Mineralogy and Petrology, 71(3), 283-288.

Cohen, K. M., Finney, S. C., Gibbard, P. L., & Fan, J. X. (2013). The ICS international chronostratigraphic chart. Episodes, 36(3), 199-204.

Cooke, R. A., & O'Brien, P. J. (2001). Resolving the relationship between high P–T rocks and gneisses in collisional terranes: an example from the Gföhl gneiss–granulite association in the Moldanubian Zone, Austria. Lithos, 58(1), 33-54.

Crowley, Q. G., Floyd, P. A., Winchester, J. A., Franke, W. T., & Holland, J. G. (2000). Early Palaeozoic rift-related magmatism in Variscan Europe: fragmentation of the Armorican Terrane Assemblage. Terra Nova, 12(4), 171-180.

Dallmeyer, R. D., Handler, R., Neubauer, F., & Fritz, H. (1998). Sequence of Thrusting Within A Thick-Skinned Tectonic Wedge: Evidence From 40Ar/39Ar and Rb-Sr Ages From the Austroalpine Nappe Complex of the Eastern Alps. The Journal of geology, 106(1), 71-86.

Dallmeyer, R. D., Neubauer, F., & Fritz, H. (2008). The Meliata suture in the Carpathians: regional significance and implications for the evolution of high-pressure wedges within collisional orogens. In Siegesmund, S., Fügenschuh, B. & Froitsheim, N. (eds) Tectonic Aspects of the Alpine-Dinaride- Carpathian System. Geological Society, London, Special Publications, 298, 101–115.

Dickinson, W. R. (2008). Impact of differential zircon fertility of granitoid basement rocks in North America on age populations of detrital zircons and implications for granite petrogenesis. Earth and Planetary Science Letters, 275(1), 80-92.

Diener, R., Kutterolf, St., Krawinkel, H. (2001). Petrographie, Geochemie und Provenanz der Hochwipfel-Formation, Karawanken (Österreich I Slowenien). Ber. Inst. f. Geol. u. Pal. d. Karl-Franzens-Universität Graz 3: 8–9; Workshop "Paläozoikumsforschung in Österreich" (19. - 20. Oktober 2001, St. Pankrazen/ Stmk.).

Domeier, M., & Torsvik, T. H. (2014). Plate tectonics in the late Paleozoic. Geoscience Frontiers, 5(3), 303-350.

Dörr, W., Zulauf, G., Gerdes, A., Lahaye, Y., & Kowalczyk, G. (2015). A hidden Tonian basement in the eastern Mediterranean: age constraints from U–Pb data of magmatic and detrital zircons of the External Hellenides (Crete and Peloponnesus). Precambrian Research, 258, 83-108.

Ebner, F., Vozárová, A., Kovács, S., Kräutner, H. G., Branislav, K., Szederkenyi, T., ... & Trajanova, M. (2008). Devonian–Carboniferous pre-flysch and flysch environments in the Circum Pannonian Region. Geologica Carpathica, 59(2), 159-195.

Edel, J.B. (2000). Hypothèse d'une ample rotation horaire tardi-varisque du bloc Maures-Estérel-Corse-Sardaigne. Geol. Fr., 1, 3-19.

Edel, J. B. (2001). The rotations of the Variscides during the Carboniferous collision: paleomagnetic constraints from the Vosges and the Massif Central (France). Tectonophysics, 332(1), 69-92.

Eichhorn, R., Höll, R., Loth, G., & Kennedy, A. (1999a). Implications of U–Pb SHRIMP zircon data on the age and evolution of the Felbertal tungsten deposit (Tauern Window, Austria). International Journal of Earth Sciences, 88(3), 496-512.

Eichhorn, R., Loth, G., Höll, R., Finger, F., Schermaier, A., & Kennedy, A. (1999b). U–Pb SHRIMP data of pre-Alpine rocks of the Tauern Window (Austria); active margin and back-arc found, but where is the adjacent continental crust. Terra nostra, 99(1), 79-80.

Eichhorn, R., Loth, G., & Kennedy, A. (2001). Unravelling the pre-Variscan evolution of the Habach terrane (Tauern Window, Austria) by U-Pb SHRIMP zircon data. Contributions to Mineralogy and Petrology, 142(2), 147-162.

Eichinger S. (2016). Provenience Post-Variszischer Sediment in der östlichen Grauwackenzone. Unpubl. Master Thesis, Uni Graz

Faryad, S. W., Melcher, F., Hoinkes, G., Puhl, J., Meisel, T., & Frank, W. (2002). Relics of eclogite facies metamorphism in the Austroalpine basement, Hochgrössen (Speik complex), Austria. Mineralogy and Petrology, 74(1), 49-73.

Floyd, P. A., Winchester, J. A., Seston, R., Kryza, R., & Crowley, Q. G. (2000). Review of geochemical variation in Lower Palaeozoic metabasites from the NE Bohemian Massif: intracratonic rifting and plume-ridge interaction. Geological Society, London, Special Publications, 179(1), 155-174.

Frank, W., Klein, P., Nowy, W., & Scharbert, S. (1976). Die Datierung geologischer Eriignisse im Altkristallin der Gleinalpe (Steiermark) mit der Rb/Sr-Methode. Tschermaks mineralogische und petrographische Mitteilungen, 23(3), 191-203.

Frank, W., Esterlus, M., Frey, I., Jung, G., Krohe, A., & Weber, J. (1983). Die Entwicklungsgeschichte von Stub-und Koralpenkristallin und die Beziehung zum Grazer Paläozoikum. Jahresber. Hochschulschwerpunkt S, 15(4), 263-293.

Frank, W., & Schlager, W. (2006). Jurassic strike slip versus subduction in the Eastern Alps. International Journal of Earth Sciences, 95(3), 431-450.

Franke, W.; Dallmeyer, D. R.; Weber, K. (1995) Geodynamic Evolution. In: David R. Dallmeyer, Wolfgang Franke und K. Weber (Hg.): Pre-permian geology of Central and Eastern Europe. Berlin, New York: Springer, 579–593.

Frey, M., Desmons, J., & Neubauer, F. (1999). The new metamorphic map of the Alps: Introduction.

Frimmel, H. (1988). Metagranitoide am Westrand der Gurktaler Decke (Oberostalpin): Genese und paläotektonische Implikationen. Jb. Geol. B.-A, 131(4), 575-592.

Frisch, W., & Neubauer, F. (1989). Pre-Alpine terranes and tectonic zoning in the eastern Alps. Geological Society of America Special Papers, 230, 91-100.

Fritz, H., & Neubauer, F. (1988). Geodynamic aspects of the Silurian and Early Devonian sedimentation in the Paleozoic of Graz (Eastern Alps). Schweizerische Mineralogische und Petrographische Mitteilungen, 68(3), 359-367.

Fritz, H., Abdelsalam, M., Ali, K. A., Bingen, B., Collins, A. S., Fowler, A. R., ... & Macey, P. (2013). Orogen styles in the East African Orogen: a review of the Neoproterozoic to Cambrian tectonic evolution. Journal of African Earth Sciences, 86, 65-106.

Froitzheim, N., SCHMID, S. M., & Conti, P. (1994). Repeated change from crustal shortening to orogen-parallel extension in the Austroalpine units of Graubünden. Eclogae Geologicae Helvetiae, 87(2), 559-612.

Froitzheim, N., & Manatschal, G. (1996). Kinematics of Jurassic rifting, mantle exhumation, and passive-margin formation in the Austroalpine and Penninic nappes (eastern Switzerland). Geological Society of America Bulletin, 108(9), 1120-1133.

Gaab, A. S., Poller, U., Janák, M., Kohút, M., & Todt, W. (2005). Zircon U-Pb geochronology and isotopic characterization for the pre-Mesozoic basement of the Northern Veporic Unit (Central Western Carpathians, Slovakia). Schweizerische Mineralogische und Petrographische Mitteilungen, 85(1), 69-88.

Gaab, A. S., Janák, M., Poller, U., & Todt, W. (2006). Alpine reworking of Ordovician protoliths in the Western Carpathians: Geochronological and geochemical data on the Muráň Gneiss Complex, Slovakia. Lithos, 87(3), 261-275.

Gawęda, A., Burda, J., Klötzli, U., Golonka, J., & Szopa, K. (2016). Episodic construction of the Tatra granitoid intrusion (Central Western Carpathians, Poland/Slovakia): consequences for the geodynamics of Variscan collision and Rheic Ocean closure. International Journal of Earth Sciences, 105(4), 1153-1174.

Gebauer, D., & Söllner, F. (1993). U–Pb dating of zircons from eclogites of the austroalpine Oetztal crystalline complex (E-Alps, Austria): conventional and SHRIMP data. In Terra Abstracts [Suppl 4] (Vol. 10).

Golonka, J. (2000). Cambrian-Neogene Plate Tectonic Maps, Wydawnictwa Uniwersytetu Jagiellońskiego, Kraków, 125 pp.

Golonka, J. (2002). Plate-tectonic maps of the Phanerozoic.

Golonka, J. (2009). Phanerozoic paleoenvironment and paleolithofacies maps: Early Paleozoic. Geologia/Akademia Górniczo-Hutnicza im. Stanisława Staszica w Krakowie, 35, 589-654.

Golonka, J. (2012). Paleozoic paleoenvironment and paleolithofacies maps of Gondwana. AGH University of Science and Technology Press.

Golonka, J., & Gaweda, A. (2012). Plate tectonic evolution of the southern margin of Laurussia in the Paleozoic. E. Sharkov.–2012.–doi, 10, 50009.

Grasemann, B., Fritz, H., & Vannay, J. C. (1999). Quantitative kinematic flow analysis from the Main Central Thrust Zone (NW-Himalaya, India): implications for a decelerating strain path and the extrusion of orogenic wedges. Journal of Structural Geology, 21(7), 837-853

Grecula, P. (1982). Gemerikum-segment riftogénneho bazénu Paleotetýdy: Mineralia Slovaca. Monografia 2/82. Alfa.

Gross, J. H. (2012). Massenspektrometrie: Ein Lehrbuch. Springer-Verlag.

Guillot F, Bertrand JM, Pidgeon RT, Leterrier J, Gattiglio M. (1998). Geochronologie U±Pb SHRIMP et IDTIMS de zircons des zones internes des Alpes occidentales .17e RST98 Brest Abstract Volume, 124.

Hammerschmidt, K. (1981). Isotopengeologische Untersuchungen am Augengneis vom Typ Campo Tures bei Rain in Taufers, Südtirol. Società Cooperativa Tipografica.

Handler, R. (1994). 40Ar/39Ar and Rb–Sr mineral dating within a complex polymetamorphic terrain: the northeastern Alps, Austria (Doctoral dissertation, PhD Thesis University of Graz).

Handler, R., Dallmeyer, R. D., & Neubauer, F. (1997). 40Ar/39Ar ages of detrital white mica from Upper Austroalpine units in the Eastern Alps, Austria: Evidence for Cadomian and contrasting Variscan sources. Geologische Rundschau, 86(1), 69-80.

Handler, R., Neubauer, F., Hermann, S., & Dallmeyer, R. D. (1999). Silurian-Devonian 40Ar/39Ar mineral ages from the Kaintaleck Nappe: Evidence for mid-Paleozoic tectonothermal activity in Upper Austroalpine basement units of the Eastern Alps (Austria). GEOLOGICA CARPATHICA-BRATISLAVA-, 50, 229-240.

Hawkesworth, C. J. (1976). Rb/Sr geochronology in the eastern Alps. Contributions to Mineralogy and Petrology, 54(3), 225-244.

Holm, R. (1971). Abbildung und Analyse von Oberflächen mit Rasterelektronenmikroskop und Elektronenspektrometer. Angewandte Chemie, 83(17-18), 632-645.

Hoinkes, G., Thöni, M., Lichem, C., Bernhard, F., Kaindl, R., Schweigl, J., ... & Cosca, M. (1997). Metagranitoids and associated metasediments as indicators for the pre-Alpine magmatic and metamorphic evolution of the western Austroalpine Ötztal Basement (Kaunertal, Tirol). Schweiz Mineral Petrogr Mitt, 77, 299-314.

Hoinkes, G., Koller, F., Rantitsch, G., Dachs, E., Höck, V., Neubauer, F. & Schuster, R. (1999). Alpine metamorphism of the Eastern Alps. – Schweiz. mineral. petr. Mitt. 79, 155–181.

Hubich, D., & Loeschke, J. (1993). Der Comelico-Porphyroid der westlichen Karnischen Alpen (ÖsterreichItalien): Stratigraphie, Petrographie, Geochemie und Zirkonmorphologie. Jahrb Geol BA, 136, 351-374.

Hubmann, B., Ebner, F., Ferretti, A., Histon, K., Kido, E., Krainer, K., Neubauer, F., Schönlaub, H.-P. & Suttner, T.J. (2013). The Paleozoic Era(them). – In: Piller, W.E. [Ed.]: The lithostratigraphic units of the Austrian Stratigraphic Chart 2004 (sedimentary successions) – Vol. I – Abh. Geol. B.-A., 66, 9–133, Wien.

Janák, M., O'Brien, P. J., Hurai, V., & Reutel, C. (1996). Metamorphic evolution and fluid composition of garnet-clinopyroxene amphibolites from the Tatra Mountains, Western Carpathians. Lithos, 39(1), 57-79.

Janák, M., Finger, F., Plašienka, D., Petrík, I., Humer, B., Méres, Š., & Lupták, B. (2002). Variscan high PT recrystallization of Ordovician granitoids in the Veporic unit (Nízke Tatry Mountains, Western Carpathians): new petrological and geochronological data. Geolines, 14, 38-39.

Johnson, P. R., Andresen, A., Collins, A. S., Fowler, A. R., Fritz, H., Ghebreab, W., ... & Stern, R. J. (2011). Late Cryogenian–Ediacaran history of the Arabian–Nubian Shield: a review of depositional, plutonic, structural, and tectonic events in the closing stages of the northern East African Orogen. Journal of African Earth Sciences, 61(3), 167-232.

Klötzli, U. S. (1995). Geochronologische Untersuchungen an Metagranitoiden im ostalpinen Altkristallin W und S des Tauernfensters. Kurzfassungen Arbeitstagung Lienz Österr Geol BA, 95-97.

Klötzli-Chowanetz, E., Klötzli, U., & Koller, F. (1997). Lower Ordovician migmatisation in the Ötztal crystalline basement (Eastern Alps, Austria): linking U–Pb and Pb–Pb dating with zircon morphology. Schweiz Mineral Petrogr Mitt, 77, 315-324.

Kohút, M., Todt, W., Janák, M., & Poller, U. (1997). Thermochronometry of the Variscan basement exhumation in the Velká Fatra Mts. Western Carpathians, Slovakia). Terra Abstracts, 9(1).

Kohút M., Poller U., Todt W. & Konečný P. (2007). Detrital zircon and monazite dating: useful tool for tracking Pan-African orogeny remnants in the Western Carpathians. CzechTec 07 Meeting, Abstr. 42-44.

Kohút, M., Poller, U., Gurk, C., & Todt, W. (2008). Geochemistry and U-Pb detrital zircon ages of metasedimentary rocks of the Lower Unit, Western Tatra Mountains (Slovakia). Acta Geologica Polonica, 58(4), 371-384.

Kohút, M., Uher, P., Putiš, M., Ondrejka, M., Sergeev, S., Larionov, A., & Paderin, I. (2009). SHRIMP U-Th-Pb zircon dating of the granitoid massifs in the Malé Karpaty Mountains (Western Carpathians): evidence of Meso-Hercynian successive S-to I-type granitic magmatism. Geologica Carpathica, 60(5), 345-350.

Kohút, M., Uher, P., Putiš, M., Broska, I., Siman, P., Rodionov, N., & Sergeev, S. (2010). Are there any differences in age of the two principal Hercynian (I-& S-) granite types from the Western Carpathians?–A SHRIMP approach. Dating of Minerals and Rocks, Metamorphic, Magmatic and Metallogenetic Processes, As Well As Tectonic Events, 17-8.

Korokovsky, S. P., Putis, M., Kotov, A. B., Sal'nikova, E. B., & Kovach, V. P. (1998). High-pressure metamorphism of Phengite Gneisses in the Lower Austro–Alpine Nappe Unit, Eastern Alps: mineral equilibria, P–T parameters, and age. Petrology (Moscow), 6, 655-672.

Kováčik, M., Konečný, P., Kollárová, V., Holický, I., & Siman, P. (2005). Electron microprobe dating of monazite in basement metamorphites from the Kohút zone of Veporicum and case correlation aspects (Western Carpathians). Slovak Geol Mag, 11, 91-105.

Kráľ, J., Hess, C., Kober, B., & Lippolt, H. J. (1997). 207Pb/206Pb and 40Ar/39Ar age data from plutonic rocks of the Strážovské vrchy Mts. basement, Western Carpathians. Geological evolution of the Western Carpathians. Mineralia Slovaca. Monograph, Bratislava, 253-260.

Krist, E., Korikovskij, S. P., Putiš, M., Janák, M., & Faryad, S. W. (1992). Geology and Petrology of Metamorphic Rocks of the Western Carpathian Crystalline Complexes; Auth. Ernest Krist, Sergej Petrovič Korikovskij, Marián Putiš, Marián Janák, Shah Wali Faryad. Univerzita Komenského.

Kroner, U.; Mansy, J. L.; Mazur, S.; Aleksandrowski, P.; Hann, H. P.; Huckriede, H. et al. (2008). Variscan tectonics. The Geology of Central Europe. London, 371–94.

Kroner, U., & Romer, R. L. (2013). Two plates—many subduction zones: the Variscan orogeny reconsidered. Gondwana Research, 24(1), 298-329.

Kruhl, J. H. (1996). Prism-and basal-plane parallel subgrain boundaries in quartz: A microstructural geothermobarometer. Journal of metamorphic Geology, 14(5), 581-589.

Kurz, W., & Froitzheim, N. (2002). The exhumation of eclogite-facies metamorphic rocks—a review of models confronted with examples from the Alps. International Geology Review, 44(8), 702-743.

Kurz, W., & Fritz, H. (2003). Tectonometamorphic evolution of the Austroalpine Nappe Complex in the central Eastern Alps—consequences for the Eo-Alpine evolution of the Eastern Alps. International Geology Review, 45(12), 1100-1127.

Law, R. D. (2014). Deformation thermometry based on quartz c-axis fabrics and recrystallization microstructures: A review. Journal of Structural Geology, 66, 129-161.

Liebetrau, V. (1996). Petrographie, Geochemie und Datierung der Fliielagranitischen Assoziation (Jiingere Orthogneise) des Silvrettakristallins-Graubiinden Schweiz (Ph. D. thesis, Univ. Fribourg).

Linnemann, U., Gerdes, A., Drost, K., & Buschmann, B. (2007). The continuum between Cadomian orogenesis and opening of the Rheic Ocean: Constraints from LA-ICP-MS U-Pb zircon dating and analysis of plate-tectonic setting (Saxo-Thuringian zone, northeastern Bohemian Massif, Germany). Geological Society of America Special Papers, 423, 61-96.

Loth, G., Eichhorn, R., Schauder, P., Höll, R., & Kennedy, A. (1999). UąPb SHRIMP data from the Wildschönau ophiolite complex: evidence for Cambro-Ordovician rifting in the Western Greywacke supergroup (Eastern Alps). Ber Dt Min Ges Eur J Mineral, 11, 149.

Loth, G., Eichhorn, R., Höll, R., Kennedy, A., Schauder, P., & Söllner, F. (2001). Cambro-Ordovician age of a metagabbro from the Wildschönau ophiolite complex, Greywacke Supergroup (eastern Alps, Austria): A U-Pb SHRIMP study. European Journal of Mineralogy, 13(1), 57-66.

Ludwig, K. (2012). User's manual for Isoplot version 3.75–4.15: a geochronological toolkit for Microsoft. Excel Berkley Geochronological Center Special Publication, (5).

Manby, G. M., & Thiedig, F. (1988). Petrology of eclogites from the Saualpe, Austria. Schweizerische Mineralogische und Petrographische Mitteilungen, 68(3), 441-466.

Maniar, P. D., & Piccoli, P. M. (1989). Tectonic discrimination of granitoids. Geological society of America bulletin, 101(5), 635-643.

Melcher, F., & Meisel, T. (2004). A metamorphosed Early Cambrian crust–mantle transition in the Eastern Alps, Austria. Journal of Petrology, 45(8), 1689-1723.

Ménot, R. P. (1987). Magmatismes paléozoiques et structuration carbonifère du Massif de Belledonne (Alpes Françaises). Contraintes nouvelles pour les schémas d'évolution de la chaîne varisque ouest-européenne (Doctoral dissertation, Université Claude Bernard-Lyon I).

Ménot, R. P., Peucat, J. J., Scarenzi, D., & Piboule, M. (1988). 496 My age of plagiogranites in the Chamrousse ophiolite complex (external crystalline massifs in the French Alps): evidence of a Lower Paleozoic oceanization. Earth and Planetary Science Letters, 88(1-2), 82-92.

Miller, C., & Thöni, M. (1995). Origin of eclogites from the Austroalpine Ötztal basement (Tirol, Austria): geochemistry and Sm-Nd vs. Rb- Sr isotope systematics. Chemical Geology, 122(1), 199-225.

Miller, C., & Thöni, M. (1997). Eo-Alpine eclogitisation of Permian MORB-type gabbros in the Koralpe (Eastern Alps, Austria): new geochronological, geochemical and petrological data. Chemical Geology, 137(3), 283-310.

Moecher, D. P., & Samson, S. D. (2006). Differential zircon fertility of source terranes and natural bias in the detrital zircon record: Implications for sedimentary provenance analysis. Earth and Planetary Science Letters, 247(3), 252-266.

Müller, B., Klötzli, U. S., & Flisch, M. (1995). U-Pb and Pb-Pb zircon dating of the older orthogneiss suite in the Silvretta nappe, eastern Alps: Cadomian magmatism in the upper Austro-Alpine realm. Geologische Rundschau, 84(3), 457-465.

Müller, B., Schaltegger, U., Klötzli, U., & Flisch, M. (1996). Early Cambrian oceanic plagiogranite in the Silvretta nappe, eastern Alps: Geochemical, zircon U-Pb and Rb-Sr data from garnet-hornblende-plagioclase gneisses. Geologische Rundschau, 85(4), 822-831.

Nance, R. D., Gutiérrez-Alonso, G., Keppie, J. D., Linnemann, U., Murphy, J. B., Quesada, C., ... & Woodcock, N. H. (2010). Evolution of the Rheic ocean. Gondwana Research, 17(2), 194-222.

Nasdala, L., Hofmeister, W., Norberg, N., Martinson, J. M., Corfu, F., Dörr, W., ... & Frei, D. (2008). Zircon M257-a Homogeneous Natural Reference Material for the Ion Microprobe U-Pb Analysis of Zircon. Geostandards and Geoanalytical Research, 32(3), 247-265.

Neubauer, F., & Pistotnik, J. (1984). Das Altpaläozoikum und Unterkarbon des Gurktaler Deckensystems (Ostalpen) und ihre paläogeographischen Beziehungen. Geologische Rundschau, 73(1), 149-174.

Neubauer, F., Frisch, W., & Hansen, B. T. (1987). Time relations between Eoalpine metamorphism and thrusting: evidence from the crystalline basement of the Eastern Greywacke Zone. Geodynamics of the Eastern Alps, 263-271.

Neubauer, F., Frisch, W., & Hansen, B. T. (1989). A Late Archean rock in the Eastern Alps. In Terra Abstr (Vol. 1, No. 5).

Neubauer, F., & Vozárová, A. (1990). The Noetsch-Veitsch-North Gemeric zone of Alps and Carpathians: correlation, paleogeography and significance for Variscan orogeny. Festive Volume: Thirty years of geol. Cooperation between Austria and Czechoslovakia, Ústr. Ústav geologický, Praha, 167-170.

Neubauer, F., & Frisch, W. (1993). The Austro-Alpine metamorphic basement east of the Tauern Window. In Pre-Mesozoic geology in the Alps (pp. 515-536). Springer Berlin Heidelberg.

Neubauer, F., Frisch, W., Hansen, BT., (1993). The pre – Alpine tectonothermal evolution of the Rennfeld region, Eastern Alps: a U – Pb zircon study. Lithos (submitted).

Neubauer, F., Handler, R., Hermann, S., & Paulus, G. (1994). Revised lithostratigraphy and structure of the eastern Graywacke Zone (Eastern Alps). Mitt. Österr. Geol. Ges, 86, 61-74.

Neubauer, F., Genser, J., & Handler, R. (2000). The Eastern Alps: result of a two-stage collision process. Mitt. österr. geol. Ges, 92(1999), 117-134.

Neubauer, F., Frisch, W., & Hansen, B. T. (2002). Early Palaeozoic tectonothermal events in basement complexes of the eastern Greywacke Zone (Eastern Alps): evidence from U–Pb zircon data. International Journal of Earth Sciences, 91(5), 775-786.

Neubauer, F., Frisch, W., & Hansen, B. T. (2002). Early Paleozoic and Variscan events in the Austroalpine Rennfeld block, Eastern Alps: a U-Pb zircon study. Jahrbuch der Geologischen Bundesanstalt, 143, 567-580.

Neubauer, F. & Genser, J. (unpubl.)

Neubauer, F., Friedl, G., Genser, J., Handler, R., Mader, D., & Schneider, D. (2007). Origin and tectonic evolution of the Eastern Alps deduced from dating of detrital white mica: a review. Austrian Journal of Earth Sciences, 100, 8-23.

Nievoll, J. (1984). Der Südrand der Grauwackenzone zwischen Stübming und Neuberg (Obersteiermark, ÖK 103 Kindberg). Mitt. Österr. Geol. Ges, 77, 63-71.

Nievoll, J. (2015) Alpidische Tektonik in der Norischen Decke der östlichen Grauwackenzone zwischen Neuberg und Turnau (GK50 Blatt 103 Kindberg). Arbeitstagung der Geologischen Bundesanstalt, 2015, Mitterdorf im Mürztal.

Nievoll, J. & Suttner, T.J. (2015) Stratigrafie der Norischen Decke auf GK50 Blatt 103 Kindberg. Arbeitstagung der Geologischen Bundesanstalt, 2015, Mitterdorf im Mürztal.

Panwitz, C. (2006). Provenienzanalyse an paläozoischen Metasedimenten der Ostalpen mit Schwerpunkt in der Nördlichen Grauwackenzone.

Passchier, C. W., & Trouw, R. A. J. (1996). Microtectonics Springer-Verlag. Berlin, Germany, 289.

Paulus, G. (1991). Die Entwicklungsgeschichte der Altkristallinschollen von Vöstenhof/Schlöglmühl sowie geochemische, geochronologische und petrogenetische Untersuchungen der Riebeckitgneise von Gloggnitz im Ostteil der nördlichen Grauwackenzone (Ostalpin). (Ph.D. thesis, Univ. Graz).

Petrík, I., Broska, I., & Uher, P. (1994). Evolution of the Western Carpathian granite magmatism: age, source rock, geotectonic setting and relation to the Variscan structure. Geol. Carpathica, 45(5), 283-291.

Poller, U., & Todt, W. (2000). U—Pb single zircon data of granitoids from the High Tatra Mountains (Slovakia): implications for the geodynamic evolution. Transactions of the Royal Society of Edinburgh: Earth Sciences, 91(1-2), 235-243.

Poller, U., Janák, M., Kohút, M., & Todt, W. (2000). Early Variscan magmatism in the Western Carpathians: U–Pb zircon data from granitoids and orthogneisses of the Tatra Mountains (Slovakia). International Journal of Earth Sciences, 89(2), 336-349.

Poller, U., Kohút, M., Anders, B., & Todt, W. (2005). Multistage geochronological evolution of the Velká Fatra Mountains—a combined TIMS and ion-microprobe study on zircons. Lithos, 82(1), 113-124.

Putiš, M., Kotov, A. B., Korikovsky, S. P., SALNIKOVA, E. B., YAKOVLEVA, S. Z., BEREZHNAYA, N. G., ... & Plotkina, J. V. (2001). U-Pb zircon ages of dioritic and trondhjemitic rocks from a layered amphibolitic complex crosscut by granite vein (Veporic basement, Western Carpathians). Geologica Carpathica, 52(1), 49-60.

Putis, M., Ketov, A. B., Petrik, I., Korikovsky, S. P., Madarás, J., Salnikova, E. B., ... & Kovach, V. P. (2003). Early-vs. Late orogenic granitoids relationships in the Variscan basement of the Western Carpathians. GEOLOGICA CARPATHICA-BRATISLAVA-, 54(3), 163-174.

Putis, M., Sergeev, S., Ondrejka, M., Larionov, A., Siman, P., Spisiak, J., ... & Paderin, I. (2008). Cambrian-Ordovician metaigneous rocks associated with Cadomian fragments in the West-Carpathian basement dated by SHRIMP on zircons: a record from the Gondwana active margin setting. GEOLOGICA CARPATHICA-BRATISLAVA-, 59(1), 3.

Radvanec, M., Sergeev, S., Putiš, M., & Larionov, A. Zircon ages from HP/UHP meta-lamprophyre (?) spheric fragment in meta-peridotite (Gemer area, W. Carpathians). DATING 2010, 33.

Ratschbacher, L. (1986). Kinematics of Austro-Alpine cover nappes: changing translation path due to transpression. Tectonophysics, 125(4), 335-356.

Ratschbacher, L., & Neubauer, F. (1989). West-directed décollement of Austro-Alpine cover nappes in the eastern Alps: geometrical and rheological considerations. Geological Society, London, Special Publications, 45(1), 243-262.

Ratschbacher, L. (1987). Stratigraphy, tectonics and paleogeography of the Veitsch Nappe/Graywackezone, Eastern Alps, Austria: A rearrangement. Mineralia Slovaca, Monogr, 1987, 407-414.

Rubatto, D. (2002). Zircon trace element geochemistry: partitioning with garnet and the link between U–Pb ages and metamorphism. Chemical Geology, 184(1), 123-138.

Schaltegger, U. (1993). The evolution of the polymetamorphic basement in the Central Alps unravelled by precise U− Pb zircon dating. Contributions to Mineralogy and Petrology, 113(4), 466-478.

Schaltegger, U., Nägler, T. F., Corfu, F., Maggetti, M., Galetti, G., & Stosch, H. G. (1997). A Cambrian island arc in the Silvretta nappe: constraints from geochemistry and geochronology. Schweizerische Mineralogische und Petrographische Mitteilungen, 77, 337-350.

Scharbert, S. (1981). Untersuchungen zum Alter des Seckauer Kristallins. Mitt Ges Geol Bergbaustud Österr, 27, 175-188.

Schätz, M., Bachtadse, V., Tait, J. A., & Soffel, H. C. (1997). Palaeomagnetic results from Lower Devonian sediments of the southern Alps. Terra Nostra, 97(5), 152-155.

Schmid, S. M., & Casey, M. (1986). Complete fabric analysis of some commonly observed quartz c-axis patterns. Mineral and Rock Deformation: Laboratory Studies: The Paterson Volume, 263-286.

Schmid, S. M., Pfiffner, O. A., Froitzheim, N., Schönborn, G., & Kissling, E. (1996). Geophysical-geological transect and tectonic evolution of the Swiss-Italian Alps. Tectonics, 15(5), 1036-1064.

Schmid, S. M., Fügenschuh, B., Kissling, E., & Schuster, R. (2004). Tectonic map and overall architecture of the Alpine orogen. Eclogae Geologicae Helvetiae, 97(1), 93-117.

Schmid, S. M., Scharf, A., Handy, M. R., & Rosenberg, C. L. (2013). The Tauern Window (Eastern Alps, Austria): a new tectonic map, with cross-sections and a tectonometamorphic synthesis. Swiss Journal of Geosciences, 106(1), 1-32.

Schmidt, K. (1999). Geochronologie entlang eines Metamorphoseprofils vom S-Rand der Nördlichen Kalkalpen bis zum Unterostalpin des Semmeringgebietes (Niederösterreich, Steiermark). (Ph.D. Thesis, Univ. Vienna).

Schönlaub, H. P. (1982). Die Grauwackenzone in den Eisenerzer Alpen (Österreich). Jb. Geol. B.-A, 124(2), 361-123.

Schulz, B., & Bombach, K. (2003). Single zircon Pb–Pb geochronology of the Early-Palaeozoic magmatic evolution in the Austroalpine basement to the south of the Tauern Window. Jahrbuch der Geologischen Bundesanstalt, 143, 303-321.

Schulz, B., Bombach, K., Pawlig, S., & Brätz, H. (2004). Neoproterozoic to Early-Palaeozoic magmatic evolution in the Gondwana-derived Austroalpine basement to the south of the Tauern Window (Eastern Alps). International Journal of Earth Sciences, 93(5), 824-843.

Schulz, B., Steenken, A., & Siegesmund, S. (2008). Geodynamic evolution of an Alpine terrane—the Austroalpine basement to the south of the Tauern Window as a part of the Adriatic Plate (eastern Alps). Geological Society, London, Special Publications, 298(1), 5-44.

Schuster, R., & Frank, W. (1999). Metamorphic evolution of the Austroalpine units east of the Tauern Window: indications for Jurassic strike slip tectonics. Mitt. Ges. Geol. Bergbaustud. Österr. (42), 37–58.

Schuster, K., Berka, R., Draganits, E., Frank, W., & Schuster, R. (2001). Lithologien, Metamorphosegeschichte und tektonischer Bau der kristallinen Einheiten am Alpenostrand. Geologische Bundesanstalt, Arbeitstagung, 29-56.

Schuster, R. (2003). Das eo-Alpine Ereigniss in den Ostalpen: Plattentektonische Situation und interne Struktur des Ostalpinen Kristallins. Geologische Bundesanstalt Arbeitstagung, 141-159.

Schuster, R. & Stüwe, K. (2010). Die Geologie der Alpen im Zeitraffer. In: Mitt. naturwiss. Ver. Steiermark 140, 5–21.

Schuster, R., Kurz, W., Krenn, K., & Fritz, H. (2013). Introduction to the Geology of the Eastern Alps. Berichte der Geologischen Bundesanstalt Wien, 99, 121-133.

Schuster R., (2015). Grauwackenzone und Grauwackenzone- Deckensystem. Arbeitstagung der Geologischen Bundesanstalt, 21-25 September 2015, Mitterdorf im Mürztal.

Shcherbak, N. P., Bartnitsky, E. N., Mitskievich, N. Y., Stepanyuk, L. M., Cambel, B., & Grecula, P. (1988). U-Pb radiometric determination of the age of zircons from Modra granodiorite, Malé Karpaty Mts., and porphyroid from Spiš-Gemer Ore Mts., Lower Paleozoic (Western Carpathians). Geol. Zbor. Geol. Carpath, 39, 427-436.

Shcherbak, N. P., Cambel, B., Bartnicky, E. N. & Stepanyuk, L .M. (1990). U – Pb age of granitoid rock from the Dubna skala – Mala Fatra Mts. Geol. Carpath. 41, 407 – 414.

Sirevaag, H., Jacobs, J., Ksienzyk, A. K., Rocchi, S., Paoli, G., Jørgensen, H., & Košler, J. (2016). From Gondwana to Europe: The journey of Elba Island (Italy) as recorded by U–Pb detrital zircon ages of Paleozoic metasedimentary rocks. Gondwana Research.

Sláma, J., Košler, J., Condon, D. J., Crowley, J. L., Gerdes, A., Hanchar, J. M., ... & Schaltegger, U. (2008). Plešovice zircon—a new natural reference material for U–Pb and Hf isotopic microanalysis. Chemical Geology, 249(1), 1-35.

Söllner, F., Höll, R., & Miller, H. (1991). U-Pb-Systematik der Zirkone in Meta-Vulkaniten (“Porphyroiden”) aus der Nördlichen Grauwackenzone und dem Tauernfenster (Ostalpen, Österreich). Z Dtsch Geol Ges, 142, 285-299.

Stampfli, G., Marcoux, J., & Baud, A. (1991). Tethyan margins in space and time. Palaeogeography, Palaeoclimatology, Palaeoecology, 87(1-4), 373-409.

Stampfli, G. M. (1993). Le Briançonnais, terrain exotique dans les Alpes?. Eclogae Geologicae Helvetiae, 86(1), 1-45.

Stampfli, G. M. (1996). The intra-Alpine terrain: a Paleotethyan remnant in the Alpine Variscides. Eclogae Geologicae Helvetiae, 89(1), 13-42.

Stampfli, G. M. (2000). Tethyan oceans. Geological society, london, special publications, 173(1), 1-23.

Stampfli, G. M., & Borel, G. D. (2002). A plate tectonic model for the Paleozoic and Mesozoic constrained by dynamic plate boundaries and restored synthetic oceanic isochrons. Earth and Planetary Science Letters, 196(1), 17-33.

Stampfli, G. M., von Raumer, J. F., & Borel, G. D. (2002). Paleozoic evolution of pre-Variscan terranes: from Gondwana to the Variscan collision. Special Papers-Geological Society of America, 263-280.

Stampfli, G. M., Von Raumer, J., & Wilhem, C. (2011). The distribution of Gondwana derived terranes in the early Paleozoic. Ordovician of the world. Cuadernos del Museo Geominero, 14, 567-574.

Stampfli, G. M., Hochard, C., Vérard, C., & Wilhem, C. (2013). The formation of Pangea. Tectonophysics, 593, 1-19.

Steiger, R., & Jäger, E. (1977). Subcommission on geochronology: convention on the use of decay constants in geo- and cosmochronology. Earth and planetary science letters, 36(3), 359-362.

Tait, J., Schätz, M., Bachtadse, V., & Soffel, H. (1998). Paleogeography of paleozoic terranes in the Variscan and Alpine fold belts. Schr Staatl Mus Min Geol Dresden, 9, 192-193.

Thöni, M. (1981). Degree and evolution of the Alpine metamorphism in the Austroalpine unit W of the Hohe Tauern in the light of K/Ar and Rb/Sr age determinations on micas. Jahrbuch der geologischen Bundesanstalt, 124(1), 111-174.

Thöni, M. (1999). A review of geochronological data from the Eastern Alps. Schweizerische Mineralogische und Petrographische Mitteilungen, 79(1), 209-230.

Thöni, M., & Miller, C. (2004). Ordovician meta-pegmatite garnet (NW Ötztal basement, Tyrol, Eastern Alps): preservation of magmatic garnet chemistry and Sm–Nd age during mylonitization. Chemical geology, 209(1), 1-26.

Thöni, M. (2006). Dating eclogite-facies metamorphism in the Eastern Alps–approaches, results, interpretations: a review. Mineralogy and Petrology, 88(1-2), 123-148.

Tollmann, A. (1964). Exkursion 11/6: Semmering—Grauwackenzone. Mitt Geol Ges Wien, 57, 193-203.

Tollmann, A. (1977). Geologie von Österreich, Band 1: Die Zentralalpen. Franz Deuticke, Wien.

Tollmann, A. (1985). Geologie von Österreich, Band 2/Fl: Nördl.

Torsvik, T. H., & Smethurst, M. A. (1994). Geographic mapping and paleoreconstruction package (GMAP). Software description and examples of paleoreconstructions.

Torsvik, T. H., & Eide, E. A. (1998). Phanerozoic palaeogeography and geodynamics with Atlantic details. NGU report, 98, 82.

Troll, G., Forst, R., Söllner, F., Brack, W., Köhler, H., & Müller-Sohnius, D. (1976). Über Bau, Alter und Metamorphose des Altkristallins der Schobergruppe, Osttirol. Geologische Rundschau, 65(1), 483-511.

von Quadt, A. (1992). U-Pb zircon and Sm—Nd geochronology of mafic and ultramafic rocks from the central part of the Tauern Window (eastern Alps). Contributions to Mineralogy and Petrology, 110(1), 57-67.

von Quadt, A., Günther, D., Frischknecht, R., Zimmermann, R., & Franz, G. (1997). The evolution of pre-Variscan eclogites of the Tauern Window (Eastern Alps): a Sm/Nd-, conventional and laser ICP-MS zircon U–Pb study. Schweizerische Mineralogische und Petrographische Mitteilungen, 77, 265-279.

Von Raumer, J. F., & Neubauer, F. (1993). Late Precambrian and Palaeozoic evolution of the Alpine basement—an overview. In Pre-Mesozoic geology in the Alps (pp. 625-639). Springer Berlin Heidelberg.

Von Raumer, J. F. (1998). The Palaeozoic evolution in the Alps: from Gondwana to Pangea. Geologische Rundschau, 87(3), 407-435.

von Raumer, J. F., Bussy, F., & Schaltegger, U. (1999) Ordovician granitoids in the Alps: significance and Peri-Gondwanan correlation. Schriften der Alfred-Wegener-Stiftung, Terra Nostra, 99(1), 165.

Von Raumer, J., Stampfli, G., Borel, G., & Bussy, F. (2002). Organization of pre-Variscan basement areas at the north-Gondwanan margin. International Journal of Earth Sciences, 91(1), 35-52.

von Raumer, J. F., Stampfli, G. M., & Bussy, F. (2003). Gondwana-derived microcontinents—the constituents of the Variscan and Alpine collisional orogens. Tectonophysics, 365(1), 7-22.

von Raumer, J. F., & Stampfli, G. M. (2008). The birth of the Rheic Ocean—Early Palaeozoic subsidence patterns and subsequent tectonic plate scenarios. Tectonophysics, 461(1), 9-20.

Von Raumer, J. F., Bussy, F., Schaltegger, U., Schulz, B., & Stampfli, G. M. (2013). Pre-Mesozoic Alpine basements—their place in the European Paleozoic framework. Geological Society of America Bulletin, 125(1-2), 89-108.

Vermeesch, P. (2012). On the visualisation of detrital age distributions. Chemical Geology, 312, 190-194.

Vozárová, A., Ebner, F., Kovács, S., Kräutner, H. G., Szederkenyi, T., Krstić, B., ... & Skaberne, D. (2009). Late Variscan (Carboniferous to Permian) environments in the Circum Pannonian Region. Geologica Carpathica, 60(1), 71-104.

Vozárová, A., Šarinová, K., Larionov, A., Presnyakov, S., & Sergeev, S. (2010). Late Cambrian/Ordovician magmatic arc type volcanism in the Southern Gemericum basement, Western Carpathians, Slovakia: U–Pb (SHRIMP) data from zircons. International Journal of Earth Sciences, 99(1), 17-37.

Vozárová, A., Lepekhina, E., Vozár, J., & Rodionov, N. (2010, Conference). In situ U-Pb (SHRIMP) zircon age dating from the Permian volcanites of the Northern Veporicum. Dating. Conference 2010: Dating of minerals and rocks, metamorphic, magmatic and metallogenetic processes, as well as tectonic events. Editor Milan Kohút. Bratislava, 2010.

VozáRová, A., Laurinc, D., Šarinová, K., Larionov, A., Presnyakov, S., Rodionov, N., & Paderin, I. (2013). Pb ages of detrital zircons in relation to geodynamic evolution: Paleozoic of the Northern Gemericum (Western Carpathians, Slovakia). Journal of Sedimentary Research, 83(11), 915-927.

Wiedenbeck, M. A. P. C., Alle, P., Corfu, F., Griffin, W. L., Meier, M., Oberli, F., ... & Spiegel, W. (1995). Three natural zircon standards for U-Th-Pb, Lu-Hf, trace element and REE analyses. Geostandards newsletter, 19(1), 1-23.

Žák, J., Verner, K., Finger, F., Faryad, S. W., Chlupáčová, M., & Veselovský, F. (2011). The generation of voluminous S-type granites in the Moldanubian unit, Bohemian Massif, by rapid isothermal exhumation of the metapelitic middle crust. Lithos, 121(1), 25-40.

Online references

Retsch solutions in Milling & Sieving. Analysesiebe.
URL: http://www.retsch.de/de/produkte/sieben/analysensiebe (status May, 2016)

Geoscience News and Information. How to Pan for Gold.
URL: http://geology.com/articles/panning-gold/ (status May, 2016)

Estwing. URL: http://www.estwing.com/ (status June, 2016)

S.G.Frantz Co. Magnetic Separators. URL: http://www.sgfrantz.com/ (status June, 2016)

TC-Tungsten Compounds-environment-friendly heavy liquid. Informationsdatenblatt.
URL: http://www.heavy-liquid.com/de/productinformation/informationdatasheet/ (status June, 2016).

Digitaler Atlas Steiermark.
URL:http://gis2.stmk.gv.at/atlas/(S(skc3oxm4ish4q5w0ltgc55wo))/init.aspx?karte=gel&ks=das&cms=da&massstab=800000 (status May, 2016).

18 Appendix

18.1 Appendix A. sample register

Table 2: This table lists all the samples taken during the mapping process

18.10.2015						
					Koordinaten	
Nr.	**Gestein**	**Decke**	**SF**	**L**	**N**	**E**
P1	Geröllführender Schiefer	Silbersberg			47°40,55'	15°43,38'
P2	Grünschiefer	Silbersberg	330/50	345/55	47°40,332	15°43,317
P3	Silbersbergphyllit	Silbersberg	13/55	292/10	47°40,332	15°43,317
P4	Phyllit	Silbersberg			47°40,332	15°43,317
P5	Phyllit	Silbersberg	10/35	320/28	47°40,28'	15°43,23'
P6	Phyllit	Silbersberg	330/40	302/35	47°40,28'	15°43,23'
P7	Gangestein	Silbersberg			47°40,28'	15°43,23'
P8	Metakonglomerat	Silbersberg			47°40,172	15°43,120
P9	Schiefer/Phyllit	Veitsch			47°40,142	15°43,076
P10	Metakonglomerat	Veitsch			47°39,901	15°42,796
P11	Metakonglomerat	Tattermann			47°39,734	15°42,777
P12	Qtz - reich mit Komponenten	Tattermann?			47°39,734	15°42,777
P13	Qtzitschiefer	Tattermann			47°39,734	15°42,777
P14	Qtz - armer Phyllit	Tattermann?			47°39,734	15°42,777
P15	Phyllit	Veitsch	10/25	300/10	47°39,792	15°41,873
P16	Ep - Chl - Schiefer	Silbersberg			47°39,97'	15°41,97'
22.10.2015						
					Koordinaten	
Nr.	**Gestein**	**Decke**	**SF**	**L**	**N**	**E**
R1	Porphyr. Tuff?	Silbersberg			47°40,366	15°41,929
R2	Metakonglomerat	Silbersberg			47°40,328	15°41,892
R3	Grünschiefer	Silbersberg			47°40,328	15°41,892
R4	Grünschiefer	Silbersberg	350/25	275/25	47°40,300	15°41,836
R5	Grünschiefer	Silbersberg			47°40,268	15°41,819
R6	saurer Vulk.	Silbersberg			47°40,489	15°42,137
R7	Metakonglomerat	Silbersberg			47°40,489	15°42,137
R8	Phyllit				47°40,32'	15°42,24'
R9	Metakonglomerat	Silbersberg			47°40,327	15°42,154
29.10.2015						
					Koordinaten	
Nr.	**Gestein**	**Decke**	**SF**	**L**	**N**	**E**
R10	Riebeckitgneis	Silbersberg			47°39,906	15°41,660
R11	vulk. Gang	Silbersberg	300/45u	270/40	47°39,971	15°41,743
R12	Phyllit + Grünschiefer	Silbersberg	0/10 ??		47°39,602	15°41,729

18.2 Appendix B

18.2.1 *Silbersberg metasandstone (G21)*

Table 3: Those tables depict the measured values of the zircons of the Silbersberg metasandstone, corrected through the EXCEL sheet LamTool U – Th – Pb VI of Košler und Klötzli (unpubl.). M257 (Nasdala et al., 2008), 91500 (Wiedenbeck et al., 1995) and Plešovice (Sláma et al., 2008) are the used standard samples. The crossed out measurements are discordant and were excluded of further steps.

File name	std.	start	end	204Pb	206Pb	207Pb	208Pb	232Th	238U	206Pb/204Pb	2RSE (%)	207Pb/235U	2RSE (%)	206Pb/238U	2RSE (%)	Rho	207Pb/206Pb	2RSE (%)	208Pb/206Pb	2RSE (%)	208Pb/232Th	2RSE (%)	238U/206Pb	2RSE (%)	207Pb/206Pb	2RSE (%)
20160707_M257_001		52	209	#DIV/0!	3.9E-03	2.9E-04	3.8E-04	1.5E-02	6.9E-02	#DIV/0!	#DIV/0!	0.7417	3.58	0.0926	3.52	0.49	0.0581	0.37	0.3002	0.31	0.0281	2.19	10.796	3.52	0.0581	0.37
20160707_M257_002		53	207	#DIV/0!	3.9E-03	2.9E-04	3.8E-04	1.5E-02	6.9E-02	#DIV/0!	#DIV/0!	0.7468	3.71	0.0933	3.63	0.49	0.0580	0.36	0.2997	0.38	0.0278	2.47	10.714	3.63	0.0580	0.36
20160707_M257_003		54	214	#DIV/0!	4.2E-03	3.0E-04	4.0E-04	1.6E-02	7.5E-02	#DIV/0!	#DIV/0!	0.7387	2.86	0.0926	2.67	0.47	0.0579	0.33	0.3105	0.24	0.0285	1.48	10.799	2.67	0.0579	0.33
20160707_M257_004		55	213	#DIV/0!	4.2E-03	3.1E-04	4.1E-04	1.6E-02	7.6E-02	#DIV/0!	#DIV/0!	0.7422	2.67	0.0932	2.60	0.49	0.0578	0.35	0.3102	0.30	0.0288	1.56	10.728	2.60	0.0578	0.35
20160707_M257_005		53	212	2.5E-06	4.0E-03	2.9E-04	3.9E-04	1.6E-02	7.1E-02	2025	1	0.7354	2.99	0.0920	3.00	0.50	0.0580	0.34	0.3147	0.32	0.0288	1.98	10.872	3.00	0.0580	0.34
20160707_M257_006		56	210	2.5E-06	4.0E-03	2.9E-04	3.9E-04	1.5E-02	7.1E-02	#DIV/0!	#DIV/0!	0.7424	3.24	0.0930	3.17	0.49	0.0579	0.33	0.3134	0.33	0.0290	2.06	10.751	3.17	0.0579	0.33
20160707_M257_007		53	211	#DIV/0!	3.8E-03	2.8E-04	3.7E-04	1.5E-02	6.9E-02	#DIV/0!	#DIV/0!	0.7306	3.16	0.0913	3.22	0.51	0.0582	0.40	0.3069	0.36	0.0284	2.20	10.957	3.22	0.0582	0.40
20160707_M257_008		56	213	#DIV/0!	3.9E-03	2.8E-04	3.7E-04	1.5E-02	6.8E-02	#DIV/0!	#DIV/0!	0.7355	3.42	0.0923	3.36	0.49	0.0579	0.37	0.3041	0.36	0.0287	2.51	10.835	3.36	0.0579	0.37
20160707_M257_009		53	202	2.9E-06	4.1E-03	3.0E-04	4.0E-04	1.6E-02	7.3E-02	842	3	0.7411	2.72	0.0925	2.68	0.49	0.0581	0.36	0.2904	0.36	0.0294	1.64	10.817	2.68	0.0581	0.36
20160707_M257_009		59	210	2.9E-06	4.0E-03	2.9E-04	3.9E-04	1.5E-02	7.2E-02	1338	0	0.7453	3.22	0.0933	2.93	0.46	0.0581	0.37	0.2839	0.37	0.0285	1.89	10.716	2.93	0.0581	0.37
20160707_M257_010		54	203	2.9E-06	4.1E-03	3.0E-04	4.0E-04	1.6E-02	7.4E-02	1793	1	0.7396	2.77	0.0926	2.68	0.48	0.0580	0.35	0.2886	0.34	0.0299	1.58	10.797	2.68	0.0580	0.35
20160707_M257_010		49	212	2.9E-06	4.1E-03	3.0E-04	3.9E-04	1.6E-02	7.3E-02	1782	0	0.7405	2.42	0.0928	2.32	0.48	0.0580	0.32	0.2826	0.31	0.0291	1.43	10.772	2.32	0.0580	0.32
20160707_M257_011		52	211	#DIV/0!	4.0E-03	2.9E-04	3.9E-04	1.6E-02	7.3E-02	#DIV/0!	#DIV/0!	0.7246	2.44	0.0904	2.37	0.49	0.0581	0.30	0.2536	0.34	0.0288	1.26	11.057	2.37	0.0581	0.30
20160707_M257_012		54	209	3.1E-06	4.0E-03	2.9E-04	3.9E-04	1.6E-02	7.2E-02	#DIV/0!	#DIV/0!	0.7278	2.42	0.0906	2.60	0.54	0.0582	0.35	0.2512	0.33	0.0290	1.30	11.032	2.60	0.0582	0.35

File name	std.	start	end	204Pb	206Pb	207Pb	208Pb	232Th	238U	206Pb/204Pb	2RSE (%)	207Pb/235U	2RSE (%)	206Pb/238U	2RSE (%)	Rho	207Pb/206Pb	2RSE (%)	208Pb/206Pb	2RSE (%)	208Pb/232Th	2RSE (%)	238U/206Pb	2RSE (%)	207Pb/206Pb	2RSE (%)
20160707_91500_1_001		56	212	2.1E-06	7.2E-04	6.8E-05	8.9E-05	1.9E-03	6.6E-03	#DIV/0!	#DIV/0!	1.8775	3.32	0.1803	3.30	0.50	0.0751	0.76	0.3809	0.84	0.0521	2.44	5.546	3.30	0.0751	0.76
20160707_91500_1_002		52	212	#DIV/0!	7.3E-04	6.9E-05	9.2E-05	2.0E-03	6.7E-03	#DIV/0!	#DIV/0!	1.8729	2.96	0.1793	2.97	0.50	0.0755	0.70	0.3875	0.76	0.0521	2.98	5.577	2.97	0.0755	0.70
20160707_91500_1_003		56	214	#DIV/0!	6.9E-04	6.5E-05	8.6E-05	1.8E-03	6.3E-03	#DIV/0!	#DIV/0!	1.8580	3.61	0.1794	3.57	0.49	0.0753	0.84	0.3986	0.63	0.0542	2.35	5.575	3.57	0.0753	0.84
20160707_91500_1_004		40	199	2.8E-06	7.1E-04	6.7E-05	8.9E-05	1.8E-03	6.5E-03	295	1	1.8385	2.42	0.1766	2.48	0.51	0.0754	0.54	0.3998	0.70	0.0545	1.79	5.662	2.48	0.0754	0.54
20160707_91500_1_005		51	210	2.9E-06	7.1E-04	6.7E-05	8.8E-05	1.8E-03	6.6E-03	#DIV/0!	#DIV/0!	1.8431	2.48	0.1770	2.71	0.55	0.0754	0.66	0.3997	0.81	0.0546	1.82	5.651	2.71	0.0754	0.66
20160707_91500_1_006		54	210	2.3E-06	7.2E-04	6.8E-05	8.9E-05	1.9E-03	6.6E-03	256	1	1.8440	2.91	0.1775	2.90	0.50	0.0753	0.64	0.4045	0.75	0.0551	1.94	5.632	2.90	0.0753	0.64
20160707_91500_1_007		53	201	2.8E-06	6.8E-04	6.4E-05	8.5E-05	1.8E-03	6.3E-03	296	0	1.8119	3.69	0.1757	3.53	0.48	0.0751	0.79	0.3948	0.65	0.0540	2.33	5.691	3.53	0.0751	0.79
20160707_91500_1_008		53	211	2.7E-06	6.9E-04	6.6E-05	8.7E-05	1.8E-03	6.4E-03	#DIV/0!	#DIV/0!	1.8217	3.24	0.1763	2.95	0.45	0.0752	0.63	0.3964	0.71	0.0552	2.04	5.673	2.95	0.0752	0.63
20160707_91500_1_009		59	210	#DIV/0!	8.0E-04	7.5E-05	9.9E-05	2.1E-03	7.5E-03	#DIV/0!	#DIV/0!	1.8555	2.56	0.1796	2.33	0.45	0.0750	0.67	0.3768	0.67	0.0573	1.89	5.569	2.33	0.0750	0.67
20160707_91500_1_009		61	210	#DIV/0!	8.0E-04	7.5E-05	9.9E-05	2.1E-03	7.5E-03	#DIV/0!	#DIV/0!	1.8573	2.70	0.1800	2.45	0.45	0.0750	0.68	0.3684	0.69	0.0559	1.90	5.556	2.45	0.0750	0.68
20160707_91500_1_010		55	208	#DIV/0!	8.0E-04	7.5E-05	9.9E-05	2.1E-03	7.5E-03	#DIV/0!	#DIV/0!	1.8604	2.14	0.1792	2.09	0.49	0.0752	0.66	0.3763	0.64	0.0574	1.84	5.580	2.09	0.0752	0.66
20160707_91500_1_010		53	202	#DIV/0!	8.1E-04	7.6E-05	1.0E-04	2.1E-03	7.6E-03	#DIV/0!	#DIV/0!	1.8654	2.07	0.1799	2.00	0.48	0.0753	0.65	0.3682	0.63	0.0563	1.88	5.558	2.00	0.0753	0.65
20160707_91500_1_011		57	205	3.4E-06	9.1E-04	8.6E-05	1.1E-04	2.2E-03	8.6E-03	#DIV/0!	#DIV/0!	1.8593	1.49	0.1794	1.35	0.45	0.0753	0.66	0.3296	0.70	0.0671	4.50	5.575	1.35	0.0753	0.66
20160707_91500_1_012		53	210	#DIV/0!	9.0E-04	8.5E-05	1.1E-04	2.2E-03	8.5E-03	#DIV/0!	#DIV/0!	1.8641	1.32	0.1782	1.35	0.51	0.0754	0.62	0.3278	0.59	0.0674	3.79	5.611	1.35	0.0754	0.62

File name	std.	start	end	204Pb	206Pb	207Pb	208Pb	232Th	238U	206Pb/204Pb	2RSE (%)	207Pb/235U	2RSE (%)	206Pb/238U	2RSE (%)	Rho	207Pb/206Pb	2RSE (%)	208Pb/206Pb	2RSE (%)	208Pb/232Th	2RSE (%)	238U/206Pb	2RSE (%)	207Pb/206Pb	2RSE (%)
20160707_ples6_001	*	52	207	#DIV/0!	1.2E-03	8.2E-05	3.9E-05	2.6E-03	3.8E-02	#DIV/0!	#DIV/0!	0.3939	3.75	0.0534	3.95	0.53	0.0536	0.66	0.0975	0.93	0.0170	2.31	18.723	3.95	0.0536	0.66
20160707_ples6_002	*	48	206	2.3E-06	1.2E-03	8.1E-05	3.9E-05	2.6E-03	3.7E-02	#DIV/0!	#DIV/0!	0.3893	3.71	0.0531	3.40	0.46	0.0530	0.62	0.0979	0.87	0.0166	2.65	18.816	3.40	0.0530	0.62
20160707_ples6_003	*	52	210	3.1E-06	1.2E-03	8.0E-05	3.8E-05	2.5E-03	3.6E-02	#DIV/0!	#DIV/0!	0.3948	3.58	0.0541	3.42	0.48	0.0531	0.67	0.0979	0.91	0.0167	2.24	18.501	3.42	0.0531	0.67
20160707_ples6_004	*	53	206	#DIV/0!	1.3E-03	8.6E-05	4.1E-05	2.7E-03	4.0E-02	#DIV/0!	#DIV/0!	0.3944	3.03	0.0536	3.06	0.50	0.0532	0.61	0.1026	1.17	0.0173	1.94	18.649	3.06	0.0532	0.61
20160707_ples6_005	*	54	207	3.8E-06	1.3E-03	8.8E-05	4.2E-05	2.8E-03	4.0E-02	#DIV/0!	#DIV/0!	0.3945	3.19	0.0540	3.31	0.52	0.0529	0.65	0.1021	1.60	0.0171	2.08	18.535	3.31	0.0529	0.65
20160707_ples6_006	*	57	212	#DIV/0!	1.3E-03	9.0E-05	4.4E-05	2.9E-03	4.1E-02	#DIV/0!	#DIV/0!	0.3961	3.27	0.0540	3.29	0.50	0.0533	0.58	0.1038	2.00	0.0170	2.34	18.519	3.29	0.0533	0.58
20160707_ples6_007	*	58	208	#DIV/0!	1.3E-03	8.8E-05	4.3E-05	2.8E-03	4.0E-02	#DIV/0!	#DIV/0!	0.3917	4.00	0.0537	3.87	0.48	0.0530	0.65	0.1046	1.77	0.0169	3.43	18.608	3.87	0.0530	0.65
20160707_ples6_008	*	52	204	#DIV/0!	1.3E-03	8.8E-05	4.2E-05	2.8E-03	4.0E-02	#DIV/0!	#DIV/0!	0.3905	3.36	0.0534	3.31	0.49	0.0532	0.59	0.1040	1.51	0.0173	2.05	18.726	3.31	0.0532	0.59
20160707_ples6_009	*	52	203	2.6E-06	1.2E-03	8.3E-05	4.0E-05	2.7E-03	3.8E-02	627	1	0.3919	3.44	0.0534	3.38	0.49	0.0532	0.75	0.1034	1.52	0.0170	2.59	18.713	3.38	0.0532	0.75
20160707_ples6_010	*	55	202	#DIV/0!	1.2E-03	8.3E-05	3.9E-05	2.4E-03	3.6E-02	#DIV/0!	#DIV/0!	0.4047	4.71	0.0543	5.07	0.54	0.0539	0.76	0.1018	2.00	0.0176	4.00	18.429	5.07	0.0539	0.76
20160707_ples6_011	*	55	205	#DIV/0!	1.2E-03	7.8E-05	3.6E-05	2.2E-03	3.4E-02	#DIV/0!	#DIV/0!	0.4011	4.72	0.0545	4.82	0.51	0.0535	0.72	0.0981	1.68	0.0177	3.90	18.357	4.82	0.0535	0.72
20160707_ples6_012	*	54	209	#DIV/0!	9.2E-04	6.0E-05	2.4E-05	1.9E-03	2.8E-02	#DIV/0!	#DIV/0!	0.3831	3.55	0.0530	3.73	0.52	0.0522	1.13	0.0863	4.72	0.0148	4.10	18.866	3.73	0.0522	1.13
20160707_ples6_013	*	52	203	#DIV/0!	9.5E-04	6.3E-05	2.9E-05	1.9E-03	2.9E-02	#DIV/0!	#DIV/0!	0.3885	4.00	0.0529	3.95	0.49	0.0534	0.72	0.0963	1.47	0.0165	3.80	18.905	3.95	0.0534	0.72
20160707_ples6_014	*	50	198	2.8E-06	1.0E-03	6.7E-05	3.0E-05	2.0E-03	3.0E-02	365	3	0.3889	4.06	0.0531	4.00	0.49	0.0533	0.67	0.0953	1.57	0.0169	3.54	18.845	4.00	0.0533	0.67
20160707_ples6_015	*	52	207	#DIV/0!	1.0E-03	7.0E-05	3.2E-05	2.1E-03	3.2E-02	#DIV/0!	#DIV/0!	0.3948	3.21	0.0538	3.02	0.47	0.0532	0.63	0.0925	1.62	0.0175	2.61	18.588	3.02	0.0532	0.63
20160707_ples6_015	*	53	205	#DIV/0!	1.0E-03	7.0E-05	3.2E-05	2.1E-03	3.2E-02	#DIV/0!	#DIV/0!	0.3916	3.36	0.0534	3.19	0.47	0.0532	0.65	0.0901	1.65	0.0172	2.74	18.715	3.19	0.0532	0.65
20160707_ples6_016	*	56	210	#DIV/0!	1.1E-03	7.5E-05	3.7E-05	2.5E-03	3.4E-02	#DIV/0!	#DIV/0!	0.3966	3.63	0.0539	3.65	0.50	0.0534	0.71	0.1037	2.62	0.0172	3.18	18.556	3.65	0.0534	0.71
20160707_ples6_016	*	54	204	#DIV/0!	1.1E-03	7.7E-05	3.8E-05	2.5E-03	3.5E-02	#DIV/0!	#DIV/0!	0.3925	3.70	0.0533	3.78	0.51	0.0534	0.72	0.1017	2.63	0.0168	3.57	18.752	3.78	0.0534	0.72
20160707_ples6_017	*	56	210	2.6E-06	1.2E-03	8.0E-05	4.3E-05	2.9E-03	3.6E-02	527	2	0.3949	3.73	0.0539	3.44	0.46	0.0531	0.72	0.1122	1.40	0.0172	2.99	18.542	3.44	0.0531	0.72
20160707_ples6_017	*	61	210	2.6E-06	1.2E-03	8.0E-05	4.3E-05	2.9E-03	3.6E-02	525	2	0.3969	4.17	0.0543	3.86	0.46	0.0531	0.80	0.1095	1.56	0.0169	3.39	18.430	3.86	0.0531	0.80
20160707_ples6_018		46	207	9.1E-06	1.3E-03	1.1E-04	1.1E-04	2.8E-03	3.8E-02	199	10	0.4270	19.91	0.0544	3.68	0.09	0.0565	14.36	0.1259	50.95	0.0218	69.25	18.379	3.68	0.0565	14.36
20160707_ples6_019	*	52	208	2.7E-06	1.9E-03	1.2E-04	6.6E-05	4.4E-03	5.7E-02	803	1	0.3925	3.54	0.0535	3.61	0.51	0.0533	0.53	0.0993	0.91	0.0167	2.41	18.705	3.61	0.0533	0.53
20160707_ples6_020	*	54	205	1.8E-06	2.0E-03	1.4E-04	7.5E-05	5.0E-03	6.2E-02	1100	2	0.3931	3.74	0.0536	3.79	0.51	0.0531	0.59	0.1025	0.75	0.0171	1.71	18.662	3.79	0.0531	0.59
20160707_ples6_021	*	57	206	2.9E-06	1.9E-03	1.3E-04	6.6E-05	4.4E-03	5.8E-02	854	2	0.3948	3.98	0.0540	3.91	0.49	0.0531	0.54	0.0979	1.06	0.0171	1.91	18.531	3.91	0.0531	0.54
20160707_ples6_022	*	57	200	#DIV/0!	1.9E-03	1.2E-04	6.5E-05	4.3E-03	5.7E-02	#DIV/0!	#DIV/0!	0.3930	4.33	0.0532	4.55	0.53	0.0537	0.65	0.0943	0.91	0.0170	2.76	18.802	4.55	0.0537	0.65
20160707_ples6_023	*	55	204	#DIV/0!	1.9E-03	1.2E-04	6.6E-05	4.4E-03	5.7E-02	#DIV/0!	#DIV/0!	0.3905	3.96	0.0534	3.83	0.48	0.0530	0.57	0.0944	0.89	0.0168	2.84	18.719	3.83	0.0530	0.57
20160707_ples6_024	*	59	205	#DIV/0!	2.0E-03	1.3E-04	7.6E-05	5.0E-03	5.9E-02	#DIV/0!	#DIV/0!	0.3967	3.91	0.0542	3.84	0.49	0.0530	0.58	0.1103	4.17	0.0170	2.88	18.439	3.84	0.0530	0.58

File name	std.	start	end	204Pb	206Pb	207Pb	208Pb	232Th	238U	206Pb/204Pb	2RSE (%)	207Pb/235U	2RSE (%)	206Pb/238U	2RSE (%)	Rho	207Pb/206Pb	2RSE (%)	208Pb/206Pb	2RSE (%)	208Pb/232Th	2RSE (%)	238U/206Pb	2RSE (%)	207Pb/206Pb	2RSE (%)
~~20160707_G21_g76R~~		~~52~~	~~167~~	~~3.6E-05~~	~~7.1E-03~~	~~1.0E-03~~	~~1.7E-03~~	~~1.0E-01~~	~~4.8E-01~~	~~206~~	~~9~~	~~0.3650~~	~~11.66~~	~~0.0230~~	~~13.34~~	~~0.57~~	~~0.1138~~	~~4.45~~	~~0.7681~~	~~5.44~~	~~0.0184~~	~~18.54~~	~~43.414~~	~~13.34~~	~~0.1138~~	~~4.45~~
20160707_G21_g62		54	269	2.5E-06	2.4E-03	1.6E-04	3.8E-05	2.1E-03	5.9E-02	1052	2	0.4663	4.07	0.0620	4.31	0.53	0.0544	0.39	0.0401	7.86	0.0196	5.29	16.136	4.31	0.0544	0.39
20160707_G21_g68R		59	242	2.8E-06	2.1E-04	1.5E-05	2.2E-05	1.3E-03	5.7E-03	107	9	0.4706	3.20	0.0613	2.93	0.46	0.0558	1.54	0.3225	2.73	0.0203	3.43	16.315	2.93	0.0558	1.54
20160707_G21_g20		40	120	2.2E-06	2.6E-04	1.9E-05	1.7E-06	1.5E-04	6.9E-03	#DIV/0!	#DIV/0!	0.4724	8.14	0.0620	7.44	0.46	0.0556	1.54	0.0174	9.41	0.0190	2.36	16.126	7.44	0.0556	1.54
~~20160707_G21_g34~~		~~58~~	~~257~~	~~1.7E-05~~	~~8.2E-03~~	~~8.2E-04~~	~~7.5E-04~~	~~5.5E-02~~	~~3.0E-01~~	~~600~~	~~10~~	~~0.4724~~	~~4.70~~	~~0.0478~~	~~5.20~~	~~0.55~~	~~0.0716~~	~~4.97~~	~~0.2192~~	~~17.46~~	~~0.0137~~	~~10.94~~	~~20.933~~	~~5.20~~	~~0.0716~~	~~4.97~~
20160707_G21_g71		59	284	2.7E-06	8.6E-04	5.9E-05	2.1E-05	1.1E-03	2.0E-02	376	1	0.4807	5.19	0.0633	5.24	0.50	0.0548	0.60	0.0740	3.05	0.0199	6.54	15.793	5.24	0.0548	0.60
20160707_G21_g16		56	246	2.3E-06	6.8E-05	4.8E-06	1.0E-06	6.0E-04	1.7E-03	53	1	0.4888	8.52	0.0624	8.46	0.50	0.0562	2.67	0.0441	23.88	0.0153	6.19	16.035	8.46	0.0562	2.67
20160707_G21_g98		65	221	2.3E-06	1.2E-04	8.3E-06	6.3E-07	1.6E-04	2.9E-03	52	3	0.5096	6.71	0.0664	5.51	0.41	0.0559	2.50	0.0119	30.75	#DIV/0!	#DIV/0!	15.059	5.51	0.0559	2.50
20160707_G21_g27		56	242	3.0E-06	9.2E-04	6.4E-05	3.9E-06	4.5E-04	2.1E-02	363	0	0.5481	6.82	0.0718	6.45	0.47	0.0551	0.71	0.0021	203.82	0.0253	10.96	13.933	6.45	0.0551	0.71
20160707_G21_g53		49	260	2.5E-06	1.8E-04	1.3E-05	3.0E-05	1.4E-03	4.2E-03	48	4	0.5503	5.64	0.0701	4.90	0.43	0.0566	1.50	0.2422	34.77	0.0231	5.17	14.258	4.90	0.0566	1.50
20160707_G21_g31		50	265	2.9E-06	2.2E-03	1.5E-04	2.9E-05	2.3E-03	4.9E-02	1911	2	0.5904	5.86	0.0765	5.84	0.50	0.0558	0.96	0.0333	34.83	0.0201	11.84	13.074	5.84	0.0558	0.96
20160707_G21_g82		58	268	2.5E-06	3.0E-04	2.2E-05	2.9E-05	1.3E-03	6.3E-03	152	2	0.6187	2.81	0.0779	2.78	0.49	0.0575	1.06	0.2137	12.12	0.0270	3.28	12.829	2.78	0.0575	1.06
20160707_G21_g81		60	274	2.3E-06	5.4E-04	3.9E-05	4.4E-05	2.0E-03	1.1E-02	273	1	0.6217	1.74	0.0772	1.58	0.45	0.0583	0.83	0.2436	2.65	0.0263	1.81	12.956	1.58	0.0583	0.83
20160707_G21_g52		62	262	2.4E-06	5.0E-04	3.7E-05	5.6E-05	2.3E-03	1.0E-02	72	7	0.6359	4.60	0.0792	4.64	0.50	0.0582	0.93	0.3068	6.50	0.0263	5.20	12.628	4.64	0.0582	0.93
20160707_G21_g100		55	266	2.2E-06	1.5E-04	1.1E-05	9.2E-06	4.1E-04	3.2E-03	86	1	0.6369	3.00	0.0790	2.55	0.43	0.0585	1.36	0.1707	2.26	0.0255	4.32	12.651	2.55	0.0585	1.36
20160707_G21_g73		56	226	2.3E-06	5.9E-04	4.3E-05	6.1E-05	2.6E-03	1.2E-02	316	1	0.6383	2.00	0.0789	1.94	0.48	0.0584	1.08	0.3603	4.47	0.0275	2.15	12.668	1.94	0.0584	1.08
20160707_G21_g69		52	269	2.2E-06	9.0E-04	6.5E-05	9.4E-05	4.1E-03	1.8E-02	386	2	0.6430	2.29	0.0809	2.22	0.48	0.0579	0.56	0.3383	3.94	0.0265	1.69	12.361	2.22	0.0579	0.56
~~20160707_G21_g108~~		~~59~~	~~217~~	~~2.3E-06~~	~~2.4E-04~~	~~1.9E-05~~	~~1.8E-05~~	~~7.4E-04~~	~~4.7E-03~~	~~141~~	~~2~~	~~0.6507~~	~~12.49~~	~~0.0797~~	~~5.20~~	~~0.21~~	~~0.0597~~	~~7.25~~	~~0.1714~~	~~24.79~~	~~0.0271~~	~~25.85~~	~~12.553~~	~~5.20~~	~~0.0597~~	~~7.25~~
20160707_G21_g106		56	259	2.4E-06	5.9E-04	4.3E-05	7.9E-05	3.5E-03	1.2E-02	256	1	0.6512	3.07	0.0806	3.23	0.53	0.0585	0.74	0.3114	14.49	0.0255	4.50	12.413	3.23	0.0585	0.74
20160707_G21_g90		61	220	2.9E-06	1.1E-04	8.0E-06	8.0E-06	4.0E-04	2.3E-03	44	10	0.6514	3.32	0.0821	2.43	0.37	0.0578	1.94	0.2067	15.60	0.0263	6.46	12.183	2.43	0.0578	1.94
20160707_G21_g118		59	246	2.8E-06	3.2E-04	2.4E-05	2.3E-05	9.5E-04	6.2E-03	165	4	0.6531	5.47	0.0802	5.69	0.52	0.0588	0.97	0.1996	1.51	0.0249	6.35	12.469	5.69	0.0588	0.97
20160707_G21_g94		53	264	2.2E-06	1.1E-04	8.2E-06	8.0E-06	3.5E-04	2.3E-03	46	1	0.6539	3.66	0.0817	2.88	0.39	0.0584	1.73	0.1867	6.59	0.0264	6.25	12.232	2.88	0.0584	1.73
20160707_G21_g72		53	271	2.3E-06	3.2E-04	2.3E-05	2.6E-05	1.1E-03	6.3E-03	207	1	0.6572	2.56	0.0815	2.49	0.49	0.0583	0.86	0.2578	1.78	0.0278	2.50	12.271	2.49	0.0583	0.86
20160707_G21_g60R		55	246	2.6E-06	9.8E-04	7.1E-05	1.1E-04	4.3E-03	1.8E-02	459	1	0.6607	4.75	0.0829	4.86	0.51	0.0579	0.59	0.3918	4.14	0.0265	4.68	12.061	4.86	0.0579	0.59
20160707_G21_g103		59	273	2.5E-06	4.9E-04	3.6E-05	5.6E-05	2.4E-03	9.7E-03	173	0	0.6647	2.79	0.0829	2.76	0.49	0.0583	0.83	0.3131	1.64	0.0261	2.28	12.070	2.76	0.0583	0.83
20160707_G21_g59		53	215	2.2E-06	1.1E-04	8.2E-06	6.5E-06	2.8E-04	2.2E-03	68	4	0.6655	4.39	0.0836	3.97	0.45	0.0575	1.94	0.1820	3.05	0.0260	9.41	11.961	3.97	0.0575	1.94
20160707_G21_g91		62	247	2.2E-06	7.3E-04	5.3E-05	2.9E-05	1.2E-03	1.4E-02	280	2	0.6664	5.26	0.0827	5.26	0.50	0.0584	0.80	0.1137	1.59	0.0241	5.77	12.095	5.26	0.0584	0.80
~~20160707_G21_g110~~		~~54~~	~~219~~	~~3.1E-06~~	~~6.5E-04~~	~~5.2E-05~~	~~4.9E-05~~	~~1.9E-03~~	~~1.2E-02~~	~~243~~	~~3~~	~~0.6683~~	~~4.38~~	~~0.0746~~	~~3.99~~	~~0.46~~	~~0.0648~~	~~2.76~~	~~0.1993~~	~~8.34~~	~~0.0342~~	~~7.33~~	~~13.402~~	~~3.99~~	~~0.0648~~	~~2.76~~
20160707_G21_g107		57	260	2.7E-06	4.7E-04	3.5E-05	5.0E-05	2.1E-03	9.3E-03	#DIV/0!	#DIV/0!	0.6712	3.86	0.0829	3.58	0.46	0.0586	0.81	0.3034	2.09	0.0259	3.27	12.066	3.58	0.0586	0.81
20160707_G21_g122		55	143	2.2E-06	5.2E-04	3.8E-05	4.3E-05	1.7E-03	9.7E-03	151	28	0.6772	16.75	0.0831	17.54	0.52	0.0586	1.46	0.2154	14.03	0.0264	19.52	12.029	17.54	0.0586	1.46
20160707_G21_g38		56	225	2.3E-06	9.9E-04	7.2E-05	3.2E-05	1.2E-03	1.8E-02	416	1	0.6793	9.90	0.0868	9.17	0.46	0.0569	0.71	0.0703	57.95	0.0253	9.57	11.517	9.17	0.0569	0.71
20160707_G21_g104		62	245	2.7E-06	4.7E-04	3.4E-05	3.4E-05	1.4E-03	9.0E-03	#DIV/0!	#DIV/0!	0.6821	4.18	0.0847	4.14	0.49	0.0584	0.82	0.2231	8.67	0.0258	5.65	11.803	4.14	0.0584	0.82
20160707_G21_g96		53	264	2.7E-06	1.4E-03	1.0E-04	1.1E-04	4.4E-03	2.8E-02	796	2	0.7009	3.35	0.0865	3.26	0.49	0.0584	0.64	0.3349	10.47	0.0296	4.35	11.566	3.26	0.0584	0.64
20160707_G21_g105		61	250	2.6E-06	8.3E-04	6.0E-05	3.3E-05	1.2E-03	1.5E-02	374	8	0.7013	5.55	0.0877	5.41	0.49	0.0577	0.74	0.1020	6.96	0.0261	7.14	11.400	5.41	0.0577	0.74
20160707_G21_g78		56	261	#DIV/0!	4.6E-04	3.4E-05	1.2E-04	4.6E-03	8.3E-03	#DIV/0!	#DIV/0!	0.7059	4.51	0.0873	4.30	0.48	0.0586	0.80	0.7276	3.43	0.0269	4.82	11.456	4.30	0.0586	0.80
20160707_G21_g57		47	277	2.5E-06	3.8E-03	2.8E-04	1.1E-04	4.1E-03	6.8E-02	1940	2	0.7170	3.70	0.0889	3.58	0.48	0.0584	0.48	0.0847	9.44	0.0305	2.97	11.249	3.58	0.0584	0.48
20160707_G21_g37		57	258	2.1E-06	7.0E-04	5.2E-05	1.1E-04	4.3E-03	1.2E-02	424	3	0.7182	4.90	0.0897	4.75	0.48	0.0583	0.69	0.4550	4.71	0.0275	5.50	11.154	4.75	0.0583	0.69
20160707_G21_g54		53	266	3.0E-06	4.8E-04	3.5E-05	1.7E-04	6.7E-03	8.8E-03	190	8	0.7208	2.43	0.0885	2.46	0.51	0.0591	0.82	1.2035	3.98	0.0293	2.01	11.297	2.46	0.0591	0.82

20160707_G21_g56		56	248	2.9E-06	1.8E-03	1.3E-04	3.2E-04	1.2E-02	3.1E-02	#DIV/0!	#DIV/0!	0.7357	3.79	0.0912	3.76	0.50	0.0586	0.48	0.5166	7.25	0.0291	3.75	10.963	3.76	0.0586	0.48
20160707_G21_g112		58	195	3.0E-06	5.1E-04	3.8E-05	1.5E-04	5.1E-03	7.8E-03	99	2	0.7624	6.81	0.0931	5.87	0.43	0.0592	1.35	0.7415	9.80	0.0291	5.33	10.746	5.87	0.0592	1.35
20160707_G21_g21		54	171	2.7E-06	1.9E-03	1.4E-04	2.0E-04	8.2E-03	3.5E-02	655	6	0.7660	6.81	0.0944	7.04	0.52	0.0589	1.82	0.4505	26.26	0.0288	12.07	10.591	7.04	0.0589	1.82
20160707_G21_g47		55	231	2.6E-06	9.5E-04	7.0E-05	1.4E-04	5.0E-03	1.6E-02	590	14	0.7664	6.28	0.0946	6.17	0.49	0.0588	0.68	0.6026	8.62	0.0279	9.03	10.567	6.17	0.0588	0.68
20160707_G21_g58		42	176	2.7E-06	1.3E-04	1.0E-05	3.2E-05	1.2E-03	2.3E-03	#DIV/0!	#DIV/0!	0.7796	5.15	0.0936	4.58	0.44	0.0610	1.82	0.6955	6.81	0.0308	3.53	10.689	4.58	0.0610	1.82
20160707_G21_g3		54	204	2.2E-06	9.5E-04	7.2E-05	1.5E-04	4.6E-03	1.5E-02	755	2	0.8092	12.94	0.0975	12.06	0.47	0.0589	2.02	0.5794	13.67	0.0331	13.85	10.256	12.06	0.0589	2.02
20160707_G21_g40R		55	247	#DIV/0!	5.5E-04	4.2E-05	1.4E-04	4.7E-03	8.7E-03	#DIV/0!	#DIV/0!	0.8408	3.44	0.1016	3.00	0.44	0.0603	0.94	0.8330	4.94	0.0318	2.93	9.844	3.00	0.0603	0.94
20160707_G21_g42R		55	245	2.5E-06	2.5E-03	1.9E-04	5.2E-04	1.7E-02	4.0E-02	1541	1	0.8428	5.78	0.1027	5.47	0.47	0.0595	0.60	0.6375	11.37	0.0335	7.12	9.741	5.47	0.0595	0.60
20160707_G21_g1		48	222	#DIV/0!	2.5E-03	1.9E-04	5.3E-04	1.3E-02	3.0E-02	#DIV/0!	#DIV/0!	0.8520	5.97	0.1047	5.89	0.49	0.0595	0.79	0.5650	13.91	0.0359	9.41	9.555	5.89	0.0595	0.79
20160707_G21_g30		52	229	1.9E-06	2.2E-03	1.7E-04	5.9E-04	2.0E-02	3.3E-02	1605	5	0.8719	5.43	0.1056	5.32	0.49	0.0601	0.49	0.8157	6.33	0.0304	5.39	9.473	5.32	0.0601	0.49
20160707_G21_g19		50	164	2.2E-06	2.3E-03	1.7E-04	4.4E-04	1.4E-02	3.4E-02	#DIV/0!	#DIV/0!	0.9009	7.12	0.1080	7.47	0.52	0.0605	0.78	0.6458	7.91	0.0327	6.46	9.262	7.47	0.0605	0.78
20160707_G21_g28		55	205	3.0E-06	6.4E-04	4.9E-05	1.4E-04	4.0E-03	8.9E-03	221	6	0.9105	6.70	0.1099	6.00	0.45	0.0607	1.24	0.5224	17.77	0.0323	9.84	9.102	6.00	0.0607	1.24
20160707_G21_g120		57	146	2.4E-06	1.2E-03	9.4E-05	2.6E-04	8.2E-03	2.0E-02	487	5	0.9724	12.98	0.1164	11.30	0.44	0.0611	3.34	0.9483	43.03	0.0344	10.95	8.593	11.30	0.0611	3.34
20160707_G21_g17		64	259	2.1E-06	1.9E-03	1.6E-04	1.5E-04	3.4E-03	2.0E-02	2211	1	1.4755	7.41	0.1554	7.06	0.48	0.0681	1.48	0.3208	20.64	0.0481	10.28	6.435	7.06	0.0681	1.48
20160707_G21_g2R		47	229	3.0E-06	2.9E-03	4.0E-04	8.1E-05	8.5E-04	4.3E-02	770	0	2.1166	22.53	0.1285	12.69	0.28	0.0958	11.33	0.0857	20.51	0.1108	13.26	7.784	12.69	0.0958	11.33
20160707_G21_g23		45	234	2.8E-06	1.9E-03	2.4E-04	4.2E-04	5.6E-03	2.1E-02	#DIV/0!	#DIV/0!	2.6651	13.55	0.1762	11.22	0.41	0.1070	3.31	0.8775	10.24	0.0892	5.29	5.676	11.22	0.1070	3.31
20160707_G21_g84		47	240	2.8E-06	2.6E-03	4.0E-04	4.0E-04	4.3E-03	1.2E-02	894	1	5.9377	3.60	0.3518	3.47	0.48	0.1226	0.57	0.4896	2.30	0.1098	2.66	2.842	3.47	0.1226	0.57
20160707_G21_g66		53	202	2.1E-06	1.2E-03	1.8E-04	2.9E-04	3.1E-03	5.4E-03	1108	2	6.0652	5.37	0.3860	5.31	0.49	0.1142	0.61	0.8201	5.95	0.1065	6.21	2.591	5.31	0.1142	0.61
20160707_G21_g36		45	257	2.7E-06	2.2E-03	3.5E-04	5.9E-04	6.2E-03	1.0E-02	990	1	6.2771	2.79	0.3625	2.60	0.47	0.1260	0.38	0.9299	3.29	0.1136	1.67	2.758	2.60	0.1260	0.38
20160707_G21_g55		54	269	3.1E-06	2.1E-03	3.9E-04	3.5E-04	3.3E-03	9.1E-03	478	3	8.6210	7.70	0.4056	7.38	0.48	0.1532	2.05	0.5139	2.13	0.1114	8.67	2.466	7.38	0.1532	2.05
20160707_G21_g86		58	277	5.0E-06	3.1E-03	7.3E-04	4.2E-04	3.0E-03	9.3E-03	625	2	13.3402	4.43	0.5198	4.53	0.51	0.1837	0.59	0.3873	7.23	0.1549	6.68	1.924	4.53	0.1837	0.59
20160707_G21_g45		54	219	#DIV/0!	4.5E-03	1.0E-03	7.7E-04	5.2E-03	1.2E-02	#DIV/0!	#DIV/0!	14.6581	6.13	0.5842	6.00	0.49	0.1825	0.34	0.5804	3.32	0.1579	6.16	1.712	6.00	0.1825	0.34
20160707_G21_g111		54	247	2.5E-06	5.4E-03	1.3E-03	1.1E-03	9.6E-03	1.9E-02	2203	9	14.7475	5.36	0.5431	4.96	0.46	0.1972	1.06	0.5195	3.98	0.1479	4.52	1.841	4.96	0.1972	1.06

18.2.2 ***Semmering quartzite (G2)***

Table 4: Those tables depict the measured values of the zircons of the Semmering quartzite, corrected with the EXCEL sheet LamTool U – Th – Pb VI of Košler und Klötzli (unpubl.). M257 (Nasdala et al., 2008), 91500 (Wiedenbeck et al., 1995) and Plešovice (Sláma et al., 2008) are the used standard samples. The crossed out measurements are discordant and were excluded of further steps.

File name	std.	start	end	204Pb	206Pb	207Pb	208Pb	232Th	238U	206Pb/204Pb	2RSE (%)	207Pb/235U	2RSE (%)	206Pb/238U	2RSE (%)	Rho	207Pb/206Pb	2RSE (%)	208Pb/206Pb	2RSE (%)	208Pb/232Th	2RSE (%)	238U/206Pb	2RSE (%)	207Pb/206Pb	2RSE (%)
20160704_M257_001		62	219	3.2E-06	4.3E-03	3.1E-04	4.1E-04	1.6E-02	7.3E-02	1707	1	0.7736	5.12	0.0962	5.10	0.50	0.0584	0.37	0.2624	0.32	0.0289	3.81	10.394	5.10	0.0584	0.37
20160704_M257_002		49	215	2.6E-06	4.4E-03	3.2E-04	4.2E-04	1.7E-02	7.6E-02	1890	1	0.7447	3.86	0.0927	3.89	0.50	0.0585	0.33	0.2621	0.29	0.0290	2.36	10.792	3.89	0.0585	0.33
20160704_M257_003		62	223	2.6E-06	5.8E-03	4.2E-04	5.6E-04	2.2E-02	1.1E-01	2592	1	0.7563	1.69	0.0943	1.71	0.51	0.0583	0.30	0.2655	0.30	0.0349	4.83	10.609	1.71	0.0583	0.30
20160704_M257_004		54	216	2.8E-06	4.4E-03	3.2E-04	4.2E-04	1.8E-02	7.9E-02	1967	2	0.7345	3.64	0.0915	3.65	0.50	0.0584	0.34	0.2647	0.27	0.0276	2.55	10.923	3.65	0.0584	0.34
20160704_M257_005		51	217	2.6E-06	4.5E-03	3.2E-04	4.3E-04	2.0E-02	8.3E-02	#DIV/0!	#DIV/0!	0.7143	3.18	0.0890	3.17	0.50	0.0584	0.31	0.2692	0.30	0.0259	2.30	11.230	3.17	0.0584	0.31
20160704_M257_006		57	216	#DIV/0!	4.5E-03	3.2E-04	4.3E-04	1.9E-02	8.3E-02	#DIV/0!	#DIV/0!	0.7213	3.54	0.0902	3.47	0.49	0.0581	0.36	0.2682	0.31	0.0260	2.63	11.087	3.47	0.0581	0.36
20160704_M257_007		56	209	2.7E-06	4.8E-03	3.4E-04	4.5E-04	2.0E-02	8.9E-02	1376	0	0.7386	2.20	0.0923	2.13	0.49	0.0581	0.32	0.2727	0.28	0.0277	1.35	10.830	2.13	0.0581	0.32
20160704_M257_008		58	202	3.3E-06	5.0E-03	3.6E-04	4.7E-04	2.2E-02	9.4E-02	#DIV/0!	#DIV/0!	0.7332	2.35	0.0916	2.30	0.49	0.0581	0.37	0.2729	0.31	0.0269	2.46	10.915	2.30	0.0581	0.37
20160704_M257_009		59	218	2.4E-06	4.6E-03	3.3E-04	4.4E-04	2.1E-02	8.7E-02	2090	1	0.7229	2.93	0.0901	2.90	0.50	0.0583	0.29	0.2787	0.30	0.0249	1.48	11.093	2.90	0.0583	0.29
20160704_M257_010		53	207	2.4E-06	4.8E-03	3.4E-04	4.5E-04	2.1E-02	9.0E-02	2096	1	0.7284	2.33	0.0911	2.31	0.50	0.0582	0.31	0.2784	0.29	0.0258	2.04	10.980	2.31	0.0582	0.31
20160705_M257_001		56	220	3.8E-06	4.1E-03	3.0E-04	4.0E-04	1.6E-02	7.4E-02	1097	0	0.7358	2.33	0.0912	2.35	0.50	0.0585	0.33	0.2877	0.31	0.0274	1.30	10.967	2.35	0.0585	0.33
20160705_M257_002		56	218	3.3E-06	4.3E-03	3.1E-04	4.1E-04	1.7E-02	7.7E-02	1212	3	0.7459	2.20	0.0927	2.17	0.49	0.0583	0.32	0.2869	0.28	0.0286	1.83	10.784	2.17	0.0583	0.32
20160705_M257_003		59	215	4.2E-06	5.0E-03	3.6E-04	4.8E-04	1.9E-02	9.1E-02	#DIV/0!	#DIV/0!	0.7472	2.15	0.0931	2.13	0.49	0.0582	0.32	0.2781	0.29	0.0299	2.18	10.740	2.13	0.0582	0.32
20160705_M257_004		58	217	4.3E-06	5.1E-03	3.7E-04	4.9E-04	1.9E-02	9.3E-02	#DIV/0!	#DIV/0!	0.7507	1.80	0.0936	1.78	0.49	0.0582	0.31	0.2775	0.28	0.0299	2.05	10.687	1.78	0.0582	0.31
20160705_M257_005		59	214	#DIV/0!	4.7E-03	3.4E-04	4.5E-04	1.8E-02	8.5E-02	#DIV/0!	#DIV/0!	0.7494	2.71	0.0932	2.76	0.51	0.0584	0.35	0.2751	0.30	0.0286	1.48	10.735	2.76	0.0584	0.35
20160705_M257_006		59	209	#DIV/0!	4.8E-03	3.5E-04	4.5E-04	1.8E-02	8.6E-02	#DIV/0!	#DIV/0!	0.7469	2.65	0.0933	2.63	0.50	0.0581	0.34	0.2746	0.29	0.0288	1.62	10.714	2.63	0.0581	0.34
20160705_M257_007		56	208	#DIV/0!	4.5E-03	3.3E-04	4.3E-04	1.7E-02	8.1E-02	#DIV/0!	#DIV/0!	0.7466	3.14	0.0930	3.18	0.51	0.0582	0.32	0.2791	0.33	0.0284	1.43	10.752	3.18	0.0582	0.32
20160705_M257_008		57	210	#DIV/0!	4.5E-03	3.2E-04	4.2E-04	1.7E-02	8.0E-02	#DIV/0!	#DIV/0!	0.7446	3.20	0.0930	3.09	0.48	0.0581	0.30	0.2795	0.30	0.0283	1.38	10.750	3.09	0.0581	0.30
20160705_M257_009		55	217	3.3E-06	4.5E-03	3.3E-04	4.3E-04	1.7E-02	8.1E-02	#DIV/0!	#DIV/0!	0.7490	2.64	0.0933	2.64	0.50	0.0583	0.31	0.2899	0.29	0.0281	1.33	10.719	2.64	0.0583	0.31
20160705_M257_010		56	216	#DIV/0!	4.5E-03	3.3E-04	4.3E-04	1.7E-02	8.1E-02	#DIV/0!	#DIV/0!	0.7453	2.69	0.0931	2.64	0.49	0.0581	0.32	0.2899	0.28	0.0282	1.44	10.741	2.64	0.0581	0.32
20160705_M257_011		54	210	2.8E-06	4.2E-03	3.1E-04	4.0E-04	1.5E-02	7.1E-02	1277	0	0.7572	4.28	0.0944	4.36	0.51	0.0583	0.35	0.2972	0.32	0.0294	2.57	10.598	4.36	0.0583	0.35
20160705_M257_012		53	208	2.3E-06	4.2E-03	3.0E-04	4.0E-04	1.5E-02	7.1E-02	1870	1	0.7536	4.26	0.0946	4.23	0.50	0.0580	0.36	0.2954	0.32	0.0291	2.51	10.574	4.23	0.0580	0.36
20160705_M257_013		57	219	#DIV/0!	4.0E-03	2.9E-04	3.8E-04	1.5E-02	7.1E-02	#DIV/0!	#DIV/0!	0.7436	3.10	0.0931	2.97	0.48	0.0581	0.33	0.2882	0.32	0.0283	1.30	10.739	2.97	0.0581	0.33
20160705_M257_014		58	203	3.0E-06	4.1E-03	3.0E-04	3.9E-04	1.6E-02	7.4E-02	#DIV/0!	#DIV/0!	0.7465	3.54	0.0933	3.59	0.51	0.0581	0.45	0.2872	0.37	0.0279	1.61	10.716	3.59	0.0581	0.45
20160705_M257_015		56	184	2.7E-06	4.3E-03	3.1E-04	4.0E-04	1.6E-02	7.3E-02	1693	0	0.7553	4.59	0.0943	4.63	0.50	0.0582	0.38	0.2838	0.40	0.0278	2.66	10.608	4.63	0.0582	0.38
20160705_M257_016		60	183	#DIV/0!	4.2E-03	3.0E-04	4.0E-04	1.6E-02	7.3E-02	#DIV/0!	#DIV/0!	0.7606	5.12	0.0951	5.07	0.50	0.0580	0.44	0.2827	0.45	0.0278	3.68	10.517	5.07	0.0580	0.44
20160705_M257_017		51	213	2.2E-06	4.7E-03	3.4E-04	4.4E-04	1.7E-02	8.4E-02	#DIV/0!	#DIV/0!	0.7466	2.30	0.0930	2.29	0.50	0.0583	0.33	0.2838	0.27	0.0301	1.43	10.754	2.29	0.0583	0.33
20160705_M257_018		57	210	2.8E-06	4.7E-03	3.4E-04	4.4E-04	1.7E-02	8.4E-02	2234	1	0.7469	2.72	0.0932	2.68	0.49	0.0582	0.30	0.2828	0.30	0.0301	1.61	10.724	2.68	0.0582	0.30

File name	std.	start	end	204Pb	206Pb	207Pb	208Pb	232Th	238U	206Pb/204Pb	2RSE (%)	207Pb/235U	2RSE (%)	206Pb/238U	2RSE (%)	Rho	207Pb/206Pb	2RSE (%)	208Pb/206Pb	2RSE (%)	208Pb/232Th	2RSE (%)	238U/206Pb	2RSE (%)	207Pb/206Pb	2RSE (%)
20160704_91500_007		57	197	2.8E-06	9.0E-04	8.3E-05	1.1E-04	2.6E-03	8.8E-03	#DIV/0!	#DIV/0!	1.8330	1.88	0.1763	1.85	0.49	0.0754	0.68	0.3476	0.69	0.0527	3.11	5.671	1.85	0.0754	0.68
20160704_91500_008		56	207	2.3E-06	9.0E-04	8.4E-05	1.1E-04	2.6E-03	8.8E-03	486	2	1.8420	1.56	0.1771	1.54	0.49	0.0754	0.63	0.3491	0.63	0.0530	2.64	5.648	1.54	0.0754	0.63
20160704_91500_009		75	219	2.6E-06	7.6E-04	7.0E-05	9.2E-05	2.1E-03	7.1E-03	#DIV/0!	#DIV/0!	1.8709	4.37	0.1812	4.06	0.46	0.0753	0.88	0.3578	0.77	0.0512	2.51	5.519	4.06	0.0753	0.88
20160704_91500_010		60	205	#DIV/0!	7.8E-04	7.2E-05	9.4E-05	2.2E-03	7.4E-03	#DIV/0!	#DIV/0!	1.8239	3.50	0.1754	3.41	0.49	0.0756	0.78	0.3607	0.85	0.0507	1.95	5.701	3.41	0.0756	0.78
20160704_91500_1_001		52	225	2.8E-06	7.3E-04	6.9E-05	8.9E-05	2.0E-03	7.0E-03	334	2	1.8174	2.79	0.1746	2.76	0.50	0.0753	0.60	0.3304	0.60	0.0522	1.78	5.726	2.76	0.0753	0.60
20160704_91500_1_002		54	216	2.6E-06	7.9E-04	7.5E-05	9.8E-05	2.2E-03	7.6E-03	305	0	1.8433	2.88	0.1775	2.61	0.45	0.0752	0.69	0.3335	1.02	0.0535	1.65	5.632	2.61	0.0752	0.69
20160704_91500_1_003		60	197	#DIV/0!	9.5E-04	8.9E-05	1.2E-04	2.9E-03	9.4E-03	#DIV/0!	#DIV/0!	1.8385	2.46	0.1768	2.41	0.49	0.0753	0.80	0.3434	0.84	0.0531	2.68	5.657	2.41	0.0753	0.80
20160704_91500_1_004		51	209	#DIV/0!	9.3E-04	8.7E-05	1.1E-04	2.7E-03	9.1E-03	#DIV/0!	#DIV/0!	1.8715	1.43	0.1783	1.57	0.55	0.0760	0.73	0.3435	0.86	0.0557	2.40	5.608	1.57	0.0760	0.73
20160704_91500_1_005		50	216	2.6E-06	8.1E-04	7.6E-05	9.8E-05	2.4E-03	7.9E-03	162	3	1.8006	2.21	0.1732	2.17	0.49	0.0756	0.63	0.3379	0.88	0.0505	1.32	5.774	2.17	0.0756	0.63
20160704_91500_1_006		53	210	#DIV/0!	8.2E-04	7.6E-05	9.9E-05	2.4E-03	8.0E-03	#DIV/0!	#DIV/0!	1.8035	2.29	0.1730	2.33	0.51	0.0756	0.69	0.3400	0.71	0.0499	1.41	5.780	2.33	0.0756	0.69
20160705_91500_1_001		58	207	#DIV/0!	6.8E-04	6.4E-05	8.3E-05	1.8E-03	6.2E-03	#DIV/0!	#DIV/0!	1.8317	3.60	0.1759	3.60	0.50	0.0756	0.79	0.3674	0.82	0.0516	1.87	5.685	3.60	0.0756	0.79
20160705_91500_1_002		56	213	4.1E-06	6.8E-04	6.4E-05	8.5E-05	1.8E-03	6.3E-03	141	0	1.8153	3.57	0.1751	3.31	0.46	0.0752	0.72	0.3693	0.78	0.0516	2.26	5.710	3.31	0.0752	0.72
20160705_91500_1_003		58	216	3.9E-06	7.9E-04	7.4E-05	9.9E-05	2.0E-03	7.3E-03	#DIV/0!	#DIV/0!	1.8595	3.34	0.1789	3.40	0.51	0.0752	0.69	0.3591	0.68	0.0543	1.92	5.590	3.40	0.0752	0.69
20160705_91500_1_004		56	219	#DIV/0!	8.0E-04	7.5E-05	9.9E-05	2.1E-03	7.3E-03	#DIV/0!	#DIV/0!	1.8558	2.64	0.1790	2.64	0.50	0.0754	0.67	0.3607	0.56	0.0542	1.58	5.586	2.64	0.0754	0.67
20160705_91500_1_005		58	210	4.0E-06	8.8E-04	8.3E-05	1.1E-04	2.3E-03	8.3E-03	262	1	1.8665	2.02	0.1803	1.87	0.46	0.0752	0.73	0.3505	0.68	0.0550	1.91	5.547	1.87	0.0752	0.73
20160705_91500_1_006		54	213	3.2E-06	8.4E-04	7.9E-05	1.0E-04	2.1E-03	7.9E-03	276	0	1.8811	1.75	0.1803	1.70	0.49	0.0758	0.65	0.3478	0.71	0.0557	2.05	5.547	1.70	0.0758	0.65
20160705_91500_1_007		61	207	#DIV/0!	7.6E-04	7.1E-05	9.1E-05	1.9E-03	7.1E-03	#DIV/0!	#DIV/0!	1.8749	3.14	0.1803	3.22	0.51	0.0754	0.83	0.3517	0.66	0.0534	1.89	5.546	3.22	0.0754	0.83
20160705_91500_1_008		61	209	#DIV/0!	7.6E-04	7.2E-05	9.3E-05	1.9E-03	7.1E-03	#DIV/0!	#DIV/0!	1.8718	3.21	0.1800	3.17	0.49	0.0756	0.81	0.3542	0.80	0.0536	1.95	5.554	3.17	0.0756	0.81
20160705_91500_1_009		59	207	#DIV/0!	8.9E-04	8.3E-05	1.1E-04	2.2E-03	8.4E-03	#DIV/0!	#DIV/0!	1.8791	2.10	0.1820	1.88	0.45	0.0750	0.61	0.3679	0.66	0.0576	3.31	5.496	1.88	0.0750	0.61
20160705_91500_1_010		55	210	3.2E-06	8.9E-04	8.3E-05	1.1E-04	2.2E-03	8.4E-03	336	1	1.8741	1.79	0.1806	1.78	0.50	0.0754	0.66	0.3716	0.62	0.0570	2.72	5.537	1.78	0.0754	0.66
20160705_91500_1_011		56	221	2.6E-06	8.4E-04	7.9E-05	1.0E-04	2.1E-03	7.9E-03	381	1	1.8814	2.06	0.1809	2.03	0.49	0.0756	0.66	0.3855	0.54	0.0557	1.45	5.528	2.03	0.0756	0.66
20160705_91500_1_012		56	221	#DIV/0!	8.5E-04	8.0E-05	1.0E-04	2.2E-03	8.0E-03	#DIV/0!	#DIV/0!	1.8816	1.93	0.1818	1.75	0.45	0.0752	0.53	0.3813	0.55	0.0566	2.11	5.502	1.75	0.0752	0.53
20160705_91500_1_013		56	216	#DIV/0!	9.1E-04	8.5E-05	1.1E-04	2.2E-03	8.6E-03	#DIV/0!	#DIV/0!	1.8680	1.79	0.1801	1.74	0.49	0.0752	0.69	0.3729	0.62	0.0605	3.05	5.553	1.74	0.0752	0.69
20160705_91500_1_014		59	208	3.5E-06	9.3E-04	8.6E-05	1.1E-04	2.3E-03	8.8E-03	#DIV/0!	#DIV/0!	1.8792	1.63	0.1821	1.48	0.45	0.0749	0.60	0.3747	0.69	0.0591	3.09	5.493	1.48	0.0749	0.60
20160705_91500_1_015		56	203	2.5E-06	7.8E-04	7.3E-05	9.6E-05	2.1E-03	7.2E-03	464	1	1.8578	3.23	0.1787	3.22	0.50	0.0753	0.68	0.3714	0.68	0.0519	2.05	5.596	3.22	0.0753	0.68
20160705_91500_1_016		55	208	#DIV/0!	7.9E-04	7.4E-05	9.8E-05	2.1E-03	7.2E-03	#DIV/0!	#DIV/0!	1.8650	3.24	0.1792	3.22	0.50	0.0755	0.73	0.3740	0.67	0.0527	2.12	5.581	3.22	0.0755	0.73
20160705_91500_1_017		55	214	#DIV/0!	8.2E-04	7.6E-05	1.0E-04	2.1E-03	7.5E-03	#DIV/0!	#DIV/0!	1.8753	2.63	0.1796	2.76	0.52	0.0757	0.69	0.3741	0.60	0.0550	1.63	5.569	2.76	0.0757	0.69
20160705_91500_1_018		56	213	2.6E-06	7.7E-04	7.2E-05	9.4E-05	1.9E-03	7.1E-03	342	1	1.8664	3.05	0.1798	2.88	0.47	0.0755	0.70	0.3678	0.65	0.0552	1.69	5.561	2.88	0.0755	0.70

File name	std.	start	end	204Pb	206Pb	207Pb	208Pb	232Th	238U	206Pb/204Pb	2RSE (%)	207Pb/235U	2RSE (%)	206Pb/238U	2RSE (%)	Rho	207Pb/206Pb	2RSE (%)	208Pb/206Pb	2RSE (%)	208Pb/232Th	2RSE (%)	238U/206Pb	2RSE (%)	207Pb/206Pb	2RSE (%)
20160705_ples9_001		54	220	#DIV/0!	1.8E-03	1.2E-04	6.0E-05	3.9E-03	5.6E-02	#DIV/0!	#DIV/0!	0.3887	2.48	0.0528	2.55	0.52	0.0534	0.51	0.0963	1.24	0.0170	1.22	18.950	2.55	0.0534	0.51
20160705_ples9_002	*	56	220	3.1E-06	1.8E-03	1.2E-04	5.8E-05	3.8E-03	5.6E-02	458	0	0.3931	2.19	0.0536	2.20	0.50	0.0533	0.51	0.0969	0.77	0.0170	1.43	18.663	2.20	0.0533	0.51
20160705_ples9_003	*	56	220	3.4E-06	2.0E-03	1.3E-04	6.7E-05	4.5E-03	6.2E-02	646	3	0.3964	1.92	0.0540	2.03	0.53	0.0531	0.46	0.0997	0.69	0.0170	1.26	18.512	2.03	0.0531	0.46
20160705_ples9_004	*	53	215	3.5E-06	2.2E-03	1.4E-04	7.5E-05	5.0E-03	6.7E-02	597	1	0.3964	1.69	0.0542	1.52	0.45	0.0532	0.47	0.1024	0.66	0.0171	1.24	18.461	1.52	0.0532	0.47
20160705_ples9_005	*	56	207	#DIV/0!	2.2E-03	1.5E-04	7.9E-05	5.2E-03	6.9E-02	#DIV/0!	#DIV/0!	0.3921	3.29	0.0533	3.49	0.53	0.0534	0.52	0.1030	0.75	0.0169	1.62	18.773	3.49	0.0534	0.52
20160705_ples9_006	*	58	217	3.1E-06	2.1E-03	1.4E-04	7.4E-05	4.9E-03	6.6E-02	747	2	0.3893	3.50	0.0531	3.48	0.50	0.0532	0.51	0.1012	0.78	0.0169	1.82	18.831	3.48	0.0532	0.51
20160705_ples9_007	*	59	219	3.7E-06	2.1E-03	1.4E-04	7.2E-05	4.8E-03	6.5E-02	661	1	0.3893	3.61	0.0532	3.57	0.49	0.0531	0.49	0.0998	0.68	0.0169	1.67	18.781	3.57	0.0531	0.49
20160705_ples9_008	*	59	210	#DIV/0!	2.1E-03	1.4E-04	7.1E-05	4.7E-03	6.3E-02	#DIV/0!	#DIV/0!	0.3948	3.89	0.0539	3.88	0.50	0.0532	0.53	0.0974	1.44	0.0165	2.70	18.566	3.88	0.0532	0.53
20160705_ples9_009	*	55	217	#DIV/0!	2.1E-03	1.4E-04	7.2E-05	4.6E-03	6.3E-02	#DIV/0!	#DIV/0!	0.3930	3.43	0.0539	3.36	0.49	0.0532	0.54	0.1008	1.34	0.0170	2.10	18.559	3.36	0.0532	0.54
20160705_ples9_010	*	56	217	#DIV/0!	1.9E-03	1.2E-04	6.4E-05	4.2E-03	5.7E-02	#DIV/0!	#DIV/0!	0.3933	3.54	0.0532	3.53	0.50	0.0532	0.63	0.0984	2.11	0.0171	2.30	18.790	3.53	0.0532	0.63
20160705_ples9_011	*	59	218	#DIV/0!	1.5E-03	1.0E-04	5.7E-05	3.7E-03	4.8E-02	#DIV/0!	#DIV/0!	0.3954	3.94	0.0532	3.61	0.46	0.0539	1.21	0.1030	6.12	0.0167	4.65	18.809	3.61	0.0539	1.21
20160705_ples9_012	*	57	215	#DIV/0!	2.1E-03	1.4E-04	7.0E-05	4.6E-03	6.5E-02	#DIV/0!	#DIV/0!	0.3965	3.04	0.0542	2.99	0.49	0.0531	0.54	0.0987	1.31	0.0167	1.75	18.450	2.99	0.0531	0.54
20160705_ples9_013	*	56	214	#DIV/0!	1.9E-03	1.3E-04	6.1E-05	4.1E-03	5.9E-02	#DIV/0!	#DIV/0!	0.3920	3.18	0.0537	3.04	0.48	0.0531	0.56	0.0939	0.86	0.0168	1.72	18.638	3.04	0.0531	0.56
20160705_ples9_014	*	58	215	#DIV/0!	2.3E-03	1.5E-04	7.7E-05	5.1E-03	7.2E-02	#DIV/0!	#DIV/0!	0.3923	2.36	0.0537	2.25	0.47	0.0530	0.42	0.1001	0.68	0.0176	2.33	18.620	2.25	0.0530	0.42
20160705_ples9_015	*	56	213	#DIV/0!	2.4E-03	1.6E-04	8.2E-05	5.5E-03	7.6E-02	#DIV/0!	#DIV/0!	0.3962	2.02	0.0540	2.16	0.54	0.0531	0.47	0.1020	0.72	0.0175	2.29	18.508	2.16	0.0531	0.47
20160705_ples9_016	*	59	210	#DIV/0!	2.5E-03	1.7E-04	8.8E-05	5.9E-03	7.9E-02	#DIV/0!	#DIV/0!	0.3956	2.24	0.0543	2.17	0.48	0.0528	0.49	0.1052	0.77	0.0172	2.19	18.402	2.17	0.0528	0.49
20160705_ples9_017	*	53	129	#DIV/0!	2.3E-03	1.5E-04	8.1E-05	4.9E-03	6.2E-02	#DIV/0!	#DIV/0!	0.3935	6.40	0.0535	6.22	0.49	0.0532	1.10	0.1082	2.55	0.0168	3.04	18.694	6.22	0.0532	1.10
20160705_ples9_020	*	54	221	#DIV/0!	1.1E-03	7.6E-05	3.5E-05	2.3E-03	3.5E-02	#DIV/0!	#DIV/0!	0.3902	3.41	0.0534	3.25	0.48	0.0532	0.61	0.0971	1.47	0.0169	1.68	18.728	3.25	0.0532	0.61
20160705_ples9_021	*	55	220	#DIV/0!	1.2E-03	7.8E-05	3.6E-05	2.3E-03	3.6E-02	#DIV/0!	#DIV/0!	0.3944	3.43	0.0536	3.42	0.50	0.0534	0.64	0.0963	1.30	0.0172	2.09	18.647	3.42	0.0534	0.64
20160705_ples9_022	*	59	219	#DIV/0!	1.4E-03	9.5E-05	4.5E-05	2.9E-03	4.4E-02	#DIV/0!	#DIV/0!	0.3959	3.35	0.0540	3.25	0.49	0.0531	0.62	0.0966	0.89	0.0171	1.88	18.506	3.25	0.0531	0.62
20160705_ples9_023	*	56	218	#DIV/0!	1.6E-03	1.1E-04	5.2E-05	3.4E-03	4.9E-02	#DIV/0!	#DIV/0!	0.3955	3.07	0.0540	3.02	0.49	0.0532	0.58	0.0957	1.55	0.0169	1.65	18.523	3.02	0.0532	0.58
20160705_ples9_024	*	55	213	#DIV/0!	1.9E-03	1.2E-04	6.3E-05	4.1E-03	5.7E-02	#DIV/0!	#DIV/0!	0.3968	2.96	0.0543	3.01	0.51	0.0530	0.44	0.1016	1.22	0.0169	1.71	18.408	3.01	0.0530	0.44
20160705_ples9_025	*	53	214	#DIV/0!	2.1E-03	1.4E-04	7.2E-05	4.8E-03	6.5E-02	#DIV/0!	#DIV/0!	0.3874	2.68	0.0529	2.78	0.52	0.0531	0.51	0.1045	0.82	0.0168	1.45	18.892	2.78	0.0531	0.51
20160705_ples9_026	*	55	121	#DIV/0!	2.0E-03	1.3E-04	6.7E-05	4.5E-03	6.6E-02	#DIV/0!	#DIV/0!	0.3857	6.66	0.0527	7.44	0.56	0.0531	1.73	0.0992	2.89	0.0171	4.02	18.972	7.44	0.0531	1.73
20160705_ples9_027	*	59	205	3.7E-06	1.8E-03	1.2E-04	6.2E-05	4.0E-03	5.4E-02	658	12	0.3999	5.10	0.0539	5.47	0.54	0.0537	0.75	0.1032	2.30	0.0169	4.36	18.545	5.47	0.0537	0.75
20160705_ples9_028	*	57	219	#DIV/0!	1.9E-03	1.3E-04	6.5E-05	4.2E-03	5.6E-02	#DIV/0!	#DIV/0!	0.3949	4.35	0.0538	4.36	0.50	0.0532	0.57	0.0998	1.80	0.0168	3.58	18.573	4.36	0.0532	0.57
20160705_ples9_029	*	56	206	#DIV/0!	1.9E-03	1.3E-04	6.5E-05	4.2E-03	5.7E-02	#DIV/0!	#DIV/0!	0.3943	4.50	0.0539	4.49	0.50	0.0531	0.64	0.0978	2.29	0.0172	2.54	18.552	4.49	0.0531	0.64
20160704_ples6_001	*	56	183	2.3E-06	2.4E-03	1.6E-04	9.2E-05	6.5E-03	7.7E-02	1008	2	0.3930	4.72	0.0535	4.86	0.52	0.0533	0.52	0.1015	0.86	0.0170	1.78	18.679	4.86	0.0533	0.52
20160704_ples6_002	*	53	181	2.8E-06	2.4E-03	1.6E-04	9.1E-05	6.5E-03	7.8E-02	#DIV/0!	#DIV/0!	0.3917	4.18	0.0534	4.30	0.51	0.0533	0.58	0.1000	0.91	0.0170	1.66	18.734	4.30	0.0533	0.58
20160704_ples6_003	*	53	215	#DIV/0!	2.3E-03	1.6E-04	8.6E-05	6.2E-03	7.4E-02	#DIV/0!	#DIV/0!	0.3902	3.46	0.0534	3.39	0.49	0.0531	0.45	0.0996	0.70	0.0167	1.76	18.741	3.39	0.0531	0.45
20160704_ples6_004	*	53	217	2.5E-06	2.3E-03	1.6E-04	8.7E-05	6.1E-03	7.4E-02	1158	1	0.3956	3.00	0.0537	2.96	0.49	0.0532	0.51	0.0990	1.16	0.0170	2.07	18.614	2.96	0.0532	0.51
20160704_ples6_005	*	52	220	#DIV/0!	2.3E-03	1.5E-04	8.3E-05	5.6E-03	6.7E-02	#DIV/0!	#DIV/0!	0.3949	4.30	0.0538	4.36	0.51	0.0534	0.54	0.1003	0.80	0.0169	3.63	18.585	4.36	0.0534	0.54
20160704_ples6_006	*	50	208	2.6E-06	2.2E-03	1.5E-04	8.2E-05	5.6E-03	6.7E-02	1133	0	0.3992	3.82	0.0545	3.60	0.47	0.0531	0.60	0.0998	0.91	0.0171	3.14	18.335	3.60	0.0531	0.60
20160704_ples6_007	*	53	213	2.9E-06	2.2E-03	1.5E-04	8.1E-05	5.6E-03	6.8E-02	963	1	0.3959	3.58	0.0541	3.65	0.51	0.0532	0.49	0.0991	0.79	0.0170	2.75	18.479	3.65	0.0532	0.49
20160704_ples6_008	*	54	213	#DIV/0!	2.3E-03	1.5E-04	8.2E-05	5.8E-03	7.1E-02	#DIV/0!	#DIV/0!	0.3908	3.42	0.0533	3.50	0.51	0.0532	0.50	0.1010	0.80	0.0168	2.13	18.761	3.50	0.0532	0.50
20160704_ples6_009	*	55	211	3.1E-06	2.2E-03	1.5E-04	8.0E-05	5.7E-03	7.0E-02	#DIV/0!	#DIV/0!	0.3925	3.36	0.0537	3.34	0.50	0.0532	0.48	0.1004	0.79	0.0170	2.25	18.632	3.34	0.0532	0.48
20160704_ples6_010	*	52	214	2.6E-06	2.2E-03	1.5E-04	8.0E-05	5.6E-03	7.0E-02	1041	0	0.3911	2.95	0.0533	2.97	0.50	0.0532	0.47	0.0991	1.00	0.0169	2.22	18.768	2.97	0.0532	0.47
20160704_ples6_011	*	57	210	#DIV/0!	2.4E-03	1.5E-04	8.4E-05	6.1E-03	7.5E-02	#DIV/0!	#DIV/0!	0.3916	2.76	0.0532	2.91	0.53	0.0533	0.59	0.1011	1.26	0.0169	2.88	18.785	2.91	0.0533	0.59
20160704_ples6_012	*	56	207	2.5E-06	2.3E-03	1.5E-04	8.2E-05	5.9E-03	7.4E-02	#DIV/0!	#DIV/0!	0.3918	2.64	0.0534	2.70	0.51	0.0531	0.61	0.1000	1.42	0.0170	2.51	18.730	2.70	0.0531	0.61
20160704_ples6_013	*	59	212	#DIV/0!	2.3E-03	1.5E-04	8.0E-05	5.6E-03	7.2E-02	#DIV/0!	#DIV/0!	0.3952	2.91	0.0537	2.87	0.49	0.0532	0.75	0.0990	1.57	0.0172	2.70	18.613	2.87	0.0532	0.75
20160704_ples6_014	*	63	213	#DIV/0!	2.3E-03	1.5E-04	7.8E-05	5.3E-03	6.3E-02	#DIV/0!	#DIV/0!	0.3947	3.09	0.0538	3.04	0.49	0.0531	0.54	0.0997	1.63	0.0165	3.02	18.597	3.04	0.0531	0.54
20160704_ples6_015	*	47	210	4.8E-06	2.3E-03	1.5E-04	8.4E-05	5.1E-03	6.1E-02	631	2	0.3967	2.14	0.0539	1.83	0.43	0.0536	0.82	0.1019	2.63	0.0175	3.76	18.543	1.83	0.0536	0.82
20160704_ples6_016	*	56	209	#DIV/0!	2.2E-03	1.5E-04	7.6E-05	5.5E-03	7.1E-02	#DIV/0!	#DIV/0!	0.3911	2.85	0.0537	2.80	0.49	0.0529	0.57	0.0984	1.24	0.0168	2.00	18.633	2.80	0.0529	0.57

File name	std.	start	end	204Pb	206Pb	207Pb	208Pb	232Th	238U	206Pb/204Pb	2RSE (%)	207Pb/235U	2RSE (%)	206Pb/238U	2RSE (%)	Rho	207Pb/206Pb	2RSE (%)	208Pb/206Pb	2RSE (%)	208Pb/232Th	2RSE (%)	238U/206Pb	2RSE (%)	207Pb/206Pb	2RSE (%)
20160705_G2_g159		50	242	3.2E-06	4.3E-04	2.8E-05	2.1E-04	1.8E-02	1.8E-02	241	1	0.2914	4.28	0.0413	3.47	0.41	0.0522	1.11	1.4346	5.24	0.0136	3.46	24.240	3.47	0.0522	1.11
20160704_G2_g6		73	248	2.3E-06	6.0E-04	4.0E-05	8.7E-05	7.5E-03	3.0E-02	387	3	0.3117	10.39	0.0430	9.95	0.48	0.0528	1.23	0.3187	19.01	0.0137	4.61	23.281	9.95	0.0528	1.23
20160704_G2_g31		59	170	#DIV/0!	1.4E-03	9.4E-05	2.2E-04	1.8E-02	5.0E-02	#DIV/0!	#DIV/0!	0.3195	7.44	0.0441	7.17	0.48	0.0528	0.76	0.4061	12.80	0.0138	5.64	22.675	7.17	0.0528	0.76
20160704_G2_g29		50	261	2.9E-06	1.6E-03	1.0E-04	2.4E-04	1.9E-02	5.2E-02	#DIV/0!	#DIV/0!	0.3347	6.22	0.0461	5.99	0.48	0.0527	0.50	0.2220	28.24	0.0140	11.32	21.699	5.99	0.0527	0.50
20160705_G2_g63		52	297	4.5E-06	1.7E-03	1.1E-04	1.7E-04	1.2E-02	6.0E-02	628	0	0.3390	2.96	0.0465	2.76	0.47	0.0527	0.52	0.3130	6.14	0.0153	2.78	21.524	2.76	0.0527	0.52
20160704_G2_g3		71	268	3.0E-06	4.5E-04	3.0E-05	7.7E-05	6.0E-03	1.6E-02	188	1	0.3417	5.21	0.0468	5.03	0.48	0.0527	1.04	0.5111	6.34	0.0148	3.82	21.373	5.03	0.0527	1.04
20160704_G2_g15		42	311	2.5E-06	1.5E-03	9.9E-05	2.0E-04	1.5E-02	5.1E-02	709	1	0.3421	2.88	0.0467	2.95	0.51	0.0529	0.40	0.3697	2.80	0.0149	3.22	21.412	2.95	0.0529	0.40
20160704_G2_g20		61	259	2.9E-06	6.8E-04	4.5E-05	8.5E-05	7.0E-03	2.3E-02	#DIV/0!	#DIV/0!	0.3436	4.83	0.0474	4.64	0.48	0.0526	0.93	0.2927	8.13	0.0135	5.02	21.089	4.64	0.0526	0.93
20160705_G2_g148		56	159	3.3E-06	1.1E-03	6.9E-05	2.1E-04	1.4E-02	3.3E-02	573	10	0.3459	7.01	0.0477	6.93	0.49	0.0529	1.53	0.6069	8.60	0.0155	2.75	20.980	6.93	0.0529	1.53
20160705_G2_g76		67	284	#DIV/0!	7.3E-04	4.8E-05	9.9E-05	7.4E-03	2.5E-02	#DIV/0!	#DIV/0!	0.3464	4.50	0.0472	4.65	0.52	0.0532	0.73	0.3848	3.89	0.0141	4.22	21.204	4.65	0.0532	0.73
20160705_G2_g107		56	279	2.9E-06	1.6E-03	1.0E-04	1.7E-04	1.2E-02	5.0E-02	861	1	0.3465	4.49	0.0481	4.37	0.49	0.0524	0.56	0.3269	5.34	0.0141	5.17	20.807	4.37	0.0524	0.56
20160704_G2_g7		60	268	3.0E-06	1.4E-03	9.4E-05	2.0E-04	1.3E-02	4.0E-02	922	1	0.3473	2.32	0.0476	2.15	0.46	0.0529	0.60	0.2823	15.66	0.0147	2.69	21.017	2.15	0.0529	0.60
20160704_G2_g16		49	274	3.2E-06	4.9E-04	3.2E-05	6.9E-05	4.5E-03	1.3E-02	#DIV/0!	#DIV/0!	0.3500	3.57	0.0467	3.45	0.48	0.0541	0.92	0.3883	1.99	0.0152	3.69	21.408	3.45	0.0541	0.92
~~20160705_G2_g136~~		~~59~~	~~260~~	~~2.5E-06~~	~~3.6E-04~~	~~2.5E-05~~	~~6.3E-05~~	~~4.1E-03~~	~~1.1E-02~~	~~#DIV/0!~~	~~#DIV/0!~~	~~0.3683~~	~~9.00~~	~~0.0507~~	~~5.12~~	~~0.28~~	~~0.0530~~	~~4.42~~	~~0.5243~~	~~4.52~~	~~0.0152~~	~~8.90~~	~~19.728~~	~~5.12~~	~~0.0530~~	~~4.42~~
20160704_G2_g19		54	324	2.6E-06	1.7E-03	1.1E-04	3.9E-04	2.7E-02	5.0E-02	1261	1	0.3972	2.84	0.0537	2.84	0.50	0.0535	0.43	0.4916	8.35	0.0160	3.46	18.610	2.84	0.0535	0.43
20160705_G2_g92		68	288	#DIV/0!	3.0E-03	2.0E-04	5.4E-04	3.4E-02	8.6E-02	#DIV/0!	#DIV/0!	0.3981	3.93	0.0544	3.93	0.50	0.0532	0.49	0.5200	21.11	0.0173	3.74	18.379	3.93	0.0532	0.49
20160705_G2_g71		75	253	#DIV/0!	3.9E-04	2.6E-05	1.6E-04	1.0E-02	1.1E-02	#DIV/0!	#DIV/0!	0.3992	6.05	0.0538	5.34	0.44	0.0536	1.49	1.0784	9.30	0.0169	5.81	18.573	5.34	0.0536	1.49
20160705_G2_g77		58	196	#DIV/0!	1.6E-03	1.1E-04	2.9E-05	1.3E-03	4.6E-02	#DIV/0!	#DIV/0!	0.4115	8.05	0.0554	8.22	0.51	0.0540	0.84	0.0548	50.02	0.0263	14.61	18.060	8.22	0.0540	0.84
20160704_G2_g32		49	236	2.5E-06	9.9E-04	6.6E-05	1.4E-04	8.7E-03	2.8E-02	338	0	0.4127	4.22	0.0559	4.26	0.50	0.0539	0.57	0.3541	10.90	0.0177	4.49	17.886	4.26	0.0539	0.57
20160705_G2_g168		62	173	2.9E-06	9.4E-04	7.2E-05	1.1E-04	3.5E-03	2.3E-02	154	9	0.4291	65.24	0.0561	48.02	0.37	0.0574	7.32	0.0971	232.79	0.0434	11.40	17.839	48.02	0.0574	7.32
20160704_G2_g33		59	283	3.3E-06	9.4E-04	6.4E-05	3.0E-04	2.1E-02	3.6E-02	354	5	0.4601	10.02	0.0577	9.67	0.48	0.0577	1.37	1.3902	13.86	0.0215	10.07	17.327	9.67	0.0577	1.37
20160705_G2_g170		53	151	2.9E-06	2.3E-03	1.6E-04	3.0E-04	1.6E-02	6.7E-02	1001	3	0.4666	19.59	0.0602	19.68	0.50	0.0567	1.29	0.3701	12.13	0.0204	10.93	16.616	19.68	0.0567	1.29
~~20160705_G2_g57~~		~~54~~	~~190~~	~~3.7E-06~~	~~4.9E-03~~	~~3.4E-04~~	~~1.7E-04~~	~~1.1E-02~~	~~1.5E-01~~	~~3416~~	~~3~~	~~0.4672~~	~~7.39~~	~~0.0612~~	~~7.30~~	~~0.49~~	~~0.0554~~	~~0.59~~	~~0.1639~~	~~22.53~~	~~0.0202~~	~~12.73~~	~~16.328~~	~~7.30~~	~~0.0554~~	~~0.59~~
20160705_G2_g171		51	294	3.9E-06	5.2E-04	3.9E-05	5.0E-05	2.4E-03	1.7E-02	#DIV/0!	#DIV/0!	0.4847	9.60	0.0591	10.55	0.55	0.0593	2.04	0.3038	7.98	0.0220	6.52	16.911	10.55	0.0593	2.04
20160705_G2_g157		49	230	2.6E-06	7.2E-04	5.1E-05	1.2E-04	5.4E-03	1.5E-02	551	2	0.4969	8.93	0.0646	8.02	0.45	0.0557	1.31	0.3368	32.45	0.0215	9.91	15.486	8.02	0.0557	1.31
~~20160704_G2_g17~~		~~43~~	~~265~~	~~5.6E-06~~	~~6.8E-04~~	~~7.3E-05~~	~~3.6E-04~~	~~2.3E-02~~	~~2.2E-02~~	~~160~~	~~7~~	~~0.5059~~	~~24.06~~	~~0.0500~~	~~8.63~~	~~0.18~~	~~0.0747~~	~~9.58~~	~~1.1857~~	~~11.28~~	~~0.0232~~	~~10.39~~	~~19.985~~	~~8.63~~	~~0.0747~~	~~9.58~~
20160705_G2_g96		40	178	3.6E-06	1.7E-03	1.2E-04	3.7E-04	6.5E-02	5.6E-02	575	1	0.5100	10.69	0.0654	11.02	0.52	0.0566	2.82	0.5983	22.34	0.0147	20.84	15.299	11.02	0.0566	2.82
~~20160705_G2_g162~~		~~56~~	~~186~~	~~9.0E-06~~	~~1.1E-03~~	~~8.2E-05~~	~~7.6E-05~~	~~3.0E-03~~	~~2.1E-02~~	~~248~~	~~6~~	~~0.5267~~	~~17.46~~	~~0.0734~~	~~3.97~~	~~0.11~~	~~0.0549~~	~~3.52~~	~~0.1390~~	~~27.77~~	~~0.0198~~	~~23.64~~	~~13.618~~	~~3.97~~	~~0.0549~~	~~3.52~~
20160704_G2_g4		53	195	#DIV/0!	7.4E-04	5.3E-05	2.5E-04	1.5E-02	1.8E-02	#DIV/0!	#DIV/0!	0.5274	5.81	0.0663	6.12	0.53	0.0575	1.06	0.2308	108.84	0.0204	14.38	15.091	6.12	0.0575	1.06
20160705_G2_g73		56	210	3.2E-06	1.1E-03	7.7E-05	8.0E-05	3.6E-03	2.8E-02	334	1	0.5461	9.39	0.0702	9.13	0.49	0.0567	0.75	0.2195	20.31	0.0240	6.70	14.238	9.13	0.0567	0.75
20160704_G2_g34		77	219	2.4E-06	3.6E-04	2.5E-05	7.9E-05	4.3E-03	7.8E-03	94	8	0.5524	12.12	0.0702	11.28	0.47	0.0573	1.82	0.9750	22.46	0.0199	9.29	14.249	11.28	0.0573	1.82
20160705_G2_g143		59	241	#DIV/0!	6.4E-04	4.5E-05	9.7E-05	4.6E-03	1.3E-02	#DIV/0!	#DIV/0!	0.5552	5.75	0.0722	4.17	0.36	0.0556	1.92	0.4815	17.37	0.0213	6.49	13.846	4.17	0.0556	1.92
20160704_G2_g18		45	276	#DIV/0!	1.9E-03	1.3E-04	2.9E-04	1.5E-02	4.0E-02	#DIV/0!	#DIV/0!	0.5554	3.47	0.0717	3.60	0.52	0.0563	0.53	0.3828	8.37	0.0218	4.47	13.945	3.60	0.0563	0.53
20160704_G2_g37		57	265	3.1E-06	1.4E-03	9.7E-05	4.4E-05	2.5E-03	3.3E-02	311	1	0.5605	4.15	0.0728	3.83	0.46	0.0562	0.55	0.0749	8.81	0.0216	5.13	13.745	3.83	0.0562	0.55
20160705_G2_g67		62	234	#DIV/0!	1.6E-03	1.1E-04	3.6E-04	1.6E-02	3.2E-02	#DIV/0!	#DIV/0!	0.5609	6.86	0.0720	6.87	0.50	0.0565	0.63	0.6799	2.28	0.0219	6.67	13.888	6.87	0.0565	0.63
20160705_G2_g74		61	286	#DIV/0!	4.6E-04	3.2E-05	2.5E-05	1.2E-03	1.0E-02	#DIV/0!	#DIV/0!	0.5619	2.83	0.0719	2.39	0.42	0.0568	0.83	0.1554	1.75	0.0229	2.30	13.907	2.39	0.0568	0.83
20160705_G2_g69		55	226	3.5E-06	9.5E-04	6.7E-05	1.5E-04	7.3E-03	2.1E-02	218	0	0.5630	4.61	0.0719	4.77	0.52	0.0568	0.73	0.6200	12.63	0.0226	3.53	13.908	4.77	0.0568	0.73
20160704_G2_g10		59	246	2.6E-06	6.5E-04	4.7E-05	3.5E-05	1.8E-03	1.3E-02	313	3	0.5630	9.71	0.0718	8.48	0.44	0.0570	1.73	0.1495	8.84	0.0213	8.61	13.922	8.48	0.0570	1.73
~~20160705_G2_g103~~		~~58~~	~~195~~	~~8.4E-06~~	~~9.0E-04~~	~~8.2E-05~~	~~6.8E-04~~	~~3.0E-02~~	~~2.1E-02~~	~~293~~	~~7~~	~~0.5655~~	~~38.96~~	~~0.0722~~	~~8.83~~	~~0.11~~	~~0.0559~~	~~16.26~~	~~1.6226~~	~~23.39~~	~~0.0236~~	~~24.12~~	~~13.859~~	~~8.83~~	~~0.0559~~	~~16.26~~
20160705_G2_g88		54	298	3.1E-06	2.5E-03	1.8E-04	1.2E-04	5.7E-03	5.5E-02	#DIV/0!	#DIV/0!	0.5655	3.04	0.0736	3.08	0.51	0.0558	0.31	0.1646	5.95	0.0215	2.97	13.590	3.08	0.0558	0.31
20160705_G2_g153		52	245	3.3E-06	1.5E-03	1.1E-04	2.7E-04	1.3E-02	3.3E-02	673	2	0.5657	3.35	0.0720	3.69	0.55	0.0567	0.60	0.5510	5.66	0.0230	3.22	13.888	3.69	0.0567	0.60
20160705_G2_g124		59	190	2.7E-06	1.8E-03	1.3E-04	6.3E-05	3.0E-03	4.2E-02	965	4	0.5661	5.50	0.0730	5.65	0.51	0.0563	0.73	0.0951	13.55	0.0240	4.71	13.698	5.65	0.0563	0.73
20160704_G2_g39		48	294	#DIV/0!	1.4E-03	9.6E-05	4.8E-05	2.4E-03	2.9E-02	#DIV/0!	#DIV/0!	0.5691	2.49	0.0735	2.24	0.45	0.0565	0.51	0.0823	6.91	0.0221	4.85	13.610	2.24	0.0565	0.51

20160705_G2_g95		57	187	#DIV/0!	3.0E-03	2.1E-04	8.1E-05	3.7E-03	6.3E-02	#DIV/0!	#DIV/0!	0.5725	7.97	0.0733	8.46	0.53	0.0564	0.62	0.0899	8.06	0.0228	5.43	13.638	8.46	0.0564	0.62
20160705_G2_g65		57	273	#DIV/0!	7.4E-04	5.2E-05	3.2E-05	1.5E-03	1.6E-02	#DIV/0!	#DIV/0!	0.5730	3.74	0.0734	3.62	0.48	0.0565	0.65	0.1641	6.28	0.0227	3.32	13.629	3.62	0.0565	0.65
20160705_G2_g135		62	256	3.0E-06	8.6E-04	6.1E-05	9.1E-05	4.3E-03	1.9E-02	#DIV/0!	#DIV/0!	0.5734	3.33	0.0736	3.35	0.50	0.0563	0.67	0.1060	78.31	0.0212	4.69	13.590	3.35	0.0563	0.67
20160705_G2_g140		56	176	#DIV/0!	1.3E-03	9.1E-05	5.4E-04	4.1E-02	3.0E-02	#DIV/0!	#DIV/0!	0.5744	4.73	0.0737	4.31	0.46	0.0566	0.93	1.2691	16.99	0.0244	8.86	13.564	4.31	0.0566	0.93
20160704_G2_g42		50	267	2.6E-06	1.3E-03	9.0E-05	1.5E-04	7.5E-03	2.8E-02	532	1	0.5767	2.64	0.0741	2.49	0.47	0.0566	0.55	0.3054	13.25	0.0228	3.05	13.502	2.49	0.0566	0.55
20160705_G2_g87		61	295	3.8E-06	2.1E-03	1.5E-04	8.3E-05	4.2E-03	4.7E-02	880	2	0.5770	2.44	0.0750	2.33	0.48	0.0559	0.41	0.0893	20.13	0.0219	2.28	13.340	2.33	0.0559	0.41
20160705_G2_g106		60	290	2.9E-06	5.9E-04	4.3E-05	9.9E-05	4.5E-03	1.2E-02	234	3	0.5842	3.37	0.0736	3.12	0.46	0.0576	1.02	0.5335	4.30	0.0224	3.20	13.594	3.12	0.0576	1.02
20160705_G2_g166		56	276	#DIV/0!	4.1E-04	2.9E-05	3.6E-05	1.6E-03	8.5E-03	#DIV/0!	#DIV/0!	0.5844	4.21	0.0739	4.23	0.50	0.0572	0.86	0.2875	7.63	0.0222	4.05	13.525	4.23	0.0572	0.86
20160704_G2_g12		60	222	3.3E-06	1.4E-03	1.0E-04	3.4E-04	1.3E-02	2.4E-02	#DIV/0!	#DIV/0!	0.5863	7.11	0.0758	6.24	0.44	0.0568	1.30	0.4182	30.31	0.0245	13.46	13.185	6.24	0.0568	1.30
20160705_G2_g59		65	187	3.7E-06	4.4E-04	3.2E-05	8.6E-05	3.8E-03	9.7E-03	103	6	0.5866	10.25	0.0724	8.99	0.44	0.0576	2.91	0.6089	36.05	0.0268	10.11	13.806	8.99	0.0576	2.91
20160704_G2_g2		48	296	2.5E-06	8.8E-04	6.3E-05	8.8E-05	4.4E-03	1.9E-02	531	2	0.5889	3.71	0.0747	3.61	0.49	0.0572	0.66	0.2806	2.95	0.0231	4.13	13.386	3.61	0.0572	0.66
20160704_G2_g1		60	316	3.0E-06	1.1E-03	8.0E-05	5.6E-05	2.9E-03	2.6E-02	381	1	0.5915	3.45	0.0756	3.49	0.51	0.0566	0.56	0.1876	6.55	0.0231	3.01	13.232	3.49	0.0566	0.56
20160705_G2_g53		61	185	3.3E-06	2.4E-03	1.7E-04	3.9E-04	1.8E-02	5.1E-02	912	5	0.5940	7.92	0.0760	8.10	0.51	0.0567	0.68	0.4985	5.79	0.0231	6.75	13.161	8.10	0.0567	0.68
20160705_G2_g51		58	187	3.3E-06	1.5E-03	1.1E-04	3.5E-05	1.4E-03	3.2E-02	371	7	0.5941	6.81	0.0753	6.69	0.49	0.0570	0.86	0.0572	39.55	0.0251	7.28	13.288	6.69	0.0570	0.86
20160704_G2_g48		52	271	3.0E-06	6.8E-04	4.8E-05	5.0E-05	2.4E-03	1.5E-02	176	1	0.5961	3.14	0.0756	3.08	0.49	0.0574	0.72	0.1364	21.75	0.0239	3.28	13.220	3.08	0.0574	0.72
20160705_G2_g55		55	185	3.9E-06	1.1E-03	7.5E-05	1.8E-04	7.7E-03	2.1E-02	#DIV/0!	#DIV/0!	0.6049	7.86	0.0767	7.99	0.51	0.0571	0.86	0.1786	93.49	0.0232	8.04	13.041	7.99	0.0571	0.86
20160705_G2_g98		55	129	3.0E-06	2.6E-03	1.8E-04	7.0E-05	3.1E-03	5.6E-02	#DIV/0!	#DIV/0!	0.6054	13.28	0.0776	13.67	0.51	0.0563	1.20	0.0735	28.35	0.0243	12.95	12.879	13.67	0.0563	1.20
20160705_G2_g167		46	299	#DIV/0!	1.0E-03	7.6E-05	1.5E-04	6.6E-03	2.3E-02	#DIV/0!	#DIV/0!	0.6091	5.07	0.0757	4.90	0.48	0.0582	0.76	0.3791	8.62	0.0254	4.91	13.208	4.90	0.0582	0.76
20160705_G2_g94		57	179	#DIV/0!	9.1E-04	6.4E-05	6.8E-05	3.0E-03	1.9E-02	#DIV/0!	#DIV/0!	0.6131	8.81	0.0785	8.66	0.49	0.0569	1.21	0.2695	16.15	0.0235	7.59	12.736	8.66	0.0569	1.21
~~20160705_G2_g172~~		~~52~~	~~141~~	~~5.2E-06~~	~~4.6E-04~~	~~4.4E-05~~	~~2.6E-04~~	~~1.2E-02~~	~~1.1E-02~~	~~199~~	~~11~~	~~0.6323~~	~~34.74~~	~~0.0697~~	~~6.52~~	~~0.09~~	~~0.0655~~	~~26.48~~	~~1.6991~~	~~10.51~~	~~0.0226~~	~~11.45~~	~~14.340~~	~~6.52~~	~~0.0655~~	~~26.48~~
20160705_G2_g89		121	239	#DIV/0!	1.4E-03	1.0E-04	2.3E-04	1.0E-02	2.9E-02	#DIV/0!	#DIV/0!	0.6493	15.62	0.0840	14.85	0.48	0.0561	2.29	0.4816	31.73	0.0245	19.98	11.906	14.85	0.0561	2.29
20160704_G2_g21		59	229	#DIV/0!	1.8E-03	1.3E-04	2.6E-04	1.2E-02	3.5E-02	#DIV/0!	#DIV/0!	0.6512	5.91	0.0824	6.09	0.52	0.0575	0.56	0.0556	370.82	0.0230	9.32	12.132	6.09	0.0575	0.56
20160705_G2_g75		59	252	3.3E-06	4.0E-04	3.0E-05	3.6E-05	2.2E-03	8.8E-03	118	2	0.6546	11.46	0.0806	10.82	0.47	0.0592	1.18	0.2271	12.20	0.0201	21.65	12.404	10.82	0.0592	1.18
20160705_G2_g86		95	246	#DIV/0!	1.2E-03	8.4E-05	6.3E-05	3.0E-03	2.5E-02	#DIV/0!	#DIV/0!	0.6619	5.57	0.0861	5.14	0.46	0.0559	1.09	0.0455	281.51	0.0240	6.44	11.621	5.14	0.0559	1.09
20160705_G2_g102		59	272	#DIV/0!	1.3E-03	9.1E-05	6.6E-05	3.0E-03	2.6E-02	#DIV/0!	#DIV/0!	0.6841	2.51	0.0852	2.43	0.48	0.0584	0.51	0.1499	6.71	0.0268	3.05	11.739	2.43	0.0584	0.51
20160704_G2_g9		50	262	2.4E-06	9.0E-04	6.6E-05	4.0E-05	1.8E-03	1.7E-02	381	0	0.6920	3.57	0.0857	3.46	0.48	0.0587	0.60	0.1195	4.43	0.0257	3.46	11.674	3.46	0.0587	0.60
20160705_G2_g104		61	172	#DIV/0!	1.4E-03	1.0E-04	8.0E-05	3.4E-03	2.6E-02	#DIV/0!	#DIV/0!	0.6967	7.34	0.0872	7.31	0.50	0.0579	0.82	0.1607	10.74	0.0256	4.86	11.469	7.31	0.0579	0.82
20160705_G2_g84		48	290	4.0E-06	2.2E-03	1.9E-04	6.4E-05	2.8E-03	3.9E-02	#DIV/0!	#DIV/0!	0.7077	13.26	0.0824	8.28	0.31	0.0602	3.66	0.1043	10.72	0.0246	7.58	12.131	8.28	0.0602	3.66
20160705_G2_g113		58	200	2.7E-06	1.6E-03	1.2E-04	1.5E-04	6.5E-03	3.0E-02	#DIV/0!	#DIV/0!	0.7151	8.14	0.0897	8.21	0.50	0.0579	0.59	0.2856	7.38	0.0274	7.67	11.154	8.21	0.0579	0.59
20160705_G2_g50		52	220	3.9E-06	1.2E-03	8.9E-05	2.9E-05	1.1E-03	2.2E-02	285	3	0.7232	3.93	0.0894	3.85	0.49	0.0586	0.52	0.0722	6.90	0.0289	3.69	11.183	3.85	0.0586	0.52
~~20160705_G2_g91~~		~~191~~	~~300~~	~~#DIV/0!~~	~~5.8E-04~~	~~4.3E-05~~	~~9.1E-05~~	~~3.8E-03~~	~~1.1E-02~~	~~#DIV/0!~~	~~#DIV/0!~~	~~0.7625~~	~~12.48~~	~~0.0903~~	~~25.25~~	~~1.01~~	~~0.0608~~	~~13.74~~	~~0.5588~~	~~91.12~~	~~0.0273~~	~~13.51~~	~~11.073~~	~~25.25~~	~~0.0608~~	~~13.74~~
20160705_G2_g111		62	193	3.0E-06	1.4E-03	1.0E-04	3.8E-04	1.3E-02	2.6E-02	398	8	0.7633	12.73	0.0921	12.93	0.51	0.0597	1.16	0.9234	21.86	0.0311	8.97	10.858	12.93	0.0597	1.16
20160704_G2_g47		67	215	3.2E-06	3.4E-03	2.4E-04	2.6E-04	1.0E-02	5.8E-02	1108	2	0.7666	7.84	0.0958	7.63	0.49	0.0583	0.58	0.1931	16.55	0.0276	9.32	10.437	7.63	0.0583	0.58
20160705_G2_g152		50	252	3.1E-06	8.2E-04	6.1E-05	4.0E-04	1.5E-02	1.4E-02	362	1	0.7724	3.68	0.0932	3.47	0.47	0.0601	0.70	1.2431	12.51	0.0303	2.19	10.731	3.47	0.0601	0.70
20160705_G2_g64K		54	186	4.8E-06	1.4E-03	1.0E-04	5.8E-04	2.0E-02	2.2E-02	#DIV/0!	#DIV/0!	0.8030	9.74	0.0968	9.74	0.50	0.0600	0.72	1.1705	7.28	0.0291	10.47	10.335	9.74	0.0600	0.72
20160705_G2_g64R		52	179	4.2E-06	1.2E-03	9.3E-05	3.5E-04	1.2E-02	2.0E-02	234	3	0.8125	8.75	0.0977	8.97	0.51	0.0602	0.77	0.4967	34.44	0.0309	10.20	10.240	8.97	0.0602	0.77
20160705_G2_g156		49	143	#DIV/0!	1.2E-03	8.9E-05	2.3E-04	8.1E-03	2.0E-02	#DIV/0!	#DIV/0!	0.8293	12.73	0.0986	12.58	0.49	0.0606	2.01	0.6629	22.91	0.0310	8.17	10.147	12.58	0.0606	2.01
20160704_G2_g22		51	301	2.7E-06	1.4E-03	1.0E-04	4.1E-04	1.3E-02	2.0E-02	346	1	0.8326	3.20	0.0990	2.95	0.46	0.0609	0.71	0.8635	6.17	0.0317	2.84	10.105	2.95	0.0609	0.71
20160705_G2_g66		63	273	#DIV/0!	1.0E-03	7.8E-05	5.2E-04	1.7E-02	1.6E-02	#DIV/0!	#DIV/0!	0.8423	6.07	0.0994	5.83	0.48	0.0611	0.79	1.3060	6.64	0.0307	6.20	10.062	5.83	0.0611	0.79
20160705_G2_g127		63	233	#DIV/0!	2.4E-03	1.8E-04	2.2E-04	7.3E-03	3.7E-02	#DIV/0!	#DIV/0!	0.8492	9.02	0.1016	8.47	0.47	0.0605	0.95	0.2336	20.48	0.0316	5.34	9.841	8.47	0.0605	0.95
20160705_G2_g85		47	287	3.2E-06	4.2E-03	3.2E-04	3.0E-04	1.1E-02	7.4E-02	#DIV/0!	#DIV/0!	0.8505	8.64	0.0994	7.11	0.41	0.0614	1.77	0.2018	13.89	0.0303	7.48	10.063	7.11	0.0614	1.77
20160705_G2_g163		45	222	4.2E-06	3.9E-03	3.0E-04	2.2E-04	6.5E-03	5.2E-02	722	1	0.8611	7.93	0.1010	8.05	0.51	0.0615	0.44	0.1400	6.93	0.0284	11.16	9.902	8.05	0.0615	0.44
20160704_G2_g23		65	201	2.6E-06	5.3E-04	4.0E-05	1.1E-04	4.4E-03	8.7E-03	60	3	0.8641	4.46	0.1027	4.27	0.48	0.0612	1.21	0.4871	15.07	0.0305	4.53	9.734	4.27	0.0612	1.21
20160705_G2_g131		70	210	3.1E-06	2.0E-03	1.5E-04	3.9E-04	1.3E-02	3.0E-02	770	1	0.8665	11.74	0.1065	11.47	0.49	0.0592	0.56	0.5958	4.60	0.0304	13.16	9.388	11.47	0.0592	0.56

20160705_G2_g128		79	233	#DIV/0!	2.1E-03	1.6E-04	7.1E-05	2.4E-03	3.4E-02	#DIV/0!	#DIV/0!	0.8740	9.42	0.1059	8.87	0.47	0.0603	0.73	0.1041	12.21	0.0329	5.93	9.443	8.87	0.0603	0.73
~~20160705_G2_g54~~		~~51~~	~~268~~	~~3.3E-06~~	~~3.5E-03~~	~~5.0E-04~~	~~1.8E-04~~	~~1.1E-02~~	~~5.2E-02~~	~~765~~	~~7~~	~~0.9041~~	~~36.70~~	~~0.0879~~	~~16.81~~	~~0.23~~	~~0.0791~~	~~12.89~~	~~0.1440~~	~~18.84~~	~~0.0240~~	~~13.99~~	~~11.382~~	~~16.81~~	~~0.0791~~	~~12.89~~
20160705_G2_g138		62	194	3.3E-06	8.7E-04	6.8E-05	1.0E-04	3.7E-03	1.4E-02	283	2	0.9078	4.03	0.1051	4.01	0.50	0.0622	1.34	0.3340	6.53	0.0321	5.31	9.513	4.01	0.0622	1.34
20160705_G2_g142		57	249	#DIV/0!	1.0E-03	7.7E-05	1.8E-04	6.2E-03	1.6E-02	#DIV/0!	#DIV/0!	0.9108	2.60	0.1069	2.57	0.50	0.0616	0.58	0.4628	8.75	0.0317	2.30	9.354	2.57	0.0616	0.58
20160704_G2_g40		96	275	4.2E-06	4.1E-03	3.1E-04	4.7E-04	4.6E-02	7.3E-02	1073	0	0.9126	11.58	0.1069	11.04	0.48	0.0622	0.78	0.3199	7.32	0.0349	17.65	9.357	11.04	0.0622	0.78
20160705_G2_g144		60	169	3.4E-06	5.1E-04	3.8E-05	4.2E-05	1.4E-03	8.0E-03	129	1	0.9219	6.29	0.1084	6.34	0.50	0.0620	2.55	0.3346	22.21	0.0317	6.89	9.222	6.34	0.0620	2.55
20160705_G2_g115		69	211	3.1E-06	1.8E-03	1.4E-04	2.1E-04	7.0E-03	2.9E-02	371	3	0.9308	9.33	0.1106	9.25	0.50	0.0606	1.82	0.5452	23.02	0.0310	8.00	9.045	9.25	0.0606	1.82
20160705_G2_g165		56	261	4.2E-06	3.1E-04	2.4E-05	4.8E-05	1.5E-03	4.7E-03	67	1	0.9375	5.18	0.1072	4.99	0.48	0.0634	1.16	0.4605	6.39	0.0324	4.50	9.331	4.99	0.0634	1.16
20160705_G2_g93		63	251	#DIV/0!	6.5E-04	5.0E-05	2.5E-04	8.2E-03	9.0E-03	#DIV/0!	#DIV/0!	0.9471	7.87	0.1115	7.41	0.47	0.0618	0.78	1.3423	11.14	0.0323	7.55	8.970	7.41	0.0618	0.78
20160704_G2_g14		44	267	3.3E-06	5.2E-04	3.9E-05	5.3E-05	1.9E-03	9.0E-03	#DIV/0!	#DIV/0!	0.9677	4.66	0.1093	4.07	0.44	0.0636	1.30	0.3731	10.61	0.0373	5.03	9.150	4.07	0.0636	1.30
20160704_G2_g41		50	271	3.0E-06	8.7E-04	6.5E-05	1.2E-04	3.8E-03	1.4E-02	734	1	0.9806	8.10	0.1082	7.72	0.48	0.0635	1.53	0.5791	9.51	0.0334	6.46	9.245	7.72	0.0635	1.53
20160704_G2_g30		46	141	4.9E-06	1.4E-03	1.1E-04	2.3E-04	6.2E-03	2.1E-02	#DIV/0!	#DIV/0!	1.0239	29.95	0.1120	22.95	0.38	0.0660	7.49	0.4290	40.67	0.0416	13.54	8.927	22.95	0.0660	7.49
20160705_G2_g60		52	162	3.2E-06	9.7E-04	7.7E-05	1.6E-04	4.8E-03	1.3E-02	203	10	1.0316	8.13	0.1182	7.54	0.46	0.0635	1.13	0.7443	24.02	0.0373	3.79	8.458	7.54	0.0635	1.13
20160705_G2_g112		63	194	2.2E-06	2.4E-03	1.8E-04	3.9E-04	1.2E-02	3.4E-02	1448	4	1.0398	5.88	0.1200	6.13	0.52	0.0629	1.47	0.6439	15.17	0.0355	5.26	8.333	6.13	0.0629	1.47
20160705_G2_g101		54	310	3.1E-06	1.6E-03	1.3E-04	5.2E-04	1.5E-02	2.7E-02	1262	0	1.0805	6.60	0.1220	6.57	0.50	0.0639	0.54	1.1142	5.16	0.0379	4.74	8.195	6.57	0.0639	0.54
20160705_G2_g154		61	214	2.9E-06	1.0E-03	8.2E-05	1.0E-04	2.9E-03	1.3E-02	451	2	1.0863	7.68	0.1228	7.71	0.50	0.0639	0.62	0.2885	1.18	0.0360	6.88	8.141	7.71	0.0639	0.62
20160704_G2_g26		56	302	2.8E-06	4.9E-04	3.8E-05	9.1E-05	3.1E-03	7.6E-03	184	0	1.1126	4.97	0.1227	4.66	0.47	0.0650	1.25	0.8190	9.27	0.0370	5.16	8.153	4.66	0.0650	1.25
20160705_G2_g149		45	230	2.9E-06	8.6E-04	6.9E-05	1.9E-04	5.4E-03	1.1E-02	507	2	1.1411	4.11	0.1284	3.95	0.48	0.0648	0.62	0.8380	6.13	0.0393	4.23	7.790	3.95	0.0648	0.62
20160704_G2_g24		102	291	2.5E-06	1.2E-03	9.7E-05	5.2E-04	1.6E-02	1.6E-02	1013	7	1.2732	10.85	0.1431	10.38	0.48	0.0647	1.50	1.4234	16.44	0.0424	13.60	6.987	10.38	0.0647	1.50
20160705_G2_g90		56	289	#DIV/0!	4.3E-04	3.6E-05	9.2E-05	2.2E-03	4.8E-03	#DIV/0!	#DIV/0!	1.3521	3.02	0.1429	2.83	0.47	0.0689	0.71	0.6177	1.71	0.0436	2.37	6.997	2.83	0.0689	0.71
20160704_G2_g13		129	262	#DIV/0!	1.5E-03	1.2E-04	2.9E-04	6.6E-03	1.7E-02	#DIV/0!	#DIV/0!	1.4252	22.28	0.1527	17.39	0.39	0.0680	8.61	0.5534	50.40	0.0548	28.53	6.547	17.39	0.0680	8.61
20160704_G2_g8		66	280	2.7E-06	1.2E-03	1.1E-04	2.5E-04	5.2E-03	1.4E-02	512	1	1.4270	11.47	0.1472	10.33	0.45	0.0691	1.32	0.4730	14.80	0.0465	13.88	6.792	10.33	0.0691	1.32
20160705_G2_g139		59	134	3.4E-06	3.0E-03	2.7E-04	4.2E-04	9.2E-03	3.1E-02	673	6	1.6096	16.18	0.1624	16.12	0.50	0.0712	2.57	0.4100	23.26	0.0522	7.05	6.159	16.12	0.0712	2.57
20160704_G2_g36		45	163	#DIV/0!	4.4E-04	4.1E-05	7.5E-05	1.8E-03	4.6E-03	#DIV/0!	#DIV/0!	1.6450	10.02	0.1563	9.62	0.48	0.0759	1.55	0.5614	9.78	0.0497	8.38	6.400	9.62	0.0759	1.55
20160705_G2_g82		66	196	4.1E-06	4.7E-04	4.2E-05	7.0E-05	1.5E-03	4.5E-03	#DIV/0!	#DIV/0!	1.7224	8.09	0.1729	7.57	0.47	0.0727	1.18	0.4386	5.28	0.0502	6.76	5.785	7.57	0.0727	1.18
20160705_G2_g62		57	197	4.1E-06	3.5E-03	3.2E-04	6.8E-04	1.5E-02	3.5E-02	#DIV/0!	#DIV/0!	1.7343	2.83	0.1732	2.75	0.49	0.0728	0.60	0.5462	4.07	0.0533	3.73	5.775	2.75	0.0728	0.60
20160705_G2_g134		58	176	2.7E-06	1.3E-03	1.2E-04	4.5E-04	8.8E-03	1.1E-02	378	5	1.7878	9.93	0.1756	9.92	0.50	0.0736	0.85	0.9069	14.91	0.0533	7.67	5.695	9.92	0.0736	0.85
20160704_G2_g27		58	265	2.4E-06	8.9E-04	9.0E-05	1.5E-04	2.7E-03	6.9E-03	464	1	2.2779	6.10	0.2007	6.07	0.50	0.0819	0.62	0.4793	2.40	0.0587	6.25	4.983	6.07	0.0819	0.62
20160705_G2_g81		56	248	#DIV/0!	3.4E-03	4.0E-04	5.5E-04	7.4E-03	2.0E-02	#DIV/0!	#DIV/0!	3.8475	4.67	0.2834	4.40	0.47	0.0984	1.48	0.6927	12.34	0.0800	3.75	3.529	4.40	0.0984	1.48
20160705_G2_g56		58	266	4.2E-06	9.0E-03	1.3E-03	6.5E-04	9.7E-03	5.0E-02	3341	3	5.0705	4.89	0.3113	4.41	0.45	0.1178	0.90	0.1536	25.70	0.0833	6.86	3.212	4.41	0.1178	0.90
20160705_G2_g61		46	199	3.8E-06	2.7E-03	4.2E-04	5.8E-04	6.2E-03	1.2E-02	#DIV/0!	#DIV/0!	5.9892	3.94	0.3555	3.83	0.49	0.1219	0.64	0.5741	5.95	0.1023	2.26	2.813	3.83	0.1219	0.64
20160704_G2_g38		46	217	3.0E-06	5.2E-03	1.0E-03	6.2E-04	6.4E-03	2.8E-02	#DIV/0!	#DIV/0!	7.3163	27.09	0.3183	22.77	0.42	0.1543	7.80	0.2838	14.49	0.1014	14.69	3.141	22.77	0.1543	7.80
20160704_G2_g11		54	258	2.5E-06	2.5E-03	4.9E-04	3.7E-04	4.0E-03	1.0E-02	1690	1	9.1964	3.31	0.4266	3.32	0.50	0.1565	0.51	0.3756	4.00	0.1081	3.15	2.344	3.32	0.1565	0.51
20160705_G2_g49		57	296	3.7E-06	7.5E-03	1.6E-03	1.6E-03	1.3E-02	2.8E-02	2383	4	10.5806	4.01	0.4545	3.32	0.41	0.1671	1.06	0.5399	9.52	0.1358	2.55	2.200	3.32	0.1671	1.06

18.2.3 *Veitscher metasandstone (G1)*

Table 5: Those tables depict the measured values of the zircons of the Veitscher metasandstone, corrected with the EXCEL sheet LamTool U – Th – Pb VI of Košler und Klötzli (unpubl.). M257 (Nasdala et al., 2008), 91500 (Wiedenbeck et al., 1995) and Plešovice (Sláma et al., 2008) are the used standard samples. The crossed out measurements are discordant and were excluded of further steps.

File name	std.	start	end	204Pb	206Pb	207Pb	208Pb	232Th	238U	206Pb/204Pb	2RSE (%)	207Pb/235U	2RSE (%)	206Pb/238U	2RSE (%)	Rho	207Pb/206Pb	2RSE (%)	208Pb/206Pb	2RSE (%)	208Pb/232Th	2RSE (%)	238U/206Pb	2RSE (%)	207Pb/206Pb	2RSE (%)
20160706_M257_001		53	202	2.6E-06	4.3E-03	3.1E-04	4.1E-04	1.6E-02	7.5E-02	#DIV/0!	#DIV/0!	0.7409	3.22	0.0927	3.16	0.49	0.0582	0.43	0.2789	0.33	0.0278	1.93	10.791	3.16	0.0582	0.43
20160706_M257_002		53	203	2.5E-06	4.4E-03	3.2E-04	4.1E-04	1.7E-02	7.6E-02	#DIV/0!	#DIV/0!	0.7315	3.42	0.0917	3.13	0.46	0.0580	0.35	0.2787	0.35	0.0277	1.71	10.908	3.13	0.0580	0.35
20160706_M257_003		52	206	#DIV/0!	4.4E-03	3.2E-04	4.2E-04	1.7E-02	7.9E-02	#DIV/0!	#DIV/0!	0.7311	2.97	0.0912	2.93	0.49	0.0582	0.37	0.2865	0.38	0.0287	1.40	10.960	2.93	0.0582	0.37
20160706_M257_004		54	205	2.3E-06	4.5E-03	3.3E-04	4.3E-04	1.7E-02	8.1E-02	2065	3	0.7392	2.95	0.0923	3.03	0.51	0.0581	0.33	0.2852	0.30	0.0289	1.42	10.839	3.03	0.0581	0.33
20160706_M257_005		57	216	3.0E-06	4.1E-03	3.0E-04	3.9E-04	1.5E-02	7.2E-02	#DIV/0!	#DIV/0!	0.7421	3.34	0.0927	3.30	0.49	0.0581	0.35	0.2912	0.35	0.0275	2.03	10.782	3.30	0.0581	0.35
20160706_M257_006		51	210	2.9E-06	4.2E-03	3.0E-04	4.0E-04	1.6E-02	7.3E-02	1914	1	0.7405	2.89	0.0928	2.85	0.49	0.0580	0.31	0.2906	0.29	0.0277	1.51	10.773	2.85	0.0580	0.31
20160706_M257_007		55	213	#DIV/0!	5.0E-03	3.6E-04	4.7E-04	1.9E-02	8.9E-02	#DIV/0!	#DIV/0!	0.7455	2.08	0.0937	1.95	0.47	0.0578	0.30	0.2948	0.29	0.0295	2.00	10.671	1.95	0.0578	0.30
20160706_M257_008		51	210	#DIV/0!	5.1E-03	3.7E-04	4.8E-04	1.9E-02	9.1E-02	#DIV/0!	#DIV/0!	0.7502	1.73	0.0944	1.59	0.46	0.0578	0.28	0.2945	0.30	0.0302	2.11	10.599	1.59	0.0578	0.28
20160706_M257_009		52	203	#DIV/0!	4.2E-03	3.0E-04	4.0E-04	1.5E-02	7.2E-02	#DIV/0!	#DIV/0!	0.7493	4.03	0.0937	4.22	0.52	0.0582	0.35	0.2968	0.33	0.0282	2.80	10.670	4.22	0.0582	0.35
20160706_M257_010		53	211	2.6E-06	4.1E-03	3.0E-04	3.9E-04	1.5E-02	7.0E-02	1401	0	0.7492	4.03	0.0944	4.00	0.50	0.0578	0.39	0.2961	0.39	0.0279	3.23	10.598	4.00	0.0578	0.39
20160706_M257_011		51	196	#DIV/0!	4.3E-03	3.1E-04	4.2E-04	1.6E-02	7.5E-02	#DIV/0!	#DIV/0!	0.7445	3.98	0.0934	4.06	0.51	0.0581	0.37	0.3013	0.29	0.0293	2.12	10.709	4.06	0.0581	0.37
20160706_M257_011		49	178	#DIV/0!	4.4E-03	3.2E-04	4.3E-04	1.6E-02	7.7E-02	#DIV/0!	#DIV/0!	0.7410	4.28	0.0925	4.40	0.51	0.0581	0.40	0.3018	0.35	0.0293	1.72	10.806	4.40	0.0581	0.40
20160706_M257_012		47	203	#DIV/0!	4.3E-03	3.1E-04	4.1E-04	1.6E-02	7.5E-02	#DIV/0!	#DIV/0!	0.7377	3.33	0.0925	3.26	0.49	0.0578	0.32	0.3007	0.30	0.0293	1.95	10.813	3.26	0.0578	0.32
20160706_M257_012		49	182	#DIV/0!	4.4E-03	3.2E-04	4.2E-04	1.6E-02	7.7E-02	#DIV/0!	#DIV/0!	0.7362	4.09	0.0927	4.06	0.50	0.0578	0.35	0.3010	0.36	0.0292	2.04	10.783	4.06	0.0578	0.35
20160706_M257_013		55	193	2.4E-06	4.3E-03	3.1E-04	4.1E-04	1.6E-02	7.3E-02	#DIV/0!	#DIV/0!	0.7430	4.75	0.0934	4.70	0.50	0.0578	0.43	0.3026	0.30	0.0283	3.17	10.710	4.70	0.0578	0.43
20160706_M257_014		54	180	#DIV/0!	4.3E-03	3.2E-04	4.2E-04	1.6E-02	7.6E-02	#DIV/0!	#DIV/0!	0.7455	4.91	0.0937	4.81	0.49	0.0579	0.41	0.3025	0.41	0.0284	3.04	10.676	4.81	0.0579	0.41
20160706_M257_015		57	206	#DIV/0!	4.3E-03	3.1E-04	4.1E-04	1.7E-02	7.7E-02	#DIV/0!	#DIV/0!	0.7386	3.65	0.0924	3.66	0.50	0.0582	0.34	0.2945	0.34	0.0278	2.01	10.826	3.66	0.0582	0.34
20160706_M257_016		59	197	2.9E-06	4.3E-03	3.1E-04	4.1E-04	1.7E-02	7.7E-02	#DIV/0!	#DIV/0!	0.7371	4.16	0.0924	4.19	0.50	0.0580	0.40	0.2930	0.37	0.0278	2.04	10.826	4.19	0.0580	0.40
20160706_M257_017		52	210	#DIV/0!	4.3E-03	3.2E-04	4.2E-04	1.7E-02	7.8E-02	#DIV/0!	#DIV/0!	0.7354	3.14	0.0914	3.15	0.50	0.0584	0.36	0.2777	0.36	0.0279	1.57	10.944	3.15	0.0584	0.36
20160706_M257_018		65	215	2.3E-06	4.3E-03	3.1E-04	4.1E-04	1.7E-02	7.5E-02	2171	3	0.7467	3.95	0.0932	3.85	0.49	0.0582	0.37	0.2755	0.36	0.0278	2.03	10.731	3.85	0.0582	0.37
20160707_M257_001		56	210	#DIV/0!	4.3E-03	3.1E-04	4.2E-04	1.6E-02	7.3E-02	#DIV/0!	#DIV/0!	0.7570	3.71	0.0941	3.76	0.51	0.0583	0.37	0.2980	0.34	0.0295	2.63	10.628	3.76	0.0583	0.37
20160707_M257_002		52	210	2.2E-06	4.3E-03	3.1E-04	4.2E-04	1.6E-02	7.3E-02	2284	0	0.7545	3.51	0.0940	3.40	0.48	0.0582	0.35	0.2986	0.35	0.0292	2.54	10.643	3.40	0.0582	0.35
20160707_M257_003		52	207	#DIV/0!	4.2E-03	3.1E-04	4.2E-04	1.6E-02	7.1E-02	#DIV/0!	#DIV/0!	0.7543	3.84	0.0939	3.81	0.50	0.0582	0.32	0.3019	0.30	0.0275	2.80	10.647	3.81	0.0582	0.32
20160707_M257_004		53	204	2.1E-06	4.2E-03	3.1E-04	4.1E-04	1.6E-02	7.1E-02	1623	3	0.7517	3.78	0.0940	3.72	0.49	0.0581	0.35	0.3021	0.30	0.0273	2.66	10.633	3.72	0.0581	0.35
20160707_M257_005		52	208	#DIV/0!	4.1E-03	3.0E-04	4.1E-04	1.6E-02	7.2E-02	#DIV/0!	#DIV/0!	0.7325	3.88	0.0912	3.91	0.50	0.0582	0.28	0.3041	0.27	0.0263	2.62	10.961	3.91	0.0582	0.28
20160707_M257_006		58	208	2.4E-06	4.1E-03	3.0E-04	4.1E-04	1.6E-02	7.1E-02	#DIV/0!	#DIV/0!	0.7341	4.42	0.0919	4.30	0.49	0.0580	0.33	0.3037	0.31	0.0265	2.80	10.878	4.30	0.0580	0.33
20160707_M257_007		51	209	2.6E-06	4.1E-03	3.0E-04	4.1E-04	1.6E-02	7.2E-02	#DIV/0!	#DIV/0!	0.7372	3.50	0.0921	3.45	0.49	0.0582	0.35	0.3058	0.34	0.0273	2.13	10.863	3.45	0.0582	0.35
20160707_M257_008		54	210	2.5E-06	4.1E-03	3.0E-04	4.0E-04	1.6E-02	7.1E-02	1696	1	0.7427	3.60	0.0926	3.49	0.49	0.0581	0.39	0.3057	0.41	0.0273	2.21	10.794	3.49	0.0581	0.39
20160707_M257_009		52	196	#DIV/0!	4.0E-03	2.9E-04	3.9E-04	1.5E-02	7.1E-02	#DIV/0!	#DIV/0!	0.7415	4.00	0.0924	3.97	0.50	0.0582	0.39	0.3035	0.32	0.0298	2.10	10.818	3.97	0.0582	0.39
20160707_M257_010		55	202	#DIV/0!	3.9E-03	2.9E-04	3.8E-04	1.5E-02	6.9E-02	#DIV/0!	#DIV/0!	0.7559	3.76	0.0943	3.71	0.49	0.0581	0.36	0.3024	0.40	0.0296	2.43	10.606	3.71	0.0581	0.36

File name	std.	start	end	204Pb	206Pb	207Pb	208Pb	232Th	238U	206Pb/204Pb	2RSE (%)	207Pb/235U	2RSE (%)	206Pb/238U	2RSE (%)	Rho	207Pb/206Pb	2RSE (%)	208Pb/206Pb	2RSE (%)	208Pb/232Th	2RSE (%)	238U/206Pb	2RSE (%)	207Pb/206Pb	2RSE (%)
20160706_91500_1_001		56	208	2.7E-06	7.6E-04	7.2E-05	9.5E-05	2.0E-03	6.8E-03	#DIV/0!	#DIV/0!	1.8619	3.66	0.1790	3.69	0.50	0.0754	0.66	0.3619	0.81	0.0529	3.27	5.588	3.69	0.0754	0.66
20160706_91500_1_002		53	217	#DIV/0!	7.7E-04	7.3E-05	9.6E-05	2.0E-03	6.9E-03	#DIV/0!	#DIV/0!	1.8361	3.47	0.1765	3.44	0.50	0.0756	0.66	0.3647	0.64	0.0538	2.43	5.665	3.44	0.0756	0.66
20160706_91500_1_003		54	210	#DIV/0!	7.8E-04	7.3E-05	9.7E-05	2.0E-03	7.1E-03	#DIV/0!	#DIV/0!	1.8358	3.22	0.1769	3.16	0.49	0.0753	0.70	0.3751	0.68	0.0548	1.63	5.652	3.16	0.0753	0.70
20160706_91500_1_004		54	208	2.3E-06	7.9E-04	7.4E-05	9.8E-05	2.0E-03	7.2E-03	#DIV/0!	#DIV/0!	1.8470	3.07	0.1781	3.10	0.50	0.0755	0.55	0.3745	0.64	0.0547	1.93	5.615	3.10	0.0755	0.55
20160706_91500_1_005		56	209	#DIV/0!	7.6E-04	7.1E-05	9.5E-05	2.0E-03	6.9E-03	#DIV/0!	#DIV/0!	1.8687	3.38	0.1802	3.37	0.50	0.0753	0.69	0.3805	0.78	0.0530	2.29	5.548	3.37	0.0753	0.69
20160706_91500_1_006		50	205	3.0E-06	7.6E-04	7.2E-05	9.5E-05	2.0E-03	7.0E-03	#DIV/0!	#DIV/0!	1.8361	3.21	0.1779	3.06	0.48	0.0749	0.64	0.3825	0.61	0.0526	2.03	5.620	3.06	0.0749	0.64
20160706_91500_1_007		62	208	#DIV/0!	7.5E-04	7.0E-05	9.3E-05	1.9E-03	6.8E-03	#DIV/0!	#DIV/0!	1.8669	4.29	0.1812	4.12	0.48	0.0749	0.78	0.3845	0.83	0.0523	2.84	5.517	4.12	0.0749	0.78
20160706_91500_1_008		54	205	2.9E-06	7.6E-04	7.2E-05	9.6E-05	1.9E-03	6.9E-03	#DIV/0!	#DIV/0!	1.8826	3.75	0.1796	3.49	0.47	0.0755	0.93	0.3879	1.65	0.0526	3.09	5.569	3.49	0.0755	0.93
20160706_91500_1_009		51	205	#DIV/0!	7.8E-04	7.3E-05	9.7E-05	2.1E-03	7.3E-03	#DIV/0!	#DIV/0!	1.8259	3.16	0.1763	3.04	0.48	0.0749	0.75	0.3872	0.63	0.0526	1.69	5.671	3.04	0.0749	0.75
20160706_91500_1_010		49	210	3.6E-06	7.9E-04	7.5E-05	9.9E-05	2.1E-03	7.4E-03	#DIV/0!	#DIV/0!	1.8268	2.82	0.1761	3.03	0.54	0.0753	0.67	0.3887	0.59	0.0521	1.87	5.678	3.03	0.0753	0.67
20160706_91500_1_011		48	214	#DIV/0!	7.7E-04	7.2E-05	9.6E-05	2.0E-03	7.0E-03	#DIV/0!	#DIV/0!	1.8448	2.68	0.1786	2.53	0.47	0.0750	0.67	0.3899	0.52	0.0531	1.96	5.598	2.53	0.0750	0.67
20160706_91500_1_011		50	188	#DIV/0!	7.9E-04	7.4E-05	9.8E-05	2.1E-03	7.3E-03	#DIV/0!	#DIV/0!	1.8374	3.48	0.1779	3.45	0.50	0.0751	0.80	0.3889	0.60	0.0532	1.84	5.622	3.45	0.0751	0.80
20160706_91500_1_012		56	213	#DIV/0!	7.7E-04	7.2E-05	9.5E-05	2.0E-03	7.0E-03	#DIV/0!	#DIV/0!	1.8532	3.47	0.1790	3.51	0.50	0.0751	0.79	0.3906	0.73	0.0526	2.45	5.588	3.51	0.0751	0.79
20160706_91500_1_012		52	188	#DIV/0!	7.9E-04	7.5E-05	9.9E-05	2.1E-03	7.3E-03	#DIV/0!	#DIV/0!	1.8415	3.57	0.1780	3.61	0.51	0.0749	0.85	0.3908	0.79	0.0529	2.00	5.617	3.61	0.0749	0.85
20160706_91500_1_013		59	200	#DIV/0!	7.9E-04	7.5E-05	9.9E-05	2.1E-03	7.3E-03	#DIV/0!	#DIV/0!	1.8554	3.50	0.1805	3.33	0.48	0.0748	0.72	0.3913	0.77	0.0535	1.91	5.540	3.33	0.0748	0.72
20160706_91500_1_014		53	210	2.2E-06	7.8E-04	7.3E-05	9.6E-05	2.0E-03	7.2E-03	354	1	1.8283	3.18	0.1766	3.18	0.50	0.0752	0.63	0.3900	0.69	0.0527	1.81	5.661	3.18	0.0752	0.63
20160706_91500_1_015		54	202	#DIV/0!	7.7E-04	7.3E-05	9.6E-05	2.0E-03	7.0E-03	#DIV/0!	#DIV/0!	1.8690	3.41	0.1810	3.75	0.55	0.0750	0.76	0.3792	0.97	0.0526	3.50	5.524	3.75	0.0750	0.76
20160706_91500_1_016		56	205	2.5E-06	7.5E-04	7.0E-05	9.3E-05	1.9E-03	6.8E-03	247	1	1.8386	4.04	0.1775	4.15	0.51	0.0753	0.76	0.3812	0.79	0.0536	3.00	5.634	4.15	0.0753	0.76
20160706_91500_1_017		59	213	#DIV/0!	7.7E-04	7.3E-05	9.5E-05	2.0E-03	7.2E-03	#DIV/0!	#DIV/0!	1.8424	3.47	0.1780	3.26	0.47	0.0754	0.74	0.3591	0.67	0.0542	1.69	5.619	3.26	0.0754	0.74
20160706_91500_1_018		61	210	#DIV/0!	7.7E-04	7.3E-05	9.6E-05	2.0E-03	7.2E-03	#DIV/0!	#DIV/0!	1.8566	3.37	0.1780	3.36	0.50	0.0754	0.79	0.3610	0.78	0.0542	2.09	5.617	3.36	0.0754	0.79
20160707_91500_1_001		50	203	#DIV/0!	7.5E-04	7.1E-05	9.5E-05	1.9E-03	6.8E-03	#DIV/0!	#DIV/0!	1.8388	3.62	0.1759	3.55	0.49	0.0757	0.75	0.3852	0.72	0.0559	2.49	5.685	3.55	0.0757	0.75
20160707_91500_1_002		53	207	2.0E-06	7.5E-04	7.1E-05	9.5E-05	1.9E-03	6.7E-03	#DIV/0!	#DIV/0!	1.8511	3.58	0.1774	3.68	0.51	0.0754	0.70	0.3852	0.71	0.0563	2.90	5.637	3.68	0.0754	0.70
20160707_91500_1_003		55	207	#DIV/0!	7.5E-04	7.1E-05	9.5E-05	1.9E-03	6.6E-03	#DIV/0!	#DIV/0!	1.8792	3.74	0.1804	3.78	0.50	0.0756	0.79	0.3912	0.74	0.0525	2.70	5.543	3.78	0.0756	0.79
20160707_91500_1_004		52	216	#DIV/0!	7.4E-04	7.1E-05	9.5E-05	1.9E-03	6.6E-03	#DIV/0!	#DIV/0!	1.8632	3.56	0.1797	3.45	0.48	0.0752	0.63	0.3910	0.59	0.0515	2.86	5.564	3.45	0.0752	0.63
20160707_91500_1_005		45	207	2.5E-06	7.7E-04	7.3E-05	9.7E-05	2.0E-03	7.1E-03	#DIV/0!	#DIV/0!	1.8019	2.69	0.1738	2.63	0.49	0.0751	0.63	0.3907	0.55	0.0502	1.93	5.755	2.63	0.0751	0.63
20160707_91500_1_007		51	207	#DIV/0!	8.0E-04	7.6E-05	1.0E-04	2.2E-03	7.5E-03	#DIV/0!	#DIV/0!	1.8370	2.55	0.1759	2.55	0.50	0.0755	0.63	0.3938	0.63	0.0507	1.87	5.685	2.55	0.0755	0.63
20160707_91500_1_008		51	211	#DIV/0!	7.9E-04	7.5E-05	1.0E-04	2.1E-03	7.3E-03	#DIV/0!	#DIV/0!	1.8412	2.77	0.1764	2.67	0.48	0.0755	0.65	0.3924	0.63	0.0504	2.02	5.669	2.67	0.0755	0.65
20160707_91500_1_009		58	207	2.1E-06	7.2E-04	6.8E-05	8.9E-05	1.9E-03	6.6E-03	#DIV/0!	#DIV/0!	1.8692	3.76	0.1799	3.76	0.50	0.0752	0.81	0.3860	0.87	0.0538	2.86	5.558	3.76	0.0752	0.81
20160707_91500_1_010		59	203	#DIV/0!	7.3E-04	6.9E-05	9.2E-05	2.0E-03	6.7E-03	#DIV/0!	#DIV/0!	1.8808	3.74	0.1803	3.81	0.51	0.0756	0.81	0.3934	0.87	0.0541	3.12	5.547	3.81	0.0756	0.81
20160707_91500_1_011		59	210	2.5E-06	6.5E-04	6.2E-05	8.0E-05	1.6E-03	6.0E-03	336	1	1.8514	4.24	0.1778	4.19	0.49	0.0755	0.72	0.3844	1.13	0.0563	4.15	5.624	4.19	0.0755	0.72

File name	std.	start	end	204Pb	206Pb	207Pb	208Pb	232Th	238U	206Pb/204Pb	2RSE (%)	207Pb/235U	2RSE (%)	206Pb/238U	2RSE (%)	Rho	207Pb/206Pb	2RSE (%)	208Pb/206Pb	2RSE (%)	208Pb/232Th	2RSE (%)	238U/206Pb	2RSE (%)	207Pb/206Pb	2RSE (%)
20160707_ples6_001		50	204	#DIV/0!	2.0E-03	1.3E-04	6.8E-05	4.8E-03	6.0E-02	#DIV/0!	#DIV/0!	0.3911	3.01	0.0530	3.12	0.52	0.0535	0.52	0.1032	1.26	0.0172	1.97	18.882	3.12	0.0535	0.52
20160707_ples6_002	*	52	206	2.8E-06	1.9E-03	1.3E-04	6.4E-05	4.5E-03	5.7E-02	681	0	0.3933	2.76	0.0537	2.71	0.49	0.0531	0.48	0.1009	1.50	0.0172	2.01	18.628	2.71	0.0531	0.48
20160707_ples6_003	*	50	203	#DIV/0!	1.8E-03	1.2E-04	6.1E-05	4.2E-03	5.5E-02	#DIV/0!	#DIV/0!	0.3915	3.07	0.0534	2.99	0.49	0.0531	0.56	0.0998	1.35	0.0170	2.17	18.710	2.99	0.0531	0.56
20160707_ples6_004	*	57	208	2.4E-06	1.7E-03	1.1E-04	5.7E-05	3.9E-03	5.1E-02	#DIV/0!	#DIV/0!	0.3976	3.50	0.0540	3.45	0.49	0.0534	0.52	0.0999	1.47	0.0168	2.45	18.511	3.45	0.0534	0.52
20160707_ples6_005	*	55	207	#DIV/0!	1.5E-03	1.0E-04	5.1E-05	3.4E-03	4.6E-02	#DIV/0!	#DIV/0!	0.3935	3.74	0.0535	3.71	0.50	0.0532	0.56	0.0999	1.38	0.0165	2.20	18.683	3.71	0.0532	0.56
20160707_ples6_006	*	55	210	#DIV/0!	1.5E-03	9.8E-05	4.9E-05	3.2E-03	4.4E-02	#DIV/0!	#DIV/0!	0.3936	3.44	0.0536	3.46	0.50	0.0533	0.64	0.0994	1.33	0.0165	2.03	18.648	3.46	0.0533	0.64
20160707_ples6_007	*	52	200	2.6E-06	1.4E-03	9.5E-05	4.7E-05	3.1E-03	4.3E-02	697	2	0.3883	3.37	0.0533	3.26	0.48	0.0532	0.53	0.0992	1.22	0.0165	1.86	18.772	3.26	0.0532	0.53
20160707_ples6_008	*	49	205	#DIV/0!	1.7E-03	1.1E-04	5.5E-05	3.6E-03	5.2E-02	#DIV/0!	#DIV/0!	0.3967	1.99	0.0538	1.93	0.49	0.0533	0.53	0.0995	0.95	0.0177	2.56	18.574	1.93	0.0533	0.53
20160707_ples6_009	*	46	201	2.4E-06	1.7E-03	1.1E-04	5.5E-05	3.5E-03	5.2E-02	940	1	0.3942	1.70	0.0537	1.75	0.51	0.0532	0.52	0.1005	0.75	0.0180	2.53	18.609	1.75	0.0532	0.52
20160707_ples6_010	*	47	205	2.7E-06	1.7E-03	1.1E-04	5.5E-05	3.4E-03	5.2E-02	643	0	0.3940	2.07	0.0538	1.89	0.46	0.0530	0.55	0.1006	0.78	0.0185	2.90	18.575	1.89	0.0530	0.55
20160707_ples6_011	*	53	210	#DIV/0!	1.3E-03	8.9E-05	4.3E-05	2.8E-03	3.9E-02	#DIV/0!	#DIV/0!	0.3923	4.26	0.0535	4.19	0.49	0.0532	0.55	0.1008	1.16	0.0161	3.41	18.699	4.19	0.0532	0.55
20160707_ples6_012	*	52	202	#DIV/0!	1.3E-03	8.8E-05	4.3E-05	2.8E-03	3.9E-02	#DIV/0!	#DIV/0!	0.3928	4.28	0.0534	4.27	0.50	0.0533	0.61	0.0998	0.97	0.0157	3.49	18.721	4.27	0.0533	0.61
20160707_ples6_013	*	55	202	2.2E-06	1.3E-03	8.7E-05	4.2E-05	2.7E-03	3.8E-02	548	2	0.3955	4.48	0.0541	4.36	0.49	0.0532	0.64	0.1001	1.08	0.0160	3.59	18.487	4.36	0.0532	0.64
20160707_ples6_014	*	52	204	#DIV/0!	1.2E-03	8.3E-05	4.0E-05	2.6E-03	3.8E-02	#DIV/0!	#DIV/0!	0.3901	3.93	0.0530	4.14	0.53	0.0535	0.67	0.0998	0.96	0.0173	2.42	18.870	4.14	0.0535	0.67
20160707_ples6_015	*	55	185	2.3E-06	1.2E-03	8.3E-05	4.0E-05	2.6E-03	3.8E-02	#DIV/0!	#DIV/0!	0.3930	4.88	0.0537	4.58	0.47	0.0530	0.82	0.1003	1.12	0.0173	2.71	18.637	4.58	0.0530	0.82
20160707_ples6_016	*	55	198	3.1E-06	1.2E-03	8.1E-05	3.9E-05	2.6E-03	3.7E-02	#DIV/0!	#DIV/0!	0.3965	3.89	0.0542	3.82	0.49	0.0531	0.75	0.0995	1.01	0.0173	2.53	18.464	3.82	0.0531	0.75
20160706_ples6_001	*	48	199	2.3E-06	2.1E-03	1.4E-04	7.3E-05	5.1E-03	6.3E-02	1087	1	0.3939	2.98	0.0534	3.09	0.52	0.0534	0.47	0.0995	1.03	0.0162	2.20	18.726	3.09	0.0534	0.47
20160706_ples6_002	*	50	204	#DIV/0!	2.1E-03	1.4E-04	7.2E-05	4.9E-03	6.2E-02	#DIV/0!	#DIV/0!	0.3901	3.17	0.0531	3.23	0.51	0.0532	0.44	0.0997	1.07	0.0166	2.03	18.822	3.23	0.0532	0.44
20160706_ples6_003	*	51	200	3.0E-06	2.1E-03	1.4E-04	7.1E-05	4.7E-03	6.2E-02	#DIV/0!	#DIV/0!	0.3929	3.36	0.0535	3.44	0.51	0.0533	0.55	0.0993	0.99	0.0168	2.19	18.686	3.44	0.0533	0.55
20160706_ples6_004	*	53	204	#DIV/0!	2.0E-03	1.3E-04	6.9E-05	4.4E-03	5.9E-02	#DIV/0!	#DIV/0!	0.3928	3.57	0.0538	3.63	0.51	0.0530	0.49	0.0997	0.85	0.0177	2.31	18.582	3.63	0.0530	0.49
20160706_ples6_005	*	52	207	#DIV/0!	1.9E-03	1.3E-04	6.6E-05	4.1E-03	5.6E-02	#DIV/0!	#DIV/0!	0.3977	3.79	0.0541	3.91	0.52	0.0533	0.50	0.1025	0.95	0.0176	2.20	18.493	3.91	0.0533	0.50
20160706_ples6_006	*	54	207	2.8E-06	1.9E-03	1.2E-04	6.3E-05	4.0E-03	5.5E-02	570	0	0.3962	4.18	0.0544	4.12	0.49	0.0531	0.65	0.1009	1.12	0.0172	2.99	18.383	4.12	0.0531	0.65
20160706_ples6_007	*	52	206	2.7E-06	1.8E-03	1.2E-04	6.1E-05	3.9E-03	5.3E-02	700	1	0.3966	4.01	0.0542	3.90	0.49	0.0530	0.60	0.1000	1.02	0.0175	2.28	18.449	3.90	0.0530	0.60
20160706_ples6_008	*	58	202	#DIV/0!	1.7E-03	1.2E-04	5.8E-05	3.8E-03	5.2E-02	#DIV/0!	#DIV/0!	0.3917	5.00	0.0532	5.09	0.51	0.0534	0.56	0.1012	1.16	0.0170	3.14	18.806	5.09	0.0534	0.56
20160706_ples6_009	*	56	202	2.6E-06	1.7E-03	1.1E-04	5.6E-05	3.6E-03	5.0E-02	510	2	0.3924	4.89	0.0534	5.03	0.51	0.0532	0.54	0.1003	1.14	0.0167	3.42	18.710	5.03	0.0532	0.54
20160706_ples6_010	*	54	204	#DIV/0!	1.6E-03	1.1E-04	5.3E-05	3.5E-03	4.9E-02	#DIV/0!	#DIV/0!	0.3923	4.10	0.0536	3.99	0.49	0.0532	0.60	0.0989	1.28	0.0167	2.56	18.641	3.99	0.0532	0.60
20160706_ples6_011	*	52	208	#DIV/0!	1.6E-03	1.1E-04	5.2E-05	3.5E-03	4.8E-02	#DIV/0!	#DIV/0!	0.3900	3.63	0.0532	3.63	0.50	0.0532	0.63	0.0991	1.24	0.0167	2.07	18.797	3.63	0.0532	0.63
20160706_ples6_012	*	51	207	#DIV/0!	1.5E-03	1.0E-04	5.0E-05	3.3E-03	4.7E-02	#DIV/0!	#DIV/0!	0.3941	3.28	0.0536	3.42	0.52	0.0533	0.56	0.0986	1.21	0.0166	2.05	18.641	3.42	0.0533	0.56
20160706_ples6_013	*	49	198	#DIV/0!	1.5E-03	1.0E-04	4.9E-05	3.3E-03	4.6E-02	#DIV/0!	#DIV/0!	0.3933	3.10	0.0538	3.13	0.51	0.0532	0.59	0.0989	1.01	0.0168	1.92	18.592	3.13	0.0532	0.59
20160706_ples6_014	*	55	204	#DIV/0!	1.5E-03	1.0E-04	4.8E-05	3.2E-03	4.7E-02	#DIV/0!	#DIV/0!	0.3910	3.78	0.0530	3.91	0.52	0.0533	0.61	0.1002	1.03	0.0170	2.16	18.861	3.91	0.0533	0.61
20160706_ples6_015	*	55	205	#DIV/0!	1.5E-03	9.7E-05	4.7E-05	3.2E-03	4.5E-02	#DIV/0!	#DIV/0!	0.3944	3.51	0.0539	3.50	0.50	0.0530	0.64	0.0997	0.92	0.0170	2.13	18.564	3.50	0.0530	0.64
20160706_ples6_016	*	54	206	2.8E-06	1.4E-03	9.5E-05	4.7E-05	3.0E-03	4.4E-02	458	0	0.3967	3.44	0.0538	3.29	0.48	0.0533	0.79	0.1013	2.51	0.0172	3.47	18.588	3.29	0.0533	0.79
20160706_ples6_017	*	56	204	#DIV/0!	1.3E-03	8.9E-05	4.3E-05	2.9E-03	4.1E-02	#DIV/0!	#DIV/0!	0.3909	3.57	0.0535	3.40	0.48	0.0531	0.67	0.0999	1.45	0.0168	2.10	18.679	3.40	0.0531	0.67
20160706_ples6_017	*	49	187	#DIV/0!	1.4E-03	9.2E-05	4.4E-05	3.0E-03	4.3E-02	#DIV/0!	#DIV/0!	0.3878	3.11	0.0530	2.99	0.48	0.0531	0.60	0.0993	1.25	0.0168	1.91	18.876	2.99	0.0531	0.60
20160706_ples6_018	*	52	180	#DIV/0!	1.4E-03	9.1E-05	4.4E-05	2.9E-03	4.2E-02	#DIV/0!	#DIV/0!	0.3941	3.41	0.0539	3.30	0.48	0.0533	0.86	0.0999	1.16	0.0171	1.99	18.550	3.30	0.0533	0.86
20160706_ples6_018	*	50	189	#DIV/0!	1.4E-03	9.1E-05	4.4E-05	2.9E-03	4.2E-02	#DIV/0!	#DIV/0!	0.3934	2.99	0.0538	2.96	0.49	0.0533	0.79	0.0995	1.18	0.0169	1.83	18.603	2.96	0.0533	0.79
20160706_ples6_019	*	55	193	#DIV/0!	1.3E-03	8.9E-05	4.3E-05	2.9E-03	4.1E-02	#DIV/0!	#DIV/0!	0.3957	3.66	0.0538	3.53	0.48	0.0532	0.85	0.1005	1.32	0.0170	2.20	18.581	3.53	0.0532	0.85
20160706_ples6_019	*	52	190	#DIV/0!	1.4E-03	9.1E-05	4.4E-05	2.9E-03	4.2E-02	#DIV/0!	#DIV/0!	0.3948	3.21	0.0536	3.35	0.52	0.0532	0.76	0.0996	1.24	0.0169	2.12	18.647	3.35	0.0532	0.76
20160706_ples6_020	*	53	182	#DIV/0!	1.3E-03	8.9E-05	4.3E-05	2.7E-03	4.0E-02	#DIV/0!	#DIV/0!	0.4012	4.74	0.0544	4.67	0.49	0.0534	0.90	0.1001	1.24	0.0171	2.96	18.366	4.67	0.0534	0.90
20160706_ples6_021	*	49	180	2.3E-06	1.4E-03	9.1E-05	4.4E-05	2.8E-03	4.1E-02	573	1	0.3944	4.51	0.0538	4.43	0.49	0.0531	0.73	0.1001	1.16	0.0172	2.93	18.575	4.43	0.0531	0.73
20160706_ples6_022	*	56	200	#DIV/0!	1.4E-03	9.6E-05	4.6E-05	3.1E-03	4.5E-02	#DIV/0!	#DIV/0!	0.3896	3.13	0.0531	3.24	0.52	0.0533	0.63	0.1014	1.14	0.0171	1.58	18.833	3.24	0.0533	0.63
20160706_ples6_023	*	55	210	#DIV/0!	1.4E-03	9.6E-05	4.7E-05	3.1E-03	4.5E-02	#DIV/0!	#DIV/0!	0.3931	3.06	0.0538	3.04	0.50	0.0530	0.56	0.1013	1.34	0.0169	2.08	18.595	3.04	0.0530	0.56

20160706_ples6_024	*	58	189	2.3E-06	1.5E-03	9.9E-05	4.8E-05	3.3E-03	4.6E-02	#DIV/0!	#DIV/0!	0.3930	3.86	0.0538	3.84	0.50	0.0530	0.63	0.1019	1.76	0.0168	2.19	18.581	3.84	0.0530	0.63
20160706_ples6_025	*	56	205	#DIV/0!	1.4E-03	9.6E-05	4.7E-05	3.1E-03	4.5E-02	#DIV/0!	#DIV/0!	0.3945	3.06	0.0537	3.13	0.51	0.0532	0.61	0.0989	2.46	0.0171	1.91	18.619	3.13	0.0532	0.61
20160706_ples6_026	*	54	207	2.3E-06	1.4E-03	9.4E-05	4.6E-05	3.1E-03	4.4E-02	486	3	0.3924	3.07	0.0535	2.99	0.49	0.0532	0.66	0.0982	2.72	0.0170	1.86	18.690	2.99	0.0532	0.66
20160706_ples6_027	*	52	204	2.7E-06	1.5E-03	9.9E-05	4.9E-05	3.3E-03	4.6E-02	683	1	0.3943	2.89	0.0535	3.05	0.53	0.0535	0.61	0.0983	3.05	0.0168	2.12	18.682	3.05	0.0535	0.61
20160706_ples6_028	*	58	208	#DIV/0!	1.4E-03	9.4E-05	4.9E-05	3.1E-03	4.2E-02	#DIV/0!	#DIV/0!	0.3938	5.45	0.0535	5.14	0.47	0.0534	0.79	0.0965	5.82	0.0172	4.31	18.686	5.14	0.0534	0.79
20160706_ples6_029	*	50	204	#DIV/0!	2.0E-03	1.3E-04	7.1E-05	4.6E-03	6.0E-02	#DIV/0!	#DIV/0!	0.3909	3.73	0.0534	3.66	0.49	0.0530	0.51	0.1044	1.05	0.0166	2.78	18.717	3.66	0.0530	0.51
20160706_ples6_030	*	54	209	2.3E-06	1.9E-03	1.3E-04	6.5E-05	4.3E-03	5.7E-02	#DIV/0!	#DIV/0!	0.3959	3.70	0.0541	3.60	0.49	0.0532	0.55	0.1003	1.23	0.0171	2.46	18.482	3.60	0.0532	0.55

File name	std.	start	end	204Pb	206Pb	207Pb	208Pb	232Th	238U	206Pb/204Pb	2RSE (%)	207Pb/235U	2RSE (%)	206Pb/238U	2RSE (%)	Rho	207Pb/206Pb	2RSE (%)	208Pb/206Pb	2RSE (%)	208Pb/232Th	2RSE (%)	238U/206Pb	2RSE (%)	207Pb/206Pb	2RSE (%)
~~20160707_G1_g90~~		~~47~~	~~172~~	~~3.3E-05~~	~~1.6E-03~~	~~4.8E-04~~	~~9.5E-04~~	~~4.1E-03~~	~~2.5E-02~~	~~546~~	~~26~~	~~0.2145~~	~~1373.78~~	~~0.0723~~	~~53.55~~	~~0.02~~	~~0.0400~~	~~154.73~~	~~0.0124~~	~~4589.57~~	~~0.0313~~	~~1129.11~~	~~13.837~~	~~53.55~~	~~0.0400~~	~~154.73~~
~~20160706_G1_g15~~		~~46~~	~~104~~	~~2.7E-06~~	~~1.4E-03~~	~~1.2E-04~~	~~1.2E-04~~	~~4.9E-03~~	~~2.6E-02~~	~~349~~	~~94~~	~~0.3708~~	~~241.93~~	~~0.0670~~	~~62.98~~	~~0.13~~	~~0.0496~~	~~54.46~~	~~0.2829~~	~~49.28~~	~~0.0212~~	~~58.63~~	~~14.935~~	~~62.98~~	~~0.0496~~	~~54.46~~
20160706_G1_g73		46	274	2.4E-06	1.1E-03	7.6E-05	1.6E-04	9.0E-03	3.1E-02	546	2	0.4112	2.94	0.0562	2.69	0.46	0.0535	0.58	0.4114	7.31	0.0183	3.43	17.792	2.69	0.0535	0.58
20160707_G1_g64		56	256	2.7E-06	7.6E-04	5.2E-05	1.5E-04	9.7E-03	2.2E-02	503	7	0.4141	3.56	0.0562	3.51	0.49	0.0536	0.70	0.8359	11.78	0.0169	5.58	17.808	3.51	0.0536	0.70
20160706_G1_g87		49	284	2.9E-06	2.3E-03	1.5E-04	3.3E-04	2.0E-02	6.4E-02	859	1	0.4157	1.71	0.0564	1.71	0.50	0.0534	0.34	0.0514	206.47	0.0186	3.19	17.724	1.71	0.0534	0.34
20160707_G1_g177		50	196	2.4E-06	6.4E-04	4.4E-05	3.3E-04	2.0E-02	1.8E-02	325	10	0.4161	4.43	0.0557	4.33	0.49	0.0542	1.13	1.1485	15.75	0.0184	4.18	17.956	4.33	0.0542	1.13
20160706_G1_g169		56	241	2.9E-06	4.8E-04	3.3E-05	7.9E-05	4.7E-03	1.4E-02	243	4	0.4171	3.09	0.0563	2.85	0.46	0.0538	0.93	0.6035	6.62	0.0187	1.76	17.749	2.85	0.0538	0.93
20160707_G1_g106		54	160	2.0E-06	5.2E-04	3.6E-05	1.4E-04	8.8E-03	1.5E-02	309	13	0.4183	6.12	0.0562	4.96	0.40	0.0541	1.98	0.7832	16.08	0.0183	3.31	17.787	4.96	0.0541	1.98
20160707_G1_g77		51	260	2.8E-06	3.0E-03	2.1E-04	5.3E-04	3.1E-02	8.4E-02	1594	4	0.4200	3.56	0.0571	3.33	0.47	0.0533	0.48	0.4462	11.45	0.0176	3.81	17.518	3.33	0.0533	0.48
20160707_G1_g179		54	238	3.0E-06	2.9E-03	2.0E-04	6.1E-04	3.2E-02	6.8E-02	922	8	0.4227	4.17	0.0567	3.54	0.42	0.0541	0.95	0.4289	15.04	0.0168	5.21	17.638	3.54	0.0541	0.95
20160706_G1_g28		62	215	3.0E-06	2.2E-03	1.5E-04	6.9E-04	3.3E-02	4.9E-02	698	6	0.4286	3.85	0.0575	3.91	0.51	0.0536	0.87	0.5090	44.48	0.0189	5.07	17.377	3.91	0.0536	0.87
20160706_G1_g22		50	221	2.2E-06	1.3E-03	8.5E-05	1.9E-04	1.0E-02	3.4E-02	609	3	0.4316	5.07	0.0586	4.97	0.49	0.0535	0.55	0.4533	6.72	0.0191	4.43	17.052	4.97	0.0535	0.55
20160706_G1_g18		56	214	2.8E-06	1.3E-03	8.9E-05	2.7E-04	1.2E-02	2.8E-02	448	9	0.4333	2.84	0.0590	2.64	0.46	0.0535	0.54	0.5561	12.68	0.0190	2.73	16.954	2.64	0.0535	0.54
20160707_G1_g140		65	254	2.4E-06	8.9E-04	6.3E-05	4.4E-05	2.6E-03	2.2E-02	452	5	0.4364	8.40	0.0578	7.03	0.42	0.0548	1.29	0.2466	20.15	0.0177	6.07	17.308	7.03	0.0548	1.29
20160707_G1_g189		55	188	3.0E-06	2.9E-03	2.0E-04	1.1E-03	6.7E-02	7.7E-02	883	3	0.4367	9.65	0.0590	9.54	0.49	0.0535	0.60	1.4505	21.74	0.0188	12.89	16.958	9.54	0.0535	0.60
20160707_G1_g66		57	228	2.2E-06	7.7E-04	5.3E-05	1.5E-04	7.2E-03	1.8E-02	175	32	0.4372	8.87	0.0585	8.95	0.50	0.0540	0.89	0.4070	14.68	0.0173	10.03	17.086	8.95	0.0540	0.89
20160706_G1_g27		46	189	2.2E-06	1.2E-03	9.8E-05	1.7E-04	4.0E-03	1.8E-02	531	5	0.4441	39.05	0.0618	25.25	0.32	0.0556	4.24	0.0098	1431.62	0.0253	18.76	16.174	25.25	0.0556	4.24
~~20160706_G1_g56~~		~~85~~	~~193~~	~~2.9E-06~~	~~4.3E-04~~	~~2.9E-05~~	~~6.8E-05~~	~~3.8E-03~~	~~1.1E-02~~	~~242~~	~~10~~	~~0.4871~~	~~15.19~~	~~0.0648~~	~~16.33~~	~~0.54~~	~~0.0546~~	~~2.50~~	~~0.4419~~	~~25.01~~	~~0.0183~~	~~21.33~~	~~15.438~~	~~16.33~~	~~0.0546~~	~~2.50~~
20160707_G1_g191		50	174	2.8E-06	9.9E-04	7.8E-05	1.0E-04	3.7E-03	1.7E-02	#DIV/0!	#DIV/0!	0.5354	37.35	0.0711	25.24	0.34	0.0561	5.34	0.3217	11.41	0.0217	22.44	14.067	25.24	0.0561	5.34
20160706_G1_g145		52	225	4.0E-06	2.8E-03	2.0E-04	1.3E-03	5.2E-02	5.4E-02	742	12	0.5514	10.15	0.0713	9.64	0.48	0.0562	0.97	0.7977	25.28	0.0203	20.82	14.022	9.64	0.0562	0.97
20160707_G1_g185		52	264	2.3E-06	3.0E-03	2.1E-04	6.5E-04	3.4E-02	6.8E-02	2298	6	0.5575	2.71	0.0729	2.66	0.49	0.0554	0.39	0.7764	8.24	0.0218	4.26	13.727	2.66	0.0554	0.39
20160707_G1_g139		50	252	2.5E-06	1.7E-03	1.2E-04	2.5E-04	1.2E-02	3.6E-02	1221	5	0.5613	4.53	0.0732	4.52	0.50	0.0559	0.63	0.5576	10.68	0.0223	6.44	13.669	4.52	0.0559	0.63
20160707_G1_g180		50	248	2.8E-06	9.5E-04	6.8E-05	1.3E-04	5.6E-03	1.9E-02	370	4	0.5638	6.01	0.0717	6.03	0.50	0.0571	0.67	0.4204	7.87	0.0225	6.28	13.940	6.03	0.0571	0.67
20160707_G1_g131		62	191	2.5E-06	1.0E-03	7.2E-05	6.4E-05	3.0E-03	1.8E-02	258	12	0.5679	18.10	0.0727	17.05	0.47	0.0571	1.20	0.2659	16.53	0.0211	15.81	13.755	17.05	0.0571	1.20
20160706_G1_g30		58	221	2.4E-06	1.8E-03	1.3E-04	1.4E-04	6.6E-03	3.8E-02	1073	7	0.5746	7.98	0.0748	7.75	0.49	0.0558	0.63	0.1122	83.53	0.0249	7.89	13.364	7.75	0.0558	0.63
20160706_G1_g16r		49	237	2.7E-06	6.1E-04	4.3E-05	5.4E-05	2.2E-03	1.3E-02	296	6	0.5778	5.22	0.0740	5.14	0.49	0.0566	0.76	0.0922	55.60	0.0232	8.08	13.515	5.14	0.0566	0.76
20160706_G1_g89		55	259	2.3E-06	1.6E-03	1.1E-04	1.5E-04	6.9E-03	3.4E-02	1047	10	0.5782	2.28	0.0754	2.21	0.48	0.0557	0.54	0.2590	9.28	0.0256	3.51	13.263	2.21	0.0557	0.54
20160707_G1_g186R		53	266	2.8E-06	1.9E-03	1.3E-04	1.6E-04	6.9E-03	3.9E-02	1050	9	0.5806	3.81	0.0744	4.16	0.54	0.0563	0.50	0.2218	11.90	0.0270	4.89	13.432	4.16	0.0563	0.50
20160706_G1_g152		55	237	2.8E-06	1.6E-03	1.1E-04	1.9E-04	9.1E-03	3.4E-02	757	4	0.5824	3.25	0.0753	3.32	0.51	0.0562	0.65	0.0759	112.32	0.0250	3.73	13.284	3.32	0.0562	0.65
20160706_G1_g120R		65	222	3.1E-06	2.0E-03	1.4E-04	7.2E-05	2.9E-03	3.1E-02	656	2	0.5836	4.35	0.0765	3.97	0.46	0.0557	0.92	0.1218	7.12	0.0249	7.40	13.068	3.97	0.0557	0.92
20160706_G1_g176		60	247	2.4E-06	2.6E-03	1.8E-04	1.9E-04	7.6E-03	4.7E-02	1155	3	0.5868	3.02	0.0752	2.67	0.44	0.0565	0.70	0.2747	13.68	0.0246	3.23	13.306	2.67	0.0565	0.70
20160706_G1_g37		53	205	2.6E-06	1.5E-03	1.0E-04	1.3E-04	5.8E-03	3.0E-02	735	10	0.5945	7.57	0.0765	7.36	0.49	0.0562	0.79	0.1556	39.25	0.0231	11.03	13.080	7.36	0.0562	0.79

20160706_G1_g6		53	187	3.0E-06	8.1E-04	5.7E-05	5.6E-05	2.5E-03	1.7E-02	277	10	0.5954	5.61	0.0764	5.43	0.48	0.0567	1.00	0.1972	29.32	0.0254	3.45	13.097	5.43	0.0567	1.00
20160706_G1_g119		46	152	2.7E-06	1.3E-03	9.2E-05	1.4E-04	5.5E-03	2.3E-02	482	7	0.5958	8.58	0.0750	8.66	0.50	0.0566	1.47	0.1540	77.67	0.0248	9.15	13.333	8.66	0.0566	1.47
20160706_G1_g4		60	220	3.4E-06	1.1E-03	7.4E-05	2.0E-04	8.4E-03	2.1E-02	367	4	0.5972	7.81	0.0774	7.64	0.49	0.0563	0.67	0.2217	117.66	0.0265	13.39	12.928	7.64	0.0563	0.67
20160706_G1_g142		59	175	2.7E-06	1.4E-03	1.0E-04	5.6E-05	2.5E-03	3.0E-02	571	3	0.5979	7.12	0.0776	7.00	0.49	0.0557	0.87	0.1297	18.43	0.0254	3.88	12.879	7.00	0.0557	0.87
20160706_G1_g17		47	243	2.9E-06	8.6E-04	6.2E-05	1.0E-04	4.5E-03	1.7E-02	546	2	0.5995	7.57	0.0766	6.42	0.42	0.0567	1.14	0.3349	37.69	0.0239	7.43	13.060	6.42	0.0567	1.14
20160707_G1_g41		59	246	2.6E-06	8.8E-04	6.3E-05	2.3E-05	1.0E-03	1.7E-02	531	4	0.6035	6.63	0.0777	6.55	0.49	0.0563	0.75	0.0913	9.04	0.0217	7.63	12.869	6.55	0.0563	0.75
20160706_G1_g85		53	218	2.9E-06	2.0E-03	1.4E-04	5.8E-05	2.4E-03	3.7E-02	790	2	0.6057	9.50	0.0789	9.33	0.49	0.0558	0.50	0.1198	9.91	0.0237	5.76	12.672	9.33	0.0558	0.50
20160706_G1_g104R		56	226	2.5E-06	2.0E-03	1.4E-04	4.7E-05	2.1E-03	4.2E-02	1030	3	0.6060	3.72	0.0782	3.65	0.49	0.0564	0.58	0.0620	11.29	0.0257	3.91	12.781	3.65	0.0564	0.58
20160706_G1_g71		49	266	7.7E-06	8.7E-04	6.4E-05	1.0E-04	8.0E-03	2.0E-02	174	15	0.6091	7.16	0.0761	7.25	0.51	0.0577	1.67	0.3348	10.30	0.0233	9.22	13.144	7.25	0.0577	1.67
20160706_G1_g55		53	235	2.7E-06	1.5E-03	1.1E-04	4.4E-04	1.9E-02	2.9E-02	1098	3	0.6149	4.74	0.0797	3.69	0.39	0.0560	2.15	1.0046	8.88	0.0244	6.53	12.553	3.69	0.0560	2.15
20160707_G1_g141R		53	271	2.2E-06	6.5E-04	4.6E-05	3.6E-05	1.7E-03	1.3E-02	467	2	0.6159	4.14	0.0787	4.06	0.49	0.0567	0.67	0.1716	2.86	0.0233	4.71	12.709	4.06	0.0567	0.67
20160706_G1_g33		50	257	#DIV/0!	6.3E-04	4.5E-05	1.3E-04	5.1E-03	1.0E-02	#DIV/0!	#DIV/0!	0.6177	6.00	0.0782	6.01	0.50	0.0567	0.70	0.9295	13.50	0.0250	4.00	12.787	6.01	0.0567	0.70
20160706_G1_g143		52	246	2.5E-06	9.1E-04	6.5E-05	4.6E-05	2.1E-03	1.9E-02	378	3	0.6194	1.76	0.0789	1.64	0.47	0.0571	0.63	0.1481	19.01	0.0257	1.79	12.678	1.64	0.0571	0.63
20160707_G1_g182		55	254	2.6E-06	2.1E-03	1.5E-04	6.4E-04	2.6E-02	4.1E-02	935	9	0.6254	5.89	0.0794	5.65	0.48	0.0570	1.19	0.7973	13.71	0.0254	10.69	12.587	5.65	0.0570	1.19
20160706_G1_g2		56	246	2.8E-06	6.8E-04	4.8E-05	8.0E-05	3.5E-03	1.4E-02	310	7	0.6271	4.08	0.0793	4.17	0.51	0.0570	0.73	0.4341	7.45	0.0243	4.10	12.613	4.17	0.0570	0.73
20160707_G1_g136		63	257	2.9E-06	1.9E-03	1.4E-04	9.2E-05	4.0E-03	3.6E-02	1043	7	0.6299	3.65	0.0808	3.35	0.46	0.0567	0.62	0.1903	12.59	0.0233	5.02	12.381	3.35	0.0567	0.62
20160706_G1_g88		57	257	2.9E-06	9.7E-04	6.9E-05	5.7E-05	2.6E-03	2.0E-02	241	1	0.6307	2.53	0.0797	2.54	0.50	0.0574	0.69	0.2218	13.77	0.0250	1.82	12.549	2.54	0.0574	0.69
20160706_G1_g35		56	248	3.1E-06	1.3E-03	9.6E-05	1.1E-04	4.1E-03	2.4E-02	523	2	0.6349	9.14	0.0803	8.34	0.46	0.0577	1.09	0.1258	47.01	0.0230	12.52	12.449	8.34	0.0577	1.09
20160706_G1_g21		51	236	2.2E-06	1.4E-03	9.9E-05	4.3E-04	1.9E-02	2.7E-02	748	10	0.6381	6.43	0.0818	6.51	0.51	0.0565	0.63	0.6447	13.67	0.0264	8.39	12.230	6.51	0.0565	0.63
20160706_G1_g10		54	276	2.8E-06	1.0E-03	7.3E-05	6.8E-05	2.8E-03	2.0E-02	513	4	0.6438	3.41	0.0814	3.43	0.50	0.0573	0.52	0.1925	9.64	0.0258	2.87	12.285	3.43	0.0573	0.52
20160706_G1_g19		57	261	2.8E-06	1.7E-03	1.2E-04	3.8E-05	1.6E-03	3.3E-02	743	5	0.6466	2.73	0.0826	2.58	0.47	0.0569	0.43	0.0270	77.24	0.0259	3.30	12.100	2.58	0.0569	0.43
20160706_G1_g170		66	239	3.0E-06	1.4E-03	1.0E-04	3.3E-04	1.4E-02	2.8E-02	439	2	0.6471	2.47	0.0809	2.34	0.47	0.0580	0.86	0.5914	10.01	0.0261	2.67	12.364	2.34	0.0580	0.86
20160706_G1_g57		66	176	2.5E-06	2.7E-03	1.8E-04	9.9E-05	3.8E-03	5.2E-02	470	2	0.6494	11.06	0.0857	10.53	0.48	0.0549	1.17	-0.0645	-352.89	0.0221	28.34	11.665	10.53	0.0549	1.17
20160706_G1_g74		55	212	2.8E-06	1.2E-03	9.0E-05	2.4E-04	7.3E-03	1.7E-02	567	3	0.6500	5.10	0.0800	4.13	0.41	0.0581	1.49	0.5300	20.55	0.0271	3.67	12.495	4.13	0.0581	1.49
20160707_G1_g156		55	215	2.7E-06	8.0E-04	5.7E-05	9.6E-05	4.3E-03	1.6E-02	509	5	0.6505	3.66	0.0836	3.76	0.51	0.0562	0.78	0.5039	10.88	0.0252	5.00	11.956	3.76	0.0562	0.78
20160706_G1_g83		61	223	3.1E-06	6.2E-04	4.5E-05	9.4E-05	3.9E-03	1.1E-02	158	6	0.6557	8.43	0.0820	8.49	0.50	0.0578	0.90	0.5536	9.58	0.0244	7.67	12.194	8.49	0.0578	0.90
20160706_G1_g39		45	235	3.0E-06	8.6E-04	6.4E-05	1.2E-04	4.2E-03	2.0E-02	307	1	0.6592	2.86	0.0823	2.29	0.40	0.0612	1.91	0.4538	18.02	0.0297	6.38	12.150	2.29	0.0612	1.91
20160707_G1_g183		61	266	2.7E-06	9.2E-04	6.7E-05	8.2E-05	3.4E-03	1.8E-02	378	2	0.6600	2.90	0.0838	2.76	0.48	0.0570	0.61	0.3929	9.31	0.0281	2.82	11.926	2.76	0.0570	0.61
20160706_G1_g29		59	262	3.1E-06	4.5E-04	3.3E-05	7.0E-05	3.1E-03	8.7E-03	135	1	0.6612	3.30	0.0831	3.27	0.49	0.0577	0.86	0.3410	10.22	0.0250	3.12	12.031	3.27	0.0577	0.86
20160706_G1_g1		56	233	2.9E-06	1.7E-03	1.2E-04	2.4E-04	8.8E-03	2.9E-02	832	11	0.6616	7.02	0.0845	6.97	0.50	0.0573	0.56	0.3688	10.38	0.0264	7.98	11.834	6.97	0.0573	0.56
20160706_G1_g116		52	240	3.0E-06	4.9E-04	3.6E-05	5.7E-05	2.2E-03	8.0E-03	241	2	0.6708	5.44	0.0849	4.67	0.43	0.0576	1.35	0.3328	3.27	0.0255	6.53	11.784	4.67	0.0576	1.35
20160707_G1_g187		58	194	2.8E-06	1.6E-03	1.2E-04	1.7E-04	6.7E-03	2.9E-02	417	3	0.6743	8.76	0.0839	9.09	0.52	0.0579	0.91	0.2988	9.68	0.0263	8.32	11.914	9.09	0.0579	0.91
20160707_G1_g109		55	269	2.6E-06	3.3E-03	2.4E-04	1.4E-04	5.3E-03	6.0E-02	1561	8	0.6816	6.91	0.0863	6.30	0.46	0.0574	0.63	0.1197	19.29	0.0259	4.45	11.591	6.30	0.0574	0.63
20160706_G1_g118		52	213	3.1E-06	1.6E-03	1.2E-04	3.5E-04	1.4E-02	3.0E-02	782	2	0.6848	3.04	0.0867	3.46	0.57	0.0573	0.75	0.6384	4.85	0.0268	4.56	11.531	3.46	0.0573	0.75
20160706_G1_g12		48	170	3.1E-06	2.7E-03	1.9E-04	4.0E-04	1.8E-02	5.5E-02	1438	15	0.6863	6.96	0.0893	6.82	0.49	0.0558	0.63	0.4867	12.35	0.0268	8.46	11.201	6.82	0.0558	0.63
20160706_G1_g147		42	131	#DIV/0!	1.7E-03	1.4E-04	1.6E-04	5.6E-03	2.8E-02	#DIV/0!	#DIV/0!	0.6942	22.89	0.0862	20.21	0.44	0.0574	6.33	0.3076	19.28	0.0304	5.79	11.596	20.21	0.0574	6.33
20160706_G1_g32		95	242	2.5E-06	2.1E-03	1.5E-04	6.1E-05	2.7E-03	3.9E-02	938	5	0.7030	7.68	0.0898	6.71	0.44	0.0563	1.11	0.1058	17.51	0.0256	6.75	11.136	6.71	0.0563	1.11
20160707_G1_g194		61	235	3.0E-06	2.2E-03	1.6E-04	2.5E-04	1.0E-02	4.1E-02	1096	4	0.7047	4.09	0.0902	4.15	0.51	0.0566	0.61	0.4466	12.68	0.0261	6.08	11.081	4.15	0.0566	0.61
20160707_G1_g62		53	253	2.7E-06	4.4E-04	3.3E-05	8.2E-05	2.8E-03	7.9E-03	129	4	0.7064	9.42	0.0879	8.88	0.47	0.0582	1.15	0.3652	29.63	0.0263	8.20	11.375	8.88	0.0582	1.15
20160706_G1_g34		51	225	2.9E-06	1.0E-03	7.7E-05	2.7E-04	1.0E-02	1.8E-02	359	1	0.7238	5.00	0.0893	5.14	0.51	0.0588	0.61	0.5430	21.66	0.0279	5.23	11.201	5.14	0.0588	0.61
20160706_G1_g38		55	260	2.7E-06	6.5E-04	4.8E-05	1.5E-04	5.5E-03	1.1E-02	306	4	0.7327	4.62	0.0908	4.53	0.49	0.0588	0.67	0.6136	6.01	0.0286	3.82	11.017	4.53	0.0588	0.67
20160706_G1_g144		49	162	2.8E-06	2.9E-04	2.1E-05	7.7E-05	2.4E-03	4.4E-03	#DIV/0!	#DIV/0!	0.7354	19.72	0.0895	19.41	0.49	0.0590	1.62	0.6784	15.26	0.0256	24.73	11.170	19.41	0.0590	1.62
20160706_G1_g60		57	265	2.8E-06	9.4E-04	6.9E-05	3.7E-04	1.4E-02	1.6E-02	200	13	0.7362	3.01	0.0897	3.11	0.52	0.0594	0.82	0.6217	18.04	0.0280	3.48	11.153	3.11	0.0594	0.82
20160706_G1_g117		47	268	2.6E-06	3.3E-04	2.6E-05	9.4E-05	2.8E-03	5.3E-03	210	1	0.7375	8.56	0.0882	8.11	0.47	0.0613	1.35	0.8387	14.31	0.0307	7.54	11.337	8.11	0.0613	1.35

20160707_G1_g166		55	213	2.5E-06	1.0E-03	7.5E-05	4.9E-04	1.7E-02	1.6E-02	628	10	0.7381	9.98	0.0910	9.92	0.50	0.0588	0.76	1.3523	9.43	0.0258	12.25	10.988	9.92	0.0588	0.76
20160707_G1_g154		56	258	2.7E-06	3.0E-04	2.2E-05	3.3E-05	1.2E-03	5.2E-03	156	4	0.7388	3.75	0.0904	3.68	0.49	0.0592	1.05	0.3295	2.77	0.0274	3.63	11.061	3.68	0.0592	1.05
20160707_G1_g195		65	230	2.4E-06	2.9E-04	2.2E-05	7.2E-05	2.7E-03	5.0E-03	154	5	0.7465	4.18	0.0890	4.04	0.48	0.0604	1.51	0.7464	5.19	0.0274	3.44	11.232	4.04	0.0604	1.51
20160706_G1_g149		49	235	2.7E-06	3.3E-04	2.6E-05	1.2E-04	3.7E-03	4.9E-03	148	1	0.7647	4.72	0.0947	2.67	0.28	0.0596	1.75	1.1535	1.23	0.0291	3.08	10.555	2.67	0.0596	1.75
20160706_G1_g105		50	208	3.0E-06	1.6E-03	1.2E-04	4.0E-04	1.5E-02	2.9E-02	548	1	0.7686	1.27	0.0939	1.23	0.49	0.0595	0.61	0.7392	2.61	0.0318	2.18	10.645	1.23	0.0595	0.61
20160706_G1_g102		52	187	2.9E-06	3.1E-04	2.3E-05	8.3E-05	3.2E-03	5.4E-03	183	6	0.7782	6.36	0.0949	6.41	0.50	0.0593	1.43	0.7997	6.74	0.0277	6.23	10.538	6.41	0.0593	1.43
20160706_G1_g209		52	222	2.7E-06	1.8E-03	1.3E-04	3.0E-04	7.4E-03	2.0E-02	477	1	0.7930	1.96	0.0970	1.85	0.47	0.0593	0.54	0.5363	2.94	0.0305	1.90	10.308	1.85	0.0593	0.54
20160706_G1_g13		52	241	3.1E-06	3.6E-03	2.7E-04	9.2E-04	3.0E-02	5.5E-02	1448	3	0.8058	5.28	0.0982	5.35	0.51	0.0594	0.32	0.7240	5.91	0.0301	5.98	10.181	5.35	0.0594	0.32
20160707_G1_g178		40	184	2.2E-06	2.5E-03	1.9E-04	4.9E-04	1.6E-02	4.1E-02	910	10	0.8184	3.04	0.0973	2.93	0.48	0.0609	0.68	0.5878	13.07	0.0333	3.18	10.281	2.93	0.0609	0.68
20160707_G1_g111		65	212	2.3E-06	9.6E-04	7.2E-05	6.6E-05	2.4E-03	1.5E-02	617	7	0.8241	10.76	0.1012	10.26	0.48	0.0591	1.01	0.2135	4.50	0.0310	8.66	9.885	10.26	0.0591	1.01
20160707_G1_g192		50	195	2.7E-06	3.9E-04	3.0E-05	3.0E-04	9.0E-03	5.8E-03	26	120	0.8259	10.49	0.0985	9.94	0.47	0.0609	1.49	2.1946	8.99	0.0268	15.38	10.153	9.94	0.0609	1.49
20160706_G1_g104K		56	228	2.5E-06	1.5E-03	1.1E-04	2.6E-04	9.4E-03	2.5E-02	678	2	0.8350	3.58	0.0997	3.52	0.49	0.0606	0.72	0.5376	16.59	0.0305	2.86	10.030	3.52	0.0606	0.72
20160706_G1_g210		49	206	2.7E-06	1.1E-03	8.5E-05	2.7E-04	8.7E-03	1.7E-02	902	9	0.8624	10.34	0.1062	10.13	0.49	0.0592	0.89	0.7030	4.51	0.0323	13.87	9.416	10.13	0.0592	0.89
20160706_G1_g14		56	201	3.0E-06	3.2E-03	2.4E-04	7.4E-04	2.4E-02	4.7E-02	1049	8	0.8648	11.29	0.1059	10.95	0.48	0.0593	0.63	0.7437	7.30	0.0311	11.10	9.444	10.95	0.0593	0.63
20160706_G1_g11		51	252	3.4E-06	9.2E-04	6.9E-05	9.6E-05	3.4E-03	1.7E-02	378	8	0.8790	5.70	0.1049	5.07	0.44	0.0604	1.13	0.5229	11.01	0.0336	3.75	9.534	5.07	0.0604	1.13
20160707_G1_g91		55	240	2.6E-06	1.1E-03	8.7E-05	1.7E-04	5.4E-03	1.6E-02	340	17	0.8820	5.53	0.1048	5.48	0.50	0.0610	0.59	0.6482	8.38	0.0307	6.03	9.541	5.48	0.0610	0.59
20160706_G1_g54		54	223	2.8E-06	3.7E-03	2.8E-04	1.0E-03	3.5E-02	5.4E-02	2114	7	0.8871	6.44	0.1080	6.35	0.49	0.0596	0.39	0.8294	4.85	0.0316	6.74	9.262	6.35	0.0596	0.39
20160706_G1_g172		88	252	3.0E-06	2.5E-04	1.9E-05	9.1E-05	3.3E-03	4.0E-03	140	5	0.8928	8.09	0.1086	7.98	0.49	0.0595	2.61	1.0339	8.72	0.0317	10.70	9.211	7.98	0.0595	2.61
20160707_G1_g125		59	215	2.8E-06	6.4E-04	4.9E-05	1.4E-04	4.6E-03	9.4E-03	203	2	0.9067	7.08	0.1065	8.01	0.57	0.0611	0.95	0.9207	15.57	0.0308	10.06	9.388	8.01	0.0611	0.95
20160706_G1_g50R		55	233	2.4E-06	2.3E-03	1.8E-04	1.1E-04	4.0E-03	3.5E-02	1048	4	0.9262	4.16	0.1089	3.95	0.47	0.0619	0.46	0.0868	31.37	0.0318	7.55	9.185	3.95	0.0619	0.46
20160706_G1_g20		54	193	3.2E-06	3.9E-04	2.9E-05	1.8E-04	5.8E-03	5.3E-03	114	7	0.9302	7.52	0.1094	7.49	0.50	0.0613	1.45	1.9441	14.75	0.0342	5.67	9.142	7.49	0.0613	1.45
20160707_G1_g174		56	248	2.5E-06	2.9E-03	2.2E-04	5.3E-04	1.5E-02	4.0E-02	1695	6	0.9441	4.75	0.1121	4.15	0.44	0.0607	1.02	0.5106	11.33	0.0340	9.32	8.922	4.15	0.0607	1.02
20160706_G1_g24		58	264	2.7E-06	7.2E-04	5.6E-05	1.7E-04	5.4E-03	1.0E-02	327	8	0.9639	6.23	0.1120	6.03	0.48	0.0626	0.73	0.7014	7.85	0.0331	9.30	8.928	6.03	0.0626	0.73
20160706_G1_g42		52	126	2.9E-06	3.0E-03	2.5E-04	7.3E-06	1.9E-04	3.4E-02	881	22	1.0793	41.04	0.1236	35.08	0.43	0.0639	3.74	0.0066	29.00	0.0430	35.51	8.091	35.08	0.0639	3.74
20160706_G1_g100		57	183	2.9E-06	1.0E-03	7.9E-05	7.5E-05	2.1E-03	1.5E-02	413	14	1.1107	7.96	0.1233	6.41	0.40	0.0659	3.34	0.3368	22.35	0.0403	5.74	8.108	6.41	0.0659	3.34
20160706_G1_g168		53	253	9.4E-06	2.0E-03	2.3E-04	3.3E-04	5.0E-03	4.1E-02	407	21	1.1440	32.72	0.0831	6.76	0.10	0.0952	21.87	0.4875	38.29	0.0877	72.72	12.031	6.76	0.0952	21.87
20160707_G1_g51		69	245	2.6E-06	8.1E-04	6.9E-05	1.0E-04	2.5E-03	9.2E-03	330	5	1.2664	6.85	0.1375	6.69	0.49	0.0668	0.64	0.2945	13.50	0.0391	7.69	7.270	6.69	0.0668	0.64
~~20160706_G1_g173~~		~~55~~	~~186~~	~~2.5E-06~~	~~3.0E-03~~	~~3.5E-04~~	~~4.2E-04~~	~~1.0E-02~~	~~3.8E-02~~	~~1017~~	~~16~~	~~1.3325~~	~~28.86~~	~~0.1134~~	~~20.41~~	~~0.35~~	~~0.0893~~	~~7.83~~	~~0.3692~~	~~15.58~~	~~0.0434~~	~~14.87~~	~~8.817~~	~~20.41~~	~~0.0893~~	~~7.83~~
20160707_G1_g52		56	262	2.4E-06	5.7E-04	5.3E-05	2.4E-04	4.9E-03	5.6E-03	251	6	1.3681	10.52	0.1381	9.36	0.44	0.0723	0.83	1.1295	6.38	0.0401	9.54	7.241	9.36	0.0723	0.83
~~20160706_G1_g151~~		~~58~~	~~125~~	~~3.0E-06~~	~~2.0E-03~~	~~1.9E-04~~	~~5.0E-04~~	~~1.0E-02~~	~~1.9E-02~~	~~1107~~	~~19~~	~~1.6129~~	~~19.48~~	~~0.1632~~	~~16.64~~	~~0.43~~	~~0.0715~~	~~3.84~~	~~0.7667~~	~~17.20~~	~~0.0518~~	~~7.68~~	~~6.127~~	~~16.64~~	~~0.0715~~	~~3.84~~
~~20160707_G1_g171~~		~~53~~	~~233~~	~~5.3E-06~~	~~8.8E-04~~	~~9.6E-05~~	~~1.7E-04~~	~~2.8E-03~~	~~1.1E-02~~	~~315~~	~~11~~	~~1.6193~~	~~29.17~~	~~0.1274~~	~~8.71~~	~~0.15~~	~~0.0757~~	~~13.89~~	~~0.4256~~	~~24.36~~	~~0.0609~~	~~32.16~~	~~7.851~~	~~8.71~~	~~0.0757~~	~~13.89~~
20160706_G1_g7		45	161	3.0E-06	4.5E-04	4.0E-05	8.9E-05	1.9E-03	4.4E-03	225	10	1.6260	7.99	0.1648	8.24	0.52	0.0719	1.72	0.6559	5.03	0.0486	8.68	6.066	8.24	0.0719	1.72
20160706_G1_g26		46	220	3.2E-06	7.5E-04	7.0E-05	1.3E-04	2.9E-03	7.5E-03	344	4	1.7334	2.41	0.1682	2.32	0.48	0.0742	0.80	0.5377	4.30	0.0534	2.91	5.947	2.32	0.0742	0.80
20160707_G1_g137		58	228	2.6E-06	2.4E-03	3.7E-04	5.2E-04	5.3E-03	1.0E-02	1123	6	5.9591	6.67	0.3566	6.58	0.49	0.1212	0.39	0.6205	3.90	0.0954	6.01	2.805	6.58	0.1212	0.39
20160706_G1_g48		50	188	2.7E-06	3.5E-03	5.5E-04	1.7E-04	1.8E-03	1.5E-02	3407	4	6.4854	6.98	0.3727	7.11	0.51	0.1262	0.57	0.3088	33.47	0.1106	7.49	2.683	7.11	0.1262	0.57
20160706_G1_g3		45	151	2.9E-06	2.1E-03	5.3E-04	2.1E-04	2.0E-03	8.9E-03	666	10	9.4082	23.45	0.3375	18.26	0.39	0.2057	4.20	0.3535	47.23	0.0987	16.78	2.963	18.26	0.2057	4.20
20160706_G1_g31		48	230	3.0E-06	7.3E-03	1.5E-03	7.6E-04	6.2E-03	2.4E-02	2335	11	10.1950	6.52	0.4506	6.07	0.47	0.1630	1.19	0.3731	5.71	0.1259	6.23	2.219	6.07	0.1630	1.19
20160707_G1_g188		47	229	4.8E-06	4.8E-03	1.0E-03	9.6E-04	7.4E-03	1.7E-02	970	7	10.8696	6.10	0.4561	5.74	0.47	0.1715	1.15	0.6740	3.49	0.1245	6.49	2.192	5.74	0.1715	1.15
20160706_G1_g205		53	138	3.1E-06	4.9E-03	9.6E-04	1.1E-03	9.5E-03	1.7E-02	1661	25	11.5304	10.61	0.5150	8.82	0.42	0.1623	3.76	0.8044	20.46	0.1324	9.79	1.942	8.82	0.1623	3.76
20160706_G1_g46		48	258	3.3E-06	8.0E-03	2.0E-03	1.3E-03	1.3E-02	3.5E-02	5625	2	12.7457	12.45	0.4260	11.09	0.45	0.2076	1.97	0.5738	3.94	0.1234	10.38	2.348	11.09	0.2076	1.97
20160707_G1_g202		57	146	2.5E-06	7.8E-03	1.7E-03	1.4E-03	1.1E-02	2.5E-02	4526	37	12.9227	9.01	0.5208	10.13	0.56	0.1733	2.64	0.6306	26.49	0.1382	8.67	1.920	10.13	0.1733	2.64
20160706_G1_g146		56	211	2.8E-06	2.8E-03	6.5E-04	5.8E-04	4.3E-03	8.3E-03	1826	8	15.5290	6.45	0.5603	4.26	0.33	0.2014	5.13	0.8516	19.61	0.1509	5.59	1.785	4.26	0.2014	5.13
20160706_G1_g59		53	235	2.5E-06	8.9E-03	2.4E-03	1.1E-03	7.6E-03	2.4E-02	3639	7	16.0938	7.68	0.5376	6.86	0.45	0.2174	1.37	0.2242	17.70	0.1404	7.06	1.860	6.86	0.2174	1.37
20160706_G1_g101		40	120	2.8E-06	#DIV/0!	#DIV/0!	#DIV/0!	4.4E-03	2.1E-02	#DIV/0!	#DIV/0!	#DIV/0!	#DIV/0!	#DIV/0!	#DIV/0!	#DIV/0!	#DIV/0!	#DIV/0!	#DIV/0!	#DIV/0!	#DIV/0!	#DIV/0!	#DIV/0!	#DIV/0!	#DIV/0!	#DIV/0!

18.2.4 *Metasandstone of the Präbichl Formation (L1)*

Table 6: Those tables depict the measured values of the zircons of the Präbichl metasandstone, corrected with the EXCEL sheet LamTool U – Th – Pb VI of Košler und Klötzli (unpubl.). M257 (Nasdala et al., 2008), 91500 (Wiedenbeck et al., 1995) and Plešovice (Sláma et al., 2008) are the used standard samples. The crossed out measurements are discordant and were excluded of further steps.

File name	std.	start	end	204Pb	206Pb	207Pb	208Pb	232Th	238U	206Pb/204Pb	2RSE (%)	207Pb/235U	2RSE (%)	206Pb/238U	2RSE (%)	Rho	207Pb/206Pb	2RSE (%)	208Pb/206Pb	2RSE (%)	208Pb/232Th	2RSE (%)	238U/206Pb	2RSE (%)	207Pb/206Pb	2RSE (%)
20160829_M257_001		60	200	#DIV/0!	3.1E-03	2.4E-04	3.2E-04	1.4E-02	5.8E-02	#DIV/0!	#DIV/0!	0.7393	4.67	0.0917	4.69	0.50	0.0587	0.42	0.2602	0.41	0.0285	4.62	10.909	4.69	0.0587	0.42
20160829_M257_002		60	200	2.8E-06	3.1E-03	2.4E-04	3.2E-04	1.4E-02	5.8E-02	1189	0	0.7355	4.84	0.0914	4.89	0.51	0.0583	0.46	0.2608	0.45	0.0283	4.47	10.938	4.89	0.0583	0.46
20160829_M257_003		59	200	2.2E-06	3.0E-03	2.3E-04	3.1E-04	1.4E-02	5.7E-02	1588	2	0.7281	4.41	0.0904	4.53	0.51	0.0583	0.46	0.2723	0.46	0.0269	3.65	11.060	4.53	0.0583	0.46
20160829_M257_004		59	200	#DIV/0!	3.1E-03	2.4E-04	3.1E-04	1.4E-02	5.7E-02	#DIV/0!	#DIV/0!	0.7307	4.27	0.0917	4.29	0.50	0.0581	0.52	0.2719	0.44	0.0271	3.63	10.907	4.29	0.0581	0.52
20160829_M257_005		57	202	2.2E-06	2.9E-03	2.2E-04	3.0E-04	1.3E-02	5.5E-02	1383	2	0.7080	4.16	0.0882	4.18	0.50	0.0585	0.46	0.2858	0.37	0.0268	3.57	11.337	4.18	0.0585	0.46
20160829_M257_006		57	202	#DIV/0!	2.9E-03	2.2E-04	3.0E-04	1.3E-02	5.6E-02	#DIV/0!	#DIV/0!	0.7087	3.90	0.0889	3.74	0.48	0.0581	0.51	0.2846	0.48	0.0268	3.60	11.246	3.74	0.0581	0.51
20160829_M257_007		58	207	#DIV/0!	2.8E-03	2.2E-04	2.9E-04	1.2E-02	5.3E-02	#DIV/0!	#DIV/0!	0.7221	4.63	0.0903	4.66	0.50	0.0583	0.44	0.2886	0.43	0.0280	4.30	11.072	4.66	0.0583	0.44
20160829_M257_008		59	203	#DIV/0!	2.8E-03	2.2E-04	2.9E-04	1.3E-02	5.4E-02	#DIV/0!	#DIV/0!	0.7227	4.80	0.0903	4.76	0.50	0.0581	0.48	0.2875	0.45	0.0280	4.63	11.072	4.76	0.0581	0.48
20160829_M257_009		57	202	2.2E-06	3.0E-03	2.3E-04	3.1E-04	1.5E-02	6.0E-02	1453	1	0.7056	3.60	0.0879	3.65	0.51	0.0583	0.47	0.2849	0.42	0.0281	2.03	11.372	3.65	0.0583	0.47
20160829_M257_009		59	202	2.2E-06	3.0E-03	2.3E-04	3.1E-04	1.4E-02	6.0E-02	1455	1	0.7050	3.86	0.0884	3.86	0.50	0.0581	0.46	0.2845	0.44	0.0277	2.16	11.314	3.86	0.0581	0.46
20160829_M257_010		55	206	#DIV/0!	3.0E-03	2.3E-04	3.1E-04	1.5E-02	6.1E-02	#DIV/0!	#DIV/0!	0.7089	3.03	0.0888	2.95	0.49	0.0580	0.46	0.2829	0.40	0.0284	1.80	11.257	2.95	0.0580	0.46
20160829_M257_010		56	202	#DIV/0!	3.0E-03	2.3E-04	3.1E-04	1.5E-02	6.1E-02	#DIV/0!	#DIV/0!	0.7028	3.35	0.0884	3.28	0.49	0.0580	0.47	0.2830	0.38	0.0278	1.89	11.310	3.28	0.0580	0.47
20160829_M257_011		55	210	8.3E-06	2.8E-03	2.2E-04	2.8E-04	1.2E-02	5.1E-02	461	5	0.7055	4.98	0.0884	5.05	0.51	0.0580	0.45	0.2788	0.39	0.0267	5.01	11.306	5.05	0.0580	0.45
20160829_M257_012		58	210	6.5E-06	2.8E-03	2.1E-04	2.8E-04	1.2E-02	5.1E-02	-1392	-5	0.7184	4.67	0.0902	4.69	0.50	0.0580	0.56	0.2779	0.53	0.0271	4.84	11.084	4.69	0.0580	0.56
20160829_M257_013		58	206	5.1E-06	2.6E-03	2.0E-04	2.7E-04	1.2E-02	4.9E-02	577	3	0.7289	3.78	0.0912	3.66	0.48	0.0581	0.52	0.2755	0.46	0.0268	4.14	10.961	3.66	0.0581	0.52
20160829_M257_014		59	207	4.5E-06	2.6E-03	2.0E-04	2.6E-04	1.2E-02	4.8E-02	796	1	0.7454	3.25	0.0933	3.33	0.51	0.0581	0.47	0.2753	0.50	0.0274	3.59	10.717	3.33	0.0581	0.47
20160829_M257_015		60	202	#DIV/0!	2.7E-03	2.1E-04	2.7E-04	1.1E-02	4.8E-02	#DIV/0!	#DIV/0!	0.8234	5.65	0.1022	5.68	0.50	0.0585	0.45	0.2713	0.52	0.0319	5.78	9.780	5.68	0.0585	0.45
20160829_M257_016		57	206	3.0E-06	2.7E-03	2.1E-04	2.7E-04	1.1E-02	4.8E-02	998	1	0.8315	4.62	0.1034	4.70	0.51	0.0586	0.62	0.2696	0.44	0.0322	4.97	9.673	4.70	0.0586	0.62

File name	std.	start	end	204Pb	206Pb	207Pb	208Pb	232Th	238U	206Pb/204Pb	2RSE (%)	207Pb/235U	2RSE (%)	206Pb/238U	2RSE (%)	Rho	207Pb/206Pb	2RSE (%)	208Pb/206Pb	2RSE (%)	208Pb/232Th	2RSE (%)	238U/206Pb	2RSE (%)	207Pb/206Pb	2RSE (%)
20160829_91500_g4_001		60	170	2.5E-06	5.7E-04	5.8E-05	7.7E-05	1.8E-03	5.6E-03	273	2	1.8869	5.66	0.1800	5.70	0.50	0.0759	1.10	0.3372	1.15	0.0564	5.00	5.555	5.70	0.0759	1.10
20160829_91500_g4_002		60	170	2.5E-06	5.8E-04	5.8E-05	7.8E-05	1.7E-03	5.6E-03	266	1	1.9171	5.32	0.1821	5.34	0.50	0.0758	1.10	0.3361	1.05	0.0568	5.47	5.491	5.34	0.0758	1.10
20160829_91500_g4_003		57	199	3.1E-06	6.0E-04	6.0E-05	8.0E-05	1.8E-03	5.8E-03	#DIV/0!	#DIV/0!	1.8666	3.49	0.1798	3.69	0.53	0.0755	0.80	0.3511	0.74	0.0540	2.99	5.562	3.69	0.0755	0.80
20160829_91500_g4_004		62	202	#DIV/0!	6.0E-04	6.1E-05	8.0E-05	1.8E-03	5.8E-03	#DIV/0!	#DIV/0!	1.8811	4.00	0.1814	3.83	0.48	0.0754	0.79	0.3534	0.81	0.0541	3.67	5.512	3.83	0.0754	0.79
20160829_91500_g4_005		57	213	#DIV/0!	5.6E-04	5.7E-05	7.6E-05	1.7E-03	5.5E-03	#DIV/0!	#DIV/0!	1.8124	3.34	0.1756	3.16	0.47	0.0750	0.73	0.3699	0.73	0.0535	3.14	5.696	3.16	0.0750	0.73
20160829_91500_g4_006		56	209	#DIV/0!	5.7E-04	5.7E-05	7.7E-05	1.8E-03	5.7E-03	#DIV/0!	#DIV/0!	1.8158	3.17	0.1747	3.13	0.49	0.0757	0.79	0.3715	0.63	0.0529	3.37	5.726	3.13	0.0757	0.79
20160829_91500_g4_007		58	208	#DIV/0!	5.6E-04	5.7E-05	7.5E-05	1.7E-03	5.4E-03	#DIV/0!	#DIV/0!	1.8245	4.33	0.1764	4.19	0.48	0.0753	0.78	0.3737	0.74	0.0537	4.37	5.670	4.19	0.0753	0.78
20160829_91500_g4_008		55	216	2.2E-06	5.7E-04	5.7E-05	7.6E-05	1.7E-03	5.5E-03	280	5	1.8392	3.87	0.1770	3.79	0.49	0.0757	0.80	0.3774	0.71	0.0544	4.20	5.649	3.79	0.0757	0.80
20160829_91500_g4_009		59	200	2.7E-06	5.7E-04	5.7E-05	7.6E-05	1.8E-03	5.6E-03	#DIV/0!	#DIV/0!	1.8324	4.53	0.1757	4.79	0.53	0.0758	0.92	0.3723	0.93	0.0546	5.21	5.692	4.79	0.0758	0.92
20160829_91500_g4_009		57	204	2.7E-06	5.7E-04	5.7E-05	7.6E-05	1.8E-03	5.6E-03	#DIV/0!	#DIV/0!	1.8464	4.34	0.1779	4.53	0.52	0.0756	0.86	0.3713	0.90	0.0548	4.74	5.621	4.53	0.0756	0.86
20160829_91500_g4_010		55	200	#DIV/0!	5.7E-04	5.7E-05	7.6E-05	1.8E-03	5.6E-03	#DIV/0!	#DIV/0!	1.8220	4.15	0.1759	4.05	0.49	0.0754	0.88	0.3714	0.70	0.0554	3.86	5.684	4.05	0.0754	0.88
20160829_91500_g4_010		55	207	#DIV/0!	5.6E-04	5.6E-05	7.5E-05	1.7E-03	5.6E-03	#DIV/0!	#DIV/0!	1.8330	4.07	0.1776	3.96	0.49	0.0753	0.84	0.3705	0.73	0.0551	3.89	5.630	3.96	0.0753	0.84
20160829_91500_g4_011		58	201	#DIV/0!	6.1E-04	6.0E-05	7.9E-05	1.8E-03	5.8E-03	#DIV/0!	#DIV/0!	1.8520	2.91	0.1793	2.88	0.49	0.0752	0.84	0.3617	0.81	0.0548	3.08	5.577	2.88	0.0752	0.84
20160829_91500_g4_012		56	204	5.9E-06	6.0E-04	6.0E-05	7.9E-05	1.8E-03	5.7E-03	#DIV/0!	#DIV/0!	1.8474	2.76	0.1803	2.46	0.44	0.0748	0.77	0.3618	0.81	0.0553	2.16	5.545	2.46	0.0748	0.77
20160829_91500_g4_013		56	200	5.8E-06	5.7E-04	5.7E-05	7.4E-05	1.7E-03	5.3E-03	119	4	1.8945	3.22	0.1821	3.53	0.55	0.0755	0.96	0.3607	0.89	0.0552	4.15	5.491	3.53	0.0755	0.96
20160829_91500_g4_014		57	199	#DIV/0!	5.7E-04	5.6E-05	7.4E-05	1.6E-03	5.3E-03	#DIV/0!	#DIV/0!	1.8686	4.16	0.1806	4.05	0.49	0.0753	0.81	0.3607	0.89	0.0548	4.95	5.536	4.05	0.0753	0.81
20160829_91500_g4_015		56	197	#DIV/0!	5.6E-04	5.5E-05	7.2E-05	1.6E-03	5.2E-03	#DIV/0!	#DIV/0!	2.0373	4.12	0.1957	4.24	0.51	0.0758	0.79	0.3538	0.80	0.0614	3.80	5.110	4.24	0.0758	0.79
20160829_91500_g4_016		61	199	#DIV/0!	5.6E-04	5.5E-05	7.3E-05	1.6E-03	5.2E-03	#DIV/0!	#DIV/0!	2.0714	4.52	0.1990	4.59	0.51	0.0755	0.97	0.3560	0.95	0.0625	3.97	5.026	4.59	0.0755	0.97

File name	std.	start	end	204Pb	206Pb	207Pb	208Pb	232Th	238U	206Pb/204Pb	2RSE (%)	207Pb/235U	2RSE (%)	206Pb/238U	2RSE (%)	Rho	207Pb/206Pb	2RSE (%)	208Pb/206Pb	2RSE (%)	208Pb/232Th	2RSE (%)	238U/206Pb	2RSE (%)	207Pb/206Pb	2RSE (%)
20160829_ples06_001		58	200	2.0E-06	1.6E-03	1.1E-04	6.4E-03	4.8E-03	5.2E-02	832	2	0.3908	3.84	0.0524	4.04	0.53	0.0541	0.65	0.0995	1.22	0.0171	3.72	19.098	4.04	0.0541	0.65
20160829_ples06_002		56	200	3.0E-06	1.6E-03	1.2E-04	7.8E-05	5.0E-03	5.4E-02	739	4	0.4011	4.72	0.0525	3.93	0.42	0.0548	2.56	0.1088	11.14	0.0189	11.17	19.041	3.93	0.0548	2.56
20160829_ples06_003	*	58	203	#DIV/0!	1.7E-03	1.2E-04	7.0E-05	5.2E-03	5.4E-02	#DIV/0!	#DIV/0!	0.3941	3.84	0.0535	3.85	0.50	0.0534	0.64	0.1034	1.14	0.0171	3.79	18.677	3.85	0.0534	0.64
20160829_ples06_004	*	58	152	#DIV/0!	1.8E-03	1.3E-04	7.5E-05	5.6E-03	5.8E-02	#DIV/0!	#DIV/0!	0.3886	8.18	0.0530	7.91	0.48	0.0533	1.20	0.1048	1.73	0.0176	4.31	18.885	7.91	0.0533	1.20
20160829_ples06_005	*	58	200	1.9E-06	1.5E-03	1.0E-04	5.6E-05	4.2E-03	4.7E-02	768	1	0.3892	4.85	0.0529	4.77	0.49	0.0532	0.63	0.0949	1.26	0.0166	5.23	18.905	4.77	0.0532	0.63
20160829_ples06_006	*	53	202	#DIV/0!	1.5E-03	1.1E-04	5.7E-05	4.1E-03	4.7E-02	#DIV/0!	#DIV/0!	0.3999	3.70	0.0546	3.80	0.51	0.0532	0.61	0.0982	1.15	0.0168	3.80	18.307	3.80	0.0532	0.61
20160829_ples06_007	*	57	208	2.5E-06	1.5E-03	1.1E-04	5.6E-05	4.0E-03	4.6E-02	847	1	0.4031	3.79	0.0555	3.59	0.47	0.0528	0.63	0.0975	1.19	0.0169	3.39	18.023	3.59	0.0528	0.63
20160829_ples06_008	*	57	201	2.7E-06	1.5E-03	1.0E-04	5.5E-05	4.0E-03	4.6E-02	621	0	0.4042	3.86	0.0553	3.87	0.50	0.0529	0.64	0.0968	1.41	0.0170	3.50	18.076	3.87	0.0529	0.64
20160829_ples06_009	*	57	211	#DIV/0!	1.4E-03	9.9E-05	5.3E-05	3.7E-03	4.5E-02	#DIV/0!	#DIV/0!	0.3828	4.86	0.0518	5.01	0.52	0.0535	0.62	0.1030	1.21	0.0165	4.82	19.315	5.01	0.0535	0.62
20160829_ples06_010	*	59	202	2.7E-06	1.4E-03	9.9E-05	5.2E-05	3.8E-03	4.6E-02	#DIV/0!	#DIV/0!	0.3825	4.48	0.0520	4.64	0.52	0.0534	0.65	0.0995	1.62	0.0163	4.63	19.226	4.64	0.0534	0.65
20160829_ples06_011	*	59	207	1.9E-06	1.4E-03	9.8E-05	5.1E-05	3.7E-03	4.5E-02	813	1	0.3888	4.11	0.0531	4.19	0.51	0.0531	0.66	0.0995	1.59	0.0166	4.34	18.837	4.19	0.0531	0.66
20160829_ples06_012	*	54	208	#DIV/0!	1.4E-03	9.9E-05	5.1E-05	3.7E-03	4.5E-02	#DIV/0!	#DIV/0!	0.3888	3.52	0.0532	3.43	0.49	0.0530	0.55	0.0994	1.33	0.0168	3.47	18.800	3.43	0.0530	0.55
20160829_ples06_013	*	57	208	#DIV/0!	1.4E-03	1.0E-04	5.2E-05	3.6E-03	4.4E-02	#DIV/0!	#DIV/0!	0.3949	4.47	0.0541	4.59	0.51	0.0531	0.69	0.1012	1.44	0.0173	4.53	18.476	4.59	0.0531	0.69
20160829_ples06_014	*	55	208	#DIV/0!	1.4E-03	1.0E-04	5.1E-05	3.5E-03	4.3E-02	#DIV/0!	#DIV/0!	0.4023	4.05	0.0546	4.10	0.51	0.0533	0.66	0.1020	1.53	0.0175	4.40	18.304	4.10	0.0533	0.66
20160829_ples06_015	*	58	206	#DIV/0!	1.4E-03	9.9E-05	5.1E-05	3.4E-03	4.3E-02	#DIV/0!	#DIV/0!	0.4051	4.39	0.0550	4.51	0.51	0.0534	0.78	0.1017	2.15	0.0178	5.17	18.184	4.51	0.0534	0.78
20160829_ples06_016	*	59	206	#DIV/0!	1.3E-03	9.4E-05	4.8E-05	3.6E-03	4.5E-02	#DIV/0!	#DIV/0!	0.3852	3.62	0.0523	3.76	0.52	0.0533	0.73	0.1011	1.32	0.0172	2.82	19.109	3.76	0.0533	0.73
20160829_ples06_016	*	54	200	#DIV/0!	1.4E-03	9.6E-05	4.9E-05	3.7E-03	4.6E-02	#DIV/0!	#DIV/0!	0.3949	3.52	0.0538	3.79	0.54	0.0533	0.72	0.1004	1.29	0.0177	2.65	18.600	3.79	0.0533	0.72
20160829_ples06_017	*	57	208	#DIV/0!	1.3E-03	9.4E-05	4.8E-05	3.6E-03	4.4E-02	#DIV/0!	#DIV/0!	0.3869	3.14	0.0526	3.30	0.53	0.0534	0.77	0.1007	1.52	0.0172	2.98	19.016	3.30	0.0534	0.77
20160829_ples06_017	*	56	200	#DIV/0!	1.3E-03	9.5E-05	4.9E-05	3.7E-03	4.5E-02	#DIV/0!	#DIV/0!	0.3953	3.48	0.0538	3.71	0.53	0.0533	0.79	0.1001	1.58	0.0177	3.00	18.584	3.71	0.0533	0.79
20160829_ples06_018	*	57	202	2.5E-06	1.3E-03	9.4E-05	4.9E-05	3.6E-03	4.4E-02	#DIV/0!	#DIV/0!	0.3883	3.50	0.0529	3.31	0.47	0.0530	0.89	0.1001	2.37	0.0172	3.95	18.899	3.31	0.0530	0.89
20160829_ples06_018	*	57	213	2.5E-06	1.3E-03	9.3E-05	4.8E-05	3.5E-03	4.4E-02	#DIV/0!	#DIV/0!	0.3963	3.36	0.0543	3.16	0.47	0.0530	0.83	0.0995	2.19	0.0175	3.49	18.410	3.16	0.0530	0.83
20160829_ples06_019	*	65	206	9.5E-05	1.4E-03	1.0E-04	5.1E-05	3.9E-03	4.5E-02	13	7	0.4010	5.41	0.0541	5.82	0.54	0.0536	0.84	0.0994	1.64	0.0168	6.45	18.479	5.82	0.0536	0.84
20160829_ples06_019	*	55	200	1.2E-04	1.5E-03	1.0E-04	5.3E-05	4.0E-03	4.7E-02	6751	3	0.3917	4.51	0.0527	5.01	0.56	0.0537	0.76	0.1006	1.56	0.0162	5.00	18.975	5.01	0.0537	0.76
20160829_ples06_020	*	69	214	#DIV/0!	1.3E-03	9.5E-05	4.8E-05	3.6E-03	4.2E-02	#DIV/0!	#DIV/0!	0.4014	6.52	0.0552	6.51	0.50	0.0527	0.83	0.0968	2.21	0.0166	8.36	18.102	6.51	0.0527	0.83
20160829_ples06_020	*	57	204	#DIV/0!	1.4E-03	9.8E-05	5.0E-05	3.8E-03	4.4E-02	#DIV/0!	#DIV/0!	0.3926	4.71	0.0535	4.97	0.53	0.0529	0.90	0.0987	2.27	0.0158	6.22	18.695	4.97	0.0529	0.90
20160829_ples06_021	*	52	160	1.2E-05	1.5E-03	1.1E-04	5.8E-05	4.5E-03	5.0E-02	144	12	0.3897	6.56	0.0536	6.47	0.49	0.0531	1.29	0.1002	3.96	0.0163	9.86	18.670	6.47	0.0531	1.29
20160829_ples06_021	*	54	160	1.2E-05	1.5E-03	1.1E-04	5.8E-05	4.5E-03	5.0E-02	241	13	0.3826	7.25	0.0526	7.02	0.48	0.0531	1.35	0.1010	4.14	0.0155	10.57	19.020	7.02	0.0531	1.35
20160829_ples06_022	*	55	205	4.8E-06	1.4E-03	1.0E-04	5.2E-05	3.5E-03	4.3E-02	169	20	0.3972	4.92	0.0543	5.07	0.52	0.0532	0.78	0.1004	1.77	0.0172	5.38	18.400	5.07	0.0532	0.78
20160829_ples06_023	*	55	208	5.8E-06	1.4E-03	9.8E-05	5.1E-05	3.4E-03	4.2E-02	326	4	0.3982	4.47	0.0547	4.62	0.52	0.0529	0.65	0.0996	1.39	0.0173	4.87	18.289	4.62	0.0529	0.65
20160829_ples06_024	*	55	204	6.4E-06	1.4E-03	9.8E-05	5.1E-05	3.4E-03	4.2E-02	219	8	0.3990	4.39	0.0548	4.49	0.51	0.0528	0.70	0.0984	1.79	0.0175	4.26	18.237	4.49	0.0528	0.70
20160829_ples06_025	*	61	213	#DIV/0!	1.4E-03	1.0E-04	5.3E-05	3.8E-03	4.5E-02	#DIV/0!	#DIV/0!	0.3940	4.23	0.0519	4.98	0.59	0.0546	0.97	0.1026	1.98	0.0171	3.87	19.282	4.98	0.0546	0.97
20160829_ples06_026		61	184	4.5E-06	1.4E-03	9.9E-05	5.2E-05	3.6E-03	4.4E-02	339	4	0.3994	4.57	0.0539	5.06	0.55	0.0534	1.53	0.1026	5.11	0.0177	6.31	18.541	5.06	0.0534	1.53
20160829_ples06_027		58	204	#DIV/0!	1.3E-03	9.5E-05	5.0E-05	3.4E-03	4.1E-02	#DIV/0!	#DIV/0!	0.3985	3.97	0.0541	4.03	0.51	0.0535	1.40	0.1033	4.95	0.0180	5.69	18.500	4.03	0.0535	1.40
20160829_ples06_028	*	55	200	5.9E-06	1.4E-03	9.8E-05	5.1E-05	3.6E-03	4.3E-02	#DIV/0!	#DIV/0!	0.3883	4.33	0.0534	4.16	0.48	0.0528	0.68	0.0997	1.45	0.0172	3.28	18.716	4.16	0.0528	0.68
20160829_ples06_029	*	55	205	#DIV/0!	1.4E-03	9.7E-05	5.0E-05	3.6E-03	4.3E-02	#DIV/0!	#DIV/0!	0.3913	4.02	0.0538	3.96	0.49	0.0529	0.73	0.0993	1.48	0.0171	3.94	18.573	3.96	0.0529	0.73
20160829_ples06_030	*	56	209	#DIV/0!	1.4E-03	9.5E-05	4.9E-05	4.0E-03	4.5E-02	#DIV/0!	#DIV/0!	0.3893	3.91	0.0531	4.00	0.51	0.0531	0.60	0.0998	1.39	0.0167	3.60	18.831	4.00	0.0531	0.60
20160829_ples06_031	*	57	203	3.1E-06	1.4E-03	9.5E-05	5.0E-05	4.0E-03	4.5E-02	#DIV/0!	#DIV/0!	0.3935	4.30	0.0536	4.35	0.51	0.0533	0.80	0.0999	1.61	0.0168	3.67	18.664	4.35	0.0533	0.80
20160829_ples06_032	*	62	207	#DIV/0!	1.3E-03	9.3E-05	4.9E-05	4.0E-03	4.5E-02	#DIV/0!	#DIV/0!	0.3986	4.26	0.0544	4.30	0.51	0.0531	0.81	0.1002	1.80	0.0171	3.76	18.366	4.30	0.0531	0.81

File name	std.	start	end	204Pb	206Pb	207Pb	208Pb	232Th	238U	206Pb/204Pb	2RSE (%)	207Pb/235U	2RSE (%)	206Pb/238U	2RSE (%)	Rho	207Pb/206Pb	2RSE (%)	208Pb/206Pb	2RSE (%)	208Pb/232Th	2RSE (%)	238U/206Pb	2RSE (%)	207Pb/206Pb	2RSE (%)
20160829_L1_g40R		58	230	2.6E-06	8.2E-04	5.8E-05	1.9E-04	1.5E-02	2.8E-02	#DIV/0!	#DIV/0!	0.3513	4.83	0.0478	4.88	0.50	0.0535	0.71	0.6408	4.26	0.0149	4.69	20.937	4.88	0.0535	0.71
~~20160829_L1_g12~~		~~57~~	~~240~~	~~5.5E-05~~	~~3.3E-03~~	~~3.0E-04~~	~~2.0E-03~~	~~3.6E-01~~	~~1.6E-01~~	~~177~~	~~45~~	~~0.3588~~	~~8.14~~	~~0.0376~~	~~16.97~~	~~1.04~~	~~0.0748~~	~~10.31~~	~~1.6741~~	~~11.65~~	~~0.0096~~	~~19.37~~	~~26.583~~	~~16.97~~	~~0.0748~~	~~10.31~~
20160829_L1_g30		60	250	2.5E-06	1.2E-03	8.4E-05	2.7E-04	2.1E-02	3.9E-02	644	3	0.3735	4.91	0.0499	5.33	0.54	0.0542	0.67	0.6180	5.80	0.0148	5.52	20.025	5.33	0.0542	0.67
20160829_L1_g80		56	241	2.3E-06	1.4E-03	1.0E-04	2.2E-04	1.9E-02	4.8E-02	1075	1	0.3781	5.58	0.0506	5.72	0.51	0.0545	0.84	0.4748	6.60	0.0148	6.89	19.751	5.72	0.0545	0.84
20160829_L1_g27		59	250	#DIV/0!	9.7E-04	6.9E-05	2.7E-04	1.4E-02	2.1E-02	#DIV/0!	#DIV/0!	0.3841	6.99	0.0524	7.08	0.51	0.0534	0.69	0.8028	4.95	0.0145	8.24	19.082	7.08	0.0534	0.69
20160829_L1_g92		53	222	4.8E-06	4.2E-04	3.0E-05	1.6E-04	1.0E-02	1.2E-02	161	3	0.3958	11.12	0.0536	10.87	0.49	0.0535	1.04	0.8719	9.26	0.0149	17.89	18.662	10.87	0.0535	1.04
20160829_L1_g101		54	208	#DIV/0!	6.7E-04	4.8E-05	1.7E-04	1.3E-02	2.0E-02	#DIV/0!	#DIV/0!	0.4049	5.19	0.0550	4.92	0.47	0.0538	0.90	0.6816	6.28	0.0161	6.13	18.167	4.92	0.0538	0.90
20160829_L1_g19		50	260	1.0E-05	1.4E-03	9.8E-05	3.6E-04	2.4E-02	3.7E-02	277	9	0.4085	4.18	0.0545	4.33	0.52	0.0544	0.53	0.6963	5.44	0.0159	4.22	18.347	4.33	0.0544	0.53
20160829_L1_g70		51	251	8.1E-06	7.0E-04	5.0E-05	1.0E-04	7.1E-03	2.1E-02	517	8	0.4133	4.21	0.0558	4.29	0.51	0.0539	0.73	0.3920	4.16	0.0163	5.31	17.916	4.29	0.0539	0.73
20160829_L1_g41K		59	230	2.7E-06	1.0E-03	7.5E-05	2.8E-04	2.1E-02	3.1E-02	389	2	0.4184	5.29	0.0563	4.51	0.43	0.0544	1.36	0.9060	12.43	0.0171	7.51	17.756	4.51	0.0544	1.36
20160829_L1_g16		60	240	#DIV/0!	7.9E-04	5.8E-05	2.2E-04	1.7E-02	2.4E-02	#DIV/0!	#DIV/0!	0.4207	4.69	0.0559	4.61	0.49	0.0546	0.82	0.5499	11.09	0.0165	6.52	17.894	4.61	0.0546	0.82
20160829_L1_g22		56	140	#DIV/0!	2.4E-04	1.8E-05	3.2E-05	2.5E-03	7.6E-03	#DIV/0!	#DIV/0!	0.4231	11.68	0.0564	7.65	0.33	0.0544	4.09	0.3242	11.50	0.0169	7.23	17.738	7.65	0.0544	4.09
20160829_L1_g65		57	256	2.0E-06	5.7E-04	4.1E-05	1.1E-04	6.6E-03	1.4E-02	333	2	0.4233	6.20	0.0562	5.97	0.48	0.0548	0.85	0.5302	2.96	0.0174	7.21	17.792	5.97	0.0548	0.85
20160829_L1_g57		55	230	3.7E-06	2.1E-03	1.6E-04	5.3E-04	3.4E-02	5.7E-02	595	3	0.4271	6.55	0.0573	6.38	0.49	0.0543	0.65	0.5772	8.93	0.0167	7.92	17.462	6.38	0.0543	0.65
20160829_L1_g15		55	196	4.5E-06	1.8E-03	1.3E-04	1.7E-04	1.1E-02	5.0E-02	1327	5	0.4278	8.35	0.0576	8.41	0.50	0.0539	0.67	0.2416	2.78	0.0165	9.78	17.369	8.41	0.0539	0.67
20160829_L1_g32		60	216	2.8E-06	8.6E-04	6.5E-05	1.4E-04	8.9E-03	2.4E-02	473	4	0.4292	12.23	0.0557	10.34	0.42	0.0549	3.24	0.4310	21.26	0.0167	18.29	17.943	10.34	0.0549	3.24
20160829_L1_g26		60	190	3.0E-06	6.4E-04	4.6E-05	5.6E-05	4.1E-03	1.9E-02	374	5	0.4306	4.72	0.0581	4.13	0.44	0.0540	1.27	0.1888	17.12	0.0167	5.46	17.224	4.13	0.0540	1.27
20160829_L1_g90		61	232	5.4E-06	1.4E-03	1.0E-04	1.4E-04	9.5E-03	3.8E-02	325	5	0.4320	4.26	0.0587	3.59	0.42	0.0539	0.82	0.2032	16.90	0.0170	3.83	17.029	3.59	0.0539	0.82
20160829_L1_g63		50	247	2.3E-06	5.6E-04	4.0E-05	9.1E-05	6.3E-03	1.6E-02	213	2	0.4322	5.01	0.0571	4.78	0.48	0.0550	0.95	0.5448	9.82	0.0179	4.01	17.498	4.78	0.0550	0.95
20160829_L1_g29		60	247	2.8E-06	8.3E-04	6.2E-05	1.2E-04	7.7E-03	2.3E-02	347	4	0.4327	9.11	0.0569	8.37	0.46	0.0551	1.48	0.1390	66.59	0.0163	15.69	17.576	8.37	0.0551	1.48
20160829_L1_g94		53	201	7.2E-06	1.8E-03	1.3E-04	2.3E-04	1.5E-02	4.8E-02	400	12	0.4424	9.61	0.0595	9.47	0.49	0.0539	0.87	0.3276	6.89	0.0166	13.23	16.806	9.47	0.0539	0.87
20160829_L1_g95		54	239	2.8E-06	4.7E-04	3.4E-05	6.4E-05	4.1E-03	1.2E-02	233	1	0.5078	7.75	0.0668	7.47	0.48	0.0553	1.08	0.3245	8.68	0.0190	9.99	14.964	7.47	0.0553	1.08
20160829_L1_g4		50	220	3.6E-05	5.6E-03	4.2E-04	6.9E-04	5.5E-02	1.5E-01	552	29	0.5115	8.57	0.0659	8.92	0.52	0.0560	0.45	0.2623	7.09	0.0160	14.64	15.176	8.92	0.0560	0.45
20160829_L1_g6		50	250	1.4E-04	3.3E-03	2.6E-04	4.1E-04	2.3E-02	7.7E-02	704	17	0.5556	9.46	0.0718	8.19	0.43	0.0569	1.12	0.2784	16.99	0.0205	10.18	13.921	8.19	0.0569	1.12
20160829_L1_g53		51	211	#DIV/0!	1.1E-03	8.6E-05	2.6E-04	1.4E-02	2.6E-02	#DIV/0!	#DIV/0!	0.5583	7.19	0.0712	7.19	0.50	0.0572	0.65	0.6036	6.65	0.0221	8.09	14.048	7.19	0.0572	0.65
20160829_L1_g55		61	220	2.5E-06	9.1E-04	7.0E-05	1.7E-04	9.5E-03	2.2E-02	#DIV/0!	#DIV/0!	0.5698	5.18	0.0718	5.37	0.52	0.0577	0.94	0.2738	48.06	0.0242	4.89	13.928	5.37	0.0577	0.94
20160829_L1_g67		57	249	7.4E-06	4.0E-04	3.0E-05	1.4E-04	7.8E-03	9.2E-03	70	7	0.5799	3.26	0.0741	3.19	0.49	0.0568	0.87	0.9553	1.40	0.0221	3.29	13.497	3.19	0.0568	0.87
20160829_L1_g28		63	255	3.1E-06	2.6E-04	2.0E-05	3.3E-05	1.9E-03	5.8E-03	109	2	0.5937	4.75	0.0748	4.52	0.48	0.0576	1.25	0.3421	2.14	0.0202	5.64	13.362	4.52	0.0576	1.25
20160829_L1_g81		55	237	2.6E-06	1.1E-03	8.1E-05	1.7E-04	9.2E-03	2.4E-02	#DIV/0!	#DIV/0!	0.5979	6.04	0.0757	5.98	0.50	0.0574	0.85	0.4867	8.17	0.0233	7.89	13.210	5.98	0.0574	0.85
20160829_L1_g77		52	192	5.4E-06	7.6E-04	5.8E-05	6.9E-05	3.3E-03	1.5E-02	193	15	0.6051	9.20	0.0767	9.58	0.52	0.0573	1.01	0.2160	9.59	0.0221	13.65	13.046	9.58	0.0573	1.01
20160829_L1_g79		57	236	7.1E-06	7.0E-04	5.4E-05	6.3E-05	3.3E-03	1.5E-02	#DIV/0!	#DIV/0!	0.6122	4.46	0.0779	4.40	0.49	0.0572	0.84	0.2353	5.21	0.0233	5.46	12.833	4.40	0.0572	0.84
~~20160829_L1_g100~~		~~58~~	~~256~~	~~1.3E-05~~	~~1.4E-03~~	~~1.1E-04~~	~~3.0E-04~~	~~2.2E-02~~	~~4.4E-02~~	~~211~~	~~13~~	~~0.6220~~	~~24.30~~	~~0.0553~~	~~6.10~~	~~0.13~~	~~0.0624~~	~~10.15~~	~~0.5724~~	~~12.80~~	~~0.0189~~	~~21.98~~	~~18.086~~	~~6.10~~	~~0.0624~~	~~10.15~~
20160829_L1_g36		54	255	2.3E-06	3.1E-04	2.5E-05	1.1E-04	5.7E-03	6.5E-03	235	2	0.6526	5.31	0.0798	4.58	0.43	0.0596	1.28	1.0702	3.63	0.0237	5.64	12.525	4.58	0.0596	1.28
20160829_L1_g61		59	235	#DIV/0!	5.4E-04	4.2E-05	1.0E-04	4.8E-03	1.0E-02	#DIV/0!	#DIV/0!	0.6603	7.84	0.0830	7.60	0.48	0.0588	0.90	0.5024	3.87	0.0235	9.31	12.048	7.60	0.0588	0.90
20160829_L1_g71		50	260	7.9E-06	5.5E-04	4.2E-05	6.7E-05	3.2E-03	1.1E-02	95	2	0.6665	2.97	0.0830	2.96	0.50	0.0583	0.84	0.2996	7.64	0.0243	3.65	12.046	2.96	0.0583	0.84
20160829_L1_g38		59	242	2.4E-06	4.9E-04	3.8E-05	5.5E-05	2.5E-03	1.0E-02	213	2	0.6896	8.79	0.0870	8.59	0.49	0.0575	1.09	0.3114	15.18	0.0260	10.38	11.490	8.59	0.0575	1.09
20160829_L1_g21		60	240	1.1E-05	4.5E-03	3.5E-04	8.9E-04	4.5E-02	8.5E-02	965	15	0.6948	7.21	0.0848	7.65	0.53	0.0591	0.79	0.4834	6.24	0.0232	9.82	11.799	7.65	0.0591	0.79
20160829_L1_g98		55	232	3.3E-06	2.2E-04	1.7E-05	7.5E-05	3.4E-03	4.1E-03	72	1	0.7036	9.04	0.0867	7.82	0.43	0.0595	1.51	0.9321	3.01	0.0240	13.39	11.536	7.82	0.0595	1.51
20160829_L1_g93		52	225	8.1E-06	1.9E-03	1.5E-04	3.6E-04	1.7E-02	3.7E-02	478	5	0.7140	7.53	0.0877	7.55	0.50	0.0595	0.59	0.2761	38.26	0.0248	12.64	11.405	7.55	0.0595	0.59
20160829_L1_g1		60	224	2.7E-06	1.1E-03	8.5E-05	2.9E-04	1.1E-02	1.6E-02	422	1	0.7594	5.84	0.0898	6.03	0.52	0.0608	0.62	0.6168	7.55	0.0249	7.86	11.138	6.03	0.0608	0.62
20160829_L1_g39		55	221	2.4E-06	8.3E-04	6.8E-05	1.5E-04	6.9E-03	1.5E-02	214	4	0.7726	5.15	0.0916	4.52	0.44	0.0613	0.89	0.5131	4.86	0.0275	4.95	10.919	4.52	0.0613	0.89
20160829_L1_g59		55	225	2.4E-06	5.3E-04	4.3E-05	5.0E-05	2.2E-03	9.9E-03	#DIV/0!	#DIV/0!	0.7731	4.94	0.0942	4.47	0.45	0.0600	0.91	0.1239	51.99	0.0268	4.74	10.618	4.47	0.0600	0.91
20160829_L1_g35		57	219	2.4E-06	5.0E-04	4.0E-05	2.3E-04	9.8E-03	9.0E-03	302	0	0.7772	5.91	0.0926	6.11	0.52	0.0603	1.04	1.3785	8.19	0.0264	8.65	10.795	6.11	0.0603	1.04

20160829_L1_g64		58	252	2.2E-06	3.0E-04	2.5E-05	8.6E-05	3.9E-03	5.7E-03	149	1	0.7800	3.61	0.0917	3.02	0.42	0.0616	1.50	0.9244	8.36	0.0278	3.21	10.900	3.02	0.0616	1.50
20160829_L1_g85		51	190	7.3E-06	6.7E-04	5.4E-05	3.9E-04	1.6E-02	1.1E-02	83	11	0.7832	7.56	0.0960	7.06	0.47	0.0599	1.22	1.4618	9.90	0.0280	7.64	10.414	7.06	0.0599	1.22
20160829_L1_g44		55	214	2.2E-06	5.8E-04	4.8E-05	1.3E-04	5.0E-03	1.0E-02	#DIV/0!	#DIV/0!	0.7916	7.49	0.0942	7.48	0.50	0.0616	0.99	0.6041	3.39	0.0286	9.42	10.612	7.48	0.0616	0.99
20160829_L1_g97		56	258	2.6E-06	1.1E-04	8.8E-06	1.1E-05	5.0E-04	1.9E-03	66	7	0.8023	7.34	0.0956	6.66	0.45	0.0610	1.82	0.2496	4.25	0.0276	10.03	10.462	6.66	0.0610	1.82
20160829_L1_g82		56	246	1.8E-06	1.4E-03	1.2E-04	2.4E-04	9.8E-03	2.5E-02	419	5	0.8355	4.61	0.0975	4.66	0.50	0.0614	0.82	0.4454	23.34	0.0304	6.75	10.254	4.66	0.0614	0.82
20160829_L1_g73		50	202	#DIV/0!	8.3E-04	6.8E-05	2.7E-04	1.1E-02	1.4E-02	#DIV/0!	#DIV/0!	0.8370	7.10	0.0996	7.24	0.51	0.0613	1.02	1.1481	9.52	0.0291	8.80	10.037	7.24	0.0613	1.02
20160829_L1_g45		61	181	2.2E-05	1.2E-03	1.1E-04	8.4E-04	3.5E-02	2.2E-02	475	17	0.8388	10.92	0.0961	8.73	0.40	0.0627	4.97	1.4648	22.09	0.0298	10.51	10.406	8.73	0.0627	4.97
20160829_L1_g87		53	208	7.4E-06	1.1E-03	9.0E-05	6.0E-05	2.3E-03	1.8E-02	619	8	0.8463	7.85	0.1021	7.67	0.49	0.0603	0.82	0.0237	337.31	0.0276	13.31	9.794	7.67	0.0603	0.82
20160829_L1_g105		59	217	#DIV/0!	3.6E-04	3.0E-05	6.6E-05	2.6E-03	5.7E-03	#DIV/0!	#DIV/0!	0.8603	6.56	0.1019	5.41	0.41	0.0613	1.30	0.4066	13.99	0.0302	8.97	9.812	5.41	0.0613	1.30
20160829_L1_g96		55	244	#DIV/0!	5.9E-04	4.8E-05	2.7E-04	1.1E-02	9.0E-03	#DIV/0!	#DIV/0!	0.9218	5.33	0.1080	5.20	0.49	0.0624	0.83	1.3233	3.17	0.0306	6.41	9.256	5.20	0.0624	0.83
20160829_L1_g56		57	220	2.2E-06	1.4E-03	1.3E-04	4.8E-04	1.5E-02	2.0E-02	662	3	1.0295	6.59	0.1141	5.56	0.42	0.0655	1.65	0.7819	7.19	0.0327	7.93	8.765	5.56	0.0655	1.65
20160829_L1_g31		67	227	3.0E-06	2.3E-04	2.3E-05	1.5E-04	4.3E-03	2.7E-03	69	2	1.4702	6.99	0.1456	6.50	0.46	0.0732	1.48	1.7787	1.99	0.0406	8.26	6.867	6.50	0.0732	1.48
20160829_L1_g66		55	158	#DIV/0!	1.8E-03	1.7E-04	5.2E-04	1.4E-02	1.9E-02	#DIV/0!	#DIV/0!	1.5558	9.29	0.1614	9.16	0.49	0.0702	0.93	1.1213	24.19	0.0449	10.71	6.196	9.16	0.0702	0.93
20160829_L1_g48		56	190	2.3E-06	1.3E-03	1.3E-04	2.1E-04	5.4E-03	1.4E-02	356	4	1.6086	9.78	0.1601	9.81	0.50	0.0735	0.99	0.7545	24.53	0.0486	9.44	6.245	9.81	0.0735	0.99
20160829_L1_g9		50	186	2.2E-06	2.9E-04	5.0E-05	8.4E-05	1.2E-03	1.5E-03	#DIV/0!	#DIV/0!	6.0424	4.67	0.3391	4.23	0.45	0.1300	1.06	0.3937	33.72	0.0943	4.75	2.949	4.23	0.1300	1.06
20160829_L1_g34		63	157	#DIV/0!	2.1E-03	3.6E-04	3.9E-04	5.4E-03	1.1E-02	#DIV/0!	#DIV/0!	6.2687	5.41	0.3490	5.93	0.55	0.1290	0.99	0.4757	6.76	0.0937	4.89	2.865	5.93	0.1290	0.99
20160829_L1_g86		52	241	4.1E-06	1.5E-03	2.6E-04	6.2E-04	7.8E-03	7.1E-03	466	6	6.3474	5.94	0.3545	4.30	0.36	0.1298	1.93	0.9563	10.94	0.0967	6.95	2.821	4.30	0.1298	1.93
20160829_L1_g68		51	227	#DIV/0!	5.8E-04	9.9E-05	1.2E-04	1.5E-03	2.8E-03	#DIV/0!	#DIV/0!	6.3820	3.07	0.3615	3.19	0.52	0.1283	0.61	0.5718	3.59	0.1023	4.74	2.767	3.19	0.1283	0.61
20160829_L1_g54		56	249	2.3E-06	3.3E-04	6.6E-05	8.0E-05	8.9E-04	1.4E-03	#DIV/0!	#DIV/0!	8.5205	5.53	0.4075	5.70	0.51	0.1514	1.08	0.6438	4.01	0.1080	7.40	2.454	5.70	0.1514	1.08
20160829_L1_g83		55	176	#DIV/0!	4.0E-03	8.0E-04	5.6E-04	5.9E-03	1.5E-02	#DIV/0!	#DIV/0!	8.7108	14.23	0.4055	14.24	0.50	0.1515	4.91	0.4730	21.52	0.1024	18.17	2.466	14.24	0.1515	4.91
20160829_L1_g62		55	200	2.2E-06	3.5E-04	8.3E-05	1.2E-04	1.2E-03	1.2E-03	209	1	11.7412	11.68	0.4712	11.16	0.48	0.1817	2.47	1.0934	10.23	0.1282	12.64	2.122	11.16	0.1817	2.47
20160829_L1_g58		51	218	2.2E-06	2.4E-03	5.6E-04	6.5E-04	6.8E-03	1.0E-02	1320	4	12.3290	8.19	0.4811	7.26	0.44	0.1864	1.89	0.9614	8.70	0.1250	4.23	2.079	7.26	0.1864	1.89
~~20160829_L1_g60~~		~~58~~	~~211~~	~~2.2E-06~~	~~2.4E-03~~	~~6.5E-04~~	~~6.1E-04~~	~~7.0E-03~~	~~1.1E-02~~	~~1131~~	~~2~~	13.2265	~~10.34~~	~~0.4549~~	~~8.97~~	~~0.43~~	~~0.2123~~	~~2.50~~	~~0.6397~~	~~8.56~~	~~0.1226~~	~~6.87~~	~~2.198~~	~~8.97~~	~~0.2123~~	~~2.50~~
20160829_L1_g25		57	237	3.1E-06	1.5E-03	3.9E-04	3.4E-04	2.6E-03	4.3E-03	674	2	14.4444	7.76	0.5225	7.84	0.51	0.2020	0.66	0.3954	18.29	0.1349	9.30	1.914	7.84	0.2020	0.66
20160829_L1_g69		50	126	1.7E-05	3.1E-03	8.7E-04	6.7E-04	5.3E-03	1.0E-02	802	21	14.5341	15.68	0.5248	13.22	0.42	0.1996	6.59	0.4262	52.65	0.1286	29.81	1.905	13.22	0.1996	6.59

18.3 Appendix C

18.3.1 *Silbersberg metasandstone*

Table 7: Register of the measured zircons of the Silbersberg metasandstone and the associated ages, two sigma errors and concordance. R: border of the zircon was measured, K: core of zircon was analysed, Diskor.: the analysed zircon is discordant.

Nummer	Alter(Ma)	Fehler(2σ)	Konkordanz	Nummer	Alter(Ma)	Fehler(2σ)	Konkordanz	Nummer	Alter(Ma)	Fehler(2σ)	Konkordanz
1	630	26	0.33	52	497	17	0.4	86	2704	42	0.89
2R	Diskordant		0	53	441	17	0.45	90	509	10	0.91
3	601	54	0.95	54	549.9	9.8	0.46	91	516	20	0.59
16	399	26	0.36	55	2296	70	0.082	94	509	12	0.59
17	923	43	0.7	56	561	15	0.76	96	538	13	0.55
19	654	33	0.67	57	549	15	0.99	98	416	19	0.76
20	391	23	0.73	58	582	20	0.49	100	495	10	0.12
21	578	29	0.81	59	518	16	0.97	103	516	11	0.49
23	Diskordant		0	60R	515	18	0.89	104	527	16	0.7
27	445	22	0.82	62	388	12	0.89	105	540	22	0.85
28	662	30	0.43	66	1984	47	0.004Diskor.	106	507	12	0.16
30	639	24	0.49	68R	387.9	9.1	0.14	107	518	14	0.35
31	472	21	0.75	69	503.2	8.4	0.6	108	496	24	0.56
34	Diskordant		0	71	398	16	0.77	110	Diskordant		0
36	2014	24	0.29	72	510.2	9.5	0.17	111	2799	51	0.96
37	551	19	0.74	73	497	7.3	0.009Diskor.	112	575	26	0.91
38	530	37	0.65	76R	Diskordant		0	118	507	21	0.29
40R	621	14	0.65	78	541	17	0.79	120	697	59	0.6
42R	624	25	0.55	81	485.8	6	0.002Diskor.	122	522	66	0.79
45	2785	59	0.007Diskor.	82	487	10	0.4				
47	579	26	0.74	84	1966	31	0.36				

18.3.2 *Semmering quartzite*

Table 8: Register of the measured zircons of the Semmering quartzite and the associated ages, two sigma errors and concordance. R: border of the zircon was measured, K: core of zircon was analysed, Diskor.: the analysed zircon is discordant.

Nummer	Alter (Ma)	Fehler (2σ)	Konkordanz	Nummer	Alter (Ma)	Fehler (2σ)	Konkordanz	Nummer	Alter (Ma)	Fehler (2σ)	Konkordanz
1	471	12	0.76	49	2480	37	0.02Diskor	101	743	33	0.94
2	468	13	0.46	50	552	16	0.96	102	528.5	9.6	0.7
3	297	12	0.6	51	471	24	0.69	103	449	38	0.93
4	425	19	0.14	53	473	28	0.94	104	537	29	0.9
6	274	22	0.74	54	554	85	0.23	106	463	11	0.16
7	301.3	5.3	0.34	55	479	28	0.81	107	302	11	0.93
8	896	64	0.72	56	1820	41	0.006Diskor.	111	574	53	0.8
9	533	14	0.62	57	387	22	0.64	112	725	30	0.71
10	450	31	0.74	59	460	33	0.38	113	549	33	0.77
11	2359	30	0.015Diskor.	60	720	39	0.98	115	670	43	0.77
12	470	23	0.85	61	1974	34	0.63	124	455	19	0.91
13	906	120	0.83	62	1023	18	0.49	127	624	39	0.99
14	680	21	0.15	63	294.7	6.6	0.36	128	641	41	0.67
15	297.1	6.9	0.25	64K	598	42	0.9	131	639	52	0.57
16	300	8.3	0.035Diskor.	64R	603	38	0.89	134	1041	63	0.96
17	318	26	0.018Diskor.	65	459	13	0.65	135	459	12	0.72
18	448	12	0.77	66	617	26	0.55	136	319	15	0.98
19	338.8	7.5	0.61	67	451	23	0.78	138	653	18	0.31
20	299	11	0.85	69	452	16	0.53	139	973	99	0.95
21	510	23	0.92	71	340	15	0.74	140	460	16	0.81
22	613	13	0.42	73	441	31	0.79	142	657	12	0.71
23	632	20	0.87	74	450.2	8.7	0.35	143	449	16	0.92
24	840	59	0.46	75	507	42	0.65	144	663	29	0.99
26	755	25	0.38	76	300	11	0.43	148	301	17	0.88
27	1202	42	0.36	77	349	22	0.84	149	774	21	0.68
29	292	14	0.74	81	1603	37	0.84	152	579	15	0.46
30	699	130	0.71	82	1019	50	0.74	153	454	12	0.31
31	280	16	0.73	84	519	37	0.26	154	747	39	0.995
32	351	12	0.99	85	618	34	0.52	156	611	55	0.83
33	374	29	0.18	86	522	21	0.2	157	407	26	0.7
34	443	39	0.69	87	463.8	8.3	0.5	159	260.2	7.8	0.85
36	974	61	0.18	88	456	10	0.68	162	455	17	0.37
37	452	14	0.92	89	512	58	0.74	163	628	36	0.63
38	2044	250	0.027Diskor.	90	866	17	0.49	165	667	24	0.3
39	457.3	8.1	0.94	92	341	10	0.83	166	465	15	0.39
40	657	52	0.9	93	678	36	0.83	167	478	18	0.24
41	683	38	0.17	94	486	32	0.93	168	355	150	0.92
42	461.7	8.9	0.74	95	459	28	0.83	170	384	58	0.72
47	581	32	0.55	96	415	34	0.61	171	391	30	0.065
48	473	11	0.48	98	481	48	0.96	172	436	27	0.37

18.3.3 *Veitscher metasandstone*

Table 9: Register of the measured zircons of the Veitscher metasandstone and the associated ages, two sigma errors and concordance. R: border of the zircon was measured, K: core of zircon was analysed, Diskor.: the analysed zircon is discordant.

Nummer	Alter(Ma)	Fehler(2σ)	Konkordanz	Nummer	Alter(Ma)	Fehler(2σ)	Konkordanz	Nummer	Alter(Ma)	Fehler(2σ)	Konkordanz
1	518	27	0.65	52	860	57	0.25	141R	488	15	0.91
2	494	15	0.79	54	649	29	0.38	142	478	25	0.69
3	Diskordant		0.001	55	491	15	0.45	143	489.4	6.2	0.992
4	477	28	0.77	57	515	41	0.38	144	558	79	0.88
6	474	20	0.997	59	2880	74	0.11	145	445	33	0.93
7	981	49	0.92	60	558	12	0.37	146	2852	59	0.69
10	505	13	0.98	62	543	36	0.98	147	534	84	0.97
11	641	24	0.87	64	351.9	9.7	0.94	149	582	14	0.53
12	536	27	0.21	66	368	25	0.91	151	975	110	0.993
13	601	23	0.78	71	480	26	0.5	152	467	11	0.79
14	637	50	0.61	73	351	7.6	0.56	154	561	15	0.68
15	407	250	0.77	74	502	17	0.27	156	511	14	0.29
16R	462	18	0.79	77	356.8	9.5	0.75	166	561	41	0.994
17	476	25	0.93	83	511	32	0.84	168	517	33	0.009Diskor.
18	367.2	7.8	0.4	85	484	34	0.67	169	353.7	8.1	0.9
19	508	10	0.37	87	353.3	4.7	0.77	170	504.7	9	0.33
20	668	35	0.95	88	495.8	9.3	0.68	171	782	63	0.042Diskor.
21	503	24	0.7	89	465.1	7.8	0.26	172	652	37	0.47
22	365	14	0.72	90	447	230	0.82	173	736	120	0.064
24	685	29	0.96	91	642	25	0.97	174	679	21	0.47
26	1005	15	0.013	100	755	37	0.72	176	468.1	9.9	0.78
27	382	85	0.83	102	584	27	0.998	177	352	12	0.58
28	362	11	0.81	104K	615	16	0.7	178	604	13	0.27
29	515	12	0.93	104R	483	13	0.57	179	357	10	0.71
30	462	27	0.8	105	578.9	5.2	0.97	180	452	20	0.54
31	2451	60	0.31	106	354	15	0.82	182	493	21	0.98
32	546	28	0.45	109	530	26	0.72	183	516	11	0.5
33	487	22	0.82	111	614	46	0.7	185	451.1	9.1	0.54
34	552	20	0.89	116	523	19	0.75	186R	464	14	0.81
35	499	32	0.96	117	555	34	0.43	187	522	34	0.85
37	474	26	0.94	118	531	12	0.38	188	2510	57	0.078
38	559	19	0.86	119	472	30	0.64	189	368	27	0.93
39	511.9	9.5	0.49	120R	470	15	0.34	191	440	96	0.92
41	480	24	0.83	125	655	34	0.89	192	609	45	0.83
42	746	190	0.95	131	455	60	0.91	194	545	16	0.12
46	Diskordant		0	136	498	13	0.56	195	560	17	0.11
48	2044	61	0.98	137	1970	58	0.93	202	2671	83	0.76
50R	666	19	0.96	139	453	15	0.76	205	2573	98	0.21
51	831	37	0.999	140	365	21	0.68	209	594.2	8.1	0.43
								210	636	46	0.5

18.3.4 *Präbichl metasandstone*

Table 10: Register of the measured zircons of the Präbichl metasandstone and the associated ages, two sigma errors and concordance. R: border of the zircon was measured, K: core of zircon was analysed, Diskor.: the analysed zircon is discordant.

Nummer	Alter(Ma)	Fehler(2σ)	Konkordanz	Nummer	Alter(Ma)	Fehler(2σ)	Konkordanz	Nummer	Alter(Ma)	Fehler(2σ)	Konkordanz
1	568	24	0.18	41K	354	13	0.84	70	351	12	0.87
4	417	28	0.62	41	361	24	0.57	71	517	11	0.51
6	448	29	0.94	44	589	32	0.54	73	616	31	0.78
9	1971	830	0.001Diskor.	45	604	42	0.33	77	479	33	0.83
15	361	23	0.96	48	971	60	0.68	79	485	16	0.9
16	354	13	0.43	53	448	24	0.62	80	323	14	0.38
19	346	11	0.39	54	2290	50	0.062	81	474	21	0.67
21	533	29	0.51	55	455	18	0.3	82	612	20	0.17
22	355	24	0.79	56	709	30	0.24	83	2308	130	0.32
25	2782	73	0.35	57	360	18	0.84	85	589	31	0.84
26	364	12	0.98	58	2625	77	0.15	86	2006	49	0.057
27	330	18	0.94	59	581	20	0.91	87	624	34	0.85
28	470	16	0.42	60	Diskordant			90	366	11	0.64
30	320	13	0.27	61	515	29	0.96	92	338	29	0.9
31	905	40	0.096Diskor	62	2584	110	0.34	93	546	30	0.77
32	355	31	0.51	63	362	14	0.43	94	372	27	0.97
34	2018	610	0.041Diskor.	64	576	200	0.025Diskor.	95	417	24	0.997
35	581	25	0.39	65	356	17	0.56	96	663	25	0.9
36	503	18	0.2	66	955	56	0.75	97	594	30	0.6
38	534	34	0.79	67	463	11	0.59	98	539	33	0.81
39	574	20	0.19	68	2030	27	0.08	100	349	370	0.004
40R	304	12	0.47	69	2781	150	0.62	101	345	14	0.98
								105	628	26	0.78

18.4 Appendix D

Table 11: This table depicts the selected ages of the literature of the Alpine-Carpathian realm.

Literature ages (Ma)	methods	Rocktype and interpretation	author	G2 - Semmering Quartzite	G1 - Veitsch Nappe	G21 - Silbersberg Nappe	L1 - Präbichl Fm.
Silvretta							
532±30	U - Pb zircon	Silvretta: Grt - Hbl - Plg gneiss; protolith	Müller et al, 1996	526	555	511, 545	519
526±7	U - Pb zircon	Silvretta: alkaline "older gneiss"	Müller et al., 1995	526	x	x	519
522±6	U - Pb zircon	Silvretta: Val Sarsura metagabbro; protolith	Schaltegger et al., 1997	526	x	x	519
523±3	U - Pb zircon	Silvretta: Val Sarsura flasergabbro; protolith	Schaltegger et al., 1997	526	x	x	x
524±6	U - Pb zircon	Silvretta: Val Sarsura metatonalit; protolith	Schaltegger et al., 1997	526	x	x	519
420 - 450	U/Pb zircon	Flüela - Granite; Silvretta	Liebetrau 1996	x	x	443 Ma	x
Seckau							
432 ±16	Rb - Sr WR	orthogneiss, protolith formation, Seckau	Schabert, 1981	x	x	443 Ma	417 Ma
353 - 363	U - Pb zircon	Rennfeld tonalite, protolith formation, Gleinalm	Neubauer & Frisch, 1993	x	356 Ma	x	356 Ma
353	U - Pb zircon	Trondhjemite, protolith formation	Neubauer & Frisch, 1993	x	356 Ma	x	356 Ma
354 ± 16	Rb - Sr WR	metagranite, protolith formation	Schabert, 1981	342 Ma	356 Ma	x	356 Ma
518 ± 44	Rb - Sr WR	plagioclase - granite	Frank et al., 1976	526 Ma	555 Ma	511 Ma, 545 Ma	519 Ma
356	U - Pb, z.I.	metatonalite	Neubauer et al., 1993	x	356 Ma	x	356 Ma
354 ±16	Rb - Sr WR	two - mica - metagranite	Schabert, 1981	342 Ma	356 Ma	x	356 Ma
331 ± 25	Rb - Sr WR	augengneiss, Rennfeld	Frank et al., 1983	342 Ma	356 Ma	x	356 Ma, 317 Ma
350	Rb - Sr WR	Orthogneiss, Seckau, Formation durign variscian tectonomorph. Event	Scharbert, 1981	342 Ma	356 Ma	x	356 Ma
367 - 353	U/Pb	Rennfeld metatonalit, Kristallisation	Neubauer et al., 2003	x	356 Ma	x	356 Ma
450 - 425	U/Pb	Rennfeld augengneiss	Neubauer et al., 2003	x	x	443 Ma	x
Ötztal							
530±2 - 516±15	Sm - Nd WR	Ötztal: metagabbro (ophiolite); protolith	Miller & Thöni, 1995	526	x	x	x

Literature ages (Ma)	**methods**	**Rocktype and interpretation**	**author**	**G2 - Semmering Quartzite**	**G1 - Veitsch Nappe**	**G21 - Silbersberg Nappe**	**L1 - Präbichl Fm.**
494±73	Sm - Nd WR	Ötztal: kaunertal metagranite; protolith	Hoinkes et al., 1997	x	498	x	x
490 ±9	U/Pb EvZrn	Ötztal migmatite	Klötzli - Chowanetz et al., 1997	x	498 Ma	x	x
494±73	Sm - Nd WR	Östztal meta - granite	Hoinkes et al., 1997	x	498 Ma	511 Ma	466, 519 Ma
343 - 331	Sm - Nd WR - garnet	Eclogite, peak conditions of metamorphism	Hoinkes et al. 1997	342 Ma	x	x	x
372 ± 29	Rb - Sr WR	Bundschuh orthogneiss	Hawkesworth, 1976	x	356 Ma	390 Ma	356 Ma
336 +- 14	U - Pb zircon	eclogite, HP - Event	Gebauer & Söllner, 1993	342 Ma	x	x	x
362 +- 29	Sm - Nd WR	Gabbro - Eclogite	Miller & Thöni, 1995	342 Ma	356 Ma	390 Ma	356 Ma
Texel/Campo							
336 ±7	Rb - Sr WR	scarl - orthogneiss	Thöni, 1981	342 Ma	x	x	x
497 ± 38	Rb - Sr WR	Paragneiss	Borsi et al. (1973)	459 Ma, 526 Ma	498 Ma, 465 Ma	511 Ma	466 Ma, 519 Ma
340	Sm - Nd	garnet - lherzolite, metamorphism, Ulten zone	Thöni (1999)	342 Ma	x	x	x
445±24	Rb/Sr WR	ms - orthogneiss, Defereggen group	Hammerschmidt, 1981	x	x	443 Ma	x
Wölz							
445 ± 44	Rb - Sr WR	villach orthogneiss	Frimmel, 1988	459 Ma	465 Ma	443 Ma	466 Ma, 417 Ma
Koralpe							
313±18	Rb - Sr WR	pegmatit (St. Radegund), protolith formation	Neubauer & Stattegger (unpubl. Data), aus: Neubauer & Frisch, 1993	297 Ma	x	x	317 Ma
693 ± 39	Sm - Nd WR - garnet	Eclogite	Manby & Thiedig, 1988	662 Ma	x	x	703 Ma
Gleinalm							
397.3±7.8	Ar/Ar	amphibole in eclogite, Plateau age, Hochgrößen	Faryad et al., 2002	x	x	390 Ma	x
S von Tauern Window							
439 ± 20	Rb - Sr WR	orthogneiss, Schober Gruppe, Wangenitzsee	Troll et al., 1976; Brack, 1977	459 Ma	x	443 Ma	x
443	U - Pb zircon	tonalitic orthogneiss, Defereggen Alps, intrusionen granitoidic bodies	Cliff, 1980	x	x	443 Ma	x
543 ± 2	Pb/Pb zircon	hbl - gneiss, northern Defereggen - Petzeck group	Schulz & Bombach, 2003	x	x	545 Ma	x

Literature ages (Ma)	**methods**	**Rocktype and interpretation**	**author**	**G2 - Semmering Quartzite**	**G1 - Veitsch Nappe**	**G21 - Silbersberg Nappe**	**L1 - Präbichl Fm.**
548 ± 4	Pb/Pb zircon	hbl - gneiss, northern Defereggen - Petzeck group	Schulz & Bombach, 2003	x	x	545 Ma	x
463 ± 8	Pb/Pb zircon	ms - orthogneiss, northern Defereggen - Petzeck group	Schulz & Bombach, 2003	459 Ma	465 Ma	x	466 Ma
471 ± 7	Pb/Pb zircon	ms - orthogneiss, northern Defereggen - Petzeck group	Schulz & Bombach, 2003	x	465 Ma	x	466 Ma
461 ± 4	Pb/Pb zircon	bt - orthogneiss, northern Defereggen - Petzeck group	Schulz & Bombach, 2003	459 Ma	465 Ma	x	x
457 ± 5	Pb/Pb zircon	ms - orthogneiss, northern Defereggen - Petzeck group	Schulz & Bombach, 2003	459 Ma	x	x	x
448 ± 6	Pb/Pb zircon	bt - orthogneiss, northern Defereggen – Petzeck group	Schulz & Bombach, 2003	x	x	443 Ma	x
468 ± 5	Pb/Pb zircon	bt - orthogneiss, Defereggen group	Schulz & Bombach, 2003	x	465 Ma	x	466 Ma
469 +- 6	Pb/Pb zircon	metaprophyroid, Thurntaler phyllite group	Schulz & Bombach, 2003	x	465 Ma	x	466 Ma
473 ± 7	Pb/Pb zircon	metaprophyroid, Thurntaler phyllite group	Schulz & Bombach, 2003	x	x	x	466 Ma
460 ± 15	Pb/Pb zircon	ms - orthogneiss, Defereggen group	Klötzli, 1995	459 Ma	465 Ma	x	466 Ma
466 +- 10	Pb/Pb zircon	bt - orthogneiss, Defereggen group	Klötzli, 1995	459 Ma	465 Ma	x	466 Ma
443 ± 13	U/Pb zircon	ms - orthogneiss, Defereggen group	Cliff, 1980	x	465 Ma	443 Ma	x
427 ± 10	U/Pb zircon	bt - orthogneiss, Defereggen group	Cliff, 1980	x	x	x	417 Ma
440± 13	Rb - Sr WR	ms - orthogneiss, northern Defereggen - Petzeck group	Brack, 1977	x	x	443 Ma	x
455 ± 4	U/Pb	ms - orthogneiss, northern Defereggen - Petzeck group	Bücksteeg, 1999	459	x	x	x
Tauern Window							
657±15	conv. U - Pb zircon	Habach C., banded amphibolite; lava extrusion	von Quadt 1992	662	646	x	x
644±12	Sm - Nd zircon - WR	Habach C., amphibolite; lava extrusion	von Quadt 1992	x	646	x	x
551±9	U - Pb zircon SHRIMP	Stubach C., hornblende plagioclase gneiss; protolith	Eichhorn et al., 2001	x	555	545	x
539±10	conv. U - Pb zircon	Stubach C., metagabbro; intrusion in magmatic arc	von Quadt 1992	x	x	545	x

Literature ages (Ma)	**methods**	**Rocktype and interpretation**	**author**	**G2 - Semmering Quartzite**	**G1 - Veitsch Nappe**	**G21 - Silbersberg Nappe**	**L1 - Präbichl Fm.**
547±27	U - Pb zircon SHRIMP	Habach C., fine - grained amphibolite; protolith	Eichhorn et al., 1999a	526	555	545	x
529±17	U - Pb zircon SHRIMP	Habach C., EOZ gneiss; protolith	Eichhorn et al., 1999a	526	x	x	519
529±18	U - Pb zircon SHRIMP	Habach C., older K2 gneiss; protolith	Eichhorn et al., 1999a	526	x	x	519
528±14	U - Pb zircon SHRIMP	Habach C., EOZ gneiss; protolith	Eichhorn et al., 1999a	526	x	x	519
519±14	U - Pb zircon SHRIMP	Habach C., younger K2 gneiss; protolith	Eichhorn et al., 1999a	526	x	511	519
496±2	conv. U - Pb zircon	Habach C., hornblendite; intrusion	von Quadt 1992	x	498	x	x
488±18	U - Pb zircon	Stubach C. (lower Schieferhülle), eclogitic amphibolite; protolith	von Quadt 1997	x	498	x	x
657±15	U - Pb; L. I	Banded amphibolite; Penninic basement TW; Protolith	Neubauer et al., 1987	662	646	x	x
644±12	Sm - Nd, mineral	Banded amphibolite; Penninic basement TW; Protolith	Neubauer et al., 1987	x	646	x	x
605±34	U - Pb; L. I	Plagioclase gneiss; Penninic basement TW; Protolith	Quadt (1992)	618	601	x	617
539±10	U - Pb; L. I	Metagabbro; Penninic basement TW; Protolith	Neubauer et al., 1987	x	x	545	x
496±2	U - Pb; L. I	Hornblendite; Penninic basement TW; Protolith	Neubauer et al., 1987	x	498	x	x
496±28	Sm - Nd, mineral	Grt - Amphibolite; Penninic basement TW; Metamorphism	Neubauer et al., 1987	x	498	x	x
500 ±10	SHRIMP	metarhyolite, Ambin	Guillot et al., 1998	x	498 Ma	511 Ma	x
500 ± 4	U/Pb zircon	alkaline granite	Bussy et al., 1996	x	498 Ma	x	x
497 ± 4	U/Pb zircon	Vanoise, granite	Bertrand & Leterrier, 1997	x	498 Ma	x	x
458 ±11	U/Pb SHRIMP	anatexis, Tauern	Eichhorn et al., 1999b	459 Ma	465 Ma	x	466 Ma
W -Greywackezone							
468	U/Pb zircon	Porphyroid Greywacke Zone	Söllner et al., 1991	459 Ma	465 Ma	x	466 Ma
476 ±14	U/Pb SHRIMP	Metagabbro Greywacke Zone	Loth et al., 1999	x	465 Ma	x	466 Ma

Literature ages (Ma)	methods	Rocktype and interpretation	author	G2 - Semmering Quartzite	G1 - Veitsch Nappe	G21 - Silbersberg Nappe	L1 - Präbichl Fm.
Wechsel							
603±18	U - Pb zircon	Wiesmath orthogneiss; protolith, Wechsel	Korikovsky et al., 1998	618	601	x	617
Kaintaleck							
514±43	U - Pb zircon	Kaintaleck C., hbl gneiss; protolith	Neubauer et al., 2002	526	498	511, 545	519
390	U - Pb zircon	paragneiss, peak conditions of metamorphism	Neubauer & Frisch, 1993	x	x	390 Ma	x
516	U - Pb, z.I.	horblende - garnet - gneiss	Neubauer et al., 1989	x	x	511 Ma	519 Ma
365 ± 20	U - Pb, z. u.	aplitic orthogneiss	Neubauer et al. (in prep)	x	356 Ma	x	356 Ma
502 ± 6	U - Pb, z. u.	orthogneiss boulder Kalwang congl.	Neubauer et al., 1987	x	498 Ma	x	x
500 +- 20	U - Pb, z. u.	orthogneiss boulder Kalwang congl.	Neubauer et al., 1987	x	498 Ma	511 Ma	519 Ma
391 ±2	U/Pb L.I.	Paragneiss, Prieselbauer unit	Frisch & Neubauer 1989	x	x	390 Ma	x
365 ± 20	U - Pb, z. u.	aplitic orthogneiss	Neubauer et al. (in prep)	x	356 Ma	x	356 Ma
Tatrikum							
380 ± 20	Rb - Sr WR	metamorphic rock	Cambel & Kral, 1989	x	x	390 Ma	x
405 - 380	U- Pb zircon	granitic orthogneiss, Jarabá complex	Poller et al., 2000 & Putis et al, 2003	x	x	390 Ma	x
650 - 500	U- Pb zircon	metasediments, protolith, middle variscan structural unit	Kohút et al., 2007	618Ma, 526 Ma	646Ma, 601Ma, 555Ma	625Ma, 571 Ma, 545 Ma, 511Ma	617Ma, 578Ma, 519 Ma
500 - 400	-	metavolcanics of lower variscan structural unit	Shcherbak et al., 1988	459 Ma	498 Ma, 465 Ma	443 Ma	466 Ma, 417 Ma
359 - 345	SHRIMP	west - carpathian granitoids	Gaab et al., 2005	x	356 Ma	x	356 Ma
472 ± 6	SHRIMP	granitic orthogneiss, Nízke Tatry Mountains	Putis et al., 2008	x	x	x	466 Ma
407 - 388	SHRIMP	granitic orthogneiss, Nízke Tatry Mountains	Putis et al., 2008	x	x	390 Ma	x
470 ± 6	SHRIMP	granitic orthogneiss, Nízke Tatry Mountains	Putis et al., 2008	x	465 Ma	x	466 Ma
617 ± 11	SHRIMP	granitic orthogneiss, Nízke Tatry Mountains	Putis et al., 2008	618 Ma	x	625 Ma	617 Ma
497 ± 6	SHRIMP	granitic to tonalitic orthogneisses, Malá Fatra Mountains	Putis et al., 2008	x	498 Ma	x	x
320	U- Pb zircon	-	Shcherbak et al., 1988	x	x	x	317 Ma
588 ± 10	SHRIMP	Bratislava Massif	Kohút et al., 2009	x	x	x	578 Ma

Literature ages (Ma)	methods	Rocktype and interpretation	author	G2 - Semmering Quartzite	G1 - Veitsch Nappe	G21 - Silbersberg Nappe	L1 - Präbichl Fm.
359 ± 5	SHRIMP	Bratislava Massif	Kohút et al., 2009		356 Ma		356 Ma
350 ± 7	SHRIMP	Bratislava Massif	Kohút et al., 2009	x	356 Ma	x	356 Ma
340 ± 5	SHRIMP	Modra Massif	Kohút et al., 2009	342 Ma	x	x	x
356 ±10	SHRIMP	Kralova Hola	Gaab et al., 2005	x	356 Ma	x	356 Ma
359 ±6	SHRIMP	Kralova Hola	Gaab et al., 2005	x	356 Ma	x	356 Ma
349 ± 26	SHRIMP	Kralova Hola	Gaab et al., 2005	342 Ma	356 Ma	x	356 Ma
345 ± 11	SHRIMP	Kralova Hola	Gaab et al., 2005	342 Ma	356 Ma	x	356 Ma
353.8 ± 3.7	SHRIMP	Kralova Hola	Gaab et al., 2005	x	356 Ma	x	356 Ma
355.8 ± 3.6	SHRIMP	Kralova Hola	Gaab et al., 2005	x	356 Ma	x	356 Ma
354 ± 3.7	SHRIMP	Kralova Hola	Gaab et al., 2005	x	356 Ma	x	356 Ma
358.8 ± 3.7	SHRIMP	Kralova Hola	Gaab et al., 2005	x	356 Ma	x	356 Ma
354.9 ± 3.7	SHRIMP	Kralova Hola	Gaab et al., 2005	x	356 Ma	x	356 Ma
354.2 ± 3.	SHRIMP	Kralova Hola	Gaab et al., 2005	x	356 Ma	x	356 Ma
359.7 ± 4	SHRIMP	Kralova Hola	Gaab et al., 2005	x	356 Ma	x	356 Ma
359.2 ± 5.6	SHRIMP	Kralova Hola	Gaab et al., 2005	x	356 Ma	x	356 Ma
341.2 ±3.6	SHRIMP	Kralova Hola	Gaab et al., 2005	342 Ma	x	x	x
359.7 ± 4	SHRIMP	Kralova Hola	Gaab et al., 2005	x	356 Ma	x	356 Ma
358.2 ± 4.4	SHRIMP	Kralova Hola	Gaab et al., 2005	x	356 Ma	x	356 Ma
390	U- Pb zircon	Kfspar - & plg - orthogneiss	Adamija et al., 1992	x	x	390 Ma	x
360 - 340	?	granitoid plutonism, Tatric basement	Petrík et al., 1994	342 Ma	356 Ma	x	356 Ma
353 ±11	U - Pb	plutonic granitoids	Shcherbak et al., 1990	x	356 Ma	x	356 Ma
526.4 ± 1.6	U - Pb zircon	orthogneiss	Putis et al., 2003	x	x	526 Ma	x
380 - 405	U- Pb zircon	granitic orthogneiss	Janák et al., 1996	x	x	390 Ma	x
415	U - Pb zircon	granitic orthogneiss	Krist et al., 1992	x	x	x	417 Ma
315.3 ± 2.8	U- Pb zircon, CLC	Smrekovica tonalite	Poller et al., 2005	x	x	x	317 Ma

Literature ages (Ma)	**methods**	**Rocktype and interpretation**	**author**	**G2 - Semmering Quartzite**	**G1 - Veitsch Nappe**	**G21 - Silbersberg Nappe**	**L1 - Präbichl Fm.**
319.9 ± 3.9	U- Pb zircon, CLC	Smrekovica tonalite	Poller et al., 2005	x	x	x	317 Ma
313.9 ± 6.9	U- Pb zircon, CLC	Smrekovica tonalite	Poller et al., 2005	x	x	x	317 Ma
297.8 ± 2.7	U- Pb zircon	Kornietov Granodiorite	Poller et al., 2005	297 Ma	x	x	x
312.1 ± 5.8	SIMS	Lipova two - mica - granite	Poller et al., 2005	x	x	x	317 Ma
467.9 ± 3.4	U - Pb zircon	Lubochna Leucogranite	Poller et al., 2005	x	465 Ma	x	466 Ma
356 ± 9	U - Pb zircon (TIMS)	S - type granite, Strázovské vrchy Mountains	Král et al., 1997	x	356 Ma	x	356 Ma
353 ± 11	U - Pb zircon (TIMS)	I - type granite, Malá Fatra Mts	Shcherbak et al., 1990	x	356 Ma	x	356 Ma
356 ± 25	U - Pb zircon (TIMS)	S - type granite, Lipová granite	Kohút et al., 1997	x	356 Ma	x	356 Ma
347 ± 14	U - Pb zircon (TIMS)	S - type granite, Tatry Mountains	Poller & Todt, 2000	342 Ma	356 Ma	x	356 Ma
314 ± 4	U - Pb zircon	I - type, High tatra tonalite	Poller & Todt, 2000	x	x	x	317 Ma
307 ± 10	U - Pb zircon	Smrekovica tonalite	Poller et al., 2005	x	x	x	317 Ma
355 ± 5	U - Pb zircon	S - type granodiorite, Malé Karpaty Mountains	Kohút et al., 2009	x	356 Ma	x	356 Ma
356	SHRIMP	Hrinová tonalite	Kohút et al., 2010 (Conference)	x	356 Ma	x	356 Ma
355	SHRIMP	Tribec granodiorite	Kohút et al., 2010 (Conference)	x	356 Ma	x	356 Ma
351	SHRIMP	Branisko granite	Kohút et al., 2010 (Conference)	x	356 Ma	x	356 Ma
348	SHRIMP	Ziar granite	Kohút et al., 2010 (Conference)	342 Ma	356 Ma	x	356 Ma
517.2 ± 4.6	U - Pb, CLC	Jalovecká Valley Micaschist	Kohút et al., 2008	x	x	x	519 Ma
633 ± 12	U - Pb zircon	Jalovecká Valley Micaschist	Kohút et al., 2008	x	x	625 Ma	x
528.7 ± 9.4	U - Pb zircon	Jalovecká Valley Micaschist	Kohút et al., 2008	526 Ma	x	x	519 Ma
535 ± 10	U - Pb zircon	Jamnická Valley Micaschist	Kohút et al., 2008	x	x	545 Ma	x
511 ± 6.4	U - Pb zircon	Jamnická Valley Micaschist	Kohút et al., 2008	x	x	511 Ma	x
513.6 ± 3.1	U - Pb zircon	Jamnická Valley Micaschist	Kohút et al., 2008	x	x	511 Ma	x
495.8 ± 4.5	U - Pb zircon	Jamnická Valley Micaschist	Kohút et al., 2008	x	498 Ma	x	x

Literature ages (Ma)	**methods**	**Rocktype and interpretation**	**author**	**G2 - Semmering Quartzite**	**G1 - Veitsch Nappe**	**G21 - Silbersberg Nappe**	**L1 - Präbichl Fm.**
363 ± 11 - 347 ± 14	U - Pb zircon	granites of common tatra type	Poller et al., 2000	342 Ma	356 Ma	x	356 Ma
350 ± 5 - 337 ±6	U - Pb zircon	granites of High Tatra type	Burda et al., 2013	342 Ma	x	x	x
518 ± 21	U - Pb zircon	granitoid, common tatra	Gaweda et al., 2016	526 Ma	498 Ma	511 Ma	519 Ma
360.2 ± 5.5	U - Pb zircon	porphyritic granitoid, common tatra	Gaweda et al., 2016	x	356 Ma	x	356 Ma
355.2 ± 8.2	U - Pb zircon	granodiorite - tonalite, common tatra	Gaweda et al., 2016	x	356 Ma	x	356 Ma
426 ± 25	U - Pb zircon	granodiorite - tonalite, common tatra	Gaweda et al., 2016	x	x	443 Ma	417 Ma
345.6 ± 3.7	U - Pb zircon	granitoid, high Tatra granites	Gaweda et al., 2016	342 Ma	x	x	x
462 ± 18	U - Pb zircon	granitoid, high Tatra granites	Gaweda et al., 2016	459 Ma	465 Ma	x	466 Ma
533 ± 19	U - Pb zircon	granitoid, high Tatra granites	Gaweda et al., 2016	526 Ma	555 Ma	545 Ma	519 Ma
Veporikum							
352 ± 15	SHRIMP	volcanites northern veporicum	Vozárová et al., 2010 (Conference)	342 Ma	356 Ma	x	356 Ma
458 ± 14	SHRIMP	volcanites northern veporicum	Vozárová et al., 2010 (Conference)	459 Ma	465 Ma	443 Ma	466 Ma
501 ± 21	SHRIMP	volcanites northern veporicum	Vozárová et al., 2010 (Conference)	x	498 Ma	511 Ma	519 Ma
655 ± 19	SHRIMP	volcanites northern veporicum	Vozárová et al., 2010 (Conference)	662 Ma	646 Ma	x	x
659 ± 18	SHRIMP	volcanites northern veporicum	Vozárová et al., 2010 (Conference)	662 Ma	646 Ma	x	x
514 ± 24	U - Pb zircon, U.I.	metatrondhjemites, layered amphibolite	Putis et al., 2001	526 Ma	498 Ma	511 Ma	519 Ma
348 ± 31	U - Pb zircon, L. I.	metatrondhjemites, layered amphibolite	Putis et al., 2001	342 Ma	356 Ma	x	356 Ma, 317 Ma
416 ± 1	U - Pb zircon	metatrondhjemites, layered amphibolite	Putis et al., 2001	x	x	x	417 Ma
464 ± 35	U - Pb, U.I.	felsic gneiss	Gaab et al., 2006	459 Ma	465 Ma, 498 Ma	443 Ma	466 Ma
444 ± 5	U- Pb zircon	felsic gneiss	Gaab et al., 2006	x	x	443 Ma	x
462 ± 10	U - Pb zircon, U.I.	Koleso & Uplaz	Gaab et al., 2005	459 Ma	465 Ma	x	466 Ma
467 ± 8	U - Pb zircon U.I.	Koleso & Uplaz	Gaab et al., 2005	459 Ma	465 Ma	x	466 Ma
440 ± 7	U - PB zircon,	Mihalikovo, intrusion age	Gaab et al., 2005	x	x	443 Ma	x

	single grain						
Literature ages (Ma)	**methods**	**Rocktype and interpretation**	**author**	**G2 - Semmering Quartzite**	**G1 - Veitsch Nappe**	**G21 - Silbersberg Nappe**	**L1 - Präbichl Fm.**
443 ± 6	U - PB zircon, U.I.	Drotacka	Gaab et al., 2005	x	x	443 Ma	x
334 ± 19	U- Pb zircon, U.I.	Hoskova & Drotacka	Gaab et al., 2005	342 Ma	x	x	x
522 ± 18	U - Pb, CLC	Drotacka	Gaab et al., 2005	526 Ma	x	511 Ma	519 Ma
553 ± 3	U- Pb , CLC	Drotacka	Gaab et al., 2005	x	555 Ma	x	x
360 ± 11	U- Pb, CLC	Hoskova	Gaab et al., 2005	x	356 Ma	x	356 Ma
294 ± 15	U- Pb, CLC	Hoskova	Gaab et al., 2005	297 Ma	x	x	x
395 ± 8	U - Pb, CLC	Hoskova	Gaab et al., 2005	x	x	390 Ma	x
492 ± 8	U - Pb, CLC	Hoskova	Gaab et al., 2005	x	498 Ma	x	x
387 ± 4	U - Pb, CLC	Hoskova	Gaab et al., 2005	x	x	390 Ma	x
349 ± 8	U - Pb, MG	Mihalikovo	Gaab et al., 2005	342 Ma	356 Ma	x	356 Ma
378 ± 23	U- Pb, MG	Mihalikovo	Gaab et al., 2005	x	356 Ma	390 Ma	356 Ma
343 ± 5	U- Pb, MG	Mihalikovo	Gaab et al., 2005	342 Ma	x	x	x
364 ± 16	U - Pb, MG	Mihalikovo	Gaab et al., 2005	x	356 Ma	x	356 Ma
343 +- 1	U - Pb, MG	Mihalikovo	Gaab et al., 2005	342 Ma	x	x	x
349 ± 13	U - Pb, MG	Mihalikovo	Gaab et al., 2005	342 Ma	356 Ma	x	356 Ma
340 ± 6	U - Pb, MG	Mihalikovo	Gaab et al., 2005	342 Ma	x	x	x
354 ± 4	U - Pb, CLC	Mihalikovo	Gaab et al., 2005	x	356 Ma	x	356 Ma
392 ± 6	U - Pb, CLC	Mihalikovo	Gaab et al., 2005	x	x	390 Ma	x
440 ± 3	U - Pb, SG	Mihalikovo	Gaab et al., 2005	x	x	443 Ma	x
462 ± 9	U - Pb, SG	Mihalikovo	Gaab et al., 2005	x	465 Ma	459 Ma	466 Ma
416 ± 2	U - Pb, CLC	Mihalikovo	Gaab et al., 2005	x	x	x	417 Ma
358 ± 3	U - Pb, SG	Koleso	Gaab et al., 2005	x	356 Ma	x	356 Ma
417 ± 3	U - Pb, SG	Koleso	Gaab et al., 2005	x	x	x	417 Ma
352 ± 8	U - Pb, SG	Koleso	Gaab et al., 2005	x	356 Ma	x	356 Ma

Literature ages (Ma)	**methods**	**Rocktype and interpretation**	**author**	**G2 - Semmering Quartzite**	**G1 - Veitsch Nappe**	**G21 - Silbersberg Nappe**	**L1 - Präbichl Fm.**
356 ± 3	U - Pb, SG	Koleso	Gaab et al., 2005	x	356 Ma	x	356 Ma
514 ± 24	U/Pb zircon	meta - leucotonalite in amphibolite	Putis et al., 2001	526 Ma	498 Ma	511 Ma	519 Ma
348 ± 31	U/Pb zircon	meta - leucotonalite in amphibolite	Putis et al., 2001	342 Ma	356 Ma	x	356 Ma
360 - 330	-	felsic layers	Gaab et al., 2005	342 Ma	356 Ma	x	356 Ma
470 - 460	-	orthogneisses	Putis et al., 2008	459 Ma	465 Ma	x	466 Ma
440	-	orthogneisses	Putis et al., 2008	x	x	443 Ma	x
490 - 450	CHIME	orthogneisses	Janák et al., 2002	459 Ma	465 Ma	x	466 Ma
ca. 500	U - Pb zircon	granitic orthogneiss	Putis et al., 2003	x	498 Ma	511 Ma	519 Ma
464 ± 40	-	Murán orthogneiss	Gaab et al., 2006	459 Ma	465 Ma	443 Ma	466 Ma
312 ± 15	CHIME	Murán orthogneiss, thermal overprint	Kovácik et al., 2005	x	x	x	317 Ma
508 - 480	U- Pb zircon	veporic basement, E - part of Nízke Tatry Mountains & Vepor mountains	Putis et al., 2008	x	498 Ma	x	x
502 ± 3	U- Pb zircon	tonalite & metaleucotonalite layers, Vepor mountains	Putis et al., 2008	x	498 Ma	x	x
549 ±18	U- Pb zircon	partially melted metagabbro, protolith age	Putis et al., 2008	x	555 Ma	545 Ma	x
516 ± 7	SHRIMP	orthogneisses, in layered amphibolite complex, North veporic basement	Putis et al., 2008	x	x	511 Ma	519 Ma
359 ± 5	SHRIMP	orthogneisses, in layered amphibolite complex, North veporic basement	Putis et al., 2008	x	356 Ma	x	356 Ma
577	SHRIMP	inherited zircon core, orthogneiss, North veporic basement	Putis et al., 2008	x	x	x	578 Ma
513 - 472	SHRIMP	granitic orthogneiss	Putis et al., 2008	x	498 Ma	511 Ma	x
462 ± 6	SHRIMP	granitic orthogneiss	Putis et al., 2008	459 Ma	465 Ma	x	466 Ma
507 ± 4	SHRIMP	tonalitic orthogneiss, south - veporic basement	Putis et al., 2008	x	x	511 Ma	x
577 ± 8	SHRIMP	tonalitic orthogneiss, south - veporic basement	Putis et al., 2008	x	601 Ma	571 Ma	578 Ma
497 ± 4	SHRIMP	granitic orthogneiss, Chorepa pass	Putis et al., 2008	x	498 Ma	x	x
607 ± 10	SHRIMP	granitic to tonalitic orthogneisses, magmatic age	Putis et al., 2008	x	601 Ma	x	617 Ma

558 ± 7	SHRIMP	garnet - rutile orthogneiss	Putis et al., 2008	x	x	555 Ma	x
Literature ages (Ma)	**methods**	**Rocktype and interpretation**	**author**	**G2 - Semmering Quartzite**	**G1 - Veitsch Nappe**	**G21 - Silbersberg Nappe**	**L1 - Präbichl Fm.**
Gemerikum							
457	U - Pb	metaleucotonalite	Putis et al., 2008	459 Ma	x	x	x
355 - 520	U- Pb zircon	quartzporphyroid, Gelnica Group	Grecula, 1982	459 Ma	356 Ma, 465 Ma, 489 Ma	390 Ma, 443 Ma, 511 Ma	356 Ma, 417 Ma, 466 Ma, 519 Ma
494	SHRIMP	Bystrý potok & Drnava Fm?	Vozárová et al., 2010	x	498 Ma	x	x
444 ± 12.6	SHRIMP	acid metavolcanites, Gelnica Group	Vozárová et al., 2010	x	x	443 Ma	x
423 ± 16.8	SHRIMP	acid metavolcanites, Gelnica Group	Vozárová et al., 2010	x	x	x	417 Ma
292 ± 6	-	NGU permian sandstones	Vozárová et al., 2013	297 Ma	x	x	x
465.8 ± 1.5	SHRIMP	Bytrý Potok, Gelnica Terrane, metasandstones	Vozárová et al., 2010	x	465 Ma	x	466 Ma
463.9 ± 1.7	SHRIMP	Drnava Formation, Gelnica Terrane, metasandstones	Vozárová et al., 2010	x	465 Ma	x	x
666 ±12	SHRIMP	Drnava Formation, Gelnica Terrane, metasandstones	Vozárová et al., 2010	662 Ma	x	x	x
657 ± 13	SHRIMP	Drnava Formation, Gelnica Terrane, metasandstones	Vozárová et al., 2010	662 Ma	646 Ma	x	x
591 ± 13	SHRIMP	Drnava Formation, Gelnica Terrane, metasandstones	Vozárová et al., 2010	x	601 Ma	x	x
653 ± 13	SHRIMP	Drnava Formation, Gelnica Terrane, metasandstones	Vozárová et al., 2010	662 Ma	646 Ma	x	x
615 ± 11	SHRIMP	Drnava Formation, Gelnica Terrane, metasandstones	Vozárová et al., 2010	618 Ma	601 Ma	625 Ma	617 Ma
612 ± 13	SHRIMP	Drnava Formation, Gelnica Terrane, metasandstones	Vozárová et al., 2010	618 Ma	601 Ma	625 Ma	617 Ma
577.2 ± 7.6	SHRIMP	Stós Formation, Gelnica Terrane, metasandstones	Vozárová et al., 2010	x	x	571 Ma	578 Ma
605.3 ± 8.9	SHRIMP	Stós Formation, Gelnica Terrane, metasandstones	Vozárová et al., 2010	x	601 Ma	x	x
617.3 ± 7.4	SHRIMP	Vlachovo Formation, Glenica Terrane, metasandstones	Vozárová et al., 2010	618 Ma	x	x	617 Ma
660.2 ± 7.4	SHRIMP	Vlachovo Formation, Glenica Terrane, metasandstones	Vozárová et al., 2010	662 Ma	x	x	x

Literature ages (Ma)	methods	Rocktype and interpretation	author	G2 - Semmering Quartzite	G1 - Veitsch Nappe	G21 - Silbersberg Nappe	L1 - Präbichl Fm.
624 ± 7.4	SHRIMP	Vlachovo Formation, Glenica Terrane, metasandstones	Vozárová et al., 2010	618 Ma	x	x	617 Ma
589 ± 25	SHRIMP	Vlachovo Formation, Glenica Terrane, metasandstones	Vozárová et al., 2010	x	601 Ma	571 Ma	578 Ma
601 ± 11	SHRIMP	Bytrý Potok, Gelnica Terrane, metasandstones	Vozárová et al., 2010	x	601 Ma	x	x
452 ± 8.4	SHRIMP	Bytrý Potok, Gelnica Terrane, metasandstones	Vozárová et al., 2010	459 Ma	x	x	x
702 ± 13	SHRIMP	Bytrý Potok, Gelnica Terrane, metasandstones	Vozárová et al., 2010	x	x	x	703 Ma
656.7 ± 7.2	SHRIMP	Roznava Formation, Gocaltovo Group, metasandstones	Vozárová et al., 2010	662 Ma	x	x	x
574.6 ±6.4	SHRIMP	Roznava Formation, Gocaltovo Group, metasandstones	Vozárová et al., 2010	x	x	x	578 Ma
644.5 ± 7.2	SHRIMP	Roznava Formation, Gocaltovo Group, metasandstones	Vozárová et al., 2010	x	646 Ma	x	x
626.4 ± 7.1	SHRIMP	Roznava Formation, Gocaltovo Group, metasandstones	Vozárová et al., 2010	x	x	625 Ma	x
658.6 ± 8.5	SHRIMP	Roznava Formation, Gocaltovo Group, metasandstones	Vozárová et al., 2010	662 Ma	x	x	x
623.1 ± 6.8	SHRIMP	Roznava Formation, Gocaltovo Group, metasandstones	Vozárová et al., 2010	618 Ma	x	625 Ma	617 Ma
608.1 ± 7.1	SHRIMP	Roznava Formation, Gocaltovo Group, metasandstones	Vozárová et al., 2010	x	601 Ma	x	x
497 ± 9.2	SHRIMP	Stítnik Formation, Gocaltovo Group, metasandstones	Vozárová et al., 2010	x	498 Ma	x	x
337 ± 8.2	SHRIMP	Stítnik Formation, Gocaltovo Group, metasandstones	Vozárová et al., 2010	342 Ma	x	x	x
461 ± 8.5	SHRIMP	Stítnik Formation, Gocaltovo Group, metasandstones	Vozárová et al., 2010	459 Ma	465 Ma	x	466 Ma
354 ± 6.8	SHRIMP	Stítnik Formation, Gocaltovo Group, metasandstones	Vozárová et al., 2010	x	356 Ma	x	356 Ma
355 ± 6.5	SHRIMP	Stítnik Formation, Gocaltovo Group, metasandstones	Vozárová et al., 2010	x	356 Ma	x	356 Ma
457 ± 8.7	SHRIMP	Stítnik Formation, Gocaltovo Group, metasandstones	Vozárová et al., 2010	459 Ma	465 Ma	x	x

Literature ages (Ma)	**methods**	**Rocktype and interpretation**	**author**	**G2 - Semmering Quartzite**	**G1 - Veitsch Nappe**	**G21 - Silbersberg Nappe**	**L1 - Präbichl Fm.**
474 ± 8.8	SHRIMP	Stítnik Formation, Gocaltovo Group, metasandstones	Vozárová et al., 2010	x	x	x	466 Ma
534 - 455	SHRIMP	Gemer area	Radvanec et al., 2010 (Conference)	526 Ma, 459 Ma	498 Ma, 465 Ma	511 Ma	519 Ma, 466 Ma
577 ± 6	U - Pb zircon	Smrecinka formation	Vozárová et al., 2013	x	x	x	578 Ma
644	U - Pb zircon	Smrecinka formation	Vozárová et al., 2013	x	646 Ma	x	x
355 ± 2	U - Pb zircon	Hrádok formation	Vozárová et al., 2013	x	356 Ma	x	356 Ma
565 ± 11	U - Pb zircon	Hrádok formation	Vozárová et al., 2013	x	555 Ma	571 Ma	x
355.8 ± 6.8	U - Pb zircon	Hrádok formation	Vozárová et al., 2013	x	356 Ma	x	356 Ma
560 - 732	U - Pb zircon	Rudnany Formation	Vozárová et al., 2013	618 Ma, 662 Ma	617 Ma, 664 Ma	571 Ma, 625 Ma	578 Ma, 601 Ma
352.4 ± 6.8	U - Pb zircon	Petrová Hora, metasandstone NGU	Vozárová et al., 2013	x	356 Ma	x	356 Ma
363 ± 12	U - Pb zircon	Petrová Hora, metasandstone NGU	Vozárová et al., 2013	x	356 Ma	x	356 Ma
458 ± 9	U - Pb zircon	Novoveská Huta	Vozárová et al., 2013	459 Ma	465 Ma	x	466 Ma
472 ± 10	U - Pb zircon	Novoveská Huta	Vozárová et al., 2013	x	465 Ma	x	466 Ma
588±12	U - Pb zircon	Novoveská Huta	Vozárová et al., 2013	x	x	x	578 Ma

18.5 Appendix E

Table 12: Occurence of ages in several areas oft he Eastern Alps in comparison to the measured sample ages. X: main ages of the samples.

	Literatur																	untersuchter Proben			
Alter	Silvretta	Seckau	Ötztal	Texel/Campo	Wölz	Koralpe	Saualpe	Gleinalm	TW	S von TW	W - GWZ	Semmering	Wechsel	Kaintaleck	Tatrikum	Veporikum	Gemerikum	Semmering	Veitscher	Silbersberg	Präbichl Fm.
662 - 600 Ma						x			xx				x			x	xx	xx	xx	x	x
580 - 490 Ma	xxx	xxx	xx	xxx					xxx	x				xxx	xx	xxx	xx	x	xx	xxx	xx
480 - 450 Ma				xxx	xxx				x	xxx	xxx				xxx	xxx	xx	x	x		x
443 - 410 Ma	x	xx		x	xx					x					x	xx	x			x	x
390 Ma			x					x						x	x	xx	xx			x	
360 - 330 Ma		xx	xx	x										x	xxx	xxx	xx	x	x		x
320 -300 Ma		x				x									x						x
297 - 250 Ma						x									x			x			